AD-A062 488 LOGICON INC LEXINGTON MA F/G 4/1
RESEARCH, ANALYSIS, DEVELOPMENT, AND APPLICATION OF HIGHLY INTE--ETC(U)
OCT 78 J N BASS, K H BHAVNANI, S T LAI F19628-78-C-0049
UNCLASSIFIED AFGL-TR-78-0204 NL

1 OF 3
AD
A062488

(12)

LEVEL II

AFGL-TR-78-0204

RESEARCH, ANALYSIS, DEVELOPMENT AND APPLICATION OF HIGHLY INTEGRATED SYSTEMS OF MULTI-PHASES OF THE PHYSICS OF THE UPPER ATMOSPHERE

James N. Bass
Krishin H. Bhavnani
Shu T. Lai
Frank R. Roberts
Donna L. Spiegelman
Leo A. Whelan

Logicon, Inc.
18 Hartwell Avenue
Lexington, Massachusetts 02173

15 October 1978

Final Report for Period 15 January 1978 - 15 July 1978

Approved for public release; distribution unlimited.

AIR FORCE GEOPHYSICS LABORATORY
AIR FORCE SYSTEMS COMMAND
UNITED STATES AIR FORCE
HANSCOM AFB, MASSACHUSETTS 01731

Unclassified

SECURITY CLASSIFICATION OF THIS PAGE (When Data Entered)

REPORT DOCUMENTATION PAGE	READ INSTRUCTIONS BEFORE COMPLETING FORM
1. REPORT NUMBER: AFGL-TR-78-0204	2. GOVT ACCESSION NO. / 3. RECIPIENT'S CATALOG NUMBER
4. TITLE (and Subtitle): RESEARCH, ANALYSIS, DEVELOPMENT, AND APPLICATION OF HIGHLY INTEGRATED SYSTEMS OF MULTI-PHASES OF THE PHYSICS OF THE UPPER ATMOSPHERE.	5. TYPE OF REPORT & PERIOD COVERED: Scientific - Final rept. 15 Jan [illegible] 15 Jul [illegible] 78
	6. PERFORMING ORG. REPORT NUMBER
7. AUTHOR(s): James N. Bass, Krishin H. Bhavnani, Shu T. Lai, Frank R. Roberts, Donna L. Spiegelman, Leo A. Whelan	8. CONTRACT OR GRANT NUMBER(s): F19628-78-C-0049 new
9. PERFORMING ORGANIZATION NAME AND ADDRESS: LOGICON, INC., 18 Hartwell Avenue, Lexington, MA, 02173	10. PROGRAM ELEMENT, PROJECT, TASK AREA & WORK UNIT NUMBERS: P- n/a; TA-n/a; WU-n/a; PE 62101F
11. CONTROLLING OFFICE NAME AND ADDRESS: Air Force Geophysics Laboratory, Hanscom AFB, Massachusetts, 01731, Contract Monitor: Edward C. Robinson/SUA	12. REPORT DATE: 15 October 1978
	13. NUMBER OF PAGES: 208 pages
14. MONITORING AGENCY NAME & ADDRESS (if different from Controlling Office) 12) 210p.	15. SECURITY CLASS. (of this report): Unclassified
	15a. DECLASSIFICATION/DOWNGRADING SCHEDULE

16. DISTRIBUTION STATEMENT (of this Report)

Approved for Public release; distribution unlimited.

17. DISTRIBUTION STATEMENT (of the abstract entered in Block 20, if different from Report)

18. SUPPLEMENTARY NOTES

Tech, Other

19. KEY WORDS (Continue on reverse side if necessary and identify by block number)

Computer Programs	Orbit Determination	Doppler Beacon
Astronomical Ephemeris	Plasma Motion	Satellite Thrusts
DMSP Project	Satellite Orbits	Geomagnetic Coordinates
Electric Field	Satellite Drag	Satellite Illumination
Ionospheric Research	Atmospheric Density Models	Proton-Electron System
		Multiple Regression

20. ABSTRACT (Continue on reverse side if necessary and identify by block number)

This report documents analyses and computer programming tasks performed in support of scientific activities at Air Force Geophysics Laboratory (AFGL). Mathematical and logical procedures are discussed; reference material and a sample of results are presented.

A variety of computer programs is used to fulfill the different requirements, generated by the various research programs, for satellite orbit data. Revisions to these programs are presented which, variously, enlarge the input/output capa-

DD FORM 1 JAN 73 1473 EDITION OF 1 NOV 65 IS OBSOLETE

Unclassified

SECURITY CLASSIFICATION OF THIS PAGE (When Data Entered)

409 990 78 12 18 160

bilities, improve the accuracy of calculations, or extend the range of problems that can be addressed. Results are presented of investigations of the comparative accuracy of available programs for satellite orbit prediction and solar ephemeris calculation.

Occasionally large scale computer codes useful for geophysical analyses, but developed elsewhere, must be adapted to the needs of AFGL research programs and modified for use on the 6600 system. Cases in point are a code for predicting the proton and electron environments in the magnetosphere and another for transforming between geomagnetic and geographical coordinate systems. Modifications to these programs and procedures for their operational usage are presented.

Atmospheric density modeling plays an important role in satellite orbit determination. Results are presented for efforts to: incorporate new density models into orbit determination programs; evaluate the performance of different density models in orbit determination applications; and provide methods for model development by applying multiple regression to experimental data.

A detailed description is provided of a software system designed to process special ion and electron sensor data from a series of polar orbiting satellites of the Defense Meteorological Systems Project.

Software systems have been developed for the extraction of plasma flow and electric field data from in situ observations made on board the polar orbiting satellites S3-2 and S3-3. The software systems, typical results, and some physical conclusions drawn from these observations are presented.

Acknowledgements

The coordination, guidance, and encouragement of our Contract Monitor, Mr. Edward C. Robinson of the Analysis and Simulation Branch, are greatly appreciated. Helpful, too, was the involvement and interest shown in many of the projects by the Acting Branch Chief, Mr. Robert E. McInerney.

Thanks are due also to the various AFGL investigators with whom we have been associated, whose motivation and direction have consistently benefitted our participation in AFGL research.

Ms. Marcia Brehm displayed commendable skill and patience in handling the technical typing, diagrams, and revisions.

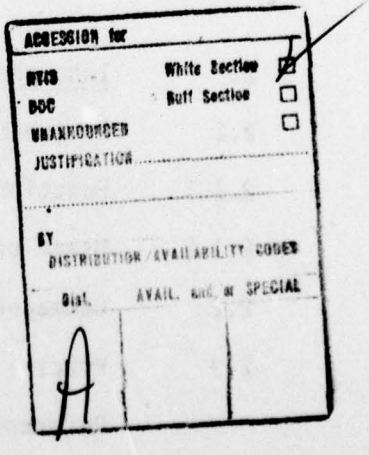

Table of Contents

Table of Contents (cont'd)

Table of Contents (cont'd)

List of Figures

List of Figures (cont'd)

List of Figures (cont'd)

List of Figures (cont'd)

List of Figures (cont'd)

List of Figures (cont'd)

List of Tables

1. Satellite Orbits

1. Satellite Orbits

Initiator: E. Robinson

Project No: 0001 Problem No: 4517

A broad range of research analyses conducted at AFGL requires, as input, precise satellite orbit data. A researcher might, for example, be interested in using on board sensors to map a particular physical quantity through space. He would need to know the satellite's position as a function of time in order to interpret telemetry data, or he might need to know the satellite's precise location relative to some spatially distributed physical quantity such as solar radiation at the edge of the earth's shadow. Programs LOKANGL, ROPP as well as other adaptations of conventional orbit determination programs are available to provide the needed data. Each has its own unique features in terms of the type of input data on which calculations are based, and methods of treating perturbations to orbital dynamics such as drag and the higher order terms of the geopotential. Efforts are continuously being conducted to evaluate and improve the accuracy of these programs and to generalize and extend their applicability. These studies are reported in the following subsections.

1.1 LOKANGL Features

Program LOKANGL has continued to be used and developed for most AFGL satellite ephemeris generation and study purposes. Improvements have been made in providing satellite observation data for flying aircraft, and in the satellite solar-illumination routine. Additional capabilities were implemented in order to handle satellite thrusting; the perigee-apogee determination algorithm was also modified to function properly under thrust adjustments. Orbital elements are now accepted in any of five formats: a) SCF position-velocity sets in subroutine DELEM; b) 2-card ADC, 3-card ADC, and osculating Keplerian sets in subroutine CONVRT; c) original 5-card ADC Keplerian sets directly in LOKANGL.

Output options include print-out of selectable station-independent or station-related parameters; and a binary ephemeris tape that is in the original format defined in the ancestral source program[1] and that is retained with minor changes. The current input format is presented in Figure 1; and the binary tape format is described in Figure 2.

Program LOKANGL is designed to convert any of the element sets provided into standard Keplerian form, and then to generate an ephemeris after revising element rates of change where interpolation is possible. The effects of first order geopotential and atmospheric perturbations only are included. Sources of inaccuracy in the trajectory may be due to element set discrepancies introduced by the orbit determination pro-

```
      PROGRAM LOKANGL(INPUT,OUTPUT,TAPE5=INPUT,TAPE6=OUTPUT,TAPE3,TAPE4,    LOKANG     2
     *  TAPE7)                                                              LOKANG     3
C.                                                                         LOKANG     4
C    LOGICON,INC.                          VERSION   SEPTEMBER   1977     LOKANG     5
C.*************************************************************           LOKANG     6
C.    INPUT FORMAT FOR PROGRAM LOKANGL                                     LOKANG     7
C.*************************************************************           LOKANG     8
C.    DATA DECK SETUP                                                      LOKANG     9
C.                                                                         LOKANG    10
C.    CARD    COLS                  DESCRIPTION                          LOKANG    11
C.    1       1       CODE OF ORBITAL DETERMINATION FORM                   LOKANG    12
C.                    1=FORM NO. 3 :   SGF 2-CARD POS.-VEL. SET            LOKANG    13
C.                    2=FORM NO. 2 :   ADC 2-CARD ELEMENT DATA SET         LOKANG    14
C                     3=3-CARD ELEMENT DATA SET                            LOKANG    15
C                     4=OSCULATING ELEMENTS                                LOKANG    16
C                     5=FORM NO.1: ADC 5-CARD DATA SET                     LOKANG    17
C.                                                                         LOKANG    18
C.    2+              ONE OR MORE ELEMENT SETS                             LOKANG    19
C.            8-9     X OR U ON FIRST CARD OF ALL SUBSEQUENT ELEMENT SETS  LOKANG    20
C.            8       T INDICATES THRUST TIME CARD: ONE CARD SET           LOKANG    21
C.                    PROVIDES TIME OF THRUST IN STANDARD COLUMNS           LOKANG    22
C.                                                                         LOKANG    23
C.    *       1-3     NO. OF STATIONS. IF NO STATIONS USE 0                LOKANG    24
C.                    FOR AIRCRAFT FLIGHT SIMULATION RUN, USE -1           LOKANG    25
C.            6       CODE 1 OR 0 FOR PRINT CONTROL OF STATION DATA        LOKANG    26
C.                    0=PRINT BY TIME ONLY                                 LOKANG    27
C.                    1=PRINT BY STATIONS                                  LOKANG    28
C.            7-10    0=STANDARD                                           LOKANG    29
C.                    IONOHT=SUB-IONOSPHERIC ALTITUDE (KM)    I3           LOKANG    30
C.            13-15   MINELV= MIN ELEVATION FOR SAT VIEWING  I3           LOKANG    31
C.            16-30   FOR AIRCRAFT FLIGHT SIMULATION RUN, ALTITUDE OF      LOKANG    32
C.                    AIRCRAFT (M) F15.1                                   LOKANG    33
C.                                                                         LOKANG    34
C.    3+              STATION LOCATION CARDS,IF NMS.GT.0                   LOKANG    35
C.            1-5     I.D. OF STATION (NUMBER)                             LOKANG    36
C.            7-8       2=GEODETIC SYSTEM                                  LOKANG    37
C.            9-23    STATION GEODETIC LATITUDE, DEGREES                   LOKANG    38
C.            24-38   STATION LONGITUDE (POSITIVE WEST), DEGREES           LOKANG    39
C.            39-53   STATION HEIGHT, METERS                               LOKANG    40
C.            61-72   NAME OF STATION                                      LOKANG    41
C.                                                                         LOKANG    42
C.    4       1-15    TIME INCREMENT IN SECONDS, F15.5                     LOKANG    43
C.            17-69   TIME INTERVAL FOR PRINT OR TAPE 7 WRITE              LOKANG    44
C.                    START COLS: 17-18:20-21:23-24:26-29:31-34:36-41      LOKANG    45
C.                    FINAL COLS: 43-44:46-47:49-50:52-55:57-60:62-67      LOKANG    46
C.                    TIME        MONTH:  DAY: YEAR: HOUR:  MIN:  SEC      LOKANG    47
C.                    FORMAT        I2:   I2:   I2: F3.1: F3.1: F5.3       LOKANG    48
C.                    FINAL TIME NOT NECESSARY IF NMS.EQ.-1                LOKANG    49
C.                                                                         LOKANG    50
C.    5               AIRCRAFT POSITION-TIME CARDS, IF NMS.EQ.-1           LOKANG    51
C.    5A              TITLE REQUIRED (4A10)                                LOKANG    52
C.     5+             TWO OR MORE POSITION-TIME CARDS                      LOKANG    53
C.            1-5     HOURS FROM STARTING TIME IS                          LOKANG    54
C.            6-10    MINUTES F5.0                                         LOKANG    55
C.            11-15   DEGREES LATITUDE IS                                  LOKANG    56
C.            16-20   MINUTES LATITUDE  IS                                 LOKANG    57
C.            21-25   DEGREES LONGITUDE IS                                 LOKANG    58
```

Figure 1a. LOKANGL Input Format

```
C.            25-30 MINUTES LONGITUDE IS                                        LOKANG     59
C.      Z     2-5   "1000" INDICATES END OF POSITION-TIME CARDS                LOKANG     60
C.                                                                              LOKANG     61
C.
C.    6             CODE FOR PRINT-OUT  0= NO PRINT; 1= PRINT FOLLOWING:        LOKANG     62
C.            2     1=POSITION AND VELOCITY                                     LOKANG     63
C.            4     1=SUB-SATELLITE DATA                                        LOKANG     64
C.            6     1=OSCULATING ELEMENTS                                       LOKANG     65
C.            8     1=OBSERVATION DATA                                          LOKANG     66
C.            9-10  0=STANDARD BINARY ON TAPE3                                  LOKANG     67
C.                  -1=PERIGEE-APOGEE DATA ON TAPE7                           LOKANG     68
C.            11-13 1.0=SINGLE PASS REFRAC. CORRECTION (STANDARD)             LOKANG     69
C.    7             "END OF PROBLEM"                                          LOKANG     70
C.                                                                              LOKANG     71
C.    ABOVE MAY BE REPEATED N TIMES                                             LOKANG     72
C.    LAST CARD: "9" IN COL. 1                                                  LOKANG     73
C.                                                                              LOKANG     74
C.*************************************************************************** LOKANG     75
C                                                                               COMM       2
C***************** COMMON AND DIMENSION PACKAGE ***************************** COMM       3
C                                                                               COMM       4
      COMMON  DPRINT, DV(3),DVP(3),ERASD(10),OMU,RALON,REARTH,                  COMM       5
     1     TIMREG,TIMSEC(2),TNORMO,TSPI(20),CON(8),DJREG,DJULN,DJULO,           COMM       6
     2     DJUPRT(2),DSPI(20),ERASE(20),FEARTH, FL0,FL1,FL2,FL3,FL4,FL5,        COMM       7
     3     FL6,FL7,FL8,FL9,FL10,FL12,FL24,FL60,FL360,FL3600,FL664M,             COMM       8
     4     FLEPS,FLP5,FL1P5,FLRAD,FL2PI, JSP,KEYTAP, KF0,KF1,KF2,KF3,           COMM       9
     5     KF4,KF5,KF6,KF7,KF8,KF9,KF10,KF100, MERASE(20),                      COMM      10
     6     NMS,NOSAT,NOSPRI,NS,NTP,OBSC(6),OBSM(7),P2(3,3),                     COMM      11
     7     PASS,PERIOD,RMEAN,REARTH,XM(3,3),XYZS(3),VVZT(3),XYZTP(3)            COMM      12
      COMMON  ALT(20),DELAT(20),NUMSTA(20),NSG(20),PHILAT(20),                  COMM      13
     1     SLAT(20),SLON(20),SRAD(20),COSLAT(20),SNSLAT(20),                    COMM      14
     2     AXSEMI,XXMEAN,XMASC,XOINCL,XWPERI,ECCEN,IPOS,IDV,IELE,ISTA,          COMM      15
     3     RADPRT,RX,RX2,TINI,TNO,IREV0,PHCCAL,MINELV,IPAP,                     COMM      16
     4     IFL(20),TITLE(4),ISTART                                              COMM      17
C                                                                               COMM      18
C***************************************************************************** COMM      19
C                                                                               COMM      20
      COMMON / CONEAR / ASUBE,F,TMU,XJ2                                         LOKANG    77
      COMMON / EL / ELO(6),PERDOT                                               LOKANG    78
      DIMENSION NAME(20,2), JMOPRT(2),JDAPRT(2),JYRPPT(2),HRPRT(2),             LOKANG    79
     1     YMIPRT(2),SECPRT(2)                                                  LOKANG    80
      DIMENSION ELM(6),X(3),V(3)                                                LOKANG    81
      EQUIVALENCE (ELM(1),XMEAN),(ELM(2),WPERI),(ELM(3),WASC),                  LOKANG    82
     1          (ELM(4),OINCL),(ELM(5),ECCEL),(ELM(6),AXSMER)                   LOKANG    83
C                                                                               LOKANG    84
      HREV(ARG)=ARG-SIGN(FL360,ARG)*AINT(ABS(ARG)/FL360+FLP5)                   LOKANG    85
C                                                                               LOKANG    86
        CALL SPSETC(0)                                                          LOKANG    87
        REWIND 3                                                                LOKANG    88
      ISTART=1                                                                  LOKANG    89
    1 READ(5,600)IXYZ                                                           LOKANG    90
  600 FORMAT(I1)                                                                LOKANG    91
      IF(IXYZ.EQ.KF9) GO TO 999                                                 LOKANG    92
      REWIND 4                                                                  LOKANG    93
      REWIND 7                                                                  LOKANG    94
      DELMAX = FL0                                                              LOKANG    95
      CALL CRMXA                                                                LOKANG    96
C  INITIALIZE FOR 6 LINE PER INCH PRINTING                                      LOKANG    97
```

Figure 1b. LOKANGL Input Format

```
C.                                                                    LOKANG   74
C.*****************************************************************  LOKANG   75
C.                                                                    LOKANG   76
C.    TAPE3 BINARY FORMAT PRODUCED BY SUBROUTINE SPPROD IS AS FOLLOWS LOKANG   77
C.                                                                    LOKANG   78
C.    FIRST RECORD      IDENTIFICATION RECORD                         LOKANG   79
C.                                                                    LOKANG   80
C.    WORD              DEFINITION                                    LOKANG   81
C.                                                                    LOKANG   82
C.      1. KF7          7,NUMBER OF WORDS REMAINING IN THIS RECORD    LOKANG   83
C.      2. NOSAT        SATELLITE NUMBER                              LOKANG   84
C.      3. TIMSEC(1)    TIME OF DAY OF INITIAL PRINT TIME (SEC)       LOKANG   85
C.      4. DJUPRT(1)    MODIFIED JULIAN DATE OF FINAL PRINT TIME      LOKANG   86
C.      5. TIMSEC(2)    TIME OF DAY OF FINAL PRINT TIME               LOKANG   87
C.      6. DJUPRT(2)    MODIFIED JULIAN DATE OF FINAL PRINT TIME      LOKANG   88
C.      7. DPRINT       PRINT INTERVAL (SEC)                          LOKANG   89
C.      8. NOSPRT       NUMBER OF SPECIAL PRINT TIMES                 LOKANG   90
C.                                                                    LOKANG   91
C.    DATA RECORDS      THIS RECORD IS REPEATED FOR EVERY PRINT TIME  LOKANG   92
C.                                                                    LOKANG   93
C.    WORD              DEFINITION                                    LOKANG   94
C.                                                                    LOKANG   95
C.      1. MERASE(1)    NUMBER OF WORDS REMAINING IN THIS RECORD=     LOKANG   96
C.                      32 + 11*IJ                                    LOKANG   97
C.      2. DAYJL        MODIFIED JULIAN DATE OF THE EPHEMERIS PRINT TIME LOKANG 98
C.      3. KMOOUT       CALENDAR MONTH                                LOKANG   99
C.      4. KDAOUT       CALENDAR DAY                                  LOKANG  100
C.      5. KYROUT       CALENDAR YEAR (LAST 2 DIGITS OF 19XX)         LOKANG  101
C.      6. KHROUT       HOUR OF DAY                                   LOKANG  102
C.      7. KMIOUT       MINUTE OF HOUR                                LOKANG  103
C.      8. SECOUT       SECONDS OF MINUTE                             LOKANG  104
C.      9. TNORMO       TIME OF DAY IN SECONDS CORRESPONDING TO DAYJL LOKANG   105
C.     10. DV(1)        X COORDINATE OF POSITION VECTOR (KM)          LOKANG  106
C.     11. DV(2)        Y COORDINATE OF POSITION VECTOR (KM)          LOKANG  107
C.     12. DV(3)        Z COORDINATE OF POSITION VECTOR (KM)          LOKANG  108
C.     13. DV(4)        X-DOT COORDINATE OF VELOCITY VECTOR (KM/SEC)  LOKANG  109
C.     14. DV(5)        Y-DOT COORDINATE OF VELOCITY VECTOR (KM/SEC)  LOKANG  110
C.     15. DV(6)        Z-DOT COORDINATE OF VELOCITY VECTOR (KM/SEC)  LOKANG  111
C.     16. ALTIO        SATELLITE ALTITUDE (KM)                       LOKANG  112
C.     17. RADPRT       SATELLITE GEOCENTRIC DISTRANCE (KM)           LOKANG  113
C.     18. VTOTPR       VELOCITY (KM/SEC)                             LOKANG  114
C.     19. GEOCEN       GEOCENTRIC LATITUDE (DEG)                     LOKANG  115
C.     20. GEODET       GEODETIC LATITUDE (DEG)                       LOKANG  116
C.     21. OLAMO        SATELLITE LONGITUDE (DEG)                     LOKANG  117
C.     22. MSTHR        HOUR OF GREENWICH MEAN SIDEREAL TIME          LOKANG  118
C.     23. MSTMIN       MINUTE OF GREENWICH MEAN SIDEREAL TIME        LOKANG  119
C.     24. STSECO       SECONDS OF GREENWICH MEAN SIDEREAL TIME       LOKANG  120
C.     25. AXSEMI       SEMI-MAJOR AXIS (KM)                          LOKANG  121
C.     26. ECCEN        ECCENTRICITY                                  LOKANG  122
C.     27. XOINCL       INCLINATION (DEG)                             LOKANG  123
C.     28. XWASC        RIGHT ASCENSION OF ASCENDING NODE (DEG)       LOKANG  124
C.     29. XWPERI       ARGUMENT OF PERIGEE (DEG)                     LOKANG  125
C.     30. XXMEAN       MEAN ANOMALY (DEG)                            LOKANG  126
C.     31. IREV         REVOLUTION NUMBER                             LOKANG  127
C.     32. IJ           NUMBER OF STATIONS IN THIS DATA RECORD (<21)  LOKANG  128
C.     33. ITYPE        =1, FINAL WORD IF IJ=0                        LOKANG  129
C.     34. NUMSTA       STATION NUMBER                                LOKANG  130
C.     35. ELRATE       ELEVATION RATE (DEG/SEC)                      LOKANG  131
C.     36. AZRATE       AZIMUTH RATE (DEG/SEC)                        LOKANG  132
C.     37. RARATE       RIGHT ASCENSION RATE (DEG/SEC)                LOKANG  133
C.     38. DCRATE       DECLINATION RATE (DEG/SEC)                    LOKANG  134
C.     39. ELEVAT       ELEVATION (DEG)                               LOKANG  135
C.     40. AZIMUT       AZIMUTH (DEG)                                 LOKANG  136
C.     41. RANGES       RANGE (KM)                                    LOKANG  137
C.     42. RANRAT       RANGE RATE (KM/SEC)                           LOKANG  138
C.     43. RTASC        RIGHT ASCENSION (DEG)                         LOKANG  139
C.     44. DECLIN       DECLINATION (DEG)                             LOKANG  140
C.                                                                    LOKANG  141
C.    THE SEQUENCE OF WORDS 34 TO 44 IS REPEATED IJ TIMES           LOKANG  142
C.                                                                    LOKANG  143
C.                                                                    LOKANG  144
C.    FINAL RECORD      IDENTIFICATION RECORD FOR THE END OF PROBLEM  LOKANG  145
C.                                                                    LOKANG  146
C.    WORD              DEFINITION                                    LOKANG  147
C.                                                                    LOKANG  148
C.      1. KF1          1                                             LOKANG  149
C.      2. BLANK        HOLLERITH BLANKS                              LOKANG  150
C.                                                                    LOKANG  151
C.    AN END OF FILE FOLLOWS THIS RECORD                            LOKANG  152
C.                                                                    LOKANG  153
C                                                                     COMM     2
```

Figure 2. Binary TAPE3 Output Format

grams, or due to the simplifications of the LOKANGL model. A third source of error entails the interpretation of element sets as provided by various agencies. Position-velocity sets are definitive in this respect, and an earlier report[2] described studies and conversions that were employed to standardize results when using mean elements. Special studies conducted to evaluate errors due to the LOKANGL simplifications are summarized in Section 1.2, and show that less than 2 sec. in-track variations occur when using daily element sets. Discrepancies between element sets are found to have comparable in-track variations, and the normal procedure is to discard erratic element sets after analytical or graphical evaluation of results with and without these sets.

1.1.1 Observing Satellite From Aircraft

Initiator: J. Buchau

Project No: 4643 Problem No: 4965

The capability of program LOKANGL to produce the position of a satellite with respect to an observation station through the use of subroutine CORFL and special service program FLTRANS was consolidated by the incorporation of subroutine FLTRANS into LOKANGL and the elimination of special service program FLTRANS. The present modification now allows the researcher direct access to LOKANGL with the aircraft position-time cards in their original format, with minimal adjustments to the standard LOKANGL input deck. Aircraft-satellite look angles continue to be simulated by a series of moving stations representing the aircraft flight segment. LOKANGL output has been modified to clearly indicate the flight parameters and flight header information of interest, and output paper requirements have been reduced by 80-85% in this consolidated presentation. Figure 1 reflects the updated input format, and Figure 3 presents sample aircraft-satellite look angle output display in its present form.

Functional Description

Subroutine CORFL interpolated the aircraft position at any desired instant in the given flight path. Since one execution of LOKANGL can now supply the user with the entire aircraft-satellite look angle history, large printout gaps and redundancy in output display information have been avoided. In the previous system, one execution of LOKANGL calculated for only one of the array of flight segments. Aircraft position

PREPARED BY/FOR THE ANALYSIS AND SIMULATION BRANCH (SUA), AIR FORCE GEOPHYSICS LABORATORY, TELEPHONE 861-4161

EPHEMERIS EXTRAPOLATION PROGRAM FOR SATELLITE MARSI1

DATE OF ELEMENTS USED IN COMPUTATION - YEAR DAY HR MN SECS REV. NO.
1978 208 0 0 .0 0

2 CARD SPADATS INPUT

	INITIAL VALUE		FIRST TIME DERIVATIVE		SECOND TIME DERIVATIVE	
INCLINATION	.4958500E+10	(DEGREES)	0.	(DEGS/DAY)		
ECCENTRICITY	.6472000E-03		0.	(/DAY)	0.	(/DAY**2)
SEMI MAJOR AXIS	.66112268E+01	(EARTH RADII)	0.	(E.R./DAY)	0.	(E.R./DAY**2)
ARGUMENT OF PERIGEE	.26710160E+03	(DEGREES)	.26922744E-01	(DEGS/DAY)	0.	(DEGS/DAY**2)
R.A. OF ASC. NODE	.2513380E+03	(DEGREES)	-.13412125E-01	(DEGS/DAY)	0.	(DEGS/DAY**2)
MEAN MOTION	.1002660E+01	(REVS/DAY)	0.	(REVS/DAY**2)	0.	(REVS/DAY**3)

THIRD TIME DERIVATIVE OF MEAN MOTION = 0. (REVS/DAY**4) MEAN ANOMALY = .13241870E+03 (DEGREES)

MOVING OBSERVATION STATION SIMULATING AIRCRAFT FLIGHT PATH

	HRS	MIN	DEG LAT	MIN LAT	DEG LONG	MIN LONG	ALT
AIRCRAFT POSITION-TIME CARDS	19	0.	-8	1	-14	25	10000.0
	19	30.	-3	-44	-23	0	10000.0
	20	30.	-1	0	-29	20	10000.0
	21	30.	2	10	-35	50	10000.0
	22	30.	5	0	-42	10	10000.0
	23	30.	8	21	-48	36	10000.0
	0	30.	11	24	-55	0	10000.0
	1	30.	13	15	-59	30	10000.0

STATION PRINTOUT REQUESTED BY STATION WITH 350 KM SUB-IDN OUTPUT

MINIMUM ELEVATION FOR SATELLITE VIEWING= 0 DEG.

EPHEMERIS PRINTOUT DATA

	MONTH	DAY	YEAR	HR.	MIN.	SEC.
START PRINT TIME	3	29	79	19.	0.	0.000
END PRINT TIME	3	30	79	1.	30.	0.000

PRINT EVERY .60000000E+02(SECONDS)

***** PREDICTION NOT RELIABLE FOR REVOLUTIONS MORE THAN 100 BEYOND LAST ELEMENT SET*******

PRINTOUT REQUESTED 1-YES 0-NO

POSITION-VELOCITY VECTOR =0 SUB-SATELLITE POSITION =0 ORBITAL ELEMENTS =0 STATION DATA =0

INITIAL COMPUTATIONS
MODIFIED JULIAN DATE (AS OF JAN.1,1950,ZERO HOURS U.T.) =11334.0 S.M.AXIS = .42167495E+05 (KILOMETERS)
P.KEPLER = .8617399E+05 (SEC.) P.ANOMALISTIC = .8617079E+05 (SEC.) P.NODAL = .8616438E+05 (SEC.) P.DECAY = 0.000 (SEC/REV)

Figure 3a. Aircraft-LOKANGL Sample Printout

PREPARED BY/FOR THE ANALYSIS AND SIMULATION BRANCH (SUA), AIR FORCE GEOPHYSICS LABORATORY, TELEPHONE 861-4161

79 089 ASC-BARBADOS

FLIGHT ALTITUDE= 100000

SEGMENT	MO DY YR	UNIVERSAL TIME				AIRCRAFT		AIRCRAFT-SATELLITE LOOKANGLES				350 KM SUB-ION		SUB-SATELLITE		
NO.		DAY	HR	MIN	SEC	LAT DEG	W.LONG DEG	ELEV DEG	AZIM DEG	RANGE KM	RANRAT KM/SEC	LAT DEG	W.LONG DEG	LAT DEG	W.LONG DEG	REV NO.
1	3/29/79	88	19	0	0	-8.00	14.42	79.75	333.16	35853.	-.00	-7.52	14.66	-.22	18.33	246
1	3/29/79	88	19	1	0	-7.80	14.71	80.05	334.49	35848.	-.00	-7.39	14.93	-.22	18.33	246
1	3/29/79	88	19	2	0	-7.72	14.99	80.35	335.90	35844.	-.00	-7.26	15.20	-.22	18.33	246
1	3/29/79	88	19	3	0	-7.59	15.28	80.63	337.40	35839.	-.00	-7.13	15.47	-.23	18.33	246
1	3/29/79	88	19	4	0	-7.45	15.57	80.91	338.98	35835.	-.00	-7.00	15.74	-.23	18.33	246
1	3/29/79	88	19	5	0	-7.31	15.86	81.18	340.66	35831.	-.00	-6.87	16.01	-.23	18.33	246
1	3/29/79	88	19	6	0	-7.17	16.14	81.44	342.45	35827.	-.00	-6.74	16.28	-.23	18.33	246
1	3/29/79	88	19	7	0	-7.03	16.43	81.70	344.34	35823.	-.00	-6.61	16.55	-.23	18.33	246
1	3/29/79	88	19	8	0	-6.89	16.72	81.94	346.35	35820.	-.00	-6.48	16.82	-.24	18.33	246
1	3/29/79	88	19	9	0	-6.75	17.01	82.18	348.47	35816.	-.00	-6.35	17.09	-.24	18.33	246
1	3/29/79	88	19	10	0	-6.62	17.29	82.41	350.73	35814.	-.00	-6.22	17.36	-.24	18.33	246
1	3/29/79	88	19	11	0	-6.48	17.58	82.61	353.11	35811.	-.00	-6.09	17.63	-.24	18.33	246
1	3/29/79	88	19	12	0	-6.34	17.87	82.81	355.63	35808.	-.00	-5.96	17.89	-.24	18.33	246
1	3/29/79	88	19	13	0	-6.20	18.15	82.99	358.29	35806.	-.00	-5.83	18.16	-.25	18.33	246
1	3/29/79	88	19	14	0	-6.06	18.44	83.16	1.07	35804.	-.00	-5.70	18.43	-.25	18.33	246
1	3/29/79	88	19	15	0	-5.92	18.72	83.31	4.00	35802.	-.00	-5.57	18.70	-.25	18.33	246
1	3/29/79	88	19	16	0	-5.78	19.01	83.45	7.04	35801.	-.00	-5.44	18.97	-.25	18.33	246
1	3/29/79	88	19	17	0	-5.64	19.30	83.58	10.21	35799.	-.00	-5.31	19.24	-.25	18.33	246
1	3/29/79	88	19	18	0	-5.50	19.58	83.69	13.48	35798.	-.00	-5.17	19.50	-.25	18.33	246
1	3/29/79	88	19	19	0	-5.35	19.87	83.78	16.83	35797.	-.00	-5.04	19.77	-.26	18.33	246
1	3/29/79	88	19	20	0	-5.21	20.15	83.79	20.25	35797.	-.00	-4.91	20.04	-.26	18.33	246
1	3/29/79	88	19	21	0	-5.07	20.44	83.82	23.72	35796.	-.00	-4.78	20.31	-.26	18.33	246
1	3/29/79	88	19	22	0	-4.93	20.72	83.82	27.21	35796.	-.00	-4.65	20.58	-.26	18.33	246
1	3/29/79	88	19	23	0	-4.79	21.01	83.81	30.69	35796.	-.00	-4.51	20.84	-.26	18.33	246
1	3/29/79	88	19	24	0	-4.65	21.29	83.77	34.15	35797.	-.00	-4.38	21.11	-.27	18.33	246
1	3/29/79	88	19	25	0	-4.51	21.58	83.71	37.55	35797.	-.00	-4.25	21.38	-.27	18.33	246
1	3/29/79	88	19	26	0	-4.37	21.86	83.63	40.87	35798.	-.00	-4.12	21.64	-.27	18.33	246
1	3/29/79	88	19	27	0	-4.23	22.15	83.53	44.11	35799.	-.00	-3.98	21.91	-.27	18.33	246
1	3/29/79	88	19	28	0	-4.08	22.43	83.41	47.23	35800.	-.00	-3.85	22.18	-.27	18.33	246
1	3/29/79	88	19	29	0	-3.94	22.72	83.27	50.23	35801.	-.00	-3.72	22.45	-.28	18.33	246
1	3/29/79	88	19	30	0	-3.80	23.00	83.11	53.10	35803.	-.00	-3.58	22.71	-.28	18.33	246
2	3/29/79	88	19	31	0	-3.75	23.11	83.05	54.09	35804.	-.00	-3.54	22.81	-.28	18.33	246
2	3/29/79	88	19	32	0	-3.71	23.21	82.98	55.47	35804.	-.00	-3.50	22.91	-.28	18.33	246
2	3/29/79	88	19	33	0	-3.66	23.32	82.91	56.82	35805.	-.00	-3.45	23.01	-.28	18.33	246
2	3/29/79	88	19	34	0	-3.61	23.42	82.83	56.96	35806.	-.00	-3.41	23.11	-.28	18.33	246
2	3/29/79	88	19	35	0	-3.57	23.53	82.75	57.87	35807.	-.00	-3.37	23.21	-.29	18.33	246
2	3/29/79	88	19	36	0	-3.52	23.63	82.66	58.77	35808.	-.00	-3.32	23.31	-.29	18.33	246
2	3/29/79	88	19	37	0	-3.48	23.74	82.51	59.65	35808.	-.00	-3.28	23.41	-.29	18.33	246
2	3/29/79	88	19	38	0	-3.43	23.85	82.53	60.51	35809.	-.00	-3.24	23.51	-.29	18.33	246
2	3/29/79	88	19	39	0	-3.38	23.95	82.45	61.35	35810.	-.00	-3.19	23.61	-.29	18.33	246
2	3/29/79	88	19	40	0	-3.34	24.06	82.36	62.18	35811.	-.00	-3.15	23.70	-.29	18.33	246
2	3/29/79	88	19	41	0	-3.29	24.16	82.26	62.98	35812.	-.00	-3.11	23.80	-.30	18.33	246
2	3/29/79	88	19	42	0	-3.24	24.27	82.19	63.77	35813.	-.00	-3.06	23.90	-.30	18.33	246
2	3/29/79	88	19	43	0	-3.20	24.37	82.11	64.55	35814.	-.00	-3.02	24.00	-.30	18.33	246
2	3/29/79	88	19	44	0	-3.15	24.48	82.02	65.30	35815.	-.00	-2.98	24.10	-.30	18.33	246
2	3/29/79	88	19	45	0	-3.10	24.59	81.93	66.04	35816.	-.00	-2.93	24.20	-.30	18.33	246
2	3/29/79	88	19	46	0	-3.06	24.69	81.84	66.76	35817.	-.00	-2.89	24.30	-.30	18.32	246
2	3/29/79	88	19	47	0	-3.01	24.80	81.74	67.46	35819.	-.00	-2.84	24.40	-.31	18.32	246
2	3/29/79	88	19	48	0	-2.96	24.90	81.65	68.15	35820.	-.00	-2.80	24.50	-.31	18.32	246
2	3/29/79	88	19	49	0	-2.92	25.01	81.55	68.83	35821.	-.00	-2.76	24.60	-.31	18.32	246
2	3/29/79	88	19	50	0	-2.87	25.11	81.45	69.49	35822.	-.00	-2.71	24.70	-.31	18.32	246

Figure 3b. Aircraft-LOKANGL Sample Printout

and time coordinates are written on TAPE7 immediately after they are read by subroutine FLTRANS, and subsequent reading of TAPE7 at the appropriate time eliminates the necessity of increased core storage, and allows for flights with a virtually unlimited number of segments.

1.1.2 Input of Elements for Thrusted Satellites

Program LOKANGL was extended to generate orbits for thrusted satellites. The standard elements are entered with single thrust cards interspersed at the appropriate times. The program was modified to discontinue use of a prior element set when the ephemeris reaches a thrust time, and then to project backward from a subsequent element set. Diagnostics are included to check for improper card sequences. Capability for handling two successive thrusts with no element set in between is feasible, but has not been implemented. The system has been used extensively with SCF element sets to generate S3-4 and PACA orbits. Section 1.3 presents the results of a short study to determine the effect of various thrust adjusts on S3-4 orbital parameters.

1.1.3 Apogee-Perigee Calculations For Thrusted Satellites

The discontinuous nature of the argument of perigee, the altitude at apogee, and the altitude at perigee necessitated a revision of the apogee-perigee calculation procedures. The epoch is advanced progressively to increase mean anomaly by 180° and then iteratively optimized to the time of apogee or perigee. As long as a thrust does not cause an adjustment of greater than 90° in the argument of perigee, the above procedure will not be confounded. Figure 4 shows a standard one-month apogee-perigee plot for S3-4.

1.1.4 ADC 3-Card Element Sets (CONVRT3)

Program LOKANGL has been modified to accept as input ADC 3-card element

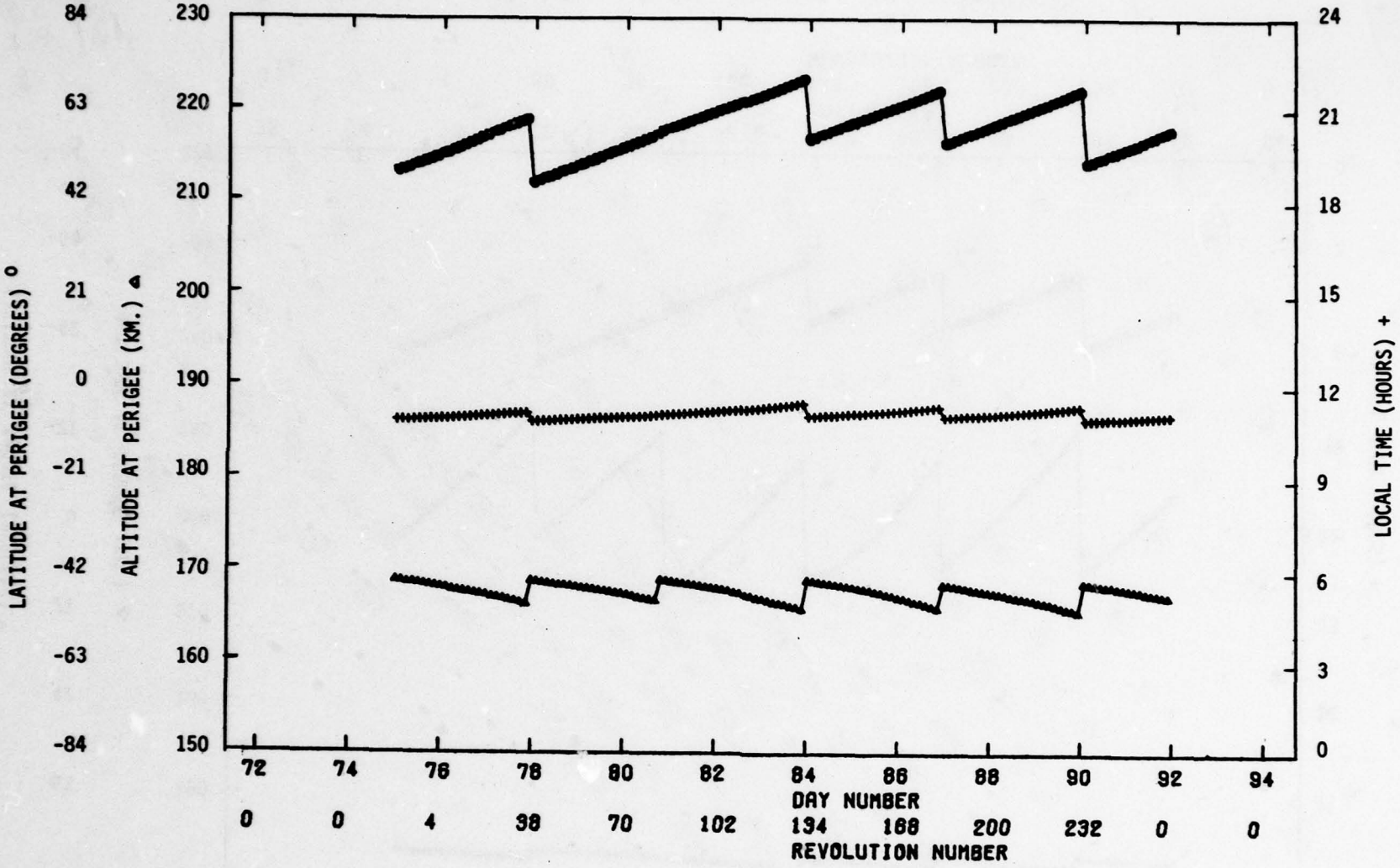

Figure 4a. Typical Apogee-Perigee Plots for a Thrusted Satellite

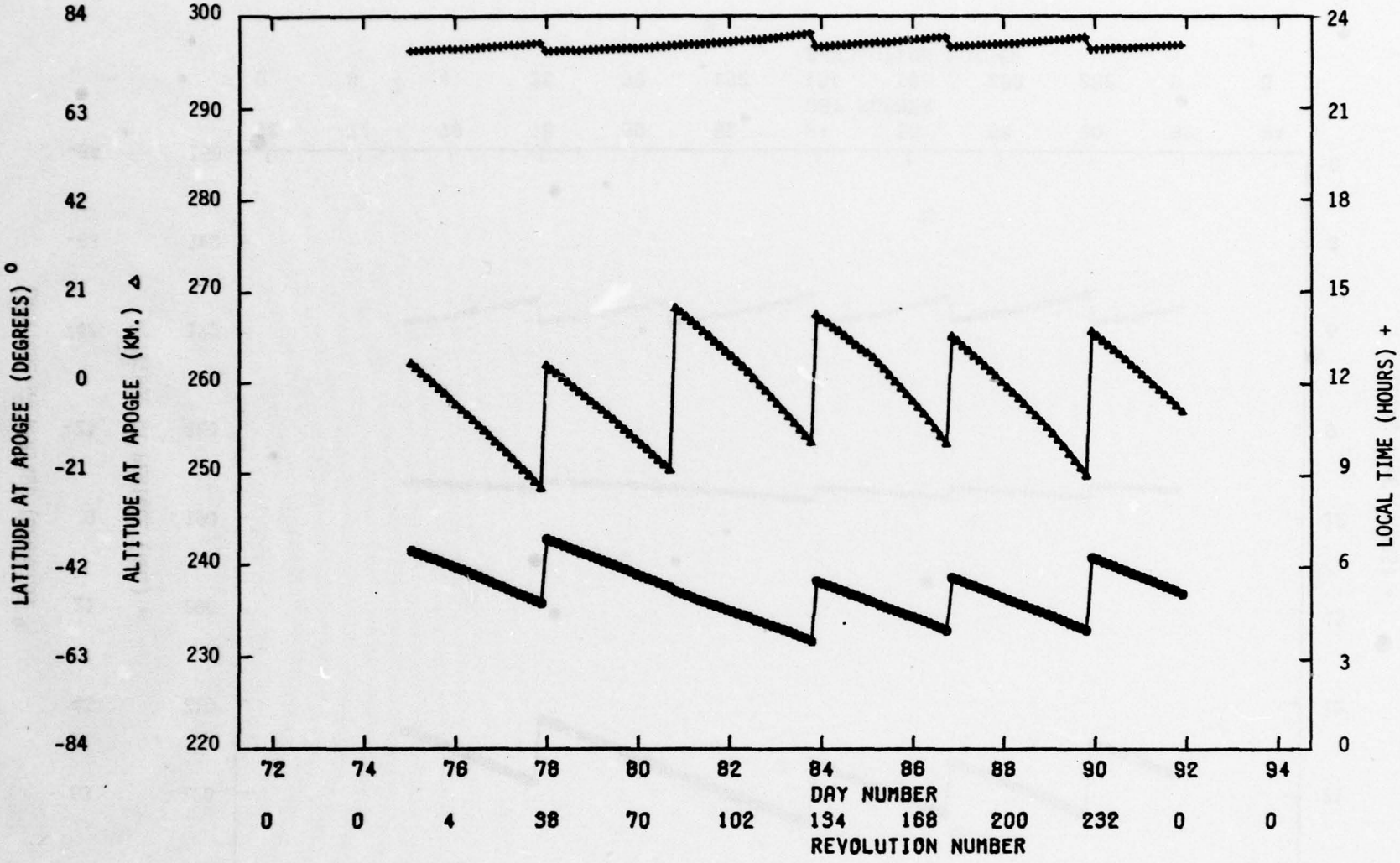

Figure 4b. Typical Apogee-Perigee Plots for a Thrusted Satellite

data sets. Required input parameters are identical to those supplied by the ADC SPADATS 2-card element sets, and scaling adjustments are made by entry point CONVRT3 of subroutine CONVRT to the argument of perigee, right ascension and year in order to standardize values for proper use by LOKANGL. Figure 1 reflects the updated input format, and Figure 5 describes the three-card format now acceptable as input to LOKANGL.

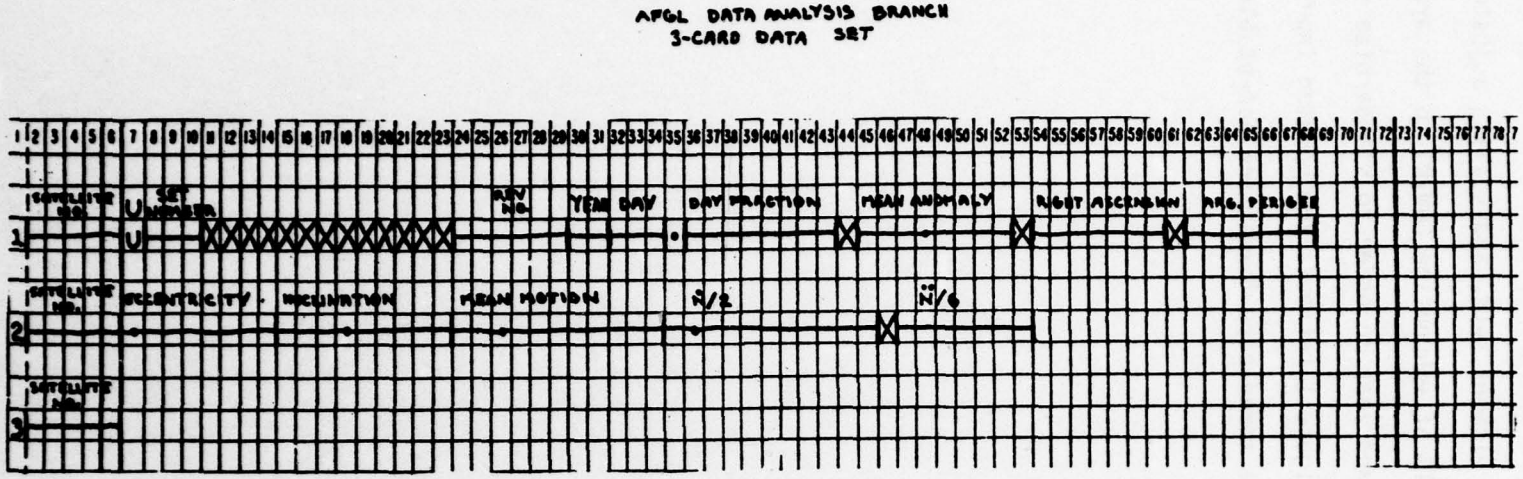

Figure 5. ADC 3-Card Element-Set Format

1.2 Orbit Estimation Accuracy Studies

The most significant variation between orbits generated by LOKANGL or ROPP using successive element sets shows up as the in-track error. Due to the earth's rotation this timing error also produces a ground track error of up to 0.5 km in longitude per second of in-track time, which clearly shows up when predicting high drag orbits. Radial and cross-track errors are generally small. The in-track difference between orbits at a given epoch may be obtained from the Keplerian elements at the epoch, using argument of perigee plus mean anomaly (W + M) as the angular measure of in-track position; or from position-velocity vectors ($\overline{P}$, $\overline{V}$) as

$$\frac{[\overline{P}_R - \overline{P}_C] \cdot \overline{V}_R}{|\overline{V}_R|}$$

where the subscripts indicate reference (R) or computed (C) quantities.

Section 1.2.1 describes a LOKANGL interpolated orbit study which used position-velocity vector comparisons, and section 1.2.2 presents a ROPP prediction study which used osculating Keplerian element comparisons.

1.2.1 LOKANGL Interpolated Orbits

Three hypothetical satellite orbits, each covering a 4-day span, were generated using CELEST with the STEM 8x8 geopotential model and the Jacchia 64 atmospheric density model. The orbits included high drag

160 km perigee altitude, moderate drag 240 km perigee altitude, and synchronous altitude cases. The trajectories could be considered to be "real" since the CELEST model included considerable fine structure. Position-velocity vectors were generated on an hourly basis; daily vectors with estimated period decays were then selected as the "SCF"-type elements for input to LOKANGL, and the resulting interpolated orbit was compared against the hourly vectors.

The original approach taken in order to match mean anomaly at the element epochs was to adjust mean motion for low drag orbits, but to adjust the derivative of mean motion for high drag orbits. Results of these tests showed that, using element sets separated by 4 days for high drag orbits, CELEST-LOKANGL in-track differences exceeded 100 km or 15 seconds of time, and that this situation could be improved only by adjusting both mean motion and its derivative. The procedure now implemented adjusts the derivative of mean motion based on the mean motions before adjusting mean motion to match mean anomaly. Maximum in-track timing error has thus been reduced to 2-3 seconds over the 4-day span. The low drag and synchronous orbit cases are essentially unaffected by this modification and have maintained less than 2 seconds of error over the 4-day span.

In addition to the above limitations, elements transmitted by agencies are subject to orbit determination inaccuracies. This problem is evidenced by erratic elements for the same epoch when transmitted on different days. 10 km or greater variations have been observed, and therefore the absolute accuracy of LOKANGL ephemerides is limited

to about 25 km.

1.2.2 ROPP Prediction Study

S3-4 orbit predictions were made over a 10 day span in April 1978 using program ROPP. A two-day thrust-free span was first employed to determine an optimized drag factor, which was established as CDAM = 0.0104796 ft^2/lb for all the runs. SCF vector and ADC 2-card Keplerian elements sets were used, and the in-track position, as measured by osculating argument of perigee plus mean anomaly, is presented in Table 1 (SCF) and Table 2 (ADC) at integral hours close after the SCF element set epochs. Various conclusions are summarized below.

1) Small initial differences in the semi-major axis cause the in-track error to build up exponentially as a function of time.

2) Following a thrust, in-track position, and consequently the ground track, rapidly diverge from the no-thrust predictions.

3) SCF and ADC elements result in comparable orbit predictions. No systematic bias is evident.

4) The first SCF element after each thrust is unreliable, probably because some pre-thrust conditions are factored into the orbit determination.

5) The most reliable positional information is, of course, obtained close to the element epochs. A LOKANGL interpolation run using all elements naturally matches this orbit closely (compare in Table 1 against diagonal entries). If one element set only is used in each thrust interval, the prediction gradually diverges as expected.

6) A separate ROPP test showed that for an S3-4 type satellite

S3-4 ARGUMENT OF PERIGEE + MEAN ANOMALY (DEG.) CDA/M = .0104796

APRIL DA/HR ELEMENT EPOCH DA/HR/MN	6/0	6/8	7/3	8/8	9/0	9/8	10/9	11/9	12/0	12/8	13/8	14/9	15/1
5/6/30	138.0	294.6	294.2	172.5	140.5	306.5	241.9	--	--	CRASHED			
THRUST -- 5/19/43													
5/22/21	134.5	284.7	264.2	123.4	77.3	236.0	245.2	384.3	482.6	301.2	--	--	CRASHED
6/6/05		284.5	262.3	117.4	66.7	222.4	218.9	338.7	418.2	222.4	363.6	411.1	--
7/7/11			262.1	117.3	66.7	222.5	219.2	339.3	419.1	223.4	365.2	414.0	--
8/6/46				117.1	66.7	222.6	219.7	340.3	420.5	225.1	367.9	418.7	--
THRUST -- 8/21/30													
8/22/33					54.7	214.9	193.7	295.2	362.4	159.5	276.7	290.0	262.8
9/6/22						214.9	193.0	292.6	357.8	153.5	265.4	270.1	235.0
10/7/28							192.8	292.6	358.0	153.8	266.0	271.1	236.5
11/7/03								292.7	358.5	154.7	267.9	274.4	240.8
THRUST -- 11/20/18													
11/22/51									356.0	146.4	241.8	228.5	181.2
12/6/39										146.4	241.3	225.8	176.1
13/6/16											241.4	226.6	177.3
14/7/19												226.6	177.7
THRUST -- 14/22/04													
14/23/08													175.3
LOKANGL (ALL ELEMENTS)	134.3	284.6	262.1	117.1	64.5	214.9	192.8	292.7	355.9	146.4	241.4	226.6	175.2
LOKANGL (2ND ELEMENTS AFTER THRUSTS)	134.4	284.5	262.5	117.8	64.6	214.9	193.1	292.9	355.9	146.4	241.7	227.5	175.3

TABLE 1. ROPP RUNS WITH SCF ELEMENTS, AND LOKANGL COMPARISONS.

S3-4 ARGUMENT OF PERIGEE + MEAN ANOMALY (DEG.) CDA/M = .0104796

APRIL DA/HR ELEMENT EPOCH DA/HR/MN	6/0	6/8	7/3	8/8	9/0	9/8	10/9	11/9	12/0	12/8	13/8	14/9	15/1
5/16/03	137.9	294.4	293.9	171.8	139.3	305.0	238.9	--	--	CRASHED			
THRUST -- 5/19/43													
5/21/57	134.4	284.4	261.7	116.4	55.5	221.0	217.2	336.7	416.1	220.1	361.0	408.0	--
7/3/30			262.1	117.1	66.4	222.1	218.7	338.6	418.2	222.4	363.8	411.7	--
8/3/05				117.1	66.3	221.9	218.7	337.9	417.4	221.4	362.3	409.0	--
THRUST -- 8/21/30													
8/23/44						214.7	192.2	291.3	356.3	152.0	263.6	268.3	233.4
11/10/45									357.8	153.6	265.6	270.5	235.7
THRUST -- 11/20/18													
12/0/04										146.3	240.7	224.6	174.6
12/11/49											241.2	225.8	176.2
14/15/25													177.8
THRUST -- 14/22/04													

TABLE 2. ROPP RUNS WITH ADC ELEMENTS.

a 20% error in the estimate of drag produces a 0.7° mean anomaly or 10 second in-track timing error after 2 days. Due to errors in determining the semi-major axis, greater variations are likely.

1.3 Satellite Thrust Effects Study

The effect of different amounts and directions of thrusting on various satellite orbits is an extensive subject, and only the special case of the S3-4 satellite was explored. The nearly circular ($e \approx .006$), 96.5° inclination, low altitude orbit is maintained with argument of perigee around 120° by periodic thrusts that cause a velocity increase of the order of 7.5 m/sec, approximately in the direction of the velocity vector.

The effect of a 0.1% increase in the velocity vector on the argument of perigee and the eccentricity was evaluated at 30° intervals of mean anomaly. The results are presented in Table 3. In all cases the mean motion decreased from 16.28 to about 16.231 revs/day and the mean anomaly change complemented the change in the argument of perigee.

This table can be used to confirm the effects of known thrusts at various latitudes, ascending and descending, and eventually to incorporate simple thrust models into LOKANGL. For example, a regular burn occurs every three days near 0° latitude descending, with a resulting 0.1% increase in velocity. The increase in the argument of perigee and the corresponding lower perigee latitude makes up for the secular -4°/day drift in the perigee. As another example, on 21 March 1978 two burns gave a 0.07% increase in velocity near 60° latitude descending (M=0°), followed by a 0.01% velocity increase near 60° latitude ascending (M=300°). The result was a minor change in the argument of perigee.

Table 3. Effect of 0.1% Velocity Increase on a Satellite with $i = 96.5°$, $e = .006$, $\omega = 120°$, and $n = 16.28$

Original Mean Anomaly °	New - Old Argument of Perigee	New Eccentricity
0	+ 0.1	.0080
30	+ 6.7	.0079
60	+ 12.5	.0073
90	+ 16.3	.0065
120	+ 15.9	.0055
150	+ 12.2	.0046
180	- 0.4	.0040
210	- 10.8	.0043
240	- 16.3	.0051
270	- 16.3	.0062
300	- 12.4	.0071
330	- 7.3	.0077

1.4 ROPP Features

The input facilities described in Reference 3 have been modified over the past several years as additional features have been incorporated in program ROPP. Drag optimization for two element-sets, and input and output of position-velocity vectors was described in Reference 2. Inclusion of geopotential resonance terms was described in Reference 4. Figure 6 reflects the up-to-date status of input facilities and options for ROPP.

```
74/74  OPT=1                    FTN 4.6+452      07/10/78  16.08.07      PAGE   1

      OVERLAY(CDCD,0,0)                                                  ROPP    2
      PROGRAM ROPP(INPUT,OUTPUT,TAPE5=INPUT,TAPE3=OUTPUT,TAPE7,TAPE2,    ROPP    3
     1TAPE6=OUTPUT,PUNCH)                                                ROPP    4
C.                                                                       ROPP    5
C.    LOGICON, INC.                VERSION  DECEMBER, 1977               ROPP    6
C.*****************************************************************    ROPP    7
C.    INPUT FORMAT FOR PROGRAM ROPP                                      ROPP    8
C.*****************************************************************    ROPP    9
C.    DATA DECK SET-UP                                                   ROPP   10
C.                                                                       ROPP   11
C.    CARD     DESCRIPTION                                               ROPP   12
C.                                                                       ROPP   13
C.     1       'NAME'                                                    ROPP   14
C.     1A      ALPHANUMERIC TITLE FOR RUN, USUALLY SATELLITE NAME        ROPP   15
C.             COLUMNS 3-48, MUST FOLLOW CARD ONE                        ROPP   16
C.                                                                       ROPP   17
C.     2       'MEAN' OR 'POVL'  (OPTIONAL)                              ROPP   18
C.     2A      2-CARD OR 5-CARD ADC SPADATS OR 2-CARD SCF POS-VEL SET    ROPP   19
C.     2B      STANDARD FORMAT REQUIRED, EXCEPT 1 IN COLUMN 71 FOR TAPE7 ROPP   20
C.             WRITE FOR USE WITH PLOTIT.                                ROPP   21
C.                                                                       ROPP   22
C.     3       'SENSR'  (OPTIONAL)                                       ROPP   23
C.     3A+     STATION COORDINATE CARDS: COLS 8-10= INDEX NUMBER         ROPP   24
C.    (20 MAX)                          COL 11-30 = GEODETIC LAT (DEG)   ROPP   25
C.                                      COL 31-50 = E LONG (DEG)         ROPP   26
C.                                      COL 51-70 = STATION HEIGHT (KM)  ROPP   27
C.                                                                       ROPP   28
C.     4       'NMLST'     INDICATES BEGINNING NAMELIST INPUT FORMAT     ROPP   29
C.     4A      -$INPUT$ REQUIRED                                         ROPP   30
C.     4A+     AN EQUAL SIGN FOLLOWS EACH INPUT VARIABLE NAME.           ROPP   31
C.             COMMAS SEPARATE EACH INDIVIDUAL ENTRY. THERE MAY BE       ROPP   32
C.             ANY NUMBER OF ENTRIES PER CARD, COLUMNS 2-72.             ROPP   33
C.                                                                       ROPP   34
C.             *  VARIABLES MAY BE INPUT ON ELEMENT SETS                 ROPP   35
C.                                                                       ROPP   36
C.             VARIABLE OPTIONS ARE AS FOLLOWS:                          ROPP   37
C.             TSTART*          F   START TIME JULIAN DATE               ROPP   38
C.                                   DEF=2439119.5                       ROPP   39
C.                                   CORRESPONDS TO EPOCH OF ELEMENT SET ROPP   40
C.             JTIME            I   PRINT-OUT START TIME:                ROPP   41
C.                                   YR,MO,DAY,HOUR,MIN,SEC              ROPP   42
C.                                   DEF=TSTART                          ROPP   43
C.             TSTOP            F   STOP TIME JULIAN DATE                ROPP   44
C.                                   DEF=2439120.5                       ROPP   45
C.             DAYS             F   NUMBER OF RUN DAYS                   ROPP   46
C.                                   TSTOP=TSTART + DAYS                 ROPP   47
C.                                   OVERRIDES TSTOP IF INPUT            ROPP   48
C.             JTIME            I   STOP TIME - OVERRIDES TSTOP AND DAYS ROPP   49
C.                                   IF INPUT.                           ROPP   50
C.                                   YR,MO,DAY,HOUR,MIN,SEC              ROPP   51
C.                                   DEF=0.                              ROPP   52
C.             PRTINT           F   PRINT INTERVAL IN DAYS   DEF=1./24.  ROPP   53
C.             PRTDAY,PRTHR,    F   PRINT INTERVAL IN DAYS, HOURS AND    ROPP   54
C.             PRTMIN               MINUTES. OVERRIDES PRTINT IF INPUT. ROPP   55
C.             HKMIN            F   STOP AT MINIMUM PERIGEE ALT. (KM)    ROPP   56
C.                                   DEF=120.0                           ROPP   57
C.             DELPRG           F   STOP AT MAXIMUM PERIGEE DROP (KM)    ROPP   58
```

Figure 6a. Program ROPP Input Format

```
C.                                DEF=100.0                                  ROPP      59
C.          SEMIAX*          F    SEMI-MAJOR AXIS (KM, OR E.R. IF            ROPP      60
C.                                AMULT =1.)                                 ROPP      61
C.          ECCEN*           F    ECCENTRICITY                               ROPP      62
C.          INCL*            F    INCLINATION (DEGREES)                      ROPP      63
C.          NODE*            F    RIGHT ASCENSION (DEGREES)                  ROPP      64
C.          OMEGA*           F    ARGUMENT OF PERIGEE (DEGREES)              ROPP      65
C.          MEAN*            F    MEAN ANOMALY (DEGREES)                     ROPP      66
C.          PERIGE*          F    PERIGEE HEIGHT: CALCULATES SEMIAX          ROPP      67
C.          AMULT            F    CONVERSION FOR SEMIAX AND PERIGE           ROPP      68
C.                                DEFAULT: KM       1= EARTH RADII           ROPP      69
C.          XAMULT           F    SAME AS AMULT FOR OUTPUT. ALSO             ROPP      70
C.                                AFFECTS A DOT AND OSC A.                   ROPP      71
C.          ERON             F    MAX RELATIVE ERROR FOR INTEGRATION         ROPP      72
C.                                WHEN DRAG PERTURBATIONS ARE USED           ROPP      73
C.                                DEF=1.E-6                                  ROPP      74
C.          EROFF            F    MAX RELATIVE ERROR USED FOR                ROPP      75
C.                                INTEGRATION WHEN DRAG PERTURBATIONS        ROPP      76
C.                                NOT USED   DEF=1.E-8                       ROPP      77
C.          INTSTP           F    INITIAL GUESS AT OPTIMUM STEP SIZE         ROPP      78
C.                                DEF=1.                                     ROPP      79
C.          HMAX             F    MAXIMUM STEP SIZE   DEF=2046.0 DAYS        ROPP      80
C.          HMIN             F    MINIMUM STEP SIZE   DEF=5.E-4 DAYS         ROPP      81
C.                                                                          ROPP      82
C.     FOR ALL PERTURBATION FLAGS,   0= NO PERTURBATION EFFECT              ROPP      83
C.                                1= INCLUDE PERTURBATION EFFECT             ROPP      84
C.          IFLGM            I    MOON - LONG PERIOD EFFECTS   DEF=1         ROPP      85
C.          IFLGHM           I    MOON - SHORT PERIOD EFFECTS   DEF=0        ROPP      86
C.          IFLGS            I    SUN - LONG PERIOD EFFECTS   DEF=1          ROPP      87
C.          IFLGHS           I    SUN - SHORT PERIOD EFFECTS   DEF=0         ROPP      88
C.          IFLGE            I    EARTH PERTURBATIONS: 1 OR 0   DEF=1        ROPP      89
C.          IF IFLGE=1, THE FOLLOWING EARTH PERTURBATIONS MAY                  ROPP      90
C.          BE CHANGED:                                                       ROPP      91
C.          NOMLPQ           I    NUMBER OF SETS OF L,M,P,Q TO USE           ROPP      92
C.                                DEF=3                                      ROPP      93
C.          L(20)            I    DEGREE SUBSCRIPTS OF HARMONICS             ROPP      94
C.                                DEF: L(1)=2,L(2)=3,L(3)=3,OTHER L=0        ROPP      95
C.          M(20)            I    DEGREE SUBSCRIPT OF SPHER HARMONICS        ROPP      96
C.                                DEF: ALL M=0                               ROPP      97
C.          P(20)            I    INCLINATION FUNCTION SUBSCRIPT OF          ROPP      98
C.                                L,M.  DEF: P(1)=1,P(2)=1,P(3)=2,           ROPP      99
C.                                OTHER P=0.                                 ROPP     100
C.          Q(20)            I    ECCENTRICITY FUNCTION SUBSCRIPT OF         ROPP     101
C.                                L,M.  DEF: Q(1)=0,Q(2)=-1,Q(3)=1,          ROPP     102
C.                                OTHER Q=0.                                 ROPP     103
C.          JLM(20,20)       F    COEFF OF J(L,M+1) TERMS IN HARMONIC        ROPP     104
C.                                ANALYSIS.     SYSTEM DEFAULT SET           ROPP     105
C.          LAMDA(20,20)     F    PHASE ANGLES ASSOCIATED WITH               ROPP     106
C.                                TESSERAL HARMONICS.  SYSTEM DEF SET        ROPP     107
C.                                                                          ROPP     108
C.          IFLGD            I    DRAG PERTURBATIONS: 1= YES 0= NO           ROPP     109
C.     IF IFLGD =1(DEF), THE FOLLOWING ARE REQUIRED:                         ROPP     110
C.          AP               F    PLANETARY GEOMAGNETIC INDEX  DEF=2.0       ROPP     111
C.          F10BAR           F    3-DAY MEAN OF 10.7 SOLAR FLUX              ROPP     112
C.                                DEF=100.0                                  ROPP     113
C.          CDAM*            F    BALLISTIC COEFFICIENT DEF=0.01             ROPP     114
C.                                SQ.FT./LB.   5-CARD ADC INPUT OPTION       ROPP     115
```

Figure 6b. Program ROPP Input Format

```
C.                                                                      ROPP      116
C.      IF CD NOT EQUAL TO 0, CDAM IS CALCULATED FROM:                  ROPP      117
C.            CD              F   DRAG COEFFICIENT                      ROPP      118
C.            AREA            F   CROSS-SECTIONAL AREA (M)              ROPP      119
C.            MASS            F   WEIGHT (KG)                           ROPP      120
C.                                                                      ROPP      121
C.      IF CDAM=0. AND CD=0., ENTER A SECOND ELEMENT SET FOR A LATER    ROPP      122
C.      TIME AFTER THE $END CARD OF THE NAMELIST INPUT. CDAM IS THEN    ROPP      123
C.      OPTIMIZED TO MATCH THE TWO ELEMENT SET NODAL PERIOD.            ROPP      124
C.                                                                      ROPP      125
C.            IDUMP           I   0 DO NOT PRINT 1 PRINT DUMPS OF EACH  ROPP      126
C.                                DERIV.      DEF=0                     ROPP      127
C.            IDUMP0          I   0 DO NOT PRINT                        ROPP      128
C.                                1  PRINT DUMPS FOR EACH OUTPUT        ROPP      129
C.            INTORV          I   0 NORMAL EXECUTION                    ROPP      130
C.                                1  QUIT AFTER 1ST OUTPUT              ROPP      131
C.                                DEF=0                                 ROPP      132
C.            NMLST           I   0 DO NOT PRINT                        ROPP      133
C.                                1  PRINT ALL NAMELIST VALUES          ROPP      134
C.            AE              F   SEMI-MAJOR AXIS OF EARTH (KM)         ROPP      135
C.                                DEF=6378.1649                         ROPP      136
C.            MU              F   GRAVITATIONAL CONSTANT OF EARTH       ROPP      137
C.                                DEF=398603.15                         ROPP      138
C.            ICONT               0  NON-CONTINUATION RUN, ALL VALUES   ROPP      139
C.                                   SAVED FROM ONE CASE TO NEXT,       ROPP      140
C.                                   EXCEPT FOR THOSE NEWLY INPUT       ROPP      141
C.                                1  CONTINUATION RUN: ONE OR MORE      ROPP      142
C.                                VARIABLES MAY BE CHANGED FOR A        ROPP      143
C.                                GIVEN TIME PERIOD. OUTPUT APPEARS     ROPP      144
C.                                AS ONE SINGLE RUN.   DEF=1            ROPP      145
C.            IOUTP(40)       I   LIST OF DESIRED OUTPUTS (DEF. BLOCK   ROPP      146
C.                                DATA)                                 ROPP      147
C.            DEGRES          F   IF TRACKS REPEAT WITHIN 'DEGRES'      ROPP      148
C.                                (DEF=1 DEGREE) , INCLUDE RESONANCE    ROPP      149
C.                                TERMS.                                ROPP      150
C.            VLMPQ           F   IF RESONANCE EXISTS, INCLUDE L,M,P,Q  ROPP      151
C.                                SUBSCRIPTS FOR GEOPOTENTIALS GREATER  ROPP      152
C.                                THAN VLMPQ (DEF=.0001)                ROPP      153
C.            LATMNP          F   LATITUDE OF MAGNETIC NORTH POLE       ROPP      154
C.                                DEF=78.5                              ROPP      155
C.            LONMNP          F   EAST LONG. OF MAGNETIC NORTH POLE     ROPP      156
C.                                DEF=291.                              ROPP      157
C.     &N     -$END:  END OF NAMELIST VARIABLES                         ROPP      158
C.                                                                      ROPP      159
C.     5A     SECOND ADC OR SCF ELEMENT SET (DRAG ESTIMATION OPTION)    ROPP      160
C.     5B     SHOULD BE AT LEAST 7 DAYS AFTER 1ST ELEMENT SET           ROPP      161
C.            TO INCLUDE TWO SETS, CDAM AND CD MUST EQUAL 0.0 IN NMLST  ROPP      162
C.                                                                      ROPP      163
C.     6      'START'   BEGINS ROPP EXECUTION TO TIME TSTOP             ROPP      164
C.                                                                      ROPP      165
C.     REPEAT CARDS 1-6 FOR EACH CASE                                   ROPP      166
C.                                                                      ROPP      167
C.     7      'STOP'   VERY LAST CARD                                   ROPP      168
C.                                                                      ROPP      169
C.     SPECIAL NOTE: TO OBTAIN BACKSPACE IN AN OVERLAY ROUTINE,         ROPP      170
C.     LDSET(USEP=$BACKSP=$)  CONTROL CARD IS REQUIRED.                 ROPP      171
C.                                                                      ROPP      172
```

Figure 6c. Program ROPP Input Format

1.5 Eclipse Calculations: Program ECLLUM

Synchronous orbit satellites have exhibited a tendency to acquire, at times, high levels of electric charge. The associated elevated voltage levels can cause breakdown with resulting adverse effects. Insulating materials, for example, can undergo irreversible damage. In addition, the impulsive flow of current accompanying breakdown can induce excessive electrical transients in on board electronics, resulting in temporary or permanent malfunctions.

Charge build-up occurs as a result of interaction of the satellite with its plasma and solar radiation environments. The solar radiation level undergoes extreme variations as the satellite proceeds into and emerges from conditions of eclipsing by the earth. To analyze the role of varying illumination intensity in the charging process, one needs to be able to calculate illumination on the satellite as a function of time. This, in turn, requires precise evaluation, as a function of time, of the relative geometry of the sun, the earth, and the satellite. An accuracy of 0.1 sec of time is the objective in these calculations.

Two approaches to these calculations are available in terms of existing software. The first is the routine ECLIPS which is used in conjunction with ROPP and is documented in Reference 4. The second is a routine, ZWEI/INTEG, prepared by the researcher and documented in Reference 5. Neither is inherently adapted to the requirement for 0.1 sec precision. In addition, these programs perform distinctly different functions.

ECLIPS solves a transcendental equation to obtain two numbers: the times at which the satellite enters and exits the earth's shadow. ZWEI/INTEG computes, at successive instants of time, the percentage obscuration of the sun as it sets and rises behind the earth limb. Since it is the UV component of the solar radiation that impacts the charging/discharging process, ZWEI/INTEG takes account of the substantial UV absorption in the earth's atmosphere. ECLIPS, on the other hand, ignores the atmosphere and calculates on the basis of shielding by the earth's surface. The objective of the present task is to identify sources of inaccuracy and develop improved calculation for eclipse phenomena.

1.5.1 Factors Affecting Accuracy

ZWEI/INTEG performs essentially two functions. First are the solar and satellite ephemeris calculations that establish the geometry. Second are the absorption/shadowing calculations involving an integration over the unobstructed portion of the solar disk using an atmospheric absorption model. Included in this calculation is the effect of variation of atmospheric absorption with altitude. The objective of the work reported here is to upgrade the first calculation while leaving the second intact. Program ECLLUM performs this function.

Factors which affect the accuracy of eclipse calculations include:

1. Precision of calculations of satellite coordinates;
2. Oblateness of the earth;
3. Solar ephemeris accuracy;
4. Time for which solar coordinates are evaluated;

5. Assumption that the satellite-sun line is parallel to the satellite-earth line.

Satellite orbit calculations must be performed to provide the changing location of the satellite as it flies into and out of the shadow region. ECLLUM employs a simple Keplerian orbit over the several minute time spans of interest during which the sun rises and sets, as observed in the UV regime, at the satellite. Orbital elements for these calculations are obtained by using ROPP to evaluate the elements applicable at eclipse-in and -out times provided by the subroutine ECLIPS. To insure accuracy, mean elements are not used; rather, the osculating (or instantaneous) elements provided by ROPP and evaluated at the estimated eclipse times are employed. A discussion of some of the sources of error and the error magnitudes inherent in using ROPP predictions has been presented above in Section 1.2.

Ignoring oblateness of the earth and treating it as a sphere of radius equal to the earth's actual equatorial radius can introduce up to approximately 20 km error in the location in space of the region of the earth's surface responsible for eclipsing. In a worst case situation this could lead to a six or seven second time error. To avoid this type of potential error, ECLLUM takes specific account of the earth's oblateness.

A major factor affecting the precision of the solar coordinates is the sophistication of the algorithm employed. As discussed in Section 2.3

three routines have been evaluated. To meet the requirement for timing precision, the routine SOLEPH has been selected for use in ECLLUM. It is expected to contribute errors no greater than 0.03 seconds of time.

Obviously, even the best algorithm will provide inaccurate solar coordinates if it is not evaluated at the proper instant of time. To insure accuracy of the solar coordinates, ROPP/ECLIPS is run to yield approximate eclipse-in and eclipse-out times. Solar coordinates are then evaluated at these two times. This is actually the second step of an iterative approach, since ECLIPS itself must evaluate solar coordinates; without a priori knowledge of eclipse times, however, ECLIPS calculates these coordinates using only very approximate times inputted to a very approximate algorithm.

To simplify calculation, the assumption is sometimes made that all rays from the sun to the satellite and to points on the earth originate from a point-source at infinity (i.e., all rays are parallel). However, this can introduce a timing error of up to 0.5 sec. In a calculation intended to provide 0.1 sec precision, this luxury cannot be afforded, and a more exact calculation is required. The approach employed in ECLLUM, including evaluation of the effect of oblateness, is presented in the following section.

1.5.2 Analysis

The routine INTEG, which embodies the physical model used to evaluate solar obscuration, requires as input the distance of closest approach,

X_m, between the surface of the earth and the line between the satellite and the center of the sun. In addition, ψ, the angle between this same line and the earth-satellite line, is also required. Figure 7 illustrates the geometry. ψ can be found from

$$\cos \psi = \frac{\bar{r} \cdot \bar{R}}{|\bar{r}|\,|\bar{R}|} = \frac{\bar{r} \cdot (\bar{R}_\odot - \bar{r})}{|\bar{R}_\odot - \bar{r}|\,|\bar{r}|}$$

where $\bar{R}_\odot$ and $\bar{r}$ can be obtained from solar and satellite ephemerides, respectively. It is convenient to express $\bar{r}$ in the $\bar{P}$, $\bar{Q}$, $\bar{W}$ coordinate system. (See Ref. 4, p. 24, and Ref. 6.)

$$\bar{r} = x_\omega \bar{P} + y_\omega \bar{Q}$$

where

$$x_\omega = r \cos v$$

$$y_\omega = r \sin v$$

$$r = \frac{p}{1 + e \cos v}$$

$$p = a(1-e)(1+e)$$

and e, a, and v are the eccentricity, semi-major axis, and true anomaly of the satellite's orbit, respectively.

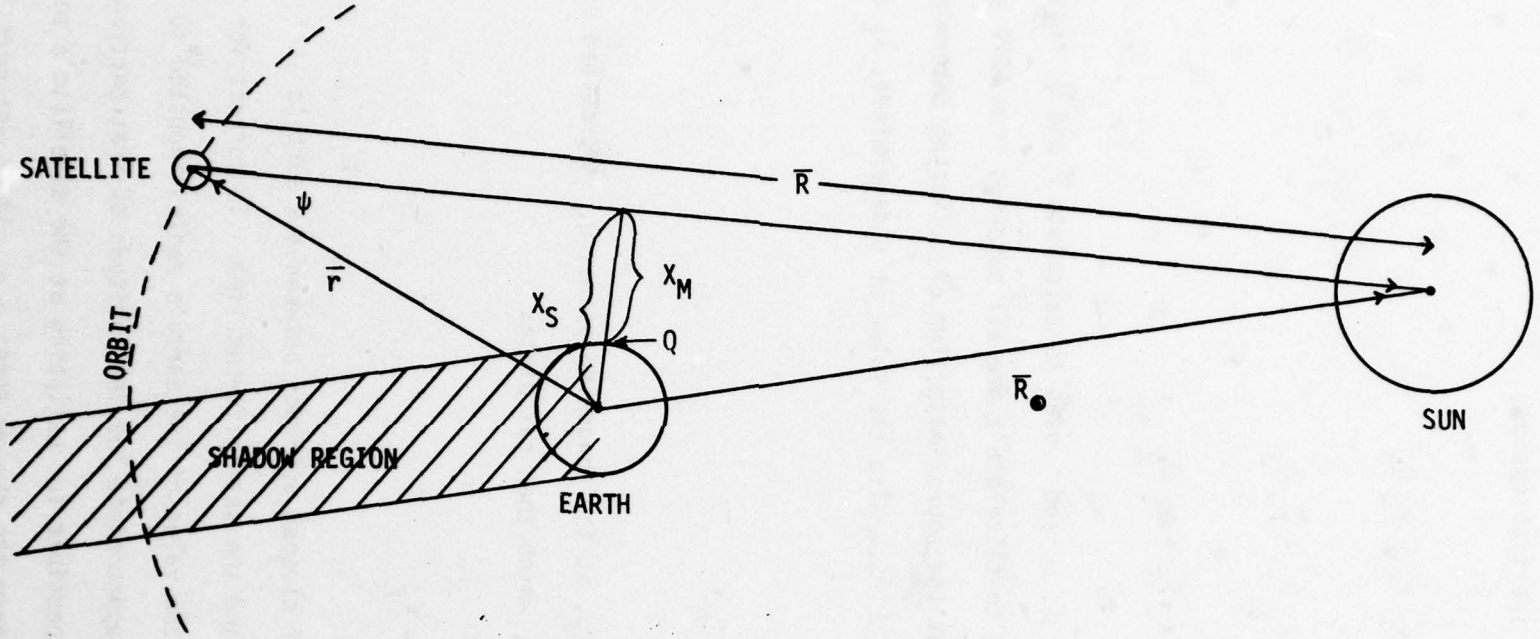

Figure 7. Geometry of Satellite Eclipsing

In the earth-centered inertial system,

$$R_x = R_{\odot x} - x_\omega P_x - y_\omega Q_x$$

$$R_y = R_{\odot y} - x_\omega P_y - y_\omega Q_y$$

$$R_z = R_{\odot z} - x_\omega P_z - y_\omega Q_z$$

The orbital elements Ω, ω, and i used to calculate $\overline{P}$ and $\overline{Q}$, together with a, e, and v used to calculate r, are all obtained from ROPP as the osculating elements at the approximate time of eclipsing determined by the ROPP subroutine ECLIPS. With the value of ψ determined, X_S can be found from

$$X_S = r\,|\sin\psi|$$

The earth's radius, R_E, at the shadowing point, Q, is provided as input to the routine INTEG, which then calculates

$$X_M = X_S - R_E$$

X_M is the distance of closest approach between the earth's surface (assumed spherical) and the satellite-sun line. To correct for the earth's oblateness, the value of the earth's radius inputted to INTEG should be the value appropriate for the latitude of that portion of the earth's limb responsible for eclipsing at the satellite's point of entrance to or exit from the shadow zone; i.e., it is not sufficient

simply to use the earth's equatorial radius.

Fig. 8a illustrates the geometry of the oblate earth. It is assumed that the earth can be represented as an oblate spheroid with its semi-major axis given by the earth's equatorial radius, A_E. All meridian cross sections are ellipses of semi-major axis, A_E and eccentricity e_E. All cross sections in planes parallel to the equator are circles.

Point Q in Fig. 8a is assumed to be the shadowing point on the earth's surface. The eclipsing calculations require the earth's radius at that point. The approach to be used is:

a) Evaluate a_z, the z-component of point Q. (i.e., its perpendicular distance from the equatorial plane.)

b) a_z defines the geocentric latitude, ϕ, of Q.

c) Knowledge of ϕ then permits calculation of the radial distance from the earth's center to Q.

To evaluate a_z, observe from Fig. 8b that

$$\overline{r} = \overline{a} + \overline{d}$$

where $|\overline{a}| = R_E$

and $\overline{d}$ is that generator of the cylinder bounding the nominal (visible) shadow region which passes through the satellite's point of entrance into the shadow region.

Therefore

$$a_z = r_z - d_z$$

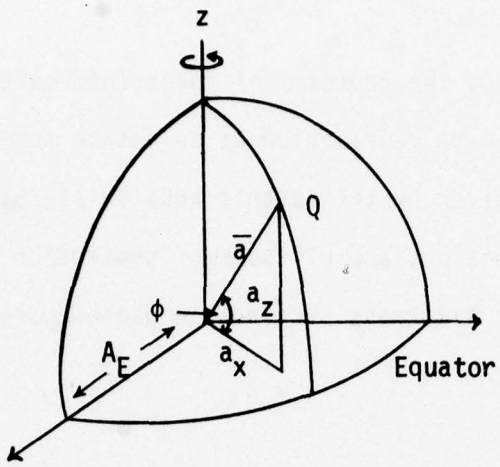

a) Oblate Spheroidal Earth

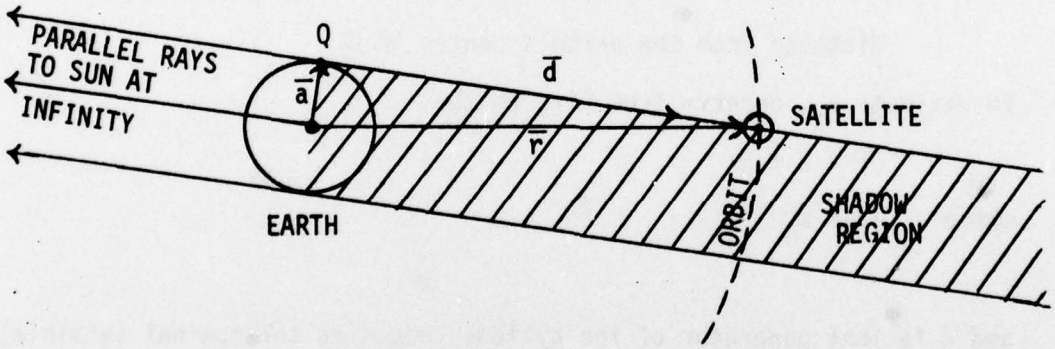

b) Simplified Eclipsing Geometry For Oblateness Calculations

Figure 8. Oblateness Geometry

Assuming a point source sun at infinite distance (an assumption that is valid for earth flattening calculations, but not elsewhere in this analysis) it is clear that the vector $\bar{d}$ is in the reverse solar direction. Therefore

$$a_z = r_z + \frac{Z_\odot}{R_\odot} |\bar{d}|$$

But $$\cos \psi = \frac{d}{r}$$

Therefore $$a_z = r_z + \frac{Z_\odot}{R_\odot} r \cos \psi$$

But from Keplerian orbit analysis,

$$r = \frac{p}{1 + e \cos v} ,$$

and therefore,

$$a_z = p \frac{(P_z \cos v + Q_z \sin v + \frac{Z_\odot}{R_\odot} \cos \psi)}{1 + e \cos v}$$

From the properties of ellipses,

$$a_z = A_E \frac{\sqrt{1 - e_E^2} \sin \phi}{\sqrt{1 - e_E^2 \cos^2 \phi}}$$

When this is solved for $\cos^2\phi$,

$$\cos^2\phi = \frac{A_E^2 [1 - e_E^2] - a_z^2}{A_E^2 [1 - e_E^2] - a_z^2 e_E^2}$$

To obtain R_E, the radius at point Q, this value of $\cos^2\phi$ is substituted into

$$R_E = \sqrt{a_x^2 + a_z^2} = \frac{A_E \sqrt{1 - e_E^2}}{\sqrt{1 - e_E^2 \cos^2\phi}}$$

At that point, all required inputs for INTEG are available:

X_s, ψ, and the value of R_F at point Q.

A grid of equi-spaced time instants is established which spans the entire eclipsing process (i.e., extending from zero to total obscuration). At each instant, the satellite's location is evaluated, using simple Keplerian orbital dynamics based on osculating elements evaluated by ROPP for the nominal times of shadow region entrance and exit. As values for X_s, ψ, and R_E are calculated, they are provided as input to subroutine INTEG, which evaluates the corresponding illumination. The result is a plot, versus time, of variation of solar UV radiation intensity incident upon the satellite during periods of penetration into and emergence from the earth's shadow.

References

1. Minka, K., J. Fein and B. Clemenz, "Orbit Determination and Ephemeris Computation", AFCRL-66-259, May 1966.

2. "Analysis and Programming for Research in Physics of the Upper Atmosphere", Logicon, Inc., AFGL-TR-76-0231, September 1976.

3. "User's Manual for the TRW Rapid Orbit Determination Program", TRW, Inc. 09967-6002-R0-00, October 1968.

4. "Analysis and Research for Integrated Systems in Physics of the Upper Atmosphere", Logicon, Inc. AFGL-TR-77-0265, November 1977.

5. Garrett, H. B., "Effects of a Time-Varying Photoelectron Flux on Spacecraft Potential", Technical Report to be published.

6. Escobal, P. R., "Methods of Orbit Determination", Wiley, New York, New York, (1965).

2. Ionospheric Research Support

2. Ionospheric Research Support

Programs to describe environmental conditions that are significant to ionospheric phenomena have been developed at AFGL and other agencies. Further work to acquire and extend capabilities for describing proton-electron, geomagnetic, and astronomical parameters is reported in this section.

2.1 Proton-Electron User System

Initiator: H. B. Garrett

Project No: 7661 Problem No: 4913

User system PROTEL consists of a series of data models describing the inner and outer radiation zone electron and proton environments and a collection of three interlocking main subroutines and various supporting subroutines which perform the following functions:

1. Subroutine ORB generates orbit tapes and calculates B-L values suitable for input to subroutine ORP using the Brouwer orbit generator suited to orbits with eccentricities > 0.1.
2. Subroutine ORP calculates the average geomagnetically trapped radiation accumulated by an orbiting vehicle.
3. Subroutine MODEL allows the user to access any of the current trapped radiation models available from the National Space Science Data Center.
4. Subroutine PREMOD selects the appropriate proton or inner and outer zone electron models from the packed binary CDC EDITLIB file PREMOD for use in subroutines ORP and MODEL.
5. Program PACKBIN prepares the eight data models for cataloguing in the EDITLIB file PREMOD from the unpacked BCD display format used for storage in the CDC UPDATE program library file PROTEL. Data models are packed and written in binary form on TAPE8.

Models now available for use at AFGL include inner zone electron model

AE5 (AE5MIN), solar minimum, at epoch October, 1967; inner zone electron model AE6 (AE6MAX), solar maximum, epoch 1980; outer zone electron models AE4, solar minimum (AE4MIN) at epoch 1964; and solar maximum (AE4MAX) at epoch 1967; interim outer zone models AEI-7, at epoch 1980 (AEI7HI and AEI7LO); and 2 AP8 proton models at solar minimum epoch 1964 (AP8MIN), and solar maximum epoch 1970 (AP8MAX). The two AEI-7 models differ in that AEI7HI favors Vampola's fits to the OUI-19 data and AEI7LO is more representative of all of the data sets available to NSSDC as of November, 1972.[1]

2.1.1 Functional Description

The complete set of all PROTEL subroutines and unpacked data models are accessible in CDC UPDATE format. CDC EDITLIB subroutine library PRELIB contains the ORB, ORP, MODEL, PREMOD and PACKBIN subroutines. The NSSDC programs ORB, ORP and MODEL were converted for use on the CDC 6600 NOS/BE system through the conversion of IBM 360 double precision variables to single precision 60-bit CDC word storage convention and required character conversions. Duplication of subroutines used by more than one of the original programs was eliminated by the EDITLIB file construction. Unnecessary input parameters were removed and other program inefficiencies were corrected in order to minimize core requirements and program execution time. Data models were packed in binary format with three data words per 60 bit CDC word, and statement function MAP was designed to unpack the appropriate word and select the relevant bits as needed during execution. In this way, run-time model storage space was reduced by one-third. NSSDC models were provided in one of two forms: as Fortran IV BLOCKDATA packages or as BCD formatted files of nine words per record. Consistency was obtained through the

elimination of BLOCKDATA format and the use of a call to subroutine PREMOD to load the requested proton model or electron models into the designated storage area. Either one proton model or an inner and outer electron model pair may be called by PREMOD.

2.1.2 Usage of the PROTEL System

Figure 1 (a & b) summarizes the rules for usage of the Proton-Electron User System. Subroutine call parameters consist of two types: those which declare input to the subroutine (subject to definition by the user); and those which control the nature and extent of the subroutine's output.

There exist certain increment and range restrictions for the inner energy (E) and logarithmic equatorial magnetic flux (L) values allowed by subroutines ORP and MODEL. The incremental restrictions are as follows:

Protons:

for $E < 1$ MeV, $\Delta E \geq 250$ keV

for $1 \leq E/(\text{MeV}) \leq 20$, $\Delta E \geq$ MeV

for $20 < E/(\text{MeV}) \leq 50$, $\Delta E \geq 5$ MeV

for $E > 50$ MeV, $\Delta E \geq 10$ MeV

Inner Zone Electrons:

for $E < 100$ keV, $\Delta E \geq 50$ keV

for $100 \leq E/(\text{keV}) \leq 250$, $\Delta E > 100$ keV

for $E > 250$ keV, $\Delta E > 200$ keV

Outer Zone Electrons:

same as inner zone electrons, except

$E > 4$ MeV, $\Delta E \geq 100$ keV

PROTON-ELECTRON USER SYSTEM

USER CONTROL CARDS:

```
ATTACH,PRELIB,ID=LOGICON.
ATTACH,TAPE8,PREMOD,ID=LOGICON.
LIBRARY,PRELIB.
```

NOTE: (1) TAPE10 CONTAINS ORBIT AND B&L PARAMETERS, AND MAY BE CATALOGUED IF ORP IS RUN LATER. THIS BINARY FILE IS GENERATED BY ORB FOR USE BY ORP. NOT REQUIRED BY MODEL.

(2) TAPE8 CONTAINS ALL PROTON AND ELECTRON MODELS INCLUDING AP8MAX,AEI7HI,AEI7LO,AE5MIN,AE6MAX,&AP3MIN. THIS FILE IS REQUIRED ONLY BY ORP OR MODEL.

(3) PRINTED OUTPUT IS ON TAPE6.

FIELD LENGTHS REQUIRED TO EXECUTE:

ORB - 46K8
ORP - 46K8 (INCLUDES PREMOD)
MODEL - 46K8 (INCLUDES PREMOD)
ORB,PREMOD,ORP,MODEL RUN TOGETHER - 116K8


```
CALL ORB(SECSPN,DSEC,XN,XE,XI,XM,XP,XR,IPR,LIMBL)
```

SECSPN	ORBIT GENERATION SPAN IN SECS. (NSSDC RECOMMENDS 20+ ORBITS FOR GOOD B-L SPACE COVERAGE)
DSEC	TIME INTERVAL BETWEEN POINTS OF GENERATED ORBIT (IF DSEC=0.,DEFAULT DSEC=20.+.0331*ALT(KM))
XN	MEAN MOTION(REVS/DAY) OR PERIGEE ALTITUDE(KM)
XE	ECCENTRICITY (>0.0)
XI	INCLINATION (DEG) (>0.0)
XM	MEAN ANOMALY (DEG)
XP	ARGUMENT OF PERIGEE (DEG)
XR	RIGHT ASCENSION (DEG)
IPR	=0 SUPPRESSES PRINT-OUT; =1 PRINT-OUT REQUESTED
LIMBL	=0 LIMITS B-L VALUES ON TAPE10; =1 NO LIMITATION ON VALUES

Figure 1a. Proton-Electron User System

```
CALL PREMOD(6HINRMOD,6HOUT10D)     OR    CALL PREMOD(6HONEMOD,1H )
   WHERE  INRMOD  OPTIONS ARE    AE5MIN,AE6MAX
          OUTMOD  OPTIONS ARE    AE17HI,AE17LO
          ONEMOD  OPTIONS ARE    AP8MIN,AP8MAX
       LOADS SPECIFIED MODELS FROM TAPE8.


CALL ORB (TABLOG,NE,ET,ISKIP,E,IORB)
   LOGICAL TABLOG(5) - EACH .TRUE. OR .FALSE.
         1  INTERMEDIATE PRINTOUT TABLE
         2  L-BAND SUMMARY TABLE
         3  INTEGRATED FLUX TABLE
         4  INTENSITY SUMMARY TABLE
         5  PEAK FLUX TABLE

   DIMENSION E(NE),IORB(2)
         NE     NUMBER OF ENERGY VALUES 'E' (<31)
         ET     THRESHOLD ENERGY FOR TABLES 1 & 5
         ISKIP  READ 1 POINT IN ISKIP FROM TAPE10
         E      ENERGY THRESHOLD ARRAY-MEV (ASCENDING ORDER)
         IORB   INDEX NUMBERS FOR FIRST & LAST ORBITS


CALL MODEL (NE,NL,IDIFF,IDEF,E,XL,B01,B02,NDELB)

   DIMENSION E(NE),XL(NL),B01(NL),B02(NL),NDELB(NL)

         NE     NUMBER OF ENERGY VALUES 'E' (<10)
         NL     NUMBER OF L VALUES (<101)
         IDIFF  0= INTEGRAL FLUX OUTPUT;1=AVG. DIFFERENTIAL FLUX OUTPUT
                2= BOTH OUTPUTS
         E      ENERGY THRESHOLD ARRAY - MEV (ASCENDING ORDER)
         XL     L VALUE ARRAY
         IDEF   0= DEFAULT 25 TO 30 LINEAR B/B0 INCREMENTS TO CUTOFF
                1= INPUT B01,B02,NDELB VALUES
      NOTE: FOR IDEF=1, ONE SET BELOW PER L VALUE-
            B01 LOWER LIMIT OF B/B0
            B02  UPPER LIMIT OF B/B0
            NDELB  NUMBER OF B/B0 INTERVALS (DEF=20)
```

Figure 1b. Proton-Electron User System

Restrictions on the range of values include the following:

for AE5MIN, $L \geq 1.2\ R_e$

for inner zone electron models, $E \leq 4.5$ MeV

Although usage of inner and outer electron models in simultaneous runs are the most physically accurate, they are not required by the PROTEL software system. In any case, simultaneous usage of inner and outer zone electron models requires that inner zone electron parameter restrictions must be followed. Failure to restrict parameters to the above specifications results in abnormal program termination. In subroutine ORB, two range restrictions exists. Variables XI and XE may not equal zero, and in the case of zero-inclination or zero-eccentricity orbits, values in the range of $10^{-9} \leq XI, XE \leq 10^{-7}$ should be entered.

Subroutine ORB allows the user the choice of a point-by-point tabular printout of the generated orbit parameters (Fig. 2) and an abbreviated printout in which the first and last few points only are displayed.

Subroutine ORP has the capability to generate the follwing tabular output:

Intermediate Printout (Fig. 3) - a point by point table of the omnidirectional integral flux at each point of the orbit for a given threshold energy.

L-Band Summary (Fig. 4) - a summary of the omnidirectional particle flux (particles/cm^2-day) accumulated in arbitrary energy and L bands.

```
BINARY TAPE10 REQUESTED.

ORBIT SPAN(SEC)  864000.0    PERIGEE ALT(KM) =   434.00    ORB RUN DATE 09/21/78

BROUWER ORBIT GENERATOR.

AXIS(ER) =   .41616144E+01
ECCENTRICITY =   .74400000E+00
INCLINATION(DEG) =   .62900000E+02
MEAN(DEG) =  0.
PERIGEE(DEG) =   .27000000E+03
NODE(DEG) =  0.

TIME INCREMENT =    0.00 SECS       ORBIT TIME =  240.00 HRS

DSEC =    20.000 + ALT *   .0331
```

LONGITUDE (DEGS)	LATITUDE (DEGS)	ALTITUDE (KM)	B (GAUSS)	L	TIME (HR)
.25999813D+03	-.62896972D+02	.42058639D+03	.38904713D+00	.24799537D+01	0.
.27617568D+03	-.62754167D+02	.42428056D+03	.37501840D+00	.24065003D+01	.94226138D-02
.28224217D+03	-.62332042D+02	.43539870+03	.35923810D+00	.23321132D+01	.18879193D-01
.28611331D+03	-.61637026D+02	.45412787D+03	.34217145D+00	.22595009D+01	.28437998D-01

-100.

```
NUMBER OF ORBIT POINTS =  1985

AVERAGE ALTITUDE(KMS) =   .13244728D+05
```

Figure 2. Printout for ORB

POINT BY POINT (INTERMEDIATE) PRINTOUT PAGE 1

ORBIT TIME INTERVAL 253200.00000 PERIGEE ALT(KM) 400.00000 INCLINATION= 84.00 ORB RUN DATE 05/11/78

INNER ZONE MODEL= AE6MAX OUTER ZONE MODEL= AE7HI THRESHOLD ENERGIES (MEV)

LONGITUDE	LATITUDE	ALTITUDE	B	L	TIME (HRS)	INCREMENT (SEC)	.050	.250	.500
.12	2.40	4.06E+02	.25206	1.083	.009	33.4	0.	0.	0.
.24	4.91	4.11E+02	.25369	1.073	.019	33.4	0.	0.	0.
.37	7.42	4.19E+02	.25629	1.068	.028	33.5	0.	0.	0.
.50	9.95	4.31E+02	.25909	1.068	.037	33.9	0.	0.	0.
.63	12.50	4.47E+02	.26260	1.074	.047	34.3	0.	0.	0.
.78	15.17	4.67E+02	.26673	1.087	.057	34.8	0.	0.	0.
.93	17.58	4.90E+02	.27136	1.107	.066	35.4	0.	0.	0.
1.09	20.32	5.19E+02	.27635	1.136	.076	36.2	0.	0.	0.
1.26	23.00	5.50E+02	.28148	1.175	.087	37.1	0.	0.	0.
1.44	25.73	5.87E+02	.28652	1.226	.097	38.2	0.	0.	0.
1.65	28.52	6.30E+02	.29122	1.291	.108	39.4	0.	0.	0.
1.88	31.37	6.79E+02	.29533	1.375	.120	40.9	0.	0.	0.
2.14	34.28	7.32E+02	.29863	1.480	.131	42.4	0.	0.	0.
2.43	37.27	7.93E+02	.30093	1.612	.144	44.2	0.	0.	0.
2.77	40.34	8.62E+02	.30203	1.777	.157	46.3	0.	0.	0.
3.17	43.49	9.38E+02	.30200	1.987	.170	48.5	0.	0.	0.
3.65	46.72	1.02E+03	.30060	2.255	.184	51.1	0.	0.	0.
4.22	50.06	1.12E+03	.29787	2.602	.199	53.9	4.79E+01	7.00E+02	1.42E+02
4.93	53.48	1.23E+03	.29381	3.061	.215	57.1	4.17E+05	1.11E+05	4.26E+04
5.84	57.00	1.34E+03	.28846	3.691	.232	60.5	2.10E+06	6.41E+05	2.45E+05
7.01	60.62	1.47E+03	.28183	4.539	.250	64.5	1.77E+06	7.00E+05	3.75E+05
8.59	64.32	1.62E+03	.27393	5.752	.269	68.8	8.56F+05	3.38E+05	1.56E+05
10.82	68.10	1.78E+03	.26475	7.553	.289	73.5	3.55E+05	6.97E+04	1.25E+04
14.13	71.93	1.95E+03	.25423	10.215	.311	78.3	1.25E+05	2.19E+02	2.15E+00
19.46	75.76	2.15E+03	.24252	14.073	.335	84.7	0.	0.	0.
28.98	79.65	2.36E+03	.22948	18.946	.360	91.1	0.	0.	0.
48.19	82.60	2.59E+03	.21525	22.909	.387	98.1	0.	0.	0.
84.66	84.00	2.84E+03	.20000	22.810	.417	105.7	0.	0.	0.
120.36	82.43	3.11E+03	.18401	18.824	.448	113.9	0.	0.	0.
139.96	79.01	3.39E+03	.16769	14.109	.482	122.9	0.	0.	0.
149.27	74.30	3.70E+03	.15117	10.414	.519	132.3	1.95E+05	1.37E+02	0.
154.35	70.49	4.02E+03	.13511	7.864	.559	142.5	6.43E+05	6.29E+04	1.16E+04
157.36	65.32	4.36E+03	.11976	6.149	.601	153.2	1.66F+06	6.55E+05	2.68E+05
159.23	61.27	4.71E+03	.10541	4.983	.647	164.4	4.19E+06	1.55E+06	7.99E+05
160.39	55.56	5.07E+03	.09225	4.172	.696	175.9	5.70E+06	2.81E+06	1.32E+06
161.09	51.17	5.43E+03	.08039	3.596	.748	187.9	8.49E+06	2.41E+06	9.12E+05
161.53	47.06	5.79E+03	.06989	3.173	.803	199.9	5.20E+06	1.66E+06	6.82E+05
161.57	42.29	6.15E+03	.06073	2.873	.862	211.7	3.60E+06	5.37E+05	2.03E+05
161.49	37.52	6.49E+03	.05286	2.646	.924	223.4	1.02E+07	1.45E+06	3.29E+05
161.27	32.76	6.81E+03	.04623	2.479	.990	234.7	4.76E+07	5.19E+06	7.18E+05
160.92	28.00	7.10E+03	.04077	2.359	1.058	245.4	1.13E+08	1.26E+07	1.34E+06
160.47	23.26	7.37E+03	.03642	2.275	1.129	255.1	1.66E+08	2.23E+07	2.18E+06
159.94	18.52	7.59E+03	.03315	2.221	1.202	263.9	2.22E+08	3.46E+07	3.18E+06
159.35	13.78	7.77E+03	.03091	2.195	1.277	271.2	2.62E+08	4.46E+07	4.05E+06
158.72	9.05	7.90E+03	.02969	2.192	1.354	277.2	2.77E+08	4.85E+07	4.44E+06
158.05	4.31	7.99E+03	.02944	2.212	1.432	281.5	2.64E+08	4.49E+07	4.15E+06
157.36	-.44	8.00E+03	.03014	2.257	1.511	284.1	2.27E+08	3.53E+07	3.44E+06
156.68	-5.21	7.97E+03	.03175	2.329	1.590	284.9	1.73E+08	2.30E+07	2.44E+06
156.01	-9.99	7.88E+03	.03423	2.434	1.669	283.9	1.02E+08	1.22E+07	1.53E+06
155.37	-14.71	7.74E+03	.03758	2.576	1.747	280.9	3.16F+07	4.39E+06	8.24E+05
154.78	-19.65	7.55E+03	.04192	2.768	1.824	275.2	5.72E+06	1.15E+06	3.54E+05
154.25	-24.54	7.31E+03	.04699	3.026	1.899	268.9	5.47E+06	1.62E+06	6.02E+05

Figure 3. Printout of Integral Flux at Points Along Orbit (ORP)

L BAND SUMMARY PAGE 1

AVERAGE INTEGRAL FLUX WITHIN ENERGY BANDS

(PARTICLES / CM2 - DAY)

ORBIT TIME INTERVAL 259200.00000 PERIGEE ALT(KM) 400.0000) INCLINATION= 84.00 ORB RUN DATE 05/11/79

MODELS USED= AE5MAX ,AE17HI

TOTAL TIME = 3.00 DAYS. TIME INTERVAL = 1.05 MIN.

ENERGY RANGES (MEV)	L VALUES 1.00 TO 1.22	1.22 TO 1.27	1.27 TO 1.32	1.32 TO 1.37	1.37 TO 1.45	1.45 TO 1.55	1.55 TO 1.65	1.65 TO 1.75	1.75 TO 1.85	1.85 TO 1.95	1.95 TO 2.05	2.05 TO 2.15
.05- .25	3.33E+05	1.50E+07	1.02E+08	9.88E+07	5.62E+08	9.25E+08	9.85E+08	7.04E+08	7.10E+08	3.70E+08	6.55E+08	4.18E+08
.25- .50	2.52E+06	7.88E+06	3.83E+07	3.31E+07	1.58E+08	1.98E+08	1.47E+08	1.01E+08	9.77E+07	3.74E+07	5.71E+07	2.48E+07
.50- .75	1.62E+05	3.97E+05	2.17E+06	2.07E+06	1.00E+07	1.25E+07	1.06E+07	7.73E+06	7.25E+06	3.34E+06	4.85E+06	1.86E+06
.75- 1.00	3.20E+04	5.91E+04	3.91E+05	4.39E+05	2.90E+05	3.34E+06	1.77E+06	9.07E+05	6.49E+05	2.45E+05	3.23E+05	1.11E+05
1.00- 1.25	9.02E+03	1.61E+04	1.18E+05	1.42E+05	1.04E+05	1.08E+06	4.59E+05	1.77E+05	9.33E+04	2.53E+04	3.25E+04	1.21E+04
1.25- 1.50	5.13E+03	8.32E+03	6.58E+04	8.20E+04	6.37E+05	6.91E+05	2.81E+05	1.04E+05	5.19E+04	1.30E+04	1.41E+04	4.76E+03
1.50- 1.75	1.97E+03	2.98E+03	2.84E+04	3.72E+04	3.36E+05	3.94E+05	1.55E+05	5.12E+04	3.21E+04	6.77E+03	5.57E+03	1.61E+03
1.75- 2.00	1.42E+03	1.98E+03	1.88E+04	2.48E+04	2.23E+05	2.67E+05	1.01E+05	3.59E+04	1.63E+04	3.17E+03	2.69E+03	7.71E+02
2.00- 2.25	1.30E+03	1.94E+03	1.23E+04	1.57E+04	1.38E+05	1.76E+05	5.82E+04	2.08E+04	7.46E+03	1.34E+03	1.25E+03	3.99E+02
2.25- 2.50	8.51E+02	9.33E+02	8.18E+03	1.07E+04	9.49E+04	1.20E+05	4.35E+04	1.25E+04	4.19E+03	6.37E+02	6.33E+02	1.84E+02
2.50- 2.75	6.43E+02	6.15E+02	7.73E+03	1.18E+04	1.23E+05	1.63E+05	4.88E+04	1.18E+04	3.26E+03	4.52E+02	3.84E+02	8.30E+01
2.75- 3.00	4.22E+02	3.50E+02	4.05E+03	5.76E+03	5.09E+04	6.13E+04	1.79E+04	4.38E+03	1.32E+03	1.30E+02	1.73E+02	0.
3.00- 3.25	2.82E+02	2.11E+02	2.95E+03	3.77E+03	2.52E+04	2.63E+04	5.88E+03	1.51E+03	4.83E+02	6.53E+01	0.	0.
3.25- 3.50	1.97E+02	1.15E+02	1.01E+03	1.17E+03	7.53E+03	7.70E+03	2.28E+03	5.57E+02	2.00E+02	0.	0.	0.
3.50- 3.75	1.57E+02	6.24E+01	3.48E+02	3.63E+02	2.26E+03	2.26E+03	7.60E+02	2.20E+02	0.	0.	0.	0.
3.75- 4.00	0.	0.	1.63E+02	1.13E+02	7.01E+02	6.91E+02	2.91E+02	0.	0.	0.	0.	0.
4.00	0.	0.	2.36E+01	5.06E+01	2.74E+02	2.51E+02	9.01E+01	0.	0.	0.	0.	0.
TOTAL =	6.69E+05	2.34E+07	1.43E+08	1.35E+08	7.36E+08	1.14E+09	1.05E+09	9.15E+08	9.06E+08	4.11E+08	7.18E+08	4.44E+08
NP1 =	24	3	4	2	8	6	7	8	8	3	7	7
NP2 =	24	3	4	2	8	6	7	8	8	3	7	7
NSIZE =	361	45	37	32	46	46	39	31	25	25	22	23

NP1 = NUMBER OF ORBIT POINTS FOR WHICH NON ZERO FLUX WAS ENCOUNTERED ABOVE .05 MEV
NP2 = NUMBER OF ORBIT POINTS FOR WHICH NON ZERO FLUX WAS ENCOUNTERED ABOVE .05 MEV
NSIZE = NUMBER OF ORBIT POINTS LYING IN L BAND.

Figure 4. Printout of Distribution of Particle Flux Within Energy Bands and L-Shells (ORP)

Integrated Flux (Fig. 5) - a summary of the integrated flux accumulated in arbitrary energy bands.

Intensity Summary (Fig. 6) - a summary of the omnidirectional particle flux accumulated in arbitrary energy and intensity bands.

Peak Flux per Orbit (Fig. 7) - a table of peak omnidirectional integral flux encountered for each revolution for a given energy threshold.

Subroutine MODEL allows the user the choice of integral (Fig. 8) and differential (Fig. 9) flux tables as output. Subroutine PREMOD prints an informative message which confirms the model(s) loaded and describes any input errors which may have occurred.

Creation of packed binary file PREMOD, which holds the trapped radiation models, involves the use of program PACKBIN and the UPDATE program library PROTEL. The following NOS/BE control cards are required to execute this mode of the system:

```
ATTACH, OLDPL, PROTELPL., ID=LOSCAG.
REQUEST, TAPE8, *PF.
UPDATE, C=TAPE7.
UPDATE.
FTN, SL, R, I.
LGO,PL=77777.
CATALOG, TAPE8, PREMOD, ID=LOGICON.
7/8/9
*C AP8MAX.AE4MIN
7/8/9
*C PACKBIN
7/8/9
6/7/8/9
```

INTEGRATED FLUX TABLE

ORBIT TIME INTERVAL 259200.00000 PERIGEE ALT(KM) 400.0000) INCLINATION= 84.00 ORB RUN DATE 05/11/78

MODELS USED= AE5MAX ,AE17HI

TOTAL TIME = 3.00 DAYS. TIME INTERVAL = 1.06 MIN.

ENERGY RANGES (MEV) E1 - E2		AVERAGED FLUX ABOVE E1 (PER DAY)	AVERAGED INTEGRAL FLUX IN ENERGY BAND E1 - E2 (PER DAY)	PER CENT
.05-	.25	4.15E+12	3.50E+12	84.47
.25-	.50	6.44E+11	5.55E+11	13.50
.50-	.75	8.41E+10	6.49E+10	1.56
.75-	1.00	1.93E+10	9.41E+09	.23
1.00-	1.25	9.91E+09	2.86E+09	.07
1.25-	1.50	6.95E+09	1.86E+09	.05
1.50-	1.75	4.98E+09	1.35E+09	.03
1.75-	2.00	3.63E+09	9.50E+09	.02
2.00-	2.25	2.67E+09	6.00E+09	.01
2.25-	2.50	2.07E+09	4.55E+09	.01
2.50-	2.75	1.61E+09	3.55E+09	.01
2.75-	3.00	1.26E+09	2.75E+09	.01
3.00-	3.25	9.82E+08	1.99E+09	.00
3.25-	3.50	7.82E+08	1.37E+08	.00
3.50-	3.75	6.26E+08	1.24E+09	.00
3.75-	4.00	5.01E+08	9.14E+07	.00
4.00		4.03E+08		.01

Figure 5. Printout of Distribution of Integrated Flux Within Energy Bands (ORP)

INTENSITY SUMMARY

AVERAGE INTEGRAL FLUX WITHIN ENERGY BANDS

ORBIT TIME INTERVAL 259200.00000 PERIGEE ALT(KM) 400.0000 INCLINATION= 84.00 ORB RUN DATE 05/11/78

MODELS USED= AE6MAX ,AE17MI

TOTAL TIME = 3.00 DAYS. TIME INTERVAL = 1.05 MIN.

ENERGY RANGES	INTENSITY RANGES															
	1.E2 OR LESS		1.E2 TO 1.E3		1.E3 TO 1.E4		1.E4 TO 1.E5		1.E5 TO 1.E6		1.E6 TO 1.E7		1.E7 TO 1.E8		1.E8 + OVER	
.05 - .25	5.37E+03	1103	6.23E+04	9	8.79E+05	15	3.56E+07	33	4.64E+09	299	1.15E+11	422	3.87E+11	114	2.99E+12	193
.25 - .50	3.10E+04	1120	3.09E+05	33	8.96E+06	60	1.65E+08	126	8.44E+09	363	5.70E+10	283	4.94E+11	193	0.	0
.50 - .75	3.99E+04	1158	7.55E+05	54	1.17E+07	103	3.70E+08	229	1.02E+10	424	5.42E+10	213	0.	0	0.	0
.75 - 1.00	5.52E+04	1193	1.05E+05	83	9.17E+06	87	6.77E+08	292	8.73E+09	523	0.	0	0.	0	0.	0
1.00 - 1.25	1.02E+05	1261	6.95E+05	59	4.17E+07	133	1.12E+09	554	1.80E+09	156	0.	0	0.	0	0.	0
1.25 - 1.50	8.83E+04	1285	7.50E+05	58	1.35E+08	391	8.08E+09	345	9.59E+08	99	0.	0	0.	0	0.	0
1.50 - 1.75	6.17E+04	1298	7.63E+05	64	1.05E+08	443	8.81E+09	326	3.64E+09	41	0.	0	0.	0	0.	0
1.75 - 2.00	5.61E+04	1311	6.87E+06	166	5.72E+07	373	8.71E+09	325	2.53E+07	3	0.	0	0.	0	0.	0
2.00 - 2.25	5.15E+04	1328	1.40E+07	367	4.31E+07	240	5.37E+09	243	0.	0	0.	0	0.	0	0.	0
2.25 - 2.50	1.65E+05	1361	8.39E+05	378	4.31E+07	235	4.02E+09	204	0.	0	0.	0	0.	0	0.	0
2.50 - 2.75	6.53E+05	1454	5.04E+05	315	5.24E+07	242	2.97E+09	157	0.	0	0.	0	0.	0	0.	0
2.75 - 3.00	1.03E+06	1657	1.71E+05	132	5.14E+07	246	2.21E+09	145	0.	0	0.	0	0.	0	0.	0
3.00 - 3.25	5.59E+05	1715	1.38E+06	102	5.10E+07	234	1.46E+09	127	0.	0	0.	0	0.	0	0.	0
3.25 - 3.50	3.24E+05	1739	1.47E+05	93	5.72E+07	243	9.79E+07	37	0.	0	0.	0	0.	0	0.	0
3.50 - 3.75	1.99E+05	1754	2.11E+05	101	7.21E+07	270	4.96E+07	53	0.	0	0.	0	0.	0	0.	0
3.75 - 4.00	1.41E+05	1761	2.46E+05	118	7.51E+07	275	2.07E+07	23	0.	0	0.	0	0.	0	0.	0
4.00	1.11E+05	1725	1.06E+05	73	4.37E+07	202	3.59E+08	178	0.	0	0.	0	0.	0	0.	0

INTENSITY RANGES HAVE UNITS OF PARTICLES PER SQCM SEC FOR THE ENERGY RANGES IN LEFT COLUMN.
THE ACCUMULATED FLUXES HAVE UNITS OF PARTICLES PER SQCM DAY FOR THE ENERGY RANGES IN LEFT COLUMN.
TOTALS FOLLOWING THE ACCUMULATED FLUXES INDICATE THE NUMBER OF FLUXES ENCOUNTERED IN BIN.
THESE TOTALS HAVE MAX VALUES OF 9999.

Figure 6. Printout of Distribution of Particle Flux Within Energy Bands and Intensity Bands (ORP)

PEAK FLUX PER ORBIT TABLE

ORBIT TIME INTERVAL 25920.00000 PERIGEE ALT(KM) 400.00000 INCLINATION= 84.00 ORB RUN DATE 05/11/78

MODELS USED= AE5MAX ,AEIPHI ENERGY = .05 MEV

TOTAL TIME = 3.00 DAYS. TIME INTERVAL = 1.05 MIN. NOMINAL PERIOD = 2.503 HRS.

ORBIT NO.	PEAK ENCOUNTERED	LONGITUDE	LATITUDE	ALTITUDE	TIME (HRS)	FIELD(B) (GAUSS)	LINE(L) (E.R.)	TOTAL FLUX/ORBIT (PARTICLES/CM**2)	S-N EQUATORIAL CROSSING (DEG)
1	2.767E+08	158.72	9.05	7901.5	1.35422	.02969	2.132	5.408E+11	359.99
2	2.843E+08	113.97	11.57	7841.7	4.32364	.03075	2.167	5.446E+11	314.88
3	2.718E+08	68.39	9.35	7900.6	7.37145	.02894	2.239	5.304E+11	269.77
4	2.453E+08	22.21	2.39	7998.4	10.49521	.02590	2.295	4.995E+11	224.54
5	2.341E+08	336.01	-4.61	7971.9	13.62308	.02468	2.331	4.937E+11	179.43
6	2.508E+08	289.22	-16.48	7653.0	16.82579	.02715	2.265	4.933E+11	134.20
7	2.605E+08	245.00	-9.11	7884.9	19.71845	.02750	2.244	5.110E+11	89.09
8	2.622E+08	201.53	2.96	7998.1	22.52324	.02815	2.234	5.255E+11	43.86
9	2.751E+08	157.37	10.21	7893.9	25.42001	.02977	2.193	5.425E+11	358.75
10	2.810E+08	112.62	12.72	7839.0	28.38973	.03083	2.170	5.451E+11	313.64
11	2.683E+08	67.03	10.48	7898.7	31.43561	.02898	2.213	5.310E+11	268.41
12	2.453E+08	20.86	3.50	7999.0	34.56285	.02579	2.294	4.976E+11	223.30
13	2.370E+08	333.98	-8.30	7885.3	37.76885	.02498	2.321	4.962E+11	178.07
14	2.547E+08	287.95	-15.40	7653.9	40.89401	.02716	2.259	4.978E+11	132.96
15	2.613E+08	243.64	-8.05	7885.0	43.78594	.02754	2.242	5.144E+11	87.73
16	2.619E+08	199.49	-.75	7934.7	46.67512	.02825	2.233	5.261E+11	42.63
17	2.725E+08	156.00	11.24	7839.3	49.48808	.02995	2.195	5.408E+11	357.39
18	2.800E+08	110.50	8.99	7946.0	52.53572	.03002	2.192	5.443E+11	312.29
19	2.662E+08	65.00	6.73	7979.1	55.58364	.02821	2.227	5.293E+11	267.18
20	2.442E+08	19.49	4.48	7999.2	58.63178	.02591	2.296	4.982E+11	221.95
21	2.382E+08	332.61	-7.34	7882.8	61.83307	.02501	2.318	4.965E+11	176.84
22	2.574E+08	286.47	-14.47	7649.2	64.96346	.02723	2.254	4.997E+11	131.61
23	2.619E+08	242.26	-7.12	7881.7	67.85572	.02772	2.240	5.152E+11	86.50
24	2.636E+08	198.11	.15	7993.6	70.74621	.02825	2.230	PARTIAL ORBIT	

Figure 7. Printout of Peak Flux Encountered Per Orbit (ORP)

INNER ZONE ELECTRON MODEL AE6 SOLAR MAX PROJECTED

INTEGRAL FLUX UNITS- ELECTRONS/SQCM.SEC

L VALUE = 2.00 EQ B = .0390 GAUSS

ENERGIES (MEV).

N	B	B/B0	0.000	.050	.250	.500	.750	1.000	1.250	1.500	1.750
1	.0390	1.000	4.607E+08	3.426E+08	7.533E+07	7.704E+06	5.400E+05	7.809E+04	3.245E+04	1.349E+04	6.567E+03
2	.0467	1.200	3.542E+08	2.651E+08	5.257E+07	5.254E+06	3.683E+05	5.325E+04	2.213E+04	9.197E+03	4.479E+03
3	.0545	1.400	2.880E+08	2.052E+08	3.803E+07	3.749E+06	2.628E+05	3.800E+04	1.579E+04	6.562E+03	3.196E+03
4	.0623	1.600	2.371E+08	1.680E+08	2.904E+07	2.800E+06	1.963E+05	2.838E+04	1.180E+04	4.902E+03	2.387E+03
5	.0701	1.800	2.014E+08	1.402E+08	2.245E+07	2.149E+06	1.506E+05	2.178E+04	9.052E+03	3.762E+03	1.832E+03
6	.0779	2.000	1.709E+08	1.169E+08	1.799E+07	1.691E+06	1.185E+05	1.714E+04	7.121E+03	2.959E+03	1.441E+03
7	.0857	2.200	1.453E+08	9.939E+07	1.441E+07	1.335E+06	9.360E+04	1.353E+04	5.625E+03	2.337E+03	1.138E+03
8	.0935	2.400	1.270E+08	8.564E+07	1.178E+07	1.085E+06	7.608E+04	1.100E+04	4.572E+03	1.900E+03	9.252E+02
9	.1013	2.600	1.110E+08	7.379E+07	9.725E+06	8.823E+05	6.184E+04	8.942E+03	3.716E+03	1.544E+03	7.521E+02
10	.1091	2.800	9.642E+07	6.368E+07	8.031E+06	7.221E+05	5.062E+04	7.320E+03	3.042E+03	1.264E+03	6.156E+02
11	.1169	3.000	8.416E+07	5.529E+07	6.704E+06	5.989E+05	4.198E+04	6.071E+03	2.523E+03	1.048E+03	5.105E+02
12	.1247	3.200	7.410E+07	4.822E+07	5.627E+06	4.957E+05	3.482E+04	5.035E+03	2.092E+03	8.695E+02	4.234E+02
13	.1325	3.400	6.524E+07	4.206E+07	4.723E+06	4.130E+05	2.895E+04	4.186E+03	1.740E+03	7.229E+02	3.520E+02
14	.1402	3.600	5.741E+07	3.669E+07	3.973E+06	3.457E+05	2.423E+04	3.504E+03	1.456E+03	6.051E+02	2.947E+02
15	.1480	3.800	5.038E+07	3.197E+07	3.352E+06	2.894E+05	2.028E+04	2.933E+03	1.219E+03	5.065E+02	2.467E+02
16	.1558	4.000	4.394E+07	2.777E+07	2.829E+06	2.422E+05	1.698E+04	2.455E+03	1.020E+03	4.240E+02	2.065E+02
17	.1636	4.200	3.833E+07	2.412E+07	2.387E+06	2.024E+05	1.419E+04	2.051E+03	8.524E+02	3.542E+02	1.725E+02
18	.1714	4.400	3.350E+07	2.092E+07	2.000E+06	1.691E+05	1.185E+04	1.714E+03	7.122E+02	2.960E+02	1.441E+02
19	.1792	4.600	2.940E+07	1.809E+07	1.676E+06	1.413E+05	9.903E+03	1.432E+03	5.951E+02	2.473E+02	1.204E+02
20	.1870	4.800	2.598E+07	1.560E+07	1.405E+06	1.187E+05	8.177E+03	1.182E+03	4.914E+02	2.042E+02	9.944E+01
21	.1948	5.000	2.322E+07	1.342E+07	1.180E+06	9.609E+04	6.736E+03	9.739E+02	4.047E+02	1.682E+02	8.191E+01
22	.2026	5.200	1.837E+07	1.112E+07	9.521E+05	7.915E+04	5.548E+03	8.022E+02	3.334E+02	1.385E+02	6.747E+01
23	.2104	5.400	1.530E+07	9.235E+06	7.815E+05	6.352E+04	4.452E+03	6.438E+02	2.675E+02	1.112E+02	5.414E+01
24	.2182	5.600	1.239E+07	7.564E+06	6.215E+05	5.176E+04	3.558E+03	5.145E+02	2.138E+02	8.886E+01	4.327E+01
25	.2259	5.800	1.035E+07	6.146E+06	4.906E+05	3.995E+04	2.800E+03	4.049E+02	1.683E+02	6.993E+01	3.405E+01
26	.2337	6.000	7.981E+06	4.783E+06	3.776E+05	3.030E+04	2.124E+03	3.071E+02	1.276E+02	5.305E+01	2.583E+01
27	.2415	6.200	6.148E+06	3.638E+06	2.788E+05	2.257E+04	1.582E+03	2.288E+02	9.508E+01	3.951E+01	1.924E+01
28	.2493	6.400	4.352E+06	2.596E+06	1.957E+05	1.570E+04	1.101E+03	1.591E+02	6.613E+01	2.748E+01	1.338E+01
29	.2571	6.600	2.981E+06	1.730E+06	1.283E+05	1.003E+04	7.028E+02	1.016E+02	4.223E+01	1.755E+01	8.546E+00
30	.2649	6.800	1.683E+06	9.708E+05	7.043E+04	5.430E+03	3.841E+02	5.555E+01	2.308E+01	9.593E+00	4.672E+00
31	.2727	7.000	6.134E+05	3.549E+05	2.537E+04	1.977E+03	1.386E+02	2.003E+01	8.326E+00	3.460E+00	1.438E+00

Figure 8. Printout of Integral Flux (MODE1)

INNER ZONE ELECTRON MODEL AE6 SOLAR MAX PROJECTED

DIFFERENTIAL FLUX UNITS- ELECTRONS/SQCM.SEC.MEV

L VALUE = 2.00 EQ B = .0390 GAUSS

ENERGIES(MEV).

N	B	B/B0	0.000 TO .050	.050 TO .250	.250 TO .500	.500 TO .750	.750 TO 1.000	1.000 TO 1.250	1.250 TO 1.500	1.500 TO 1.750
1	.0390	1.000	2.361E+09	1.337E+09	2.705E+08	2.566E+07	1.848E+06	1.825E+05	7.586E+04	2.768E+04
2	.0467	1.200	1.982E+09	1.063E+09	1.893E+08	1.954E+07	1.260E+06	1.245E+05	5.174E+04	1.887E+04
3	.0545	1.400	1.656E+09	8.357E+08	1.371E+08	1.394E+07	8.991E+05	8.882E+04	3.691E+04	1.347E+04
4	.0623	1.600	1.382E+09	6.949E+08	1.049E+08	1.042E+07	6.716E+05	6.635E+04	2.757E+04	1.006E+04
5	.0701	1.800	1.225E+09	5.885E+08	8.122E+07	7.394E+06	5.154E+05	5.092E+04	2.116E+04	7.720E+03
6	.0779	2.000	1.080E+09	4.948E+08	6.518E+07	6.238E+06	4.055E+05	4.006E+04	1.665E+04	6.073E+03
7	.0857	2.200	9.185E+08	4.249E+08	5.229E+07	4.957E+06	3.207E+05	3.164E+04	1.315E+04	4.797E+03
8	.0935	2.400	8.269E+08	3.693E+08	4.277E+07	4.037E+06	2.603E+05	2.572E+04	1.069E+04	3.899E+03
9	.1013	2.600	7.435E+08	3.203E+08	3.537E+07	3.282E+06	2.116E+05	2.090E+04	8.688E+03	3.169E+03
10	.1091	2.800	6.549E+08	2.782E+08	2.923E+07	2.686E+06	1.732E+05	1.711E+04	7.111E+03	2.594E+03
11	.1169	3.000	5.773E+08	2.430E+08	2.442E+07	2.228E+06	1.436E+05	1.419E+04	5.897E+03	2.151E+03
12	.1247	3.200	5.175E+08	2.130E+08	2.052E+07	1.848E+06	1.191E+05	1.177E+04	4.891E+03	1.784E+03
13	.1325	3.400	4.536E+08	1.867E+08	1.724E+07	1.536E+06	9.905E+04	9.785E+03	4.067E+03	1.484E+03
14	.1402	3.600	4.144E+08	1.636E+08	1.451E+07	1.286E+06	8.291E+04	8.191E+03	3.404E+03	1.242E+03
15	.1480	3.800	3.693E+08	1.431E+08	1.225E+07	1.076E+06	6.940E+04	6.856E+03	2.849E+03	1.039E+03
16	.1558	4.000	3.235E+08	1.247E+08	1.035E+07	9.009E+05	5.809E+04	5.739E+03	2.385E+03	8.700E+02
17	.1636	4.200	2.841E+08	1.087E+08	8.739E+06	7.527E+05	4.854E+04	4.795E+03	1.993E+03	7.270E+02
18	.1714	4.400	2.536E+08	9.462E+07	7.326E+06	6.289E+05	4.056E+04	4.006E+03	1.665E+03	6.074E+02
19	.1792	4.600	2.264E+08	8.205E+07	6.140E+06	5.255E+05	3.389E+04	3.348E+03	1.391E+03	5.075E+02
20	.1870	4.800	1.915E+08	6.999E+07	5.153E+06	4.339E+05	2.798E+04	2.764E+03	1.149E+03	4.191E+02
21	.1948	5.000	1.620E+08	5.979E+07	4.254E+06	3.574E+05	2.305E+04	2.277E+03	9.462E+02	3.452E+02
22	.2026	5.200	1.451E+08	5.083E+07	3.492E+06	2.944E+05	1.898E+04	1.875E+03	7.794E+02	2.843E+02
23	.2104	5.400	1.213E+08	4.227E+07	2.873E+06	2.363E+05	1.523E+04	1.505E+03	6.254E+02	2.282E+02
24	.2182	5.600	9.649E+07	3.471E+07	2.283E+06	1.888E+05	1.217E+04	1.203E+03	4.998E+02	1.823E+02
25	.2259	5.800	8.417E+07	2.828E+07	1.802E+06	1.486E+05	9.582E+03	9.466E+02	3.934E+02	1.435E+02
26	.2337	6.000	6.397E+07	2.203E+07	1.389E+06	1.127E+05	7.268E+03	7.180E+02	2.984E+02	1.089E+02
27	.2415	6.200	5.020E+07	1.679E+07	1.025E+06	8.396E+04	5.414E+03	5.348E+02	2.223E+02	8.108E+01
28	.2493	6.400	3.510E+07	1.200E+07	7.198E+05	5.840E+04	3.766E+03	3.720E+02	1.546E+02	5.640E+01
29	.2571	6.600	2.502E+07	8.009E+06	4.730E+05	3.729E+04	2.405E+03	2.376E+02	9.872E+01	3.602E+01
30	.2649	6.800	1.424E+07	4.502E+06	2.598E+05	2.038E+04	1.314E+03	1.298E+02	5.396E+01	1.969E+01
31	.2727	7.000	5.170E+06	1.648E+06	9.359E+04	7.352E+03	4.741E+02	4.683E+01	1.946E+01	8.088E+00

Figure 9. Printout of Differential Flux (MODE1)

Program PACKBIN supplies a printout of the contents of the packed binary file.

2.2 Geomagnetic-Geographic Coordinate Conversion

Initiator: J. Buchau

Project No: 4643 Problem No: 4965

Geographic to geomagnetic coordinate conversion and its inversion require the availability of a one-to-one transformation model for latitude and longitude. The centered dipole model with the prime geomagnetic meridian containing the south geographic pole is the simplest approximation for this purpose, where the location of the dipole poles are prescribed for the epoch by any selected field model. Since the reference longitude and latitude are hereby established, transformation from geocentric to geomagnetic coordinates follows by application of spherical trigonometry.

Hakura[5], Gustafsson[6], and others have introduced "corrected" geomagnetic coordinates to account for the asymmetric field lines represented by the higher order spherical harmonic terms in any field model such as GSFC 12/66, IGRF (1975), etc. The correction to the dipole coordinates is given by the displacement, due to the higher order terms, of a field line starting in the geomagnetic equatorial plane and terminating at the altitude at which the coordinates are desired. Gustafsson tabulates results for the earth's surface using the GSFC field 12/66 for epoch 1965, based on an elaborate analytical derivation. A purpose in his approach was to evaluate the contribution from additional higher order terms, but this procedure could not be readily implemented at

AFGL for use with recent field models. A computerized technique for obtaining a constant altitude geographic-geomagnetic coordinate conversion based on IGRF (1975) is however worth investigating.

Two alternate programs, MAGCON and MAGFLN, were implemented to tabulate geographic contours of constant geomagnetic latitude and longitude by examining the field line models. Both programs make use of the MGFLD2 magnetic field package which was obtained from the SUA program library, and which is an updated version of the package described in Reference 7. MGFLD2 calculates the L shell value and the magnetic field components for a specified field model, location and epoch, using either the SHELLG/FELDG or the slower but equivalent INVAR/FIELDG system of routines. In addition, field line tracing and conjugate point calculations are available through subroutine LINTRA.

Program MAGCON tabulates geographic latitude vs. magnetic dip latitude at 5° geographic longitude intervals. Since the magnetic dip latitude (DL) is given by

$$\tan (DL) = 0.5 \left(\frac{Z}{H}\right)$$

where Z is the vertical and H is the horizontal magnetic field component, the geographic latitude is iteratively obtained. Figure 10 shows sample print-out using IGRF (1975) updated to 1978 for an altitude of 100 km.

Program MAGFLN tabulates the geographic longitude trace of field lines starting at 40°N magnetic dip latitude and 100 km altitude, vs. geo-

GEOG. LONGITUDE (EAST)

GMLAT	-180	-175	-170	-165	-160	-155	-150	-145	-140	-135	-130	-125	-120	-115	-110	-105	-100	-95	-90
45.0	52.64	52.12	51.57	50.45	49.36	48.13	46.80	45.45	44.08	42.75	41.46	40.21	39.01	37.86	36.75	35.66	34.64	33.69	32.89
44.0	51.69	51.12	50.56	49.40	48.28	47.04	45.73	44.39	43.04	41.74	40.48	39.27	38.10	36.98	35.89	34.82	33.80	32.86	32.05
43.0	50.69	50.10	49.31	48.33	47.19	45.94	44.63	43.30	42.00	40.72	39.50	38.33	37.19	36.10	35.03	33.97	32.96	32.02	31.20
42.0	49.66	49.06	48.24	47.23	46.07	44.82	43.52	42.21	40.94	39.70	38.52	37.38	36.27	35.21	34.18	33.19	32.11	31.17	30.35
41.0	48.65	48.00	47.14	46.10	44.93	43.68	42.40	41.12	39.86	38.68	37.53	36.42	35.35	34.31	33.28	32.27	31.26	30.32	29.49
40.0	47.60	46.91	46.03	44.97	43.79	42.53	41.26	40.00	38.81	37.65	36.53	35.47	34.42	33.41	32.40	31.40	30.42	29.47	28.63
39.0	46.53	45.81	44.89	43.81	42.61	41.35	40.11	38.89	37.73	36.61	35.53	34.51	33.49	32.49	31.51	30.53	29.55	28.61	27.76
38.0	45.43	44.66	43.72	42.61	41.41	40.17	38.95	37.77	36.65	35.57	34.52	33.51	32.50	31.52	30.55	29.59	28.62	27.74	26.88
37.0	44.32	43.52	42.57	41.40	40.20	38.97	37.78	36.64	35.56	34.52	33.51	32.56	31.61	30.67	29.72	28.77	27.81	26.87	26.00
36.0	43.18	42.34	41.39	40.18	38.97	37.76	36.61	35.51	34.47	33.47	32.51	31.59	30.66	29.75	28.82	27.86	26.93	25.99	25.12
35.0	42.02	41.14	40.13	38.93	37.74	36.55	35.42	34.33	33.37	32.42	31.50	30.60	29.71	28.82	27.90	26.98	26.04	25.10	24.23
34.0	40.84	39.93	38.85	37.68	36.49	35.33	34.24	33.24	32.27	31.37	30.48	29.62	28.76	27.89	26.99	26.06	25.15	24.21	23.33
33.0	39.65	38.69	37.59	36.41	35.23	34.11	33.06	32.09	31.18	30.31	29.46	28.63	27.80	26.95	26.08	25.18	24.25	23.32	22.47
32.0	38.44	37.44	36.31	35.13	33.98	32.88	31.89	30.96	30.09	29.26	28.44	27.64	26.84	26.01	25.16	24.26	23.35	22.42	21.52
31.0	37.22	36.14	35.04	33.86	32.72	31.67	30.71	29.83	28.99	28.20	27.42	26.65	25.87	25.06	24.23	23.35	22.44	21.51	20.61
30.0	35.98	34.92	33.75	32.58	31.46	30.45	29.54	28.70	27.90	27.15	26.40	25.65	24.90	24.11	23.30	22.43	21.52	20.60	19.69
29.0	34.74	33.65	32.47	31.31	30.21	29.24	28.37	27.57	26.82	26.10	25.37	24.65	23.92	23.16	22.36	21.51	20.61	19.68	18.77
28.0	33.50	32.38	31.19	30.04	28.98	28.04	27.21	26.48	25.74	25.05	24.35	23.65	22.95	22.20	21.42	20.58	19.68	18.76	17.84
27.0	32.25	31.11	29.92	28.78	27.75	26.86	26.06	25.34	24.66	24.00	23.33	22.65	21.97	21.24	20.47	19.65	18.76	17.83	16.91
26.0	31.01	29.85	28.66	27.53	26.54	25.68	24.92	24.24	23.59	22.95	22.31	21.65	20.98	20.29	19.52	18.71	17.83	16.91	15.98
25.0	29.76	28.59	27.41	26.30	25.33	24.52	23.79	23.14	22.53	21.91	21.28	20.65	20.00	19.32	18.57	17.77	16.89	15.97	15.04
24.0	28.55	27.35	26.17	25.08	24.14	23.37	22.67	22.05	21.46	20.87	20.26	19.65	19.01	18.35	17.61	16.82	15.96	15.03	14.10
23.0	27.32	26.12	24.94	23.88	22.98	22.22	21.56	20.97	20.40	19.83	19.26	18.65	18.02	17.37	16.65	15.87	15.01	14.09	13.16
22.0	26.11	24.90	23.73	22.69	21.82	21.10	20.46	19.90	19.35	18.80	18.23	17.64	17.03	16.39	15.69	14.92	14.06	13.15	12.21
21.0	24.92	23.69	22.54	21.52	20.68	19.98	19.33	18.74	18.21	17.77	17.21	16.64	16.04	15.41	14.73	13.96	13.11	12.20	11.25
20.0	23.72	22.51	21.37	20.37	19.55	18.88	18.30	17.78	17.26	16.74	16.20	15.64	15.05	14.43	13.76	13.00	12.16	11.24	10.29
19.0	22.55	21.34	20.21	19.23	18.44	17.79	17.23	16.73	16.23	15.71	15.18	14.63	14.06	13.45	12.78	12.03	11.20	10.29	9.33
18.0	21.39	20.19	19.07	18.11	17.34	16.71	16.17	15.69	15.20	14.69	14.17	13.63	13.06	12.46	11.81	11.07	10.24	9.33	8.37
17.0	20.25	19.05	17.94	17.00	16.25	15.64	15.12	14.64	14.17	13.68	13.16	12.63	12.07	11.48	10.83	10.10	9.27	8.36	7.40
16.0	19.12	17.93	16.83	15.92	15.18	14.58	14.08	13.61	13.15	12.66	12.15	11.62	11.07	10.49	9.85	9.13	8.30	7.40	6.43
15.0	18.00	16.82	15.74	14.84	14.11	13.53	13.04	12.59	12.13	11.65	11.15	10.62	10.08	9.50	8.87	8.15	7.34	6.43	5.46
14.0	16.90	15.71	14.65	13.77	13.06	12.49	12.01	11.57	11.12	10.64	10.14	9.62	9.08	8.51	7.88	7.17	6.37	5.46	4.49
13.0	15.80	14.63	13.58	12.71	12.02	11.46	10.99	10.55	10.11	9.64	9.14	8.63	8.08	7.51	6.89	6.19	5.39	4.48	3.51
12.0	14.72	13.56	12.53	11.67	10.99	10.44	9.99	9.56	9.10	8.63	8.13	7.62	7.08	6.52	5.91	5.21	4.41	3.50	2.52
11.0	13.64	12.50	11.48	10.63	9.96	9.43	8.97	8.54	8.10	7.63	7.13	6.62	6.08	5.53	4.92	4.22	3.43	2.52	1.54
10.0	12.59	11.45	10.44	9.62	8.95	8.42	7.97	7.55	7.11	6.64	6.14	5.62	5.08	4.53	3.93	3.24	2.44	1.54	.55
9.0	11.54	10.41	9.40	8.59	7.95	7.42	6.97	6.54	6.10	5.63	5.14	4.62	4.08	3.53	2.93	2.25	1.45	.55	-.44
8.0	10.48	9.37	8.39	7.58	6.94	6.42	5.97	5.55	5.10	4.63	4.13	3.62	3.08	2.54	1.94	1.26	.47	-.44	-1.44
7.0	9.46	8.35	7.37	6.58	5.93	5.43	4.99	4.56	4.12	3.63	3.13	2.62	2.08	1.54	.94	.27	-.53	-1.43	-2.44
6.0	8.44	7.33	6.37	5.58	4.95	4.44	4.00	3.57	3.12	2.64	2.13	1.62	1.08	.54	-.05	-.73	-1.52	-2.43	-3.44
5.0	7.42	6.33	5.36	4.58	3.96	3.46	3.02	2.59	2.14	1.65	1.14	.61	.09	-.46	-1.05	-1.72	-2.51	-3.43	-4.44
4.0	6.40	5.33	4.33	3.60	2.99	2.49	2.04	1.61	1.15	.66	.14	-.39	-.91	-1.47	-2.05	-2.72	-3.51	-4.43	-5.45
3.0	5.40	4.33	3.41	2.67	2.01	1.51	1.06	.62	.16	-.33	-.86	-1.39	-1.91	-2.46	-3.05	-3.72	-4.51	-5.43	-6.46
2.0	4.40	3.34	2.42	1.65	1.04	.54	.09	-.35	-.82	-1.32	-1.85	-2.39	-2.91	-3.46	-4.05	-4.72	-5.51	-6.44	-7.47
1.0	3.41	2.36	1.44	.68	.07	-.43	-.88	-1.33	-1.81	-2.31	-2.85	-3.39	-3.91	-4.46	-5.06	-5.72	-6.52	-7.45	-8.48
0.0	2.42	1.38	.47	-.26	-.89	-1.40	-1.85	-2.31	-2.79	-3.30	-3.84	-4.39	-4.91	-5.46	-6.05	-6.73	-7.53	-8.45	-9.50
-1.0	1.44	.41	-.50	-1.24	-1.85	-2.36	-2.82	-3.28	-3.77	-4.29	-4.84	-5.38	-5.92	-6.47	-7.06	-7.73	-8.53	-9.47	-10.53
-2.0	.46	-.56	-1.46	-2.21	-2.81	-3.32	-3.79	-4.25	-4.75	-5.28	-5.83	-6.36	-6.93	-7.48	-8.07	-8.75	-9.55	-10.49	-11.56
-3.0	-.51	-1.53	-2.41	-3.16	-3.76	-4.28	-4.75	-5.21	-5.73	-6.27	-6.83	-7.36	-7.93	-8.48	-9.08	-9.76	-10.56	-11.52	-12.59
-4.0	-1.48	-2.49	-3.37	-4.11	-4.72	-5.24	-5.72	-6.20	-6.71	-7.26	-7.82	-8.38	-8.93	-9.49	-10.09	-10.77	-11.58	-12.54	-13.63
-5.0	-2.44	-3.44	-4.32	-5.06	-5.66	-6.19	-6.68	-7.17	-7.69	-8.25	-8.82	-9.38	-9.94	-10.50	-11.10	-11.79	-12.61	-13.56	-14.65
-6.0	-3.40	-4.39	-5.26	-6.00	-6.61	-7.14	-7.64	-8.14	-8.67	-9.23	-9.81	-10.38	-10.95	-11.51	-12.11	-12.81	-13.64	-14.62	-15.74
-7.0	-4.36	-5.34	-6.20	-6.93	-7.55	-8.09	-8.60	-9.11	-9.65	-10.22	-10.81	-11.38	-11.95	-12.52	-13.13	-13.83	-14.67	-15.67	-16.81
-8.0	-5.30	-6.28	-7.14	-7.87	-8.50	-9.04	-9.56	-10.08	-10.63	-11.21	-11.80	-12.36	-12.96	-13.53	-14.15	-14.86	-15.71	-16.73	-17.88
-9.0	-6.24	-7.22	-8.08	-8.81	-9.44	-9.99	-10.51	-11.05	-11.61	-12.20	-12.80	-13.38	-13.97	-14.55	-15.17	-15.86	-16.75	-17.79	-18.96
-10.0	-7.18	-8.15	-9.01	-9.75	-10.38	-10.94	-11.47	-12.02	-12.59	-13.19	-13.80	-14.40	-14.98	-15.57	-16.20	-16.93	-17.81	-18.86	-20.06

Figure 10a. Geographic Latitude vs. Magnetic Dip Latitude at 100 km Altitude - Sample MAGCON Printout

-11.0	-8.12	-9.08	-9.94	-10.68	-11.31	-11.86	-12.43	-12.98	-13.57	-14.18	-14.80	-15.40	-15.99	-16.59	-17.23	-17.97	-18.87	-19.94	-21.16		
-12.0	-9.05	-10.01	-10.87	-11.61	-12.25	-12.83	-13.38	-13.95	-14.55	-15.17	-15.80	-16.41	-17.01	-17.61	-18.26	-19.03	-19.94	-21.03	-22.28		
-13.0	-9.98	-10.93	-11.79	-12.53	-13.18	-13.77	-14.34	-14.92	-15.53	-16.16	-16.80	-17.41	-18.02	-18.63	-19.30	-20.08	-21.02	-22.14	-23.42		
-14.0	-10.90	-11.85	-12.70	-13.46	-14.12	-14.71	-15.30	-15.89	-16.51	-17.15	-17.80	-18.42	-19.04	-19.66	-20.34	-21.15	-22.11	-23.25	-24.56		
-15.0	-11.82	-12.77	-13.62	-14.38	-15.05	-15.66	-16.25	-16.86	-17.49	-18.14	-18.79	-19.44	-20.06	-20.70	-21.40	-22.22	-23.20	-24.36	-25.75		
-16.0	-12.74	-13.68	-14.54	-15.30	-15.97	-16.60	-17.21	-17.83	-18.48	-19.14	-19.79	-20.45	-21.09	-21.74	-22.46	-23.30	-24.32	-25.54	-26.94		
-17.0	-13.65	-14.59	-15.45	-16.22	-16.90	-17.54	-18.16	-18.80	-19.46	-20.13	-20.81	-21.46	-22.11	-22.78	-23.52	-24.39	-25.44	-26.71	-28.15		
-18.0	-14.56	-15.50	-16.36	-17.14	-17.83	-18.43	-19.12	-19.77	-20.44	-21.13	-21.81	-22.48	-23.14	-23.84	-24.60	-25.49	-26.59	-27.89	-29.38		
-19.0	-15.47	-16.41	-17.27	-18.06	-18.76	-19.42	-20.08	-20.74	-21.43	-22.13	-22.82	-23.51	-24.18	-24.89	-25.66	-26.61	-27.75	-29.11	-30.66		
-20.0	-16.38	-17.32	-18.19	-18.98	-19.69	-20.37	-21.04	-21.72	-22.42	-23.13	-23.87	-24.53	-25.22	-25.95	-26.77	-27.74	-28.92	-30.33	-31.95		
-21.0	-17.28	-18.22	-19.09	-19.88	-20.62	-21.31	-22.00	-22.69	-23.41	-24.13	-24.85	-25.56	-26.26	-27.02	-27.87	-28.89	-30.12	-31.59	-33.27		
-22.0	-18.18	-19.12	-20.00	-21.80	-21.55	-22.25	-22.96	-23.67	-24.40	-25.13	-25.87	-26.59	-27.32	-28.10	-28.98	-30.05	-31.33	-32.87	-34.61		
-23.0	-19.08	-20.02	-20.90	-21.72	-22.48	-23.20	-23.92	-24.65	-25.39	-26.14	-26.89	-27.62	-28.36	-29.19	-30.11	-31.22	-32.56	-34.18	-36.00		
-24.0	-19.96	-20.92	-21.81	-22.63	-23.41	-24.16	-24.88	-25.63	-26.39	-27.15	-27.91	-28.66	-29.44	-30.28	-31.24	-32.41	-33.83	-35.51	-37.41		
-25.0	-20.87	-21.82	-22.72	-23.55	-24.34	-25.10	-25.85	-26.61	-27.39	-28.16	-28.93	-29.71	-30.52	-31.39	-32.41	-33.62	-35.12	-36.87	-38.85		
-26.0	-21.76	-22.72	-23.62	-24.47	-25.27	-26.05	-26.82	-27.60	-28.39	-29.18	-29.96	-30.76	-31.59	-32.50	-33.57	-34.85	-36.42	-38.27	-40.31		
-27.0	-22.66	-23.62	-24.53	-25.39	-26.21	-27.00	-27.79	-28.59	-29.39	-30.19	-31.00	-31.82	-32.68	-33.63	-34.76	-36.10	-37.75	-39.69	-41.79		
-28.0	-23.55	-24.52	-25.44	-26.31	-27.15	-27.95	-28.76	-29.57	-30.38	-31.21	-32.04	-32.88	-33.78	-34.77	-35.95	-37.39	-39.11	-41.13	-43.31		
-29.0	-24.44	-25.42	-26.35	-27.23	-28.09	-28.91	-29.74	-30.57	-31.40	-32.24	-33.08	-33.95	-34.88	-35.93	-37.17	-38.68	-40.50	-42.59	-44.83		
-30.0	-25.34	-26.32	-27.26	-28.15	-29.03	-29.87	-30.71	-31.57	-32.41	-33.27	-34.17	-35.03	-35.99	-37.10	-38.40	-40.00	-41.90	-44.07	-46.35		
-31.0	-26.23	-27.22	-28.17	-29.05	-29.97	-30.83	-31.70	-32.56	-33.43	-34.30	-35.18	-36.11	-37.12	-38.28	-39.65	-41.33	-43.33	-45.57	-47.87		
-32.0	-27.12	-28.12	-29.09	-30.02	-30.92	-31.79	-32.68	-33.56	-34.44	-35.33	-36.25	-37.20	-38.25	-39.47	-40.93	-42.69	-44.77	-47.07	-49.39		
-33.0	-28.02	-29.03	-30.00	-30.96	-31.87	-32.76	-33.68	-34.56	-35.47	-36.37	-37.31	-38.30	-39.41	-40.66	-42.22	-44.07	-46.23	-48.56	-50.90		
-34.0	-28.92	-29.93	-30.93	-31.90	-32.82	-33.74	-34.66	-35.57	-36.49	-37.42	-38.38	-39.41	-40.56	-41.91	-43.53	-45.47	-47.69	-50.08	-52.39		
-35.0	-29.82	-30.84	-31.85	-32.83	-33.78	-34.71	-35.65	-36.58	-37.52	-38.47	-39.46	-40.53	-41.74	-43.15	-44.85	-46.86	-49.17	-51.58	-53.87		
-36.0	-30.72	-31.76	-32.79	-33.78	-34.74	-35.69	-36.65	-37.60	-38.55	-39.52	-40.55	-41.65	-42.92	-44.41	-46.19	-48.30	-50.65	-53.06	-55.33		
-37.0	-31.62	-32.67	-33.71	-34.72	-35.71	-36.69	-37.65	-38.61	-39.59	-40.59	-41.64	-42.79	-44.12	-45.68	-47.55	-49.73	-52.13	-54.54	-56.76		
-38.0	-32.53	-33.59	-34.64	-35.67	-36.68	-37.66	-38.65	-39.63	-40.63	-41.65	-42.74	-43.94	-45.33	-46.97	-48.93	-51.17	-53.60	-55.99	-58.17		
-39.0	-33.43	-34.52	-35.58	-36.63	-37.65	-38.66	-39.65	-40.66	-41.67	-42.72	-43.85	-45.10	-46.55	-48.28	-50.31	-52.62	-55.07	-57.44	-59.56		
-40.0	-34.35	-35.44	-36.52	-37.59	-38.63	-39.65	-40.66	-41.69	-42.72	-43.80	-44.96	-46.27	-47.79	-49.59	-51.71	-54.07	-56.53	-58.86	-60.93		
-41.0	-35.26	-36.37	-37.49	-38.56	-39.61	-40.65	-41.67	-42.72	-43.77	-44.88	-46.09	-47.45	-49.04	-50.93	-53.12	-55.52	-57.90	-60.26	-62.29		
-42.0	-36.19	-37.31	-38.43	-39.52	-40.59	-41.65	-42.70	-43.75	-44.83	-45.98	-47.22	-48.65	-50.32	-52.28	-54.54	-56.97	-59.41	-61.66	-63.63		
-43.0	-37.10	-38.24	-39.33	-40.48	-41.57	-42.65	-43.71	-44.79	-45.89	-47.07	-48.37	-49.86	-51.60	-53.64	-55.96	-58.42	-60.83	-63.04	-64.95		
-44.0	-38.03	-39.18	-40.34	-41.46	-42.56	-43.65	-44.73	-45.83	-46.97	-48.18	-49.53	-51.08	-52.91	-55.03	-57.40	-59.97	-62.26	-64.41	-66.27		
-45.0	-38.96	-40.13	-41.29	-42.43	-43.55	-44.66	-45.76	-46.87	-48.04	-49.29	-50.70	-52.32	-54.22	-56.43	-58.84	-61.32	-63.67	-65.78	-67.58		

Figure 10b. Geographic Latitude vs. Magnetic Dip Latitude at 100 km Altitude - Sample MAGCON Printout

detic latitude at 5° geographic longitude intervals. Figure 11 shows a sample print-out. Subroutine LINTRA was modified by an entry point CONTRA which returns to the calling program at any specified geodetic latitude GDLATF, but resumes field line tracing from this point on a subsequent call. If GDLATF > 90°, a normal conjugate point calculation terminating at a specified altitude is performed.

IGRF1975.1 UPDATED TO 1978.000 USER SHELLG/FELLG

NORTH-SOUTH FIELD LINE TRACE FROM GDLAT,HKM = 40.000 100.000 ON A 5 DEGREE LONGITUDE GRID

GEOG. LONGITUDE (EAST)

GDLAT	-120	-115	-110	-105	-100	-95	-90	-85	-80	-75	-70	-65	-60
60.0	.00	.00	.00	.00	.00	.00	.00	.00	.00	.00	.00	.00	.00
59.0	.00	.00	.00	.00	.00	.00	.00	.00	.00	.00	.00	.00	.00
58.0	.00	.00	.00	.00	.00	.00	.00	.00	.00	.00	.00	.00	.00
57.0	.00	.00	.00	.00	.00	.00	.00	.00	.00	.00	.00	.00	.00
56.0	.00	.00	.00	.00	.00	.00	.00	.00	.00	.00	.00	.00	.00
55.0	.00	.00	.00	.00	.00	.00	.00	.00	.00	.00	.00	.00	.00
54.0	.00	.00	.00	.00	.00	.00	.00	.00	.00	.00	.00	.00	.00
53.0	.00	.00	.00	.00	.00	.00	.00	.00	.00	.00	.00	.00	.00
52.0	.00	.00	.00	.00	.00	.00	.00	.00	.00	.00	.00	.00	.00
51.0	.00	.00	.00	.00	.00	.00	.00	.00	.00	.00	.00	.00	.00
50.0	.00	.00	.00	.00	.00	.00	.00	.00	.00	.00	.00	.00	.00
49.0	.00	.00	.00	.00	.00	.00	.00	.00	.00	.00	.00	.00	.00
48.0	.00	.00	.00	.00	.00	.00	.00	.00	.00	.00	.00	.00	.00
47.0	.00	.00	.00	.00	.00	.00	.00	.00	.00	.00	.00	.00	.00
46.0	.00	.00	.00	.00	.00	.00	.00	.00	.00	.00	.00	.00	.00
45.0	.00	.00	.00	.00	.00	.00	.00	.00	.00	.00	.00	.00	.00
44.0	.00	.00	.00	.00	.00	.00	.00	.00	.00	.00	.00	.00	.00
43.0	.00	.00	.00	.00	.00	.00	.00	.00	.00	.00	.00	.00	.00
42.0	.00	.00	.00	.00	.00	.00	.00	.00	.00	.00	.00	.00	.00
41.0	.00	.00	.00	.00	.00	.00	.00	.00	.00	.00	.00	.00	.00
40.0	.00	.00	.00	.00	.00	.00	.00	.00	.00	.00	.00	.00	.00
39.0	.00	.00	.00	.00	.00	.00	.00	.00	.00	.00	.00	.00	.00
38.0	.00	.00	.00	.00	.00	.00	.00	.00	.00	.00	.00	.00	.00
37.0	.00	.00	.00	.00	.00	.00	.00	.00	.00	.00	.00	.00	.00
36.0	.00	.00	.00	.00	.00	.00	.00	.00	.00	.00	.00	.00	.00
35.0	.00	.00	.00	.00	.00	.00	.00	.00	.00	.00	.00	.00	.00
34.0	-120.13	.00	.00	.00	.00	.00	.00	.00	.00	.00	.00	.00	.00
33.0	-120.44	-115.12	.00	.00	.00	.00	.00	.00	.00	.00	.00	.00	.00
32.0	-120.72	-115.39	-110.10	.00	.00	.00	.00	.00	.00	.00	.00	.00	.00
31.0	-121.00	-115.65	-110.35	-105.09	.00	.00	.00	.00	.00	.00	.00	.00	.00
30.0	-121.26	-115.91	-110.58	-105.30	-100.07	.00	.00	.00	.00	.00	.00	.00	-55.65
29.0	-121.51	-116.15	-110.81	-105.50	-100.25	-95.06	.00	.00	.00	.00	.00	.00	-59.54
28.0	-121.76	-116.37	-111.02	-105.70	-100.41	-95.19	-90.05	.00	.00	.00	.00	-64.75	-59.24
27.0	-121.99	-116.60	-111.23	-105.88	-100.58	-95.32	-90.17	-85.03	-79.98	-74.94	-69.82	-64.52	-58.96
26.0	-122.22	-116.82	-111.43	-106.07	-100.73	-95.44	-90.31	-85.05	-79.95	-74.84	-69.66	-64.29	-58.69
25.0	-122.45	-117.03	-111.63	-106.24	-100.86	-95.56	-90.29	-85.08	-79.92	-74.75	-69.50	-64.08	-58.43
24.0	-122.67	-117.24	-111.82	-106.42	-101.03	-95.68	-90.37	-85.11	-79.89	-74.66	-69.35	-63.87	-58.19
23.0	-122.86	-117.44	-112.01	-106.59	-101.18	-95.79	-90.45	-85.14	-79.87	-74.56	-69.21	-63.66	-57.95
22.0	-123.09	-117.64	-112.19	-106.75	-101.32	-95.90	-90.52	-85.17	-79.85	-74.50	-69.07	-63.49	-57.72
21.0	-123.29	-117.84	-112.38	-106.91	-101.46	-96.02	-90.60	-85.21	-79.83	-74.43	-68.94	-63.31	-57.50
20.0	-123.50	-118.03	-112.55	-107.07	-101.60	-96.13	-90.67	-85.24	-79.81	-74.36	-68.82	-63.13	-57.28
19.0	-123.70	-118.22	-112.73	-107.23	-101.73	-96.23	-90.75	-85.27	-79.80	-74.29	-68.70	-62.96	-57.07
18.0	-123.89	-118.41	-112.90	-107.39	-101.87	-96.34	-90.82	-85.31	-79.79	-74.23	-68.59	-62.80	-56.87
17.0	-124.09	-118.59	-113.07	-107.54	-102.00	-96.45	-90.90	-85.35	-79.78	-74.17	-68.48	-62.64	-56.67
16.0	-124.28	-118.77	-113.24	-107.69	-102.13	-96.56	-90.97	-85.38	-79.77	-74.12	-68.37	-62.49	-56.48
15.0	-124.47	-118.95	-113.41	-107.85	-102.26	-96.66	-91.05	-85.42	-79.77	-74.07	-68.27	-62.34	-56.29
14.0	-124.66	-119.13	-113.58	-108.00	-102.39	-96.77	-91.13	-85.46	-79.77	-74.02	-68.17	-62.20	-56.11
13.0	-124.85	-119.31	-113.74	-108.15	-102.52	-96.87	-91.20	-85.50	-79.77	-73.97	-68.08	-62.06	-55.93
12.0	-125.04	-119.49	-113.91	-108.30	-102.65	-96.98	-91.28	-85.54	-79.77	-73.93	-67.98	-61.92	-55.75
11.0	-125.22	-119.67	-114.07	-108.45	-102.79	-97.09	-91.36	-85.59	-79.77	-73.88	-67.90	-61.79	-55.58
10.0	-125.41	-119.84	-114.24	-108.60	-102.92	-97.19	-91.44	-85.63	-79.78	-73.84	-67.81	-61.65	-55.41
9.0	-125.61	-120.02	-114.40	-108.75	-103.05	-97.30	-91.51	-85.68	-79.78	-73.81	-67.73	-61.53	-55.24
8.0	-125.78	-120.21	-114.57	-108.90	-103.18	-97.41	-91.60	-85.72	-79.79	-73.77	-67.64	-61.40	-55.08

THIS PAGE IS BEST QUALITY PRACTICABLE
FROM COPY FURNISHED TO DDC

Figure 11a. Geographic Longitude Trace of Field Line from Magnetic Dip Latitude 40°N, 100 km Altitude - Sample MAGFLN Printout

THIS PAGE IS BEST QUALITY PRACTICABLE
FROM COPY FURNISHED TO DDC

7.0	-126.97	-120.37	-114.73	-109.05	-103.31	-97.52	-91.68	-85.77	-79.80	-73.74	-67.57	-61.28	-54.92
6.0	-126.19	-120.53	-114.94	-109.20	-103.44	-97.63	-91.76	-85.82	-79.81	-73.71	-67.49	-61.16	-54.76
5.0	-126.34	-120.73	-115.06	-109.35	-103.57	-97.74	-91.84	-85.87	-79.82	-73.68	-67.41	-61.04	-54.60
4.0	-126.52	-120.97	-115.23	-109.50	-103.71	-97.86	-91.93	-85.93	-79.84	-73.65	-67.34	-60.92	-54.45
3.0	-126.71	-121.09	-115.39	-109.65	-103.84	-97.96	-92.01	-85.98	-79.86	-73.62	-67.27	-60.81	-54.30
2.0	-126.90	-121.26	-115.56	-109.80	-103.98	-98.06	-92.10	-86.04	-79.88	-73.60	-67.20	-60.70	-54.14
1.0	-127.09	-121.44	-115.73	-109.96	-104.12	-98.19	-92.19	-86.10	-79.90	-73.58	-67.14	-60.59	-53.99
0.0	-127.27	-121.62	-115.90	-110.11	-104.25	-98.31	-92.29	-86.15	-79.92	-73.56	-67.07	-60.48	-53.85
-1.0	-127.47	-121.80	-116.07	-110.27	-104.39	-98.43	-92.39	-86.22	-79.94	-73.54	-67.01	-60.37	-53.70
-2.0	-127.65	-121.99	-116.24	-110.43	-104.54	-98.55	-92.47	-86.28	-79.97	-73.53	-66.95	-60.27	-53.55
-3.0	-127.85	-122.17	-116.42	-110.59	-104.69	-98.67	-92.57	-86.34	-80.00	-73.51	-66.89	-60.16	-53.41
-4.0	-128.04	-122.35	-116.59	-110.75	-104.82	-98.80	-92.66	-86.41	-80.02	-73.50	-66.83	-60.06	-53.27
-5.0	-128.24	-122.54	-116.77	-110.92	-104.97	-98.92	-92.76	-86.46	-80.06	-73.49	-66.76	-59.96	-53.12
-6.0	-128.44	-122.71	-116.95	-111.08	-105.12	-99.05	-92.87	-86.55	-80.09	-73.48	-66.72	-59.86	-52.98
-7.0	-128.64	-122.90	-117.13	-111.25	-105.27	-99.18	-92.97	-86.62	-80.13	-73.47	-66.67	-59.76	-52.84
-8.0	-128.84	-123.12	-117.32	-111.42	-105.43	-99.32	-93.08	-86.70	-80.16	-73.47	-66.62	-59.66	-52.70
-9.0	-129.05	-123.32	-117.50	-111.60	-105.58	-99.45	-93.19	-86.78	-80.20	-73.46	-66.57	-59.56	-52.56
-10.0	-129.25	-123.52	-117.69	-111.77	-105.74	-99.59	-93.30	-86.86	-80.25	-73.46	-66.52	-59.47	-52.42
-11.0	-129.46	-123.72	-117.88	-111.95	-105.89	-99.73	-93.42	-86.94	-80.29	-73.46	-66.47	-59.37	-52.28
-12.0	-129.68	-123.92	-118.08	-112.13	-106.07	-99.88	-93.53	-87.03	-80.34	-73.47	-66.43	-59.28	-52.14
-13.0	-129.89	-124.13	-118.28	-112.32	-106.24	-100.02	-93.66	-87.12	-80.39	-73.47	-66.38	-59.19	-52.00
-14.0	-130.11	-124.35	-118.48	-112.51	-106.41	-100.17	-93.79	-87.21	-80.44	-73.48	-66.34	-59.09	-51.86
-15.0	-130.34	-124.56	-118.69	-112.70	-106.59	-100.33	-93.91	-87.30	-80.50	-73.49	-66.30	-59.00	-51.72
-16.0	-130.56	-124.73	-118.90	-112.90	-106.77	-100.49	-94.04	-87.40	-80.56	-73.50	-66.26	-58.91	-51.58
-17.0	-130.80	-125.01	-119.11	-113.10	-106.95	-100.65	-94.18	-87.51	-80.62	-73.52	-66.23	-58.82	-51.44
-18.0	-131.03	-125.24	-119.33	-113.31	-107.14	-100.82	-94.32	-87.61	-80.69	-73.54	-66.19	-58.73	-51.30
-19.0	-131.28	-125.47	-119.56	-113.52	-107.34	-100.99	-94.46	-87.72	-80.76	-73.56	-66.16	-58.65	-51.16
-20.0	-131.52	-125.71	-119.79	-113.73	-107.54	-101.17	-94.61	-87.84	-80.83	-73.58	-66.13	-58.56	-51.02
-21.0	-131.77	-125.96	-120.02	-113.96	-107.74	-101.35	-94.77	-87.96	-80.91	-73.61	-66.10	-58.47	-50.88
-22.0	-132.04	-126.21	-120.26	-114.19	-107.95	-101.54	-94.93	-88.08	-80.99	-73.64	-66.07	-58.39	-50.74
-23.0	-132.30	-126.46	-120.51	-114.42	-108.17	-101.74	-95.10	-88.22	-81.07	-73.67	-66.05	-58.30	-50.60
-24.0	-132.57	-126.71	-120.77	-114.66	-108.40	-101.94	-95.27	-88.35	-81.16	-73.71	-66.03	-58.22	-50.46
-25.0	-132.85	-127.00	-121.03	-114.91	-108.63	-102.15	-95.45	-88.49	-81.26	-73.75	-66.01	-58.14	-50.31
-26.0	-133.13	-127.23	-121.30	-115.17	-108.87	-102.37	-95.64	-88.64	-81.36	-73.80	-65.99	-58.06	-50.17
-27.0	-133.43	-127.57	-121.58	-115.43	-109.12	-102.59	-95.83	-88.80	-81.47	-73.85	-65.98	-57.98	-50.03
-28.0	-133.73	-127.87	-121.86	-115.71	-109.37	-102.83	-96.03	-88.96	-81.59	-73.91	-65.97	-57.90	-49.88
-29.0	-134.05	-128.17	-122.16	-115.99	-109.64	-103.07	-96.25	-89.13	-81.71	-73.97	-65.96	-57.82	-49.74
-30.0	-134.37	-128.48	-122.47	-116.29	-109.92	-103.32	-96.47	-89.31	-81.84	-74.03	-65.96	-57.74	-49.59
-31.0	-134.70	-128.80	-122.79	-116.59	-110.21	-103.59	-96.70	-89.51	-81.97	-74.11	-65.96	-57.67	-49.44
-32.0	-135.05	-129.16	-123.12	-116.91	-110.51	-103.88	-96.94	-89.71	-82.12	-74.19	-65.97	-57.60	-49.29
-33.0	-135.41	-129.51	-123.46	-117.25	-110.82	-104.18	-97.20	-89.92	-82.27	-74.28	-65.98	-57.53	-49.14
-34.0	-135.78	-129.93	-123.82	-117.59	-111.15	-104.48	-97.47	-90.14	-82.44	-74.37	-66.00	-57.46	-48.98
-35.0	-136.17	-130.26	-124.20	-117.95	-111.49	-104.78	-97.75	-90.38	-82.62	-74.48	-66.02	-57.40	-48.85
-36.0	-136.57	-130.65	-124.59	-118.33	-111.86	-105.11	-98.05	-90.63	-82.81	-74.59	-66.05	-57.34	-48.70
-37.0	-136.97	-131.07	-125.00	-118.73	-112.23	-105.47	-98.37	-90.89	-83.01	-74.72	-66.09	-57.28	-48.55
-38.0	-137.41	-131.51	-125.41	-119.15	-112.61	-105.84	-98.70	-91.18	-83.23	-74.85	-66.13	-57.23	-48.40
-39.0	-137.89	-131.96	-125.87	-119.59	-113.05	-106.23	-99.06	-91.48	-83.46	-75.00	-66.18	-57.18	-48.25
-40.0	-138.37	-132.44	-126.35	-120.05	-113.50	-106.63	-99.44	-91.80	-83.71	-75.17	-66.25	-57.14	-48.10
-41.0	-138.87	-132.94	-126.84	-120.53	-113.97	-107.05	-99.84	-92.15	-83.98	-75.35	-66.32	-57.10	-47.95
-42.0	-139.40	-133.47	-127.37	-121.05	-114.47	-107.57	-100.27	-92.52	-84.27	-75.54	-66.41	-57.07	-47.80
-43.0	-139.95	-134.03	-127.92	-121.60	-115.00	-108.07	-100.73	-92.92	-84.59	-75.76	-66.51	-57.04	-47.66
-44.0	-140.53	-134.60	-128.50	-122.18	-115.57	-108.61	-101.22	-93.35	-84.93	-75.99	-66.62	-57.02	-47.52
-45.0	.00	.00	-129.12	-122.79	-116.17	-109.19	-101.75	-93.81	-85.30	-76.25	-66.75	-57.02	-47.38
-46.0	.00	.00	-129.77	-123.45	-116.82	-109.81	-102.33	-94.31	-85.70	-76.53	-66.90	-57.03	-47.24
-47.0	.00	.00	.00	-124.14	-117.51	-110.47	-102.94	-94.85	-86.14	-76.85	-67.07	-57.05	-47.11
-48.0	.00	.00	.00	.00	-118.25	-111.19	-103.61	-95.44	-86.62	-77.19	-67.26	-57.08	-46.99
-49.0	.00	.00	.00	.00	.00	-111.97	-104.34	-96.08	-87.14	-77.57	-67.46	-57.13	-46.87
-50.0	.00	.00	.00	.00	.00	.00	-105.13	-96.78	-87.71	-77.98	-67.72	-57.20	-46.76
-51.0	.00	.00	.00	.00	.00	.00	.00	-97.54	-88.34	-78.45	-68.00	-57.28	-46.66
-52.0	.00	.00	.00	.00	.00	.00	.00	-98.36	-89.03	-78.95	-68.31	-57.39	-46.57

Figure 11b. Geographic Longitude Trace of Field Line from Magnetic Dip Latitude 40°N, 100 km Altitude - Sample MAGFLN Printout

-53.0	.00	.00	.00	.00	.00	.00	.00	.00	-89.79	-79.52	-68.66	-57.52	-46.50
-54.0	.00	.00	.00	.00	.00	.00	.00	.00	-90.63	-80.14	-69.05	-57.66	-46.44
-55.0	.00	.00	.00	.00	.00	.00	.00	.00	.00	-80.63	-69.49	-57.82	-46.39
-56.0	.00	.00	.00	.00	.00	.00	.00	.00	.00	.00	-69.99	-58.10	-46.37
-57.0	.00	.00	.00	.00	.00	.00	.00	.00	.00	.00	.00	.00	.00
-58.0	.00	.00	.00	.00	.00	.00	.00	.00	.00	.00	.00	.00	.00
-59.0	.00	.00	.00	.00	.00	.00	.00	.00	.00	.00	.00	.00	.00
-60.0	.00	.00	.00	.00	.00	.00	.00	.00	.00	.00	.00	.00	.00

Figure 11c. Geographic Longitude Trace of Field Line from Magnetic Dip Latitude 40°N, 100 km Altitude - Sample MAGFLN Printout

2.3 Precise Solar Ephemeris Routine

Initiator: E. Robinson

Project No: 0001 Problem No: 4517

Routines at three levels of speed, core memory, and accuracy are available for various solar and lunar ephemeris requirements. SOLUN[8] approximates these ephemerides using about ten coefficients for the sun. A limited test showed that solar ephemeris accuracy is 75" arc in right ascension and 10" arc in declination when compared to the U.S. Naval Observatory Ephemeris. This routine is satisfactory for many experimental data correlation requirements.

Program SOLLUN is a higher accuracy, self-contained package that was obtained from the SUA program library (Project 0001; Problems 1131, 1461), and which is used to provide most of the print-outs or plots requested for various observing stations. The solar ephemeris is based on about thirty coefficients and in a comparative test gave accuracies of 15" arc in right ascension and 7" arc in declination.

Subroutine SLEPHEM[8] was developed earlier for the highest accuracy requirements at AFGL, such as eclipse time calculations. For this purpose, celestial latitude and longitude calculations are carried out including all periodic coefficients that are greater than .025" arc. The sun-moon coefficients comprise 789 argument-index sets and are stored on permanent file for execution of SLEPHEM. A comparative test

showed right ascension and declination accurate to 0.5" arc. For future high accuracy satellite eclipsing calculations, the approximately sixty solar coefficient-index sets were incorporated into a self-contained subroutine SOLEPH. Right ascension, declination, radius vector and semi-diameter are calculated for any universal time, with specified or default correction for ephemeris time. Optional print-out for checking against the American Ephemeris and Nautical Almanac verifies and calibrates the calculations.

References

1. Teague, Michael; Stein, Joel and Vette, James, The Use of the Inner Zone Electron Model AE-5 and Associated Computer Programs, Greenbelt, MD: NSSDC, NASA, Goddard Space Flight Center; November, 1972.

2. Teague, Michael and Vette, James, A Model of the Trapped Electron Population for Solar Minimum, Greenbelt, MD: NSSDC, NASA, Goddard Space Flight Center; April, 1974.

3. Teague, Michael; Chan, King and Vette, James, AE6: A Model Environment of Trapped Electrons for Solar Maximum, Greenbelt, MD: NSSDC, NASA, Goddard Space Flight Center; December, 1976.

4. Sawyer, Donald and Vette, James, AP-8 Trapped Proton Environment for Solar Maximum and Solar Minimum, Greenbelt, MD: NSSDC, NASA, Goddard Space Flight Center; December, 1976.

5. Hakura, Y., "Tables and Maps of Geomagnetic Coordinates Corrected by the Higher Order Spherical Harmonic Terms", Report on Ionospheric Space Res. Japan, 19, pp. 121-157, (1965).

6. Gustafsson, G., "A Revised Corrected Geomagnetic Coordinate System", Arkiv för Geofysik, 5, p. 40.

7. McInerney, R., and Abelowitz, A., "MFP (Magnetic Field Package): A Flexible System of Computer Programs for Theoretical Magnetic Field Calculations", AFCRL-TR-73-0356, June 1973.

8. "Analysis and Programming for Scientific Research", Logicon, Inc., AFGL-TR-77-0265, November 1977.

3. Atmospheric Density Models

3. Atmospheric Density Models

Initiator: K. S. W. Champion

Project No: 6690 Problem No: 4867

The continuing need for accuracy in satellite tracking and ephemerides prediction in high atmospheric drag situations results in the need for improved modeling of the complex lower thermospheric density variations. A case in point concerns the Skylab, orbiting space laboratory, whose orbit is decaying at a faster rate than predicted from density models based on the previous solar activity cycle. This clearly points up the need for better understanding of interactions of solar radiation with the neutral atmosphere. Geomagnetic activity remains the dominating factor in short term density variations and orbit determination. Recent in-situ accelerometer and mass spectrometer data provide fuel for these studies. Support for this work has taken three forms:

1) Evaluation of recent density models for ephemeris prediction accuracy.

2) Assistance in development of empirical density models by adaptation of multiple linear regression software.

3) Analysis of high quality Doppler beacon satellite tracking data, with program CELEST, to obtain new satellite drag density data for new model development and checking of accelerometer data.

3.1 Recent Density Model Evaluation

AFGL has an on-going program of evaluating atmospheric density models for their satellite ephemeris prediction capabilities. The primary

software vehicles for this are the CADNIP/BADMEP[1] package and program CELEST.[2] Both systems determine a satellite trajectory, using specified models, by least-squares fitting of tracking observations with the resulting trajectory propagated through numerical integration into a prediction realm. When the tracking observations consists of positional information (i.e., range, azimuth, elevation), as is the case with the data handled by CADNIP/BADMEP, then a direct comparison of the predicted trajectory with the observations is possible. In the case of Doppler data handled by CELEST, it is more convenient to make a second fit over the prediction realm, for comparison with the predicted trajectory. Program TRDIFF has been developed for computing and outputting differences between CELEST-determined trajectories resulting from the use of various models. As new models are developed they may be added to, or replace, existing models in the orbit-determination programs. Recently this approach has been applied to evaluation of geopotential models.[3]

3.1.1 Additions to Existing Programs

Among recently developed density models, the Jacchia 1977(J77),[4] the Mass Spectrometer and Incoherent Scatter (MSIS) model of Hedin, et al.,[5] and the USSR Apollo-Soyuz model[6] have been selected for incorporation into the orbit determination programs. Subroutine decks provided to AFGL by developing or using agencies simplified this task. Figure 1 shows a schematic diagram of the interphasing developed in program CELEST. Subroutine DENS had been adopted from CADNIP earlier in adding the Jacchia 1964 and other densities to CELEST.[7] Hence the interphasing for CADNIP/BADMEP is the same except for the integration

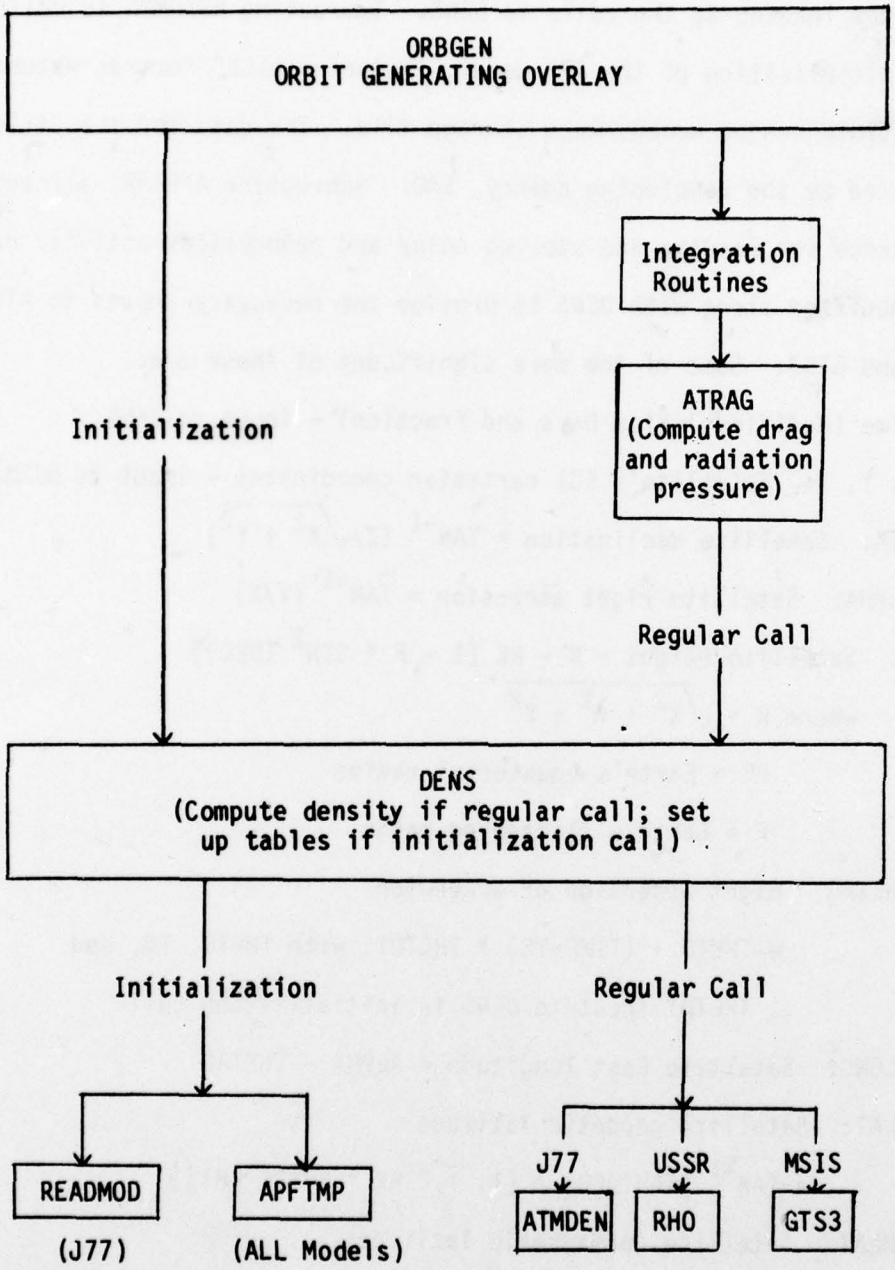

Figure 1. CELEST Density Model Flow

routines leading to the calls to DENS. Subroutine READMOD is called for initialization of the J77 model, including a CDC Fortran extended-compatible random access mass storage file. The data for this file was supplied by the developing agency, SAO. Subroutine APFTMP, already in existence for reading and storing solar and geophysical activity data, was modified along with DENS to provide the necessary inputs to ATMDEN, RHO and GTS3. Some of the more significant of these are:

Time (Modified Julian Days and Fraction) - input to DENS

X, Y, Z: Satellite's ECI cartesian coordinates - input to DENS

DEC: Satellite declination = $\text{TAN}^{-1}\ (Z/\sqrt{X^2 + Y^2})$

ALPHA: Satellite right ascension = $\text{TAN}^{-1}\ (Y/X)$

H: Satellite height = R - RE [1 - F * SIN^2 (DEC)]

where $R = \sqrt{X^2 + Y^2 + Z^2}$

RE = Earth's equatorial radius

F = Earth's flattening ratio

THETAG: Right ascension of Greenwich

= THETO + (TIME-TO) * THETDT, with THETO, TO, and THETDT input to DENS in initialization call

XLONG: Satellite East longitude = ALPHA - THETAG

GLAT: Satellite geodetic latitude

$= \text{TAN}^{-1}\ \{\text{TAN(DEC)} * [1. + 2\ \text{RE} * F/(\text{RE} + H)]\}$

GMLAT: Satellite geomagnetic latitude

$= \text{SIN}^{-1}\ [.9792\ \text{SIN(DEC)} + .2028\ \text{COS(DEC)}\ \text{COS(XLONG} - 291°)]$

RSUN, DSUN: Solar right ascension and declination, - obtained from already existing subroutine SOL

Solar Obliquity = 23.44°

Solar Distance = 1 A.U.

Solar and Geomagnetic Activity - From APFTMP

3.1.2 Separate Programs

Separate programs, SOVTEST and JAC77, have been produced as requested for the USSR and J77 models. The inputs include time (calendar date, hour, minute), height, west longitude, latitude, solar flux (smoothed and instantaneous) and geomagnetic activity index. These are input either interactively, using INTERCOM, or non-interactively, one card per computation desired. In the former case INTERCOM types a header to cue the user for typing in the data. From these inputs the quantities required for the subroutines are computed as described in section 3.1.1 except that solar position is obtained as described in Reference 8.

3.1.3 Ephemeris Prediction Accuracy Evaluations

Using program CELEST, updated as described in section 3.1.1, satellite ephemeris prediction accuracy evaluations may be carried out for the various models. For each density model and time span, two CELEST orbit determination runs are required: one for the initial fit span terminated by integration of trajectory into the prediction period, and a second run determining a second trajectory from a fit of data over this prediction period. The resulting trajectories can then be compared. A comparison of 5 models thus requires 10 CELEST runs per case. To streamline the procedure the system depicted in Figure 2 has been developed. Program CELUPF reads a set of run parameters from cards (usually only 2 cards are required). These include parameters of existing preprocessed observation permanent file, if any, parameters of output permanent file, day number to be processed, model indicator, indicators

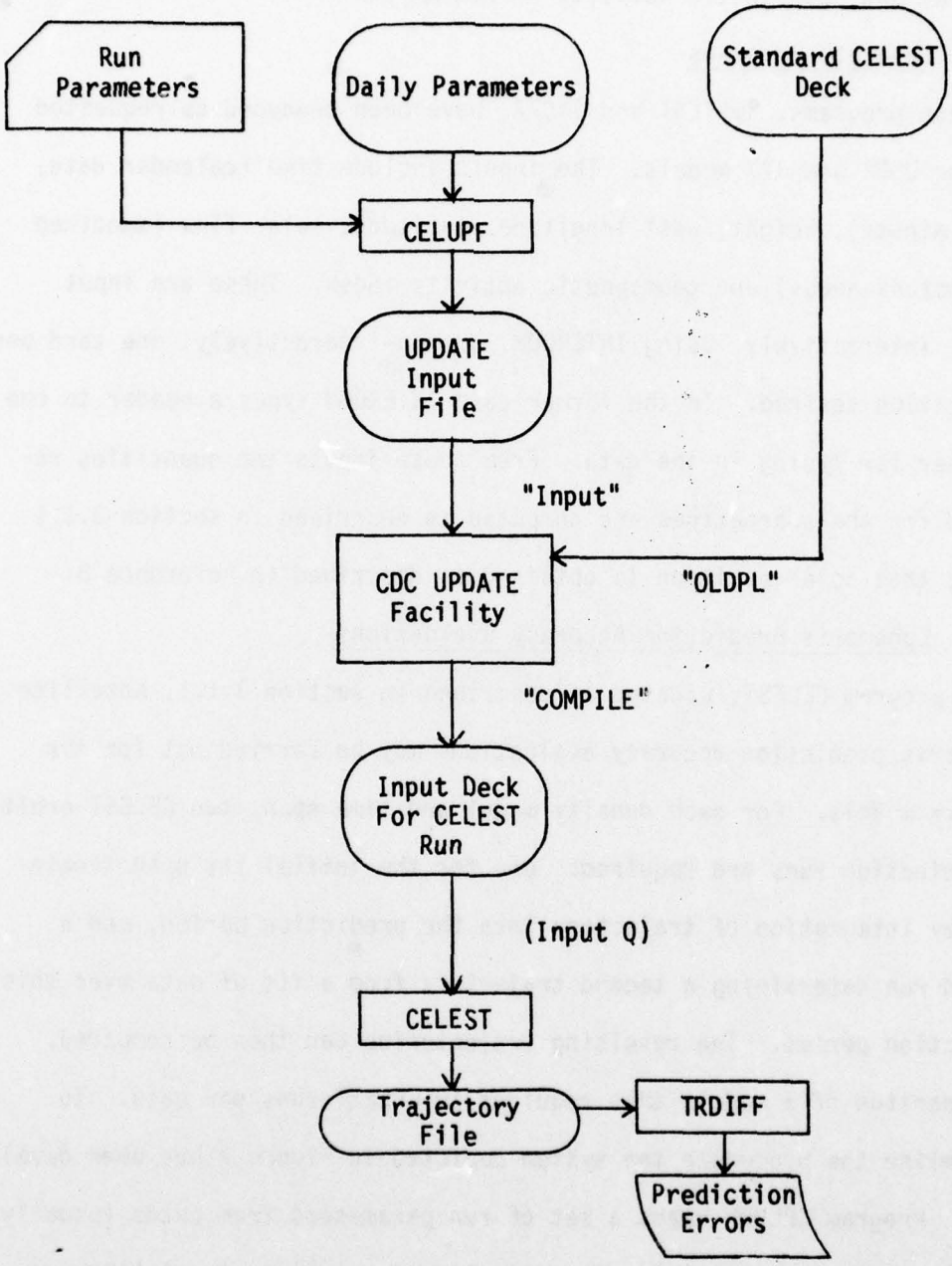

Figure 2. CELEST Run Setup

for any input or output initial conditions permanent files. These are combined with inputs from the "Daily Parameters" file, which are appropriate to the day number to be processed (daily polar motion, time span to be processed, initial conditions, etc.) to produce an input stream for the CDC UPDATE facility. Using this with a standard CELEST input deck, in program library format, as OLDPL, UPDATE creates the BCD file COMPILE which contains the desired CELEST run input deck suitable for routing to the input queue. The resulting run produces, as its main output, a trajectory file, plus optional updated initial conditions and/or preprocessed observation files.

When the required trajectory files (2 for each model) have been produced they may be input to TRDIFF to produce a printout of prediction errors of various components (radial, in-track, cross-track) for the different models for easy comparison.

3.2 Density Modeling - Stepwise Multiple Regression

A stepwise multiple regression program to produce empirical density models from experimental data has been developed from the IBM Scientific Subroutine Package Program STEPR.[9] This program fits the density data to the functional form

$$\rho = a_0 + \sum_{i=1}^{m} a_i F_i$$

where the a_i are the adjustable coefficients to be determined and the variables F_i are functions of various correlative parameters such as solar flux, geomagnetic activity, etc.

Models are constructed from successively larger subsets of the variables F_i, in each step adding the variable which most reduces the residuals between model and data. After each step, the latest model is output with statistics and the procedure terminated or continued according to the percentage reduction in residuals in this step.

Figure 3 shows a block diagram of the program. The major addition is the user supplied routine PREPRO to generate the observation file required by DATA. This is called only if the number of observations specified on the parameter input card read by STEPR is not positive; i.e., if the required data file already exists, the call to this routine can be skipped. The actual number of observations is re-

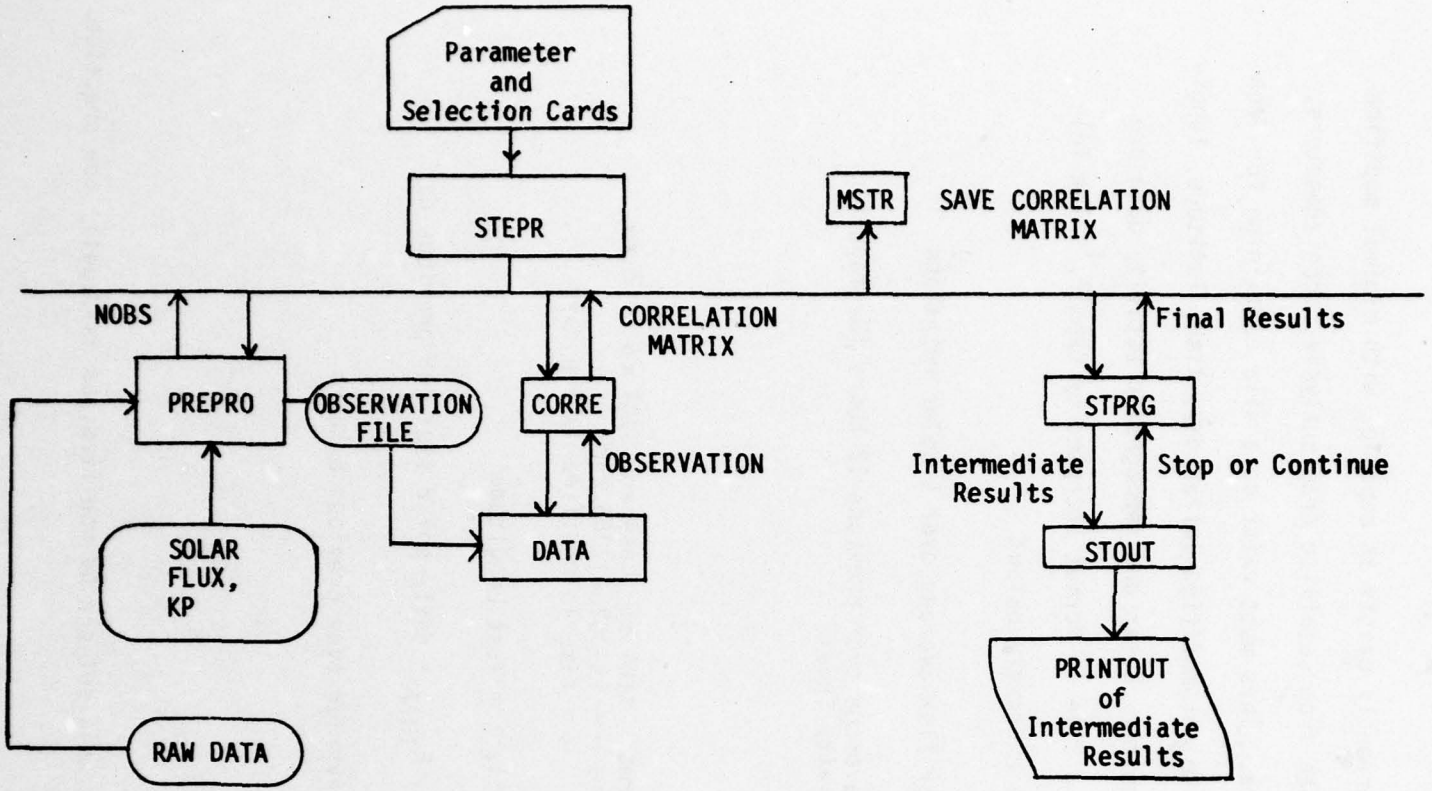

Figure 3. Multiple Regression Program STEPR

turned by this routine to STEPR for use by the other structures.

The version which currently exists is capable, with minimal modification, of handling data from satellite drag analysis, accelerometers, or mass spectrometers. This must exist on a file containing for each observation: the date, or modified Julian day, time, latitude, longitude, height and density. Solar and geomagnetic activity data are assumed to exist on a file in format accepted by CADNIP.[1] The following variables are currently output

$\overline{F_{10.7}}$ Solar flux average over 4 solar rotations

$\langle KP \rangle_{12}$ KP average over previous 12 hours (Geomagnetic activity index

$\left(\overline{F_{10.7}}\right)^2$

semiannual terms: $\sin 4\pi\alpha$, $\cos 4\pi\alpha$, $\sin 4\pi\alpha \cos 2\pi\alpha$,
where $\alpha = (t-36204)/365.2422$
t = time in modified Julian days

$\cos 2(\lambda + 30°)$, λ = West Longitude

$F_{10.7} - \overline{F_{10.7}}$, $F_{10.7}$ = daily solar flux for previous day

$\langle KP \rangle_6$ KP average over previous 6 hours

KP(t-3hr)

Density

With minimal effort this set can be modified, as is usually the practice.

3.3 Accelerometer Data Support

Traditional satellite orbit determinations by CADNIP and CELEST provide useful checks or comparison for accelerometer measurements made on board the same satellite, in addition to providing drag density data. If high quality Doppler Beacon observations are available, CELEST is particularly useful because of the capability to subdivide the drag into 4-6 hour segments.

Data has been requested by AFGL and received from Defense Mapping Agency (DMA) for satellite DB-16, including the following:

1) Preprocessed observation files in BCD format, for specific time periods

2) Punch card deck containing data for Sun-Moon/coordinate transformation file

3) Sample output of CELEST run

4) Thrust start-stop times and values (TWX reports).

Data was transmitted by BCD to circumvent incompatibilities between DMA's Univac 1100 and AFGL's CDC 6600. This data has been successfully converted to files needed by CELEST with programs DMABIN (for the preprocessed observations) and SNMNBN (for Sun-Moon/transformation data). Because preprocessed data has been supplied it will not be necessary to enter CELEST's preprocessor module, as was done for satellites DB-7 through DB-9. Thus the rather large station data file is not needed.

CELEST is now totally operational with this data.

References

1. Bramson, A. S., and Slowey, J. W., "Some Recent Innovations in Atmospheric Density Programs", AFCRL-TR-74-0370, 1974.

2. O'Toole, J. W., "Naval Surface Weapons Center Reduction and Analysis of Doppler Satellite Receivers Using the CELEST Computer Program", Satellite Doppler Positioning, Volume 2 of Proceedings of the International Geodetic Symposium, October 1976.

3. Private Communication, K. S. W. Champion, J. M. Forbes, H. B. Garrett, and J. W. Slowey.

4. Jacchia, L. G., "Thermospheric Temperature, Density, and Composition: New Models", Smithsonian Astrophysical Observatory, Special Report Number 375, 1977.

5. Hedin, A. E., Salah, J. E., Evans, J. V., Reber, C. A., Newton, G. P., Spencer, N. W., Kayser, D. C., Alcayde, D., Bauer, P., Cogger, L., and McClure, J. P., "A Global Thermospheric Model Based on Mass Spectrometer and Incoherent Scatter Data - MSIS 1. N_2 Density and Temperature", J. Geophys. Res. 82, P. 2139, 1977.; Hedin, A. E., Reber, C. A., Newton, G. P., Spencer, N. W., Brinton, H. C., Mayr, H. G., and Potter, W. E., "A Global Thermospheric Model Based on

AD-A062 488 LOGICON INC LEXINGTON MA F/G 4/1
RESEARCH, ANALYSIS, DEVELOPMENT, AND APPLICATION OF HIGHLY INTE--ETC(U)
OCT 78 J N BASS, K H BHAVNANI, S T LAI F19628-78-C-0049
UNCLASSIFIED AFGL-TR-78-0204 NL

2 OF 3
AD
A062488

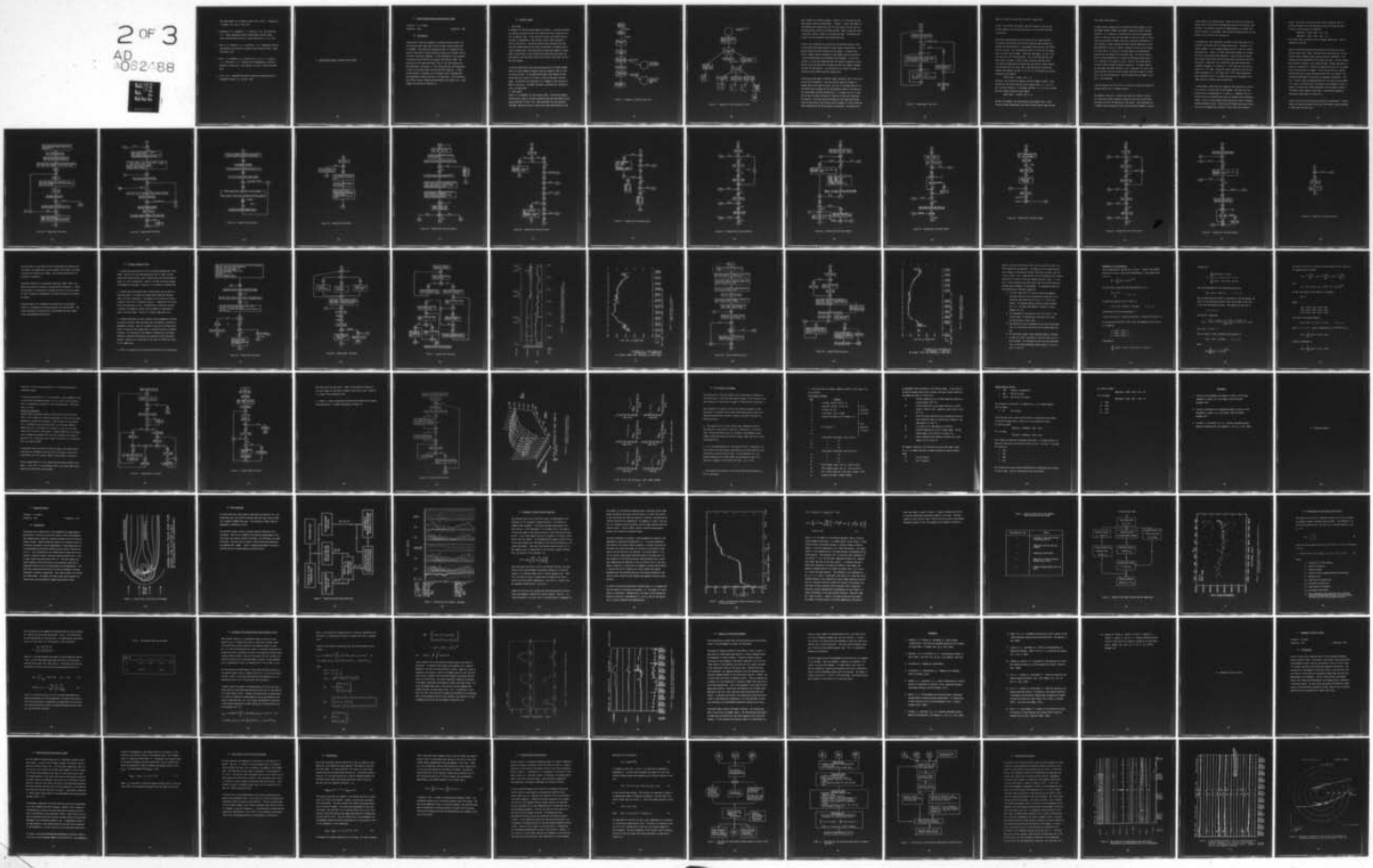

Mass Spectrometer and Incoherent Scatter Data - MSIS 2. Composition", J. Geophys. Res., 82, p. 2148, 1977.

6. Elyasberg, P. E., Kugaenko, B. V., Synitsyn, V. M., and Voiskovsky, M. I., "Upper Atmosphere Density Determination from the Cosmos Satellite Deceleration Results", Space Research XII, p. 727, 1972.

7. Bass, J. N., Bhavnani, K. H., and Hussey, I. M., "Atmospheric Density Determination from Analysis of Doppler Beacon Satellite Data", AFCRL-TR-75-0176, 1975.

8. Bass, J. N., Bhavnani, K. H., Hurwitz, M. G., Lai, S. T., Stancik, J. L., and Whelan, L. A., "Analysis and Programming for Scientific Research", (Logicon Inc. Final Report), pp. 106-7, AFCRL-TR-74-0480, 1974.

9. I.B.M., Inc., "System/360 Scientific Subroutine Package Version III Programmer's Manual", pp. 413-418, 1970.

4. Defense Meteorological Systems Project (DMSP)

4. Defense Meteorological Systems Project (DMSP)

Initiator: R. C. Sagalyn

Project No: DMSP Problem No: 4836

4.0 Introduction

Program SSIE is the main program of a system to process special ion and electron sensor data from a series of polar orbiting satellites of the DMSP. The program was developd at AFGL for integration into the real time satellite data processing system at Air Weather Service, Offutt Air Force Base, Nebraska. In the development it was necessary to simulate the AWS UNIVAC 1110 System on the AFGL CDC 6600. The structures of the input and output files for the SSIE program have been described in Reference 1. This report describes the integration of SSIE into the AWS System, and into the AFGL operation. At AFGL the AWS system is simulated, and in addition several programs have been developed to display the data in various ways. Since Reference 1 was written, several changes have been made to the output file. These changes are described in Section 4.3.

4.1 AWS/AFGL System

1. AWS System

A schematic for the AWS System appears as Figure 1. Currents generated by electrons and positive ions are recorded from their respective sensors on magnetic tape. As the satellite passes over ground stations, the data is telemetered as the recorder rewinds (hence backward in time) to the station. The ground station then retransmits the data from that readout (usually one orbit) to AWS where it becomes preprocessor program input. The preprocessor program adds ephemeris information to each minute of data creating one minute data sets which are then placed in the raw data circular file, which is the input file for the SSIE program.

In the pre-operational phase the pre-processed file at Global Weather Central has been dumped to magnetic tape and shipped to AFGL to save for future studies. In the operational phase, SSIE outputs the processed data to a circular file which is used for GWC modelling programs. Periodically the processed file is dumped to tape and sent to NOAA for archiving. From NOAA, the data is available to a variety of users, including AFGL.

2. AFGL System

Figure 2 is a schematic for the system at AFGL. During the pre-operational phase, input to the AFGL system has been the tape copies of the preprocessed AWS circular file. When processed files are available from NOAA, they may be used as input after minor modifications to the

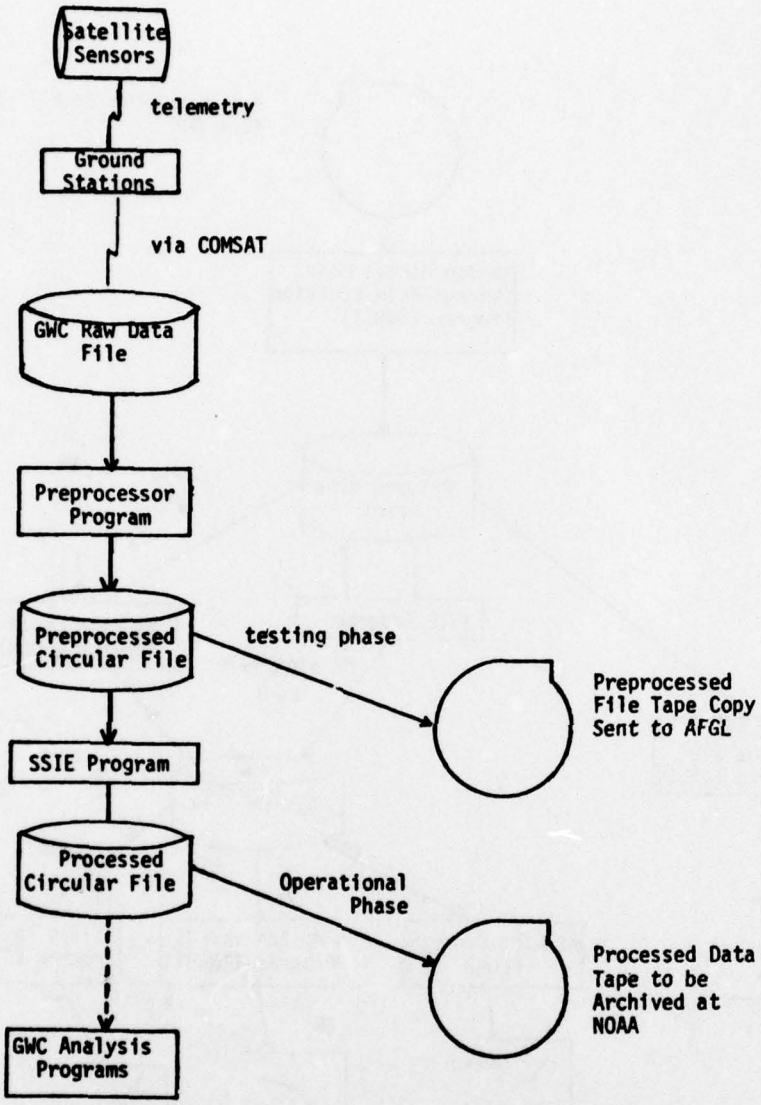

Figure 1. Schematic of GWC SSIE Data Flow

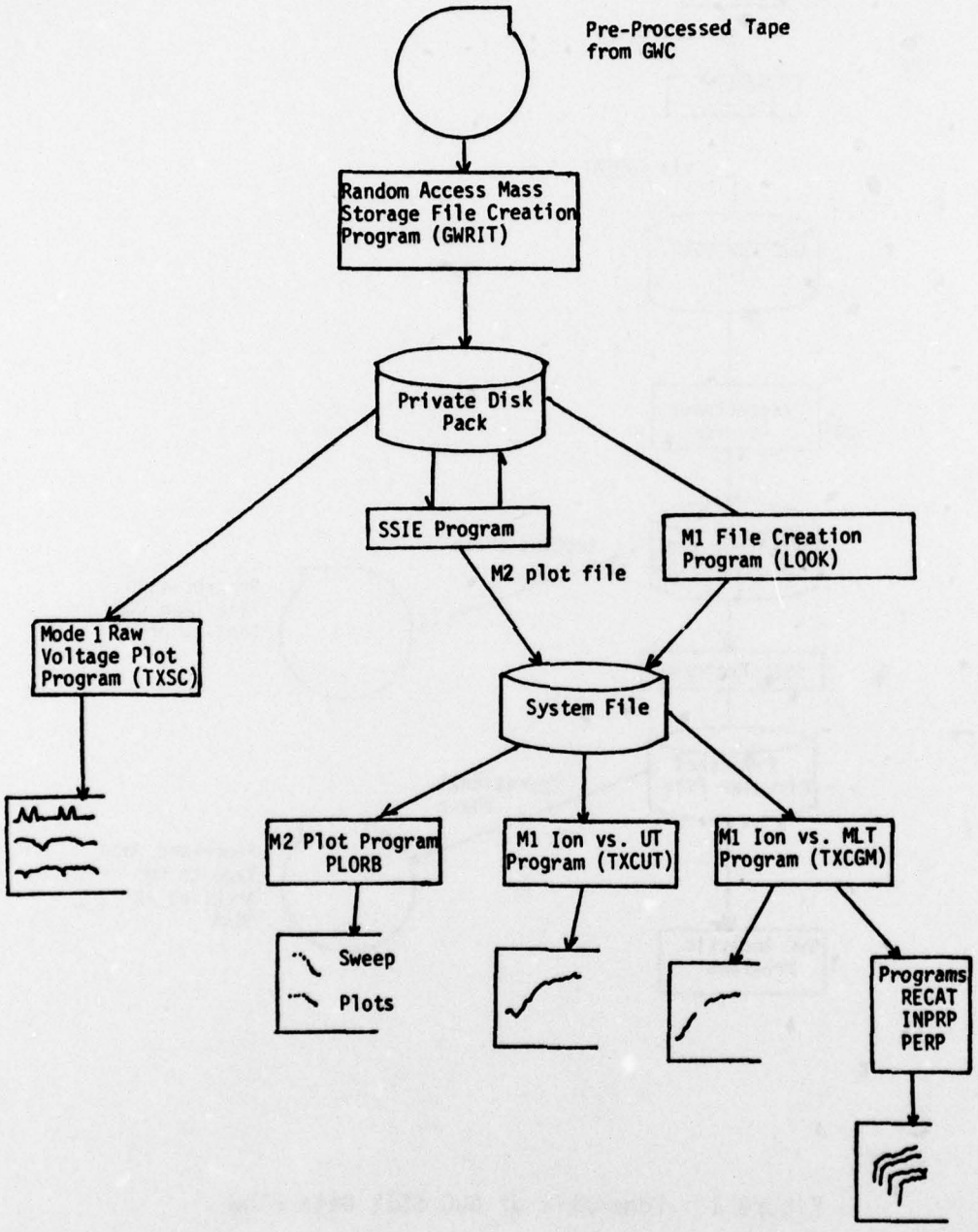

Figure 2. Schematic of SSIE Processing at AFGL

mass storage file creation program. Figure 3 is a flow chart for the mass storage creation program GWRIT. In GWRIT, L counts the number of 1120 UNIVAC word records read, and M is the count of the 112 word addressable blocks written on CDC mass storage. GWRIT creates the input to the AFGL version of SSIE on a private disk pack. The output (processed) file also resides on the private disk pack.

In the first instrument to carry the ion and electron sensors, noise in the monitor word amplification circuit caused irregularities in the monitor words during the electron and ion sweeps. In normal operations, however, applied voltages for the sweeps would be obtained by a linear transformation on the monitor word voltages. In the first satellite, it has been determined that the nominal voltages are nearly correct, and since the actual voltages are noisy the nominal voltages are used for the analysis. The electron and ion nominal voltages are carried in arrays APEVL and APIVL respectively.

Provision has been made in SSIE for normal operation, that is for valid monitor word information. Over one electron sweep (10 seconds in length) there are 60 monitor words, and over an ion sweep there are 72. The monitor word voltages and the corresponding times are collected in the arrays EMVOL and EMTIM respectively. A straight line fit is done on this data to obtain voltage as a function of time with intercept A and slope B. The actual applied voltages are then obtained from the times of data words of the electron and ion sweeps (in arrays XTIME and XTIMI respectively) and the straight line equation. The applied vol-

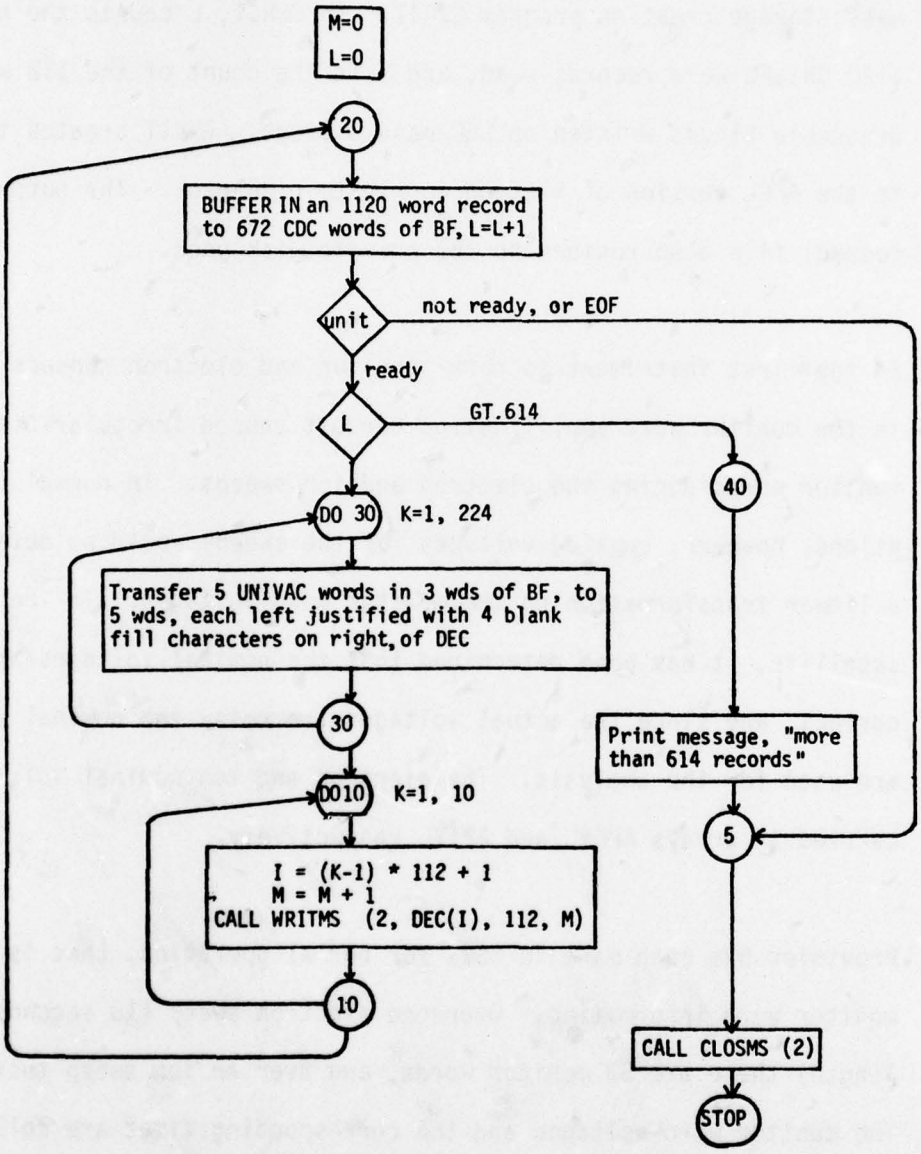

Figure 3. Program GWRIT Flow Chart

tages are stored in arrays APEVL and APIVL respectively.

In SSIE, lines 43-62, the nominal applied voltages for the ion and electron sweeps are calculated and placed in arrays APIVL and APEVL respectively.

Since each second contains 20 data words, the ion sweep (duration 12 seconds) has 240 data points and the electron sweep (duration 10 seconds) has 200 data points. Both sweeps start with the last monitor word in a second. This starting point then is -5V for the ion sweep, and 5V for the electron sweep. The end of the sweep is at 12V in the ion case and at -8V in the electron. Thus in filling the APIVL and APEVL arrays, we take, in the ion case, 84 points from the 240 by calculating voltage at the 2nd point (the last of the initial second), then the 2nd, 5th, 7th, 11th, 14th, 17th, 20th points from the 2nd through 12th seconds, and the 2, 5, 8, 11, 14, 17 from the last second according to the formula

APIVL (KAP) = 17/240 * (M-1) - 5.

Similarly, we calculate the nominal electron voltages in APEVL, using the next to last point from the initial second, the 1, 4, 7, 10, 13, 16, 17 points from the 2 - 10 seconds, and the 1, 4, 7, 10, 13, 16 from the last second according to the formula

APEVL (KAP) = -13/209 * (M-1) + 5.

The GWC 1110 computer has random access mass storage files. These files are sector addressable, each sector being 28 words long, and the

first sector being sector 0.

To mimic the GWC random access on the AFGL CDC 6600 computer, we use the READMS, WRITMS, OPENMS, and CLOSEMS, random access mass storage functions. It is possible to directly mimic the 28 word addressable sectors in this way, but since the number of sectors at GWC is usually large (on the order of 25000), and since at AFGL each addressable record requires an index, directly mimicking the GWC RAMS would utilize large portions of core for indeces. Because of this and also because all I/O at GWC is in 112 wd, or 4 sector modules, the addressable records at GL are chosen to be 112 words long. This would indicate that all sector addresses of I/O blocks at GWC would be multiples of 4 (-1 since the first sector is at 0). Thus for the record address of sector #ISAD, we would divide by 4 and add 1. To ensure against the case where the sector address is not a 4 multiple, we read in two 112 wd records, the first at the integer less than or equal to ISAD/4 plus 1, and the following one. Then we tabulate by the number of sectors in the remainder.

Line 309 through line 331 of SSIE is a section to calculate spacecraft average velocity for a 1 minute interval.

The ephemeris group of a 1 minute input data set contains in words 11-13 the earth center coordinate cosines for the end of the minute, and words 14-16 for the beginning of the minute. The coordinates are in UNIVAC 1100 floating point form, and the routine BLKCONV is used to

convert them to CDC floating point. FACTA and FACTB are latitude corrected radii of the earth at the beginning and end of the minute, respectively. The distance travelled is approximated by a straight line and the velocity is calculated. AVEL contains average velocity for the minute, and is available for further use.

In program SSIE, the arrays AMPEL and AMPIO contain logs (base 10) of currents from electron and ion sweeps respectively. The data is received, however, in raw voltages between 0 and 5.11 volts in digital form from 0-511. There is a linear relationship between raw voltages and logs of the currents they represent. There are two calibration cycles every 1024 seconds, which are detected by the monitor word voltage level. During the first calibration cycle the electron word voltages correspond to a current of -1×10^{-6} amps and ion word voltages to 5×10^{-8} amps. During the second calibration cycle the voltages correspond to -1×10^{-9} amps and 5×10^{-11} amps respectively. Each calibration cycle is 2 seconds long and thus corresponds to 14 sample points of electron and ion data words.

In the program, calibrations are flagged by the variables IC1 and IC2. IC1 is set at -1 at the start of the program. When the first calibration cycle is encountered, IC1 is set to 1. Otherwise, IC1 is 1 during the first calibration cycle and 0 in between first calibration cycles. IC2 is 1 during second calibration cycles, and 0 in between second calibration cycles. During the calibration cycles the 14 electron and ion voltages are collected in KC1E, KC2E, KC1I, and KC2I

arrays. At the end of the calibration cycles, subroutine CAL1B is called to average the 14 voltage arrays, and to calculate the coefficients in the straight line equations

```
AMPEL(NEL) = AINE + BSLE * IEL * .01
AMPIO(NIO) = AINI + BSLI * ION * .01
```

which gives logs of electron and ion voltages respectively, from raw voltages IEL and ION.

Several plotting programs have been written to display the ion and electron sensor data. Mode 1 raw data plots display monitor, ion and electron sensor voltages versus time and location information. The program uses the preprocessed file directly as input. The SSIE program has an option to create a file containing mode 2 (sweep) data which is placed on a system file. The M2 plot program uses this file to produce plots of electron and ion sweeps. The M1 ion density file creation program LOOK uses as input the preprocessed file, and creates a file containing approximate ion densities and ephemeris information. This file is used as input to programs which plot ion density versus ephemeris linear in universal time; ion density versus ephemeris linear in magnetic latitude; and a three dimensional plot of several orbits of ion density versus magnetic local time. The plotting programs are described in more detail in Section 4.2.

Figures 4 and 5 are flow charts of the logic of program SSIE. Figure 4 covers the input and output of data sets, and Figure 5 covers handling of data within the data sets.

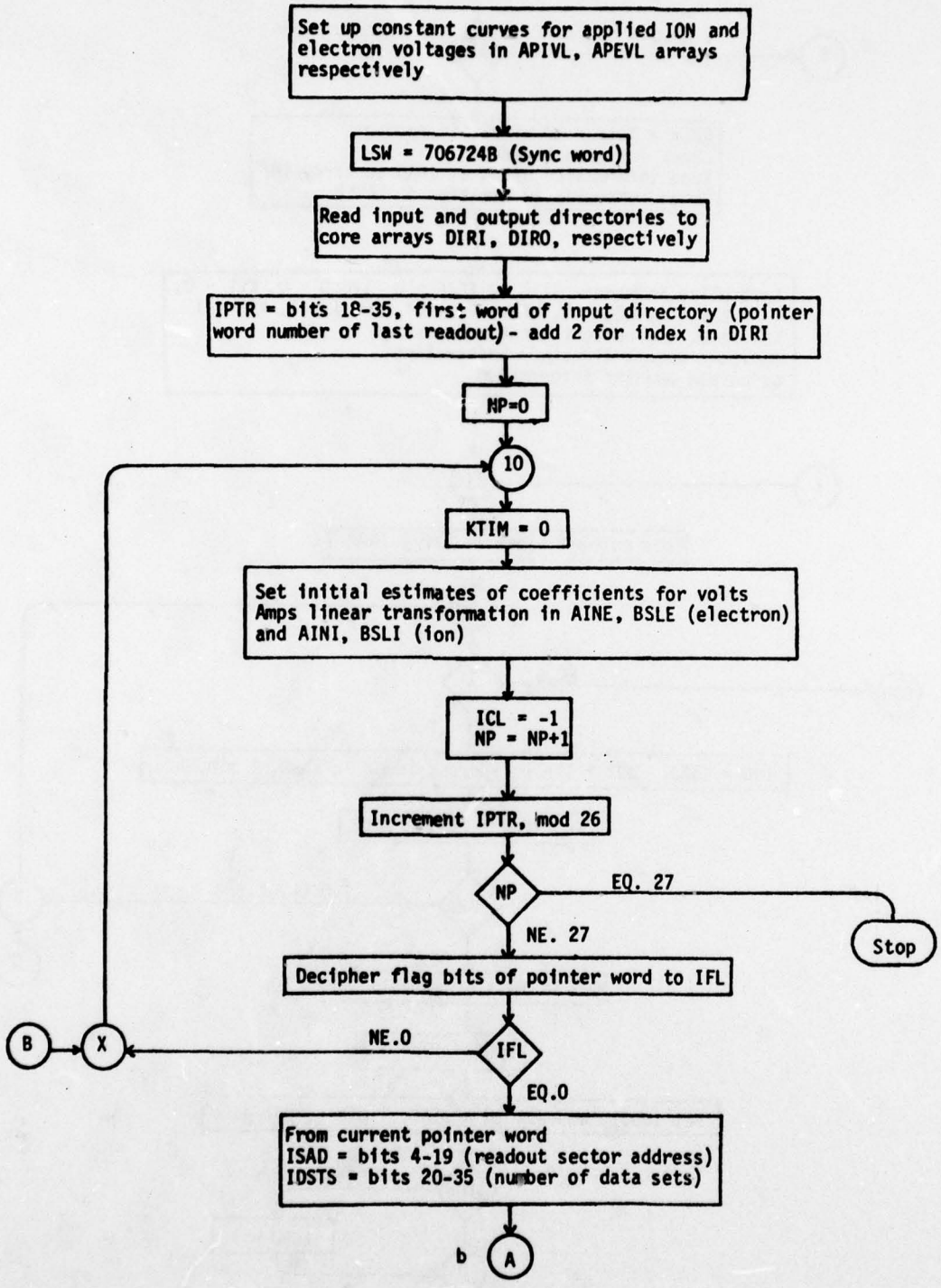

Figure 4a. Program SSIE Flow Chart

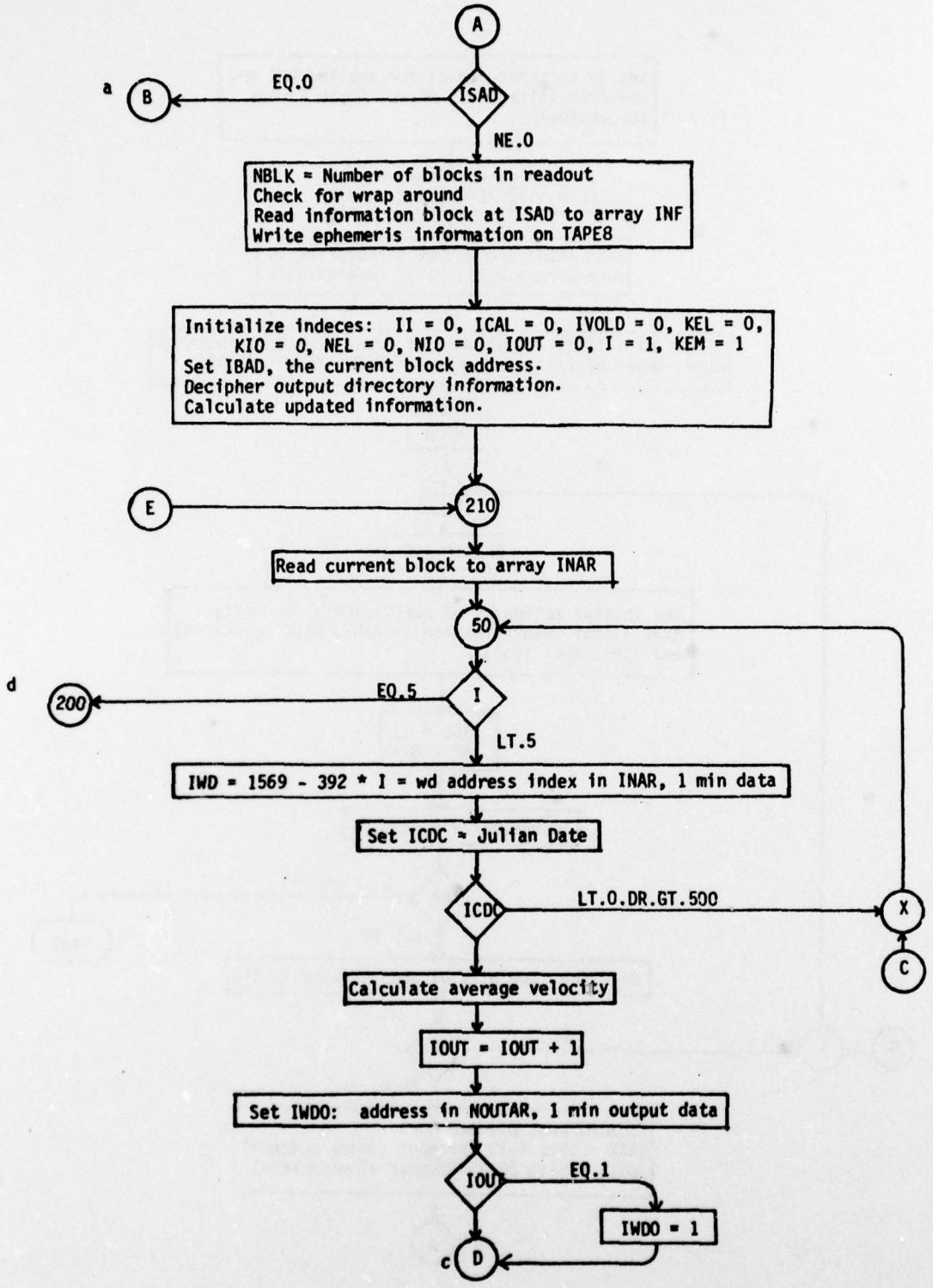

Figure 4b. Program SSIE Flow Chart

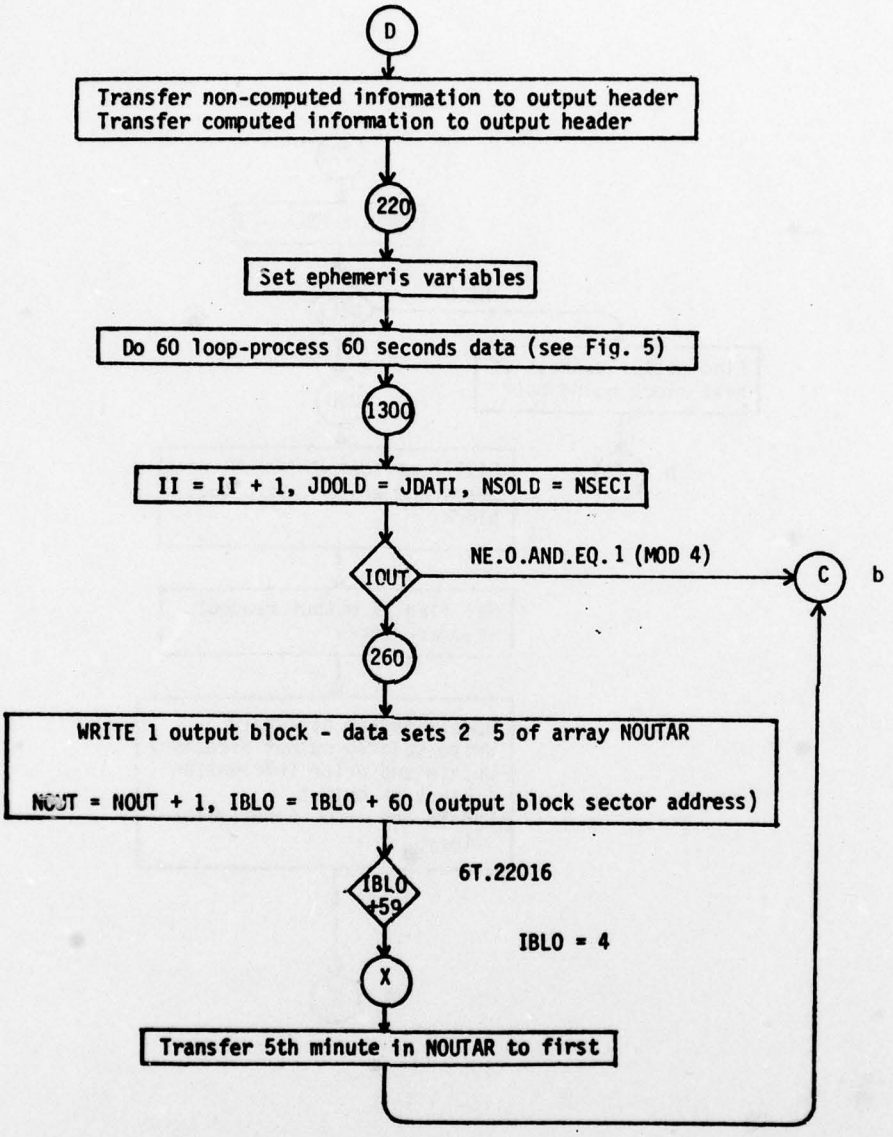

Figure 4c. Program SSIE Flow Chart

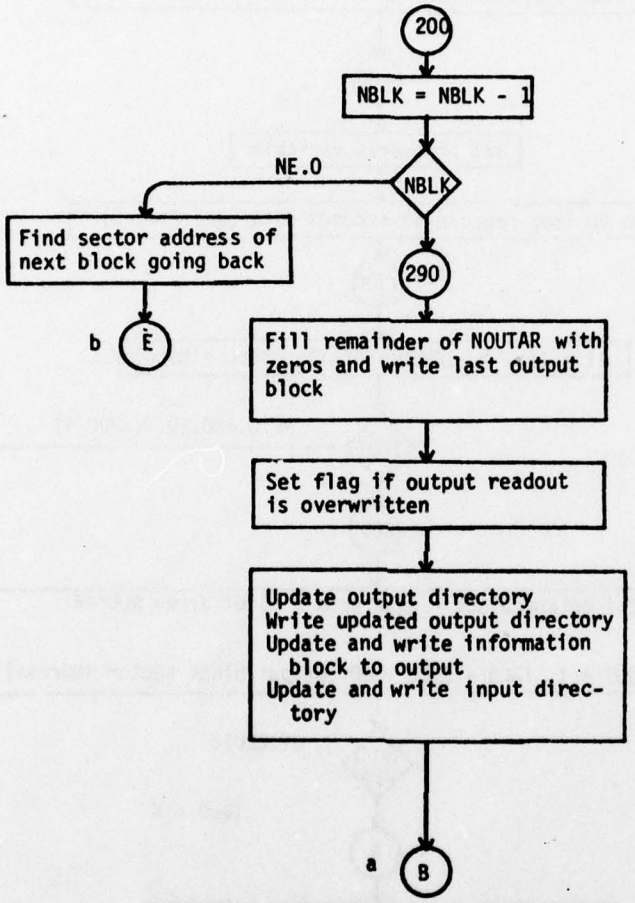

Figure 4d. Program SSIE Flow Chart

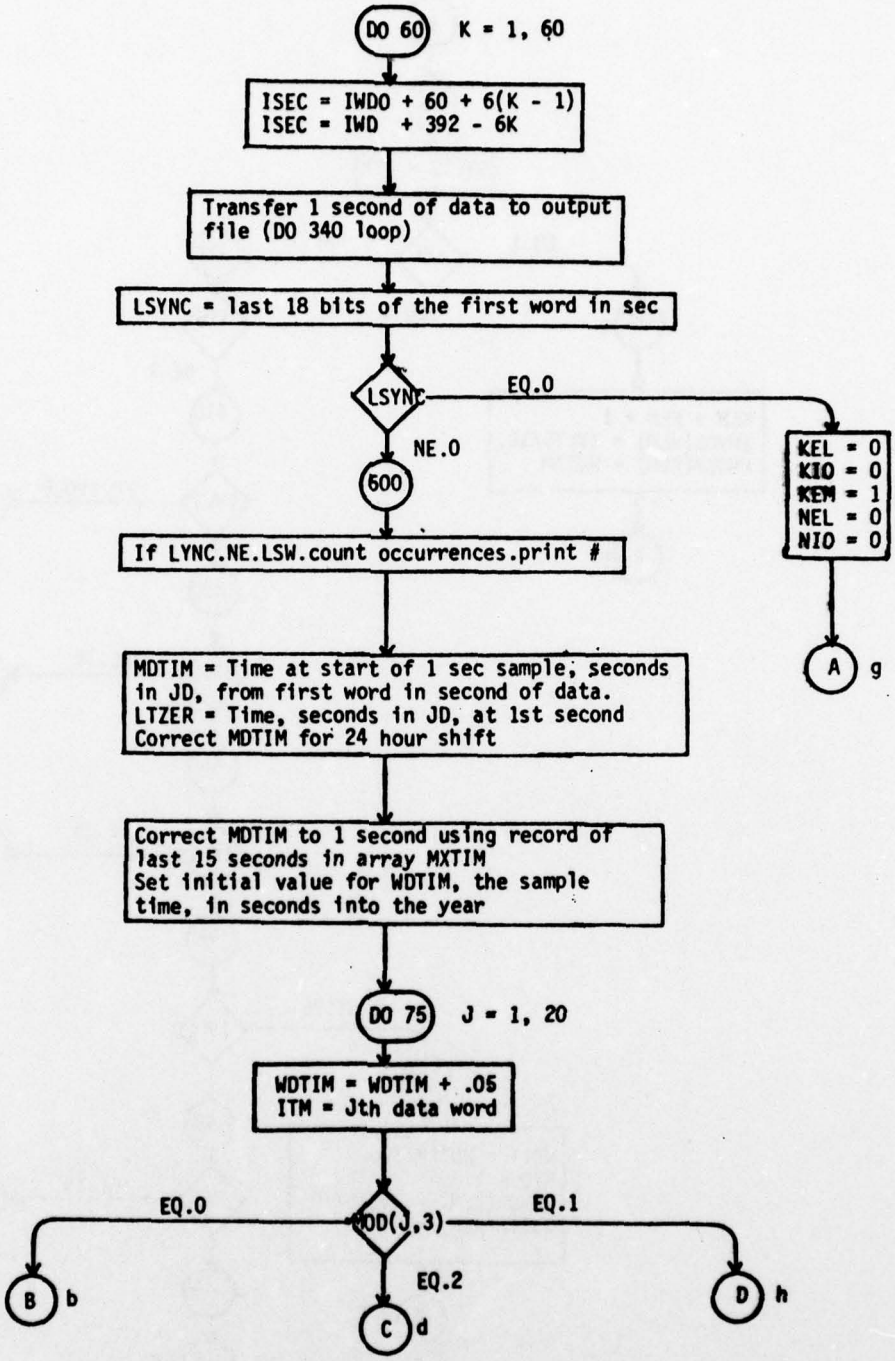

Figure 5a. Program SSIE Flow Chart Detail

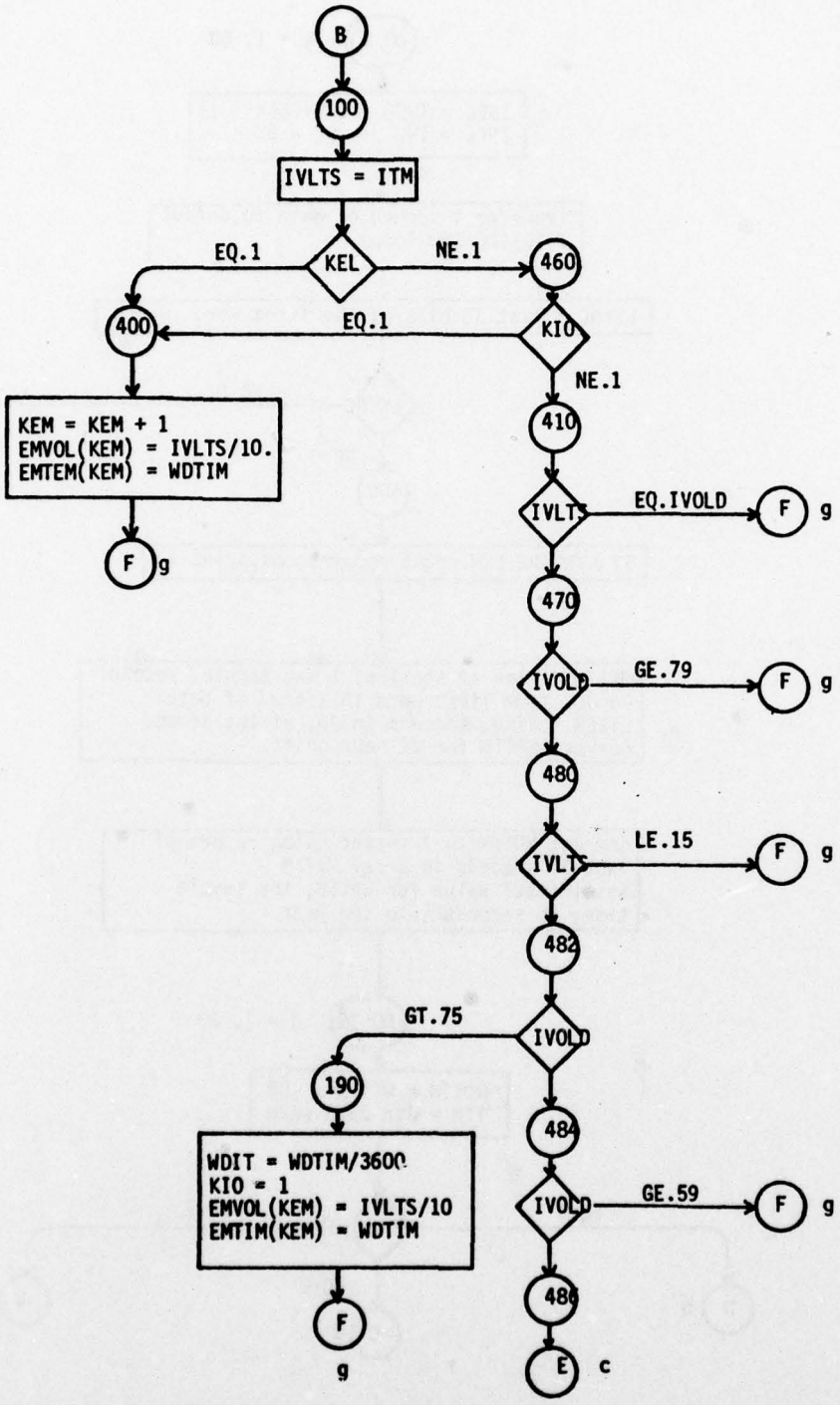

Figure 5b. Program SSIE Flow Chart Detail

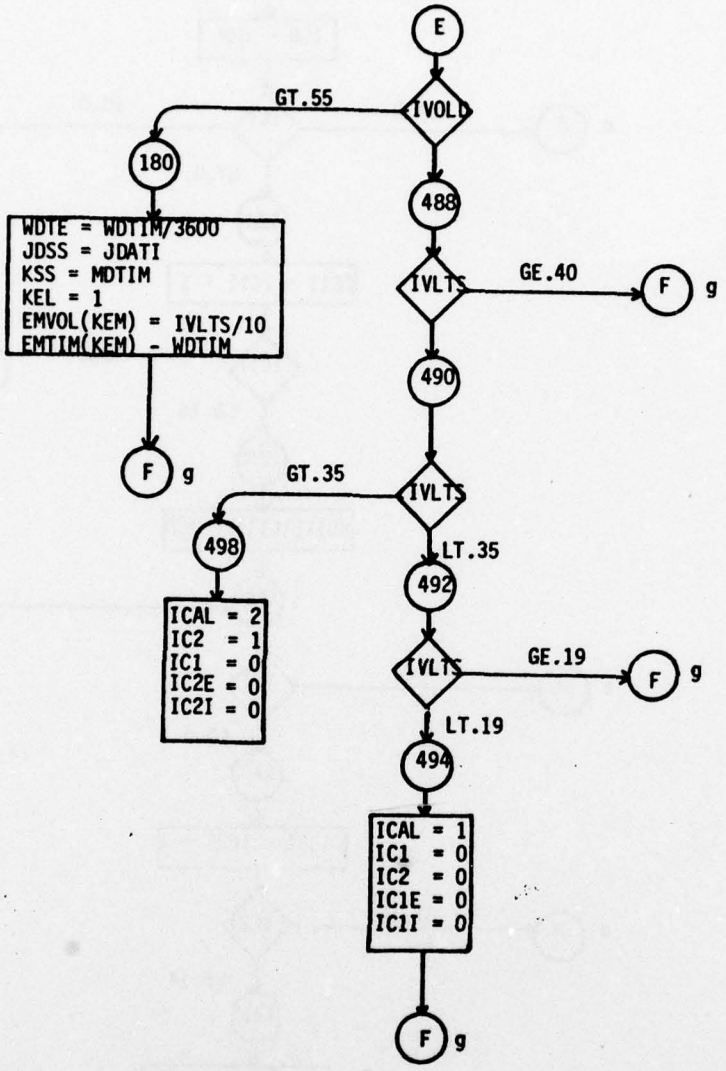

Figure 5c. Program SSIE Flow Chart Detail

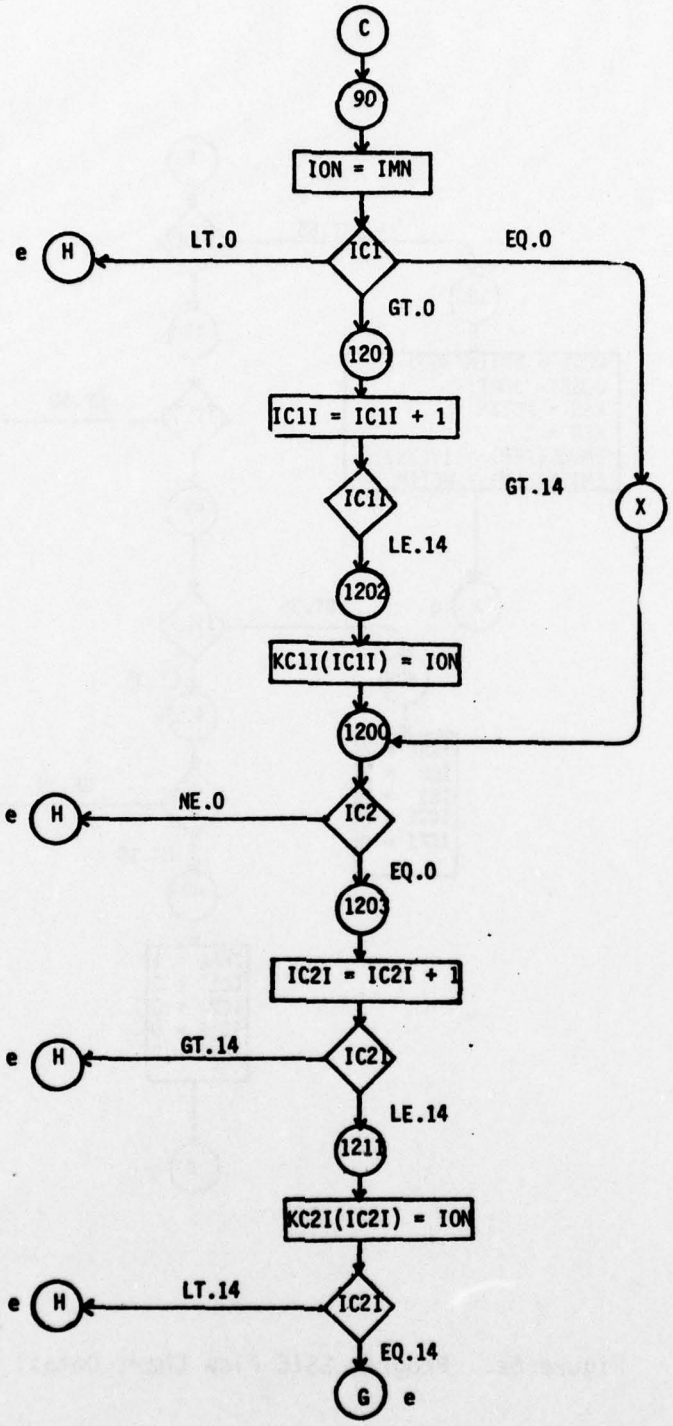

Figure 5d. Program SSIE Flow Chart Detail

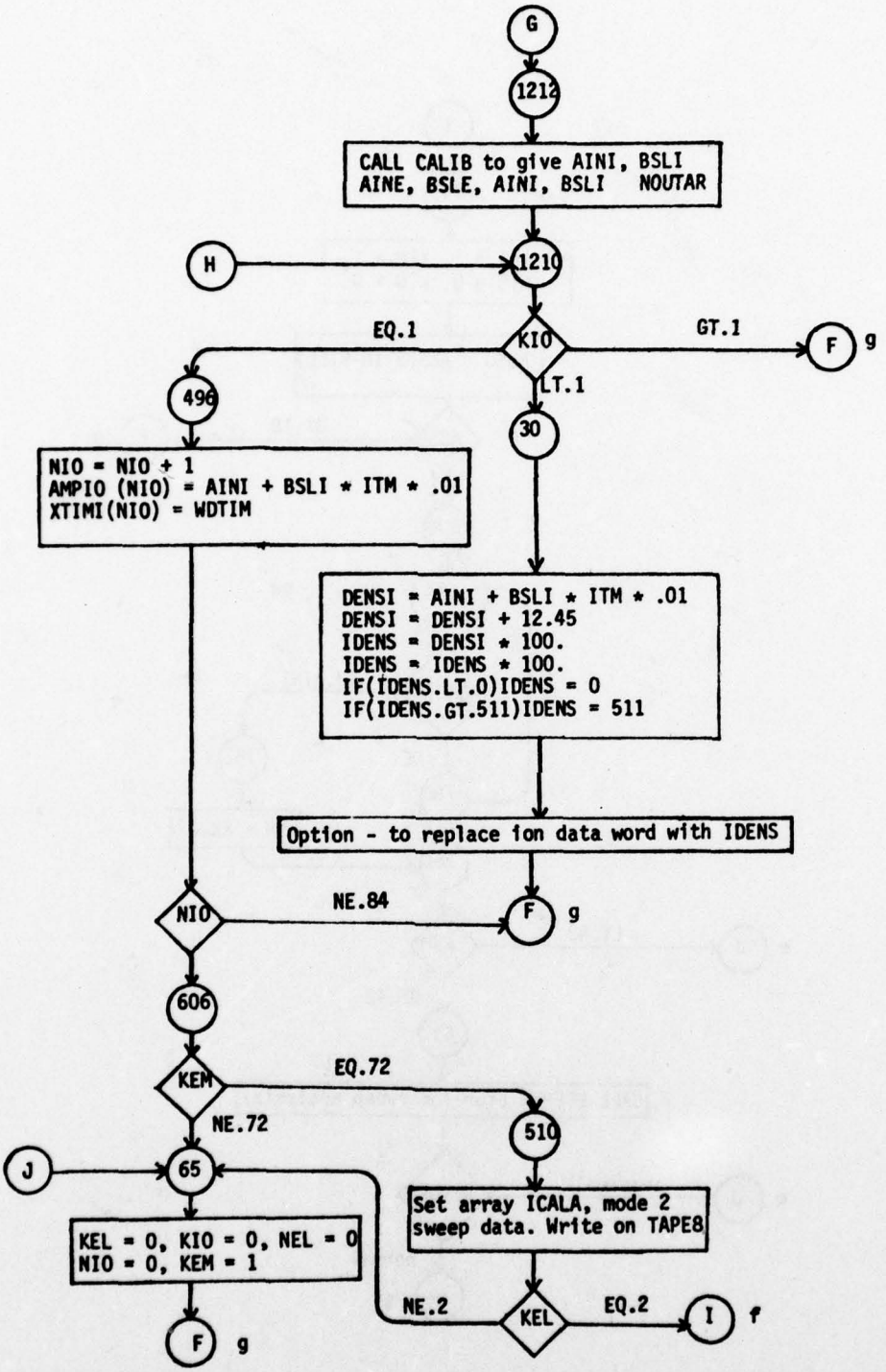

Figure 5e. Program SSIE Flow Chart Detail

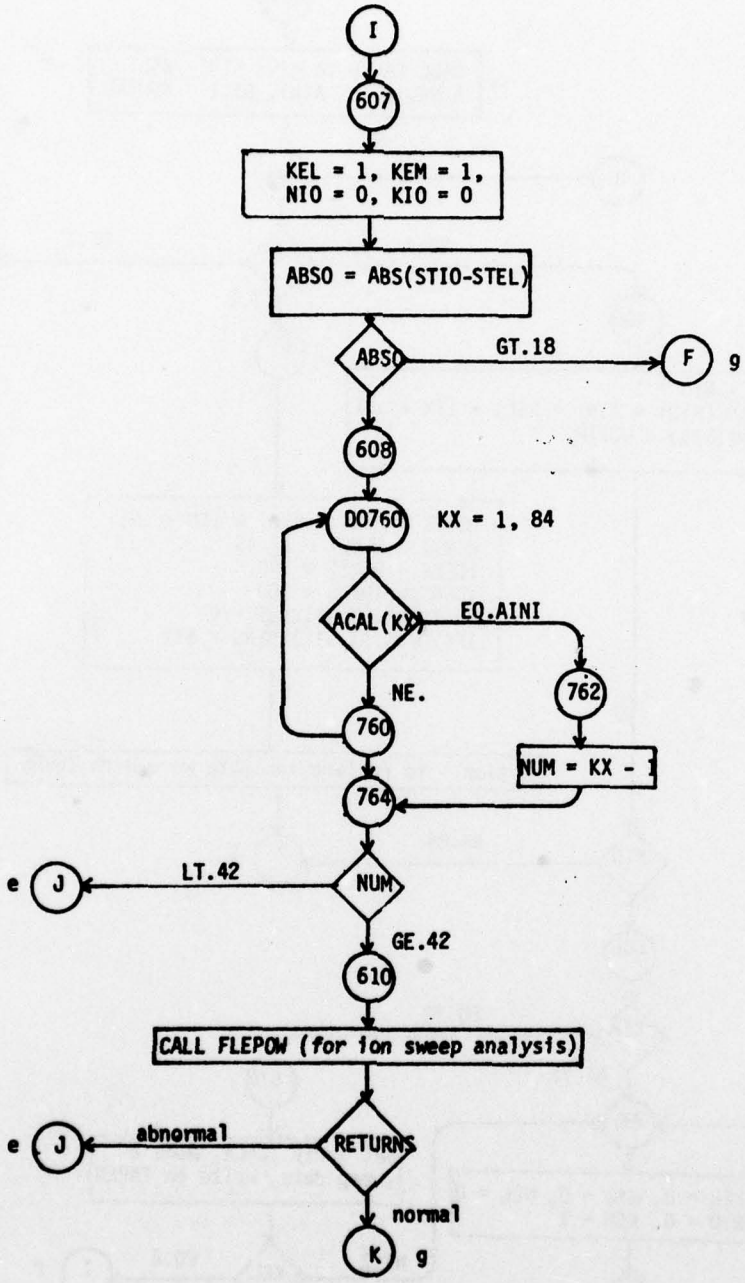

Figure 5f. Program SSIE Flow Chart Detail

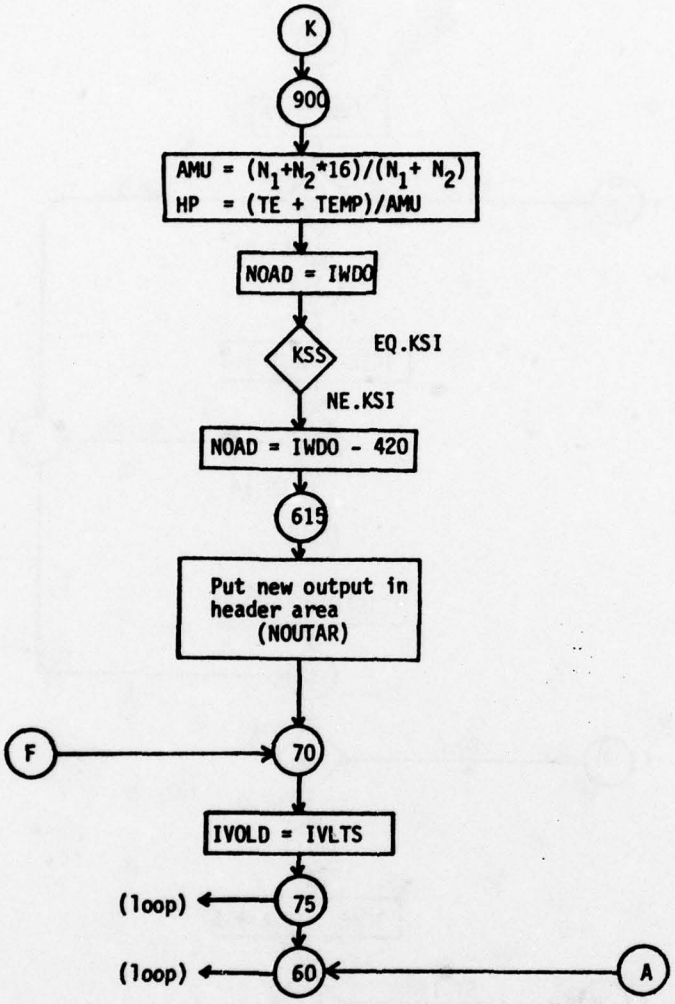

Figure 5g. Program SSIE Flow Chart Detail

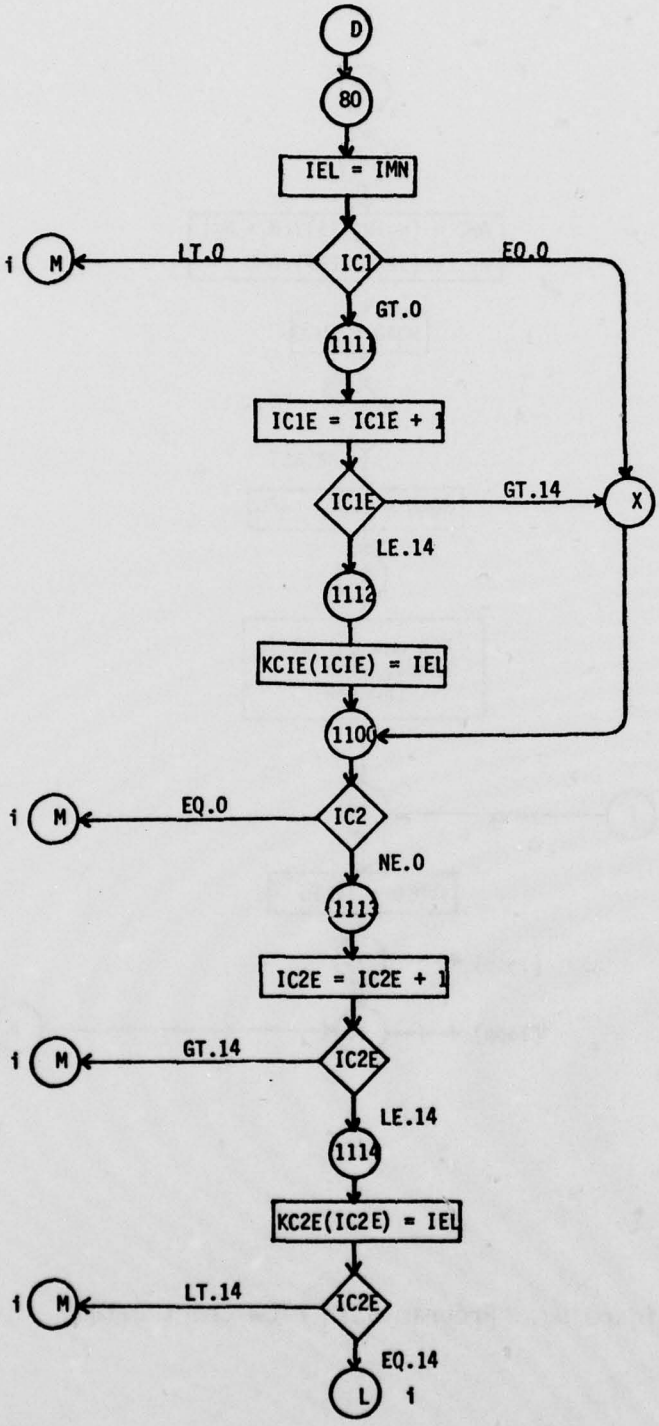

Figure 5h. Program SSIE Flow Chart Detail

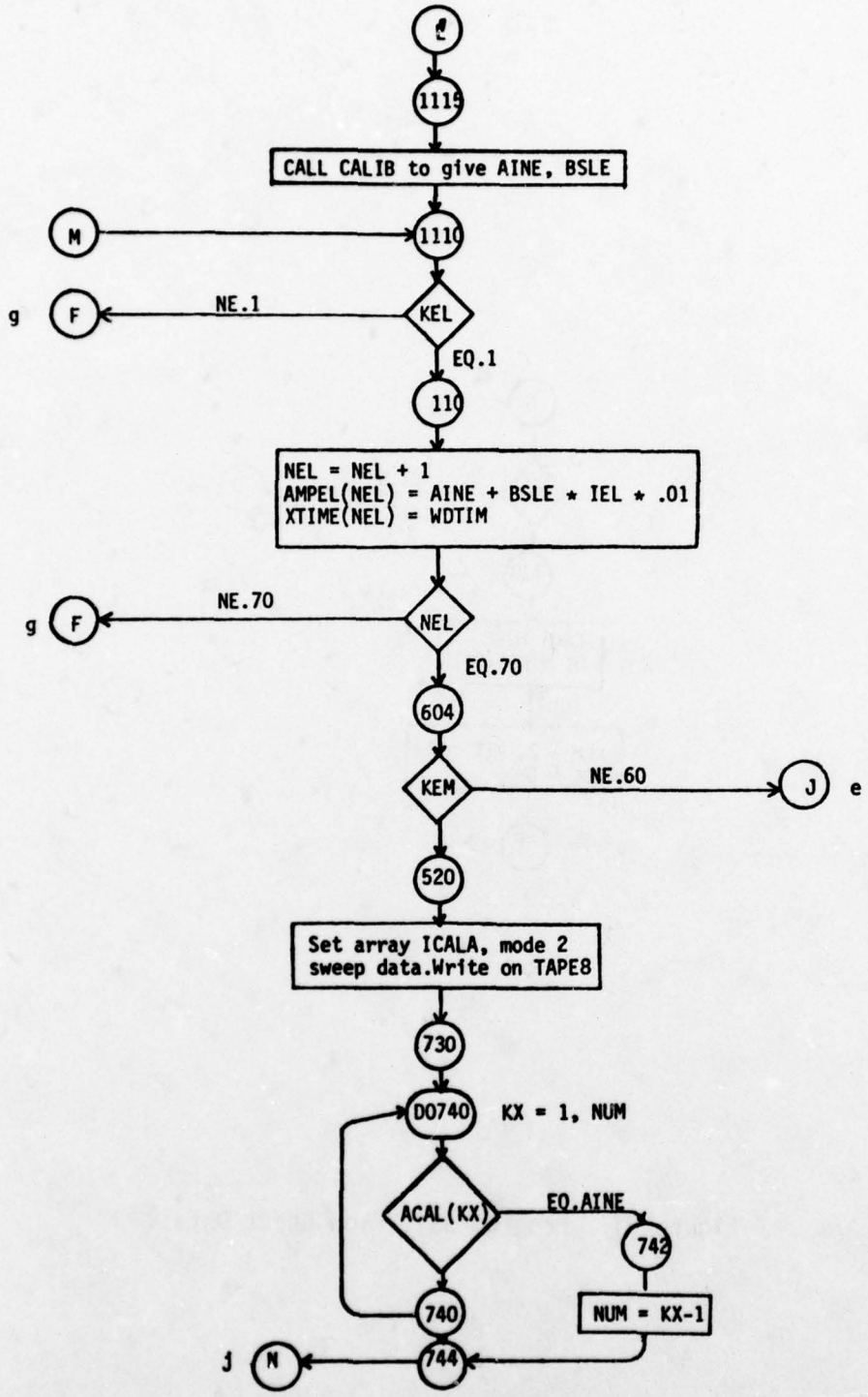

Figure 5i. Program SSIE Flow Chart Detail

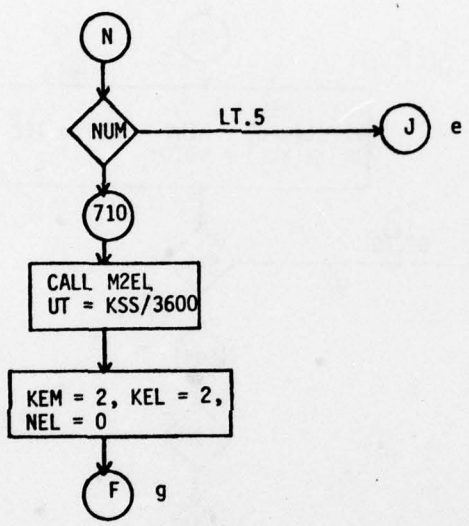

Figure 5j. Program SSIE Flow Chart Detail

Subroutine M2EL utilizes mode 2 electron sweep data and produces electron density and temperature, vehicle potential with respect to plasma, and current at resting bias voltage. The electron sweep analysis is discussed in Reference 1.

Subroutine FLEPOW and its associated subroutines SEARCH, FUNCT, and CERF were written by M. Smiddy in accordance with Reference 3. FLEPOW utilizes mode 2 ion sweep data to produce densities of the two species H^+ and O^+, average ion temperature, and vehicle potential with respect to plasma.

Subroutine NTRP is for straight-line interpolation, used by M2EL. FITLIN is a straight-line fitting subroutine, also used by M2EL. The CALIB subroutine is called by SSIE to recalibrate the volts→amps linear transformation coefficients.

4.2 Plotting Programs at AFGL

1. Program LOOK prepares data files for plotting programs TXSC, TXCUT, TXCGM. LOOK utilizes the preprocessed data file as input, and separates and transfers monitor word, electron word, and ion word data to tapes 2, 3, and 4 respectively. Tape 5 is written on once per minute with ephemeris information. Figure 6 is a flow chart of program LOOK.

2. Program TXSC plots monitor data, electron data, and ion data on a long strip chart. All three are plotted versus universal time and other positional information. The program is flow charted in Figure 7. A sample of the plot is included as Figure 8. Program TXCUT has essentially the same logic as TXSC. The difference is that only ion data is plotted, one datum per second, and the readout is compressed to about a one-foot length. Figure 9 is a sample compressed orbit.

3. Program TXCGM plots ion data linearity versus geomagnetic latitude. The abscissa displays other positional data information in addition to geomagnetic latitude. Gaps are included in the plot to indicate where there is no data at the extreme poles. To achieve linearity in magnetic latitude, it is necessary to use ephemeris information at one-minute intervals, accumulate differences, and interpolate within one-minute periods. Figure 10 is a flow chart of the logic for TXCGM, and Figure 11 is a sample plot.

4. PERP is a program to plot successive half orbits of ion data versus

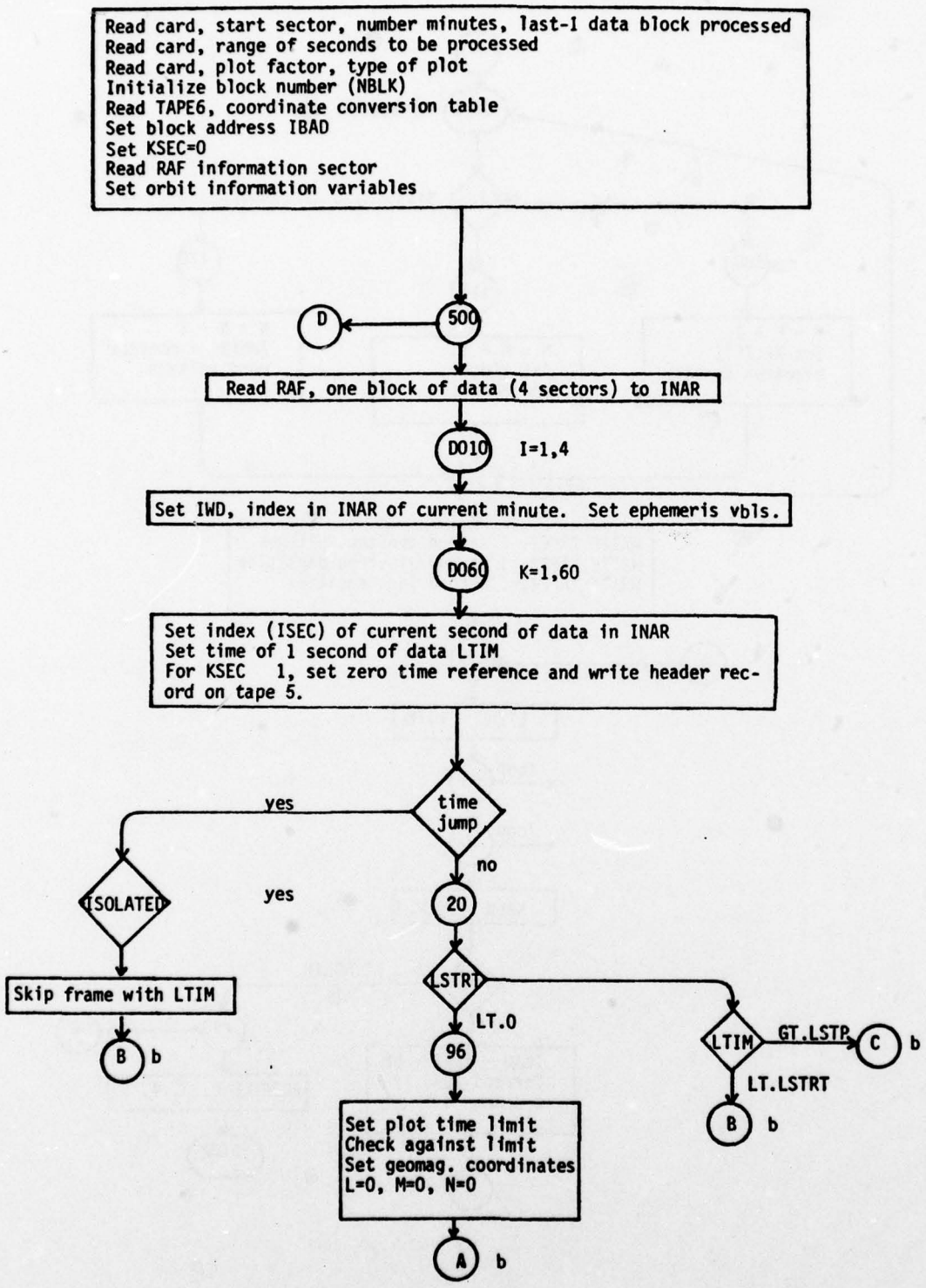

Figure 6a. Program LOOK Flow Chart

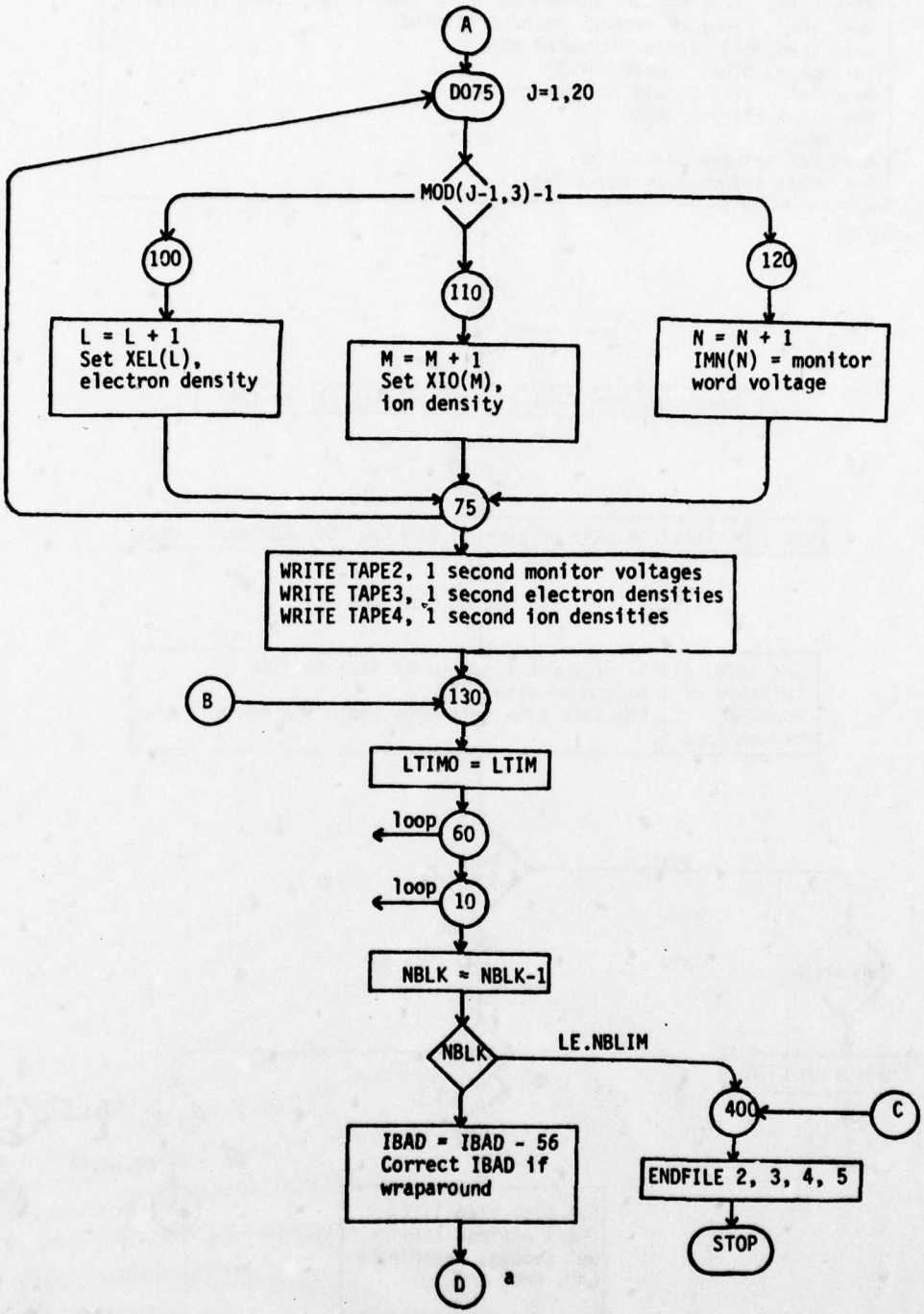

Figure 6b. Program LOOK Flow Chart

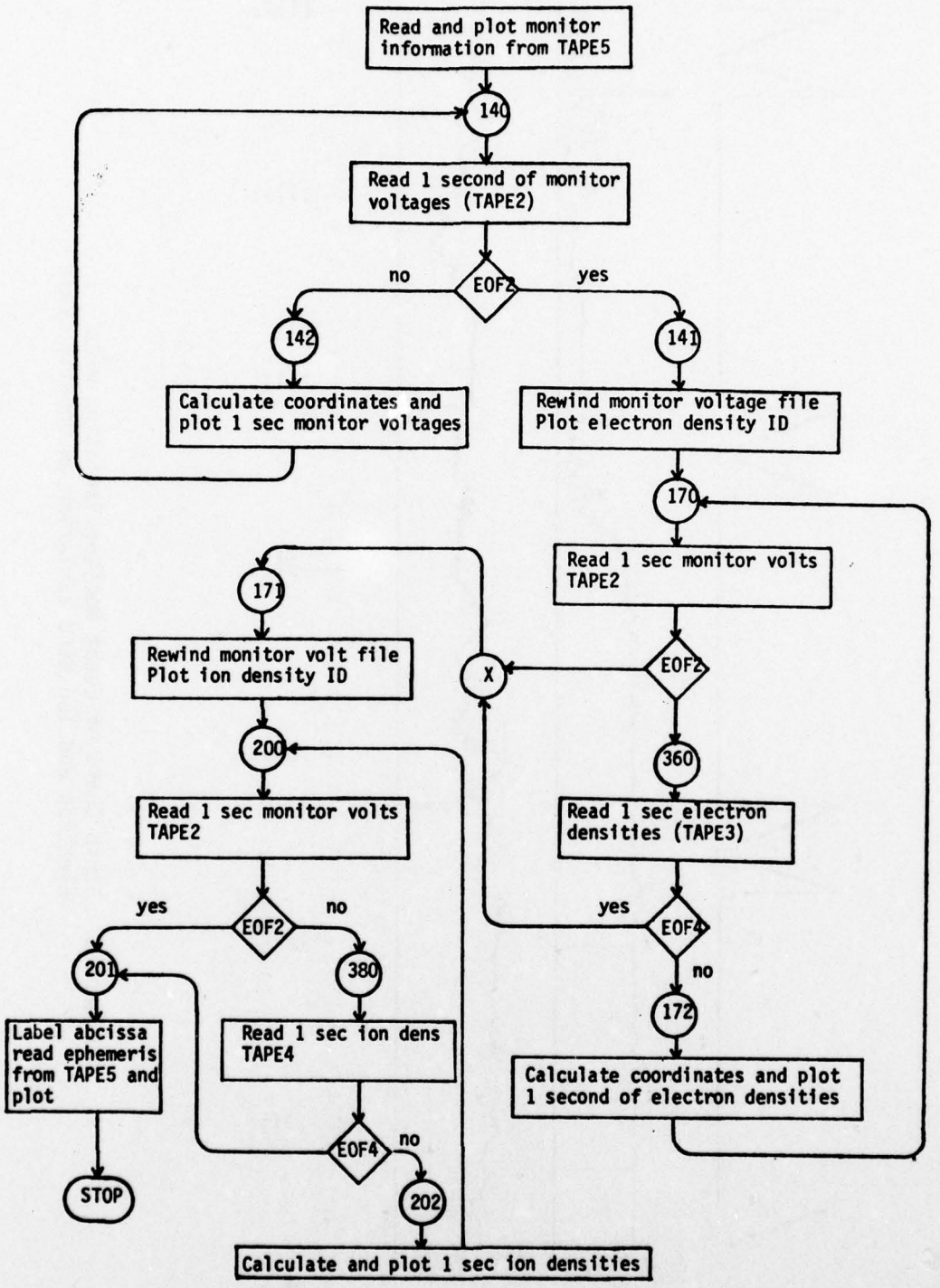

Figure 7. Program TXSC Flow Chart

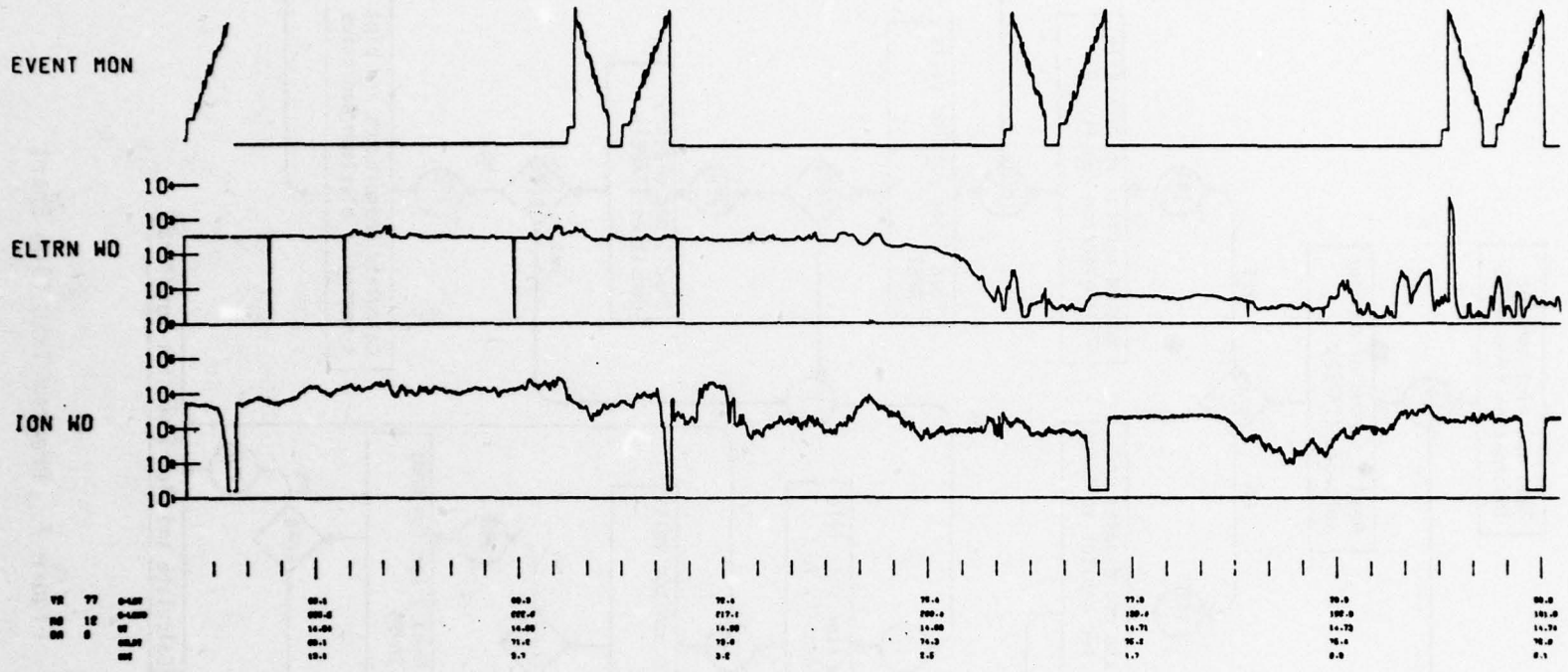

Figure 8. Strip Chart of Event Monitor Variation with Electron and Ion Word Variation on Density Scale

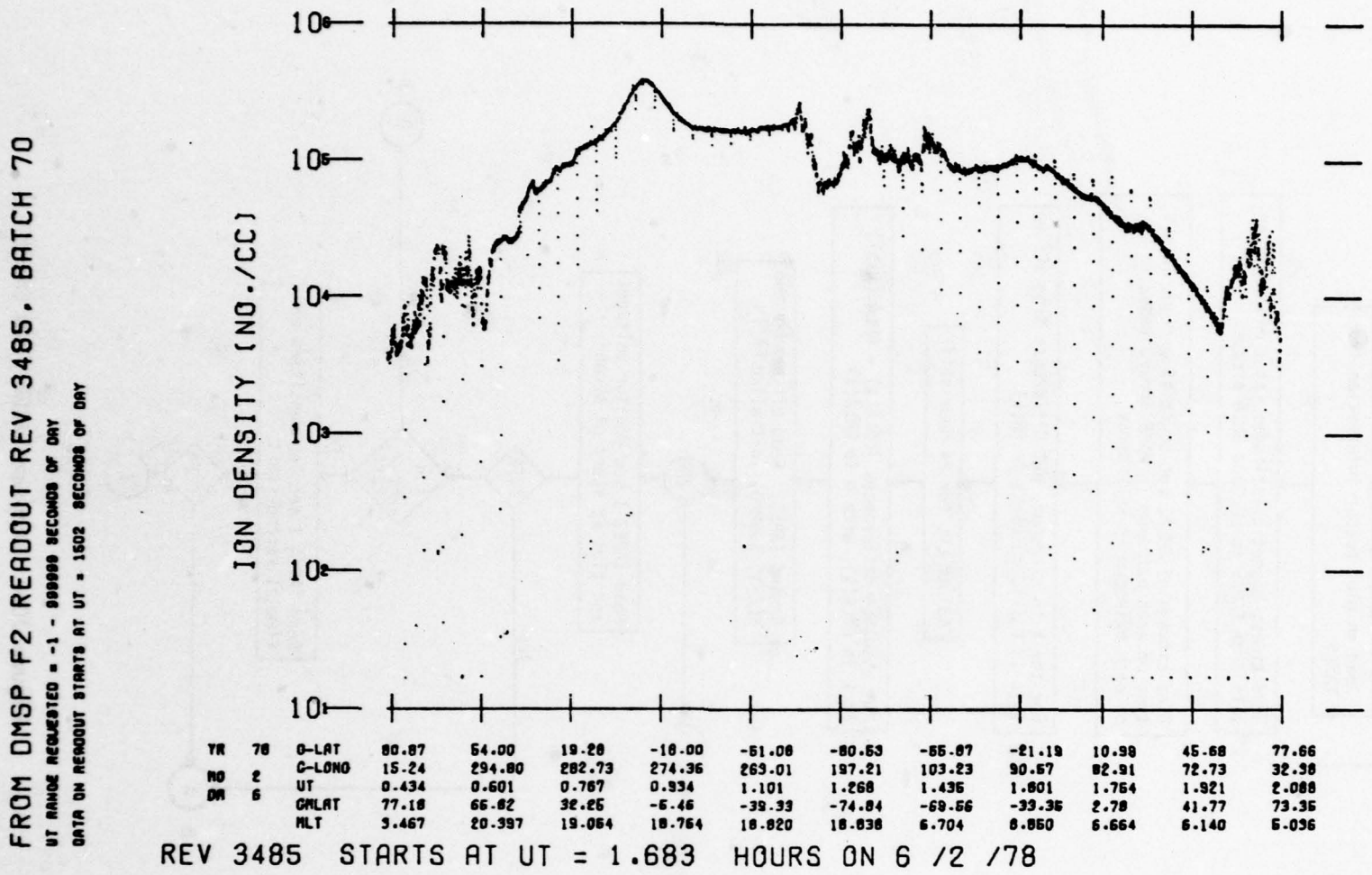

Figure 9. Compressed Mode 1 Ion Density.
Linear in Universal Time

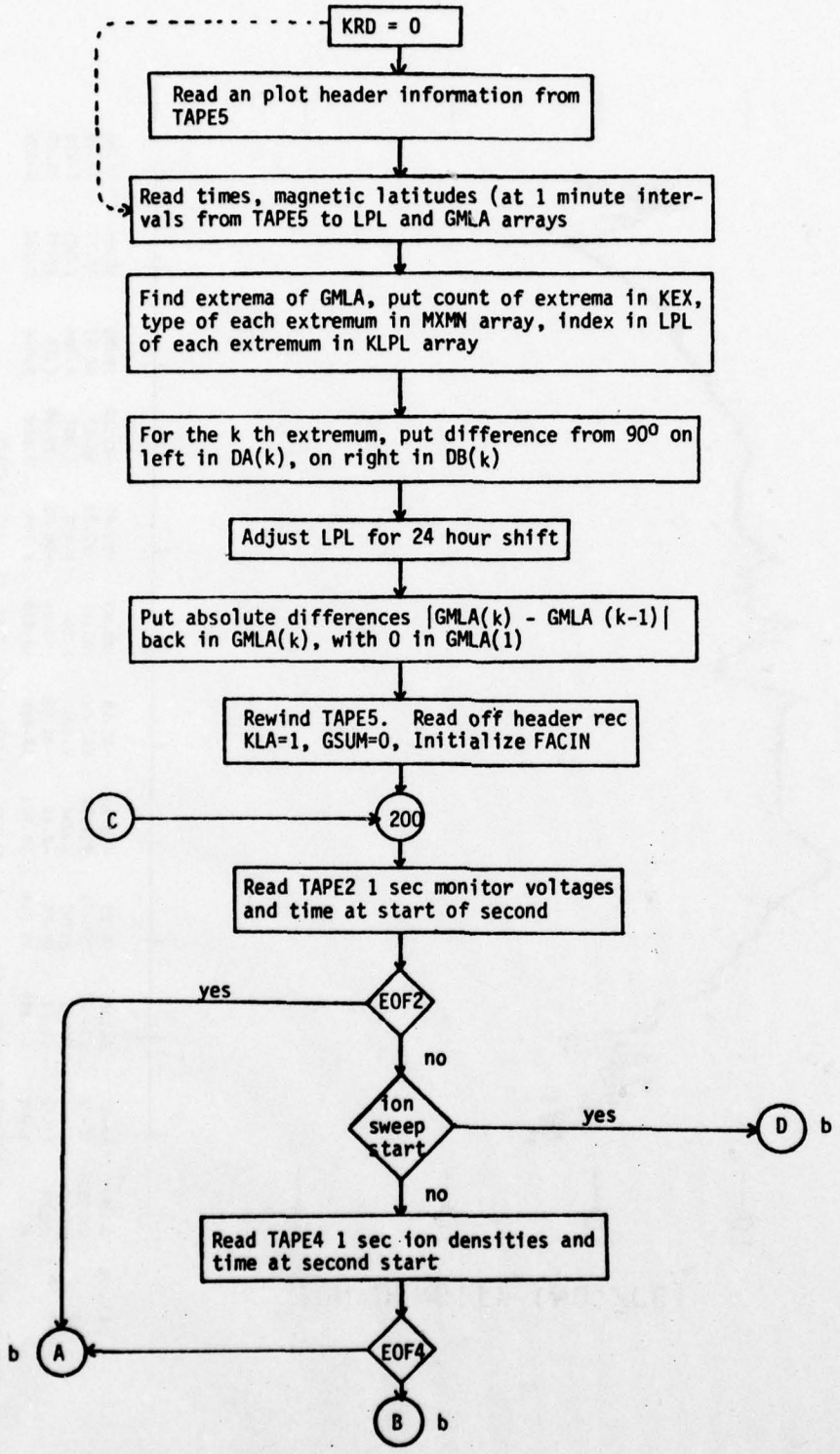

Figure 10a. Program TXCGM Flow Chart

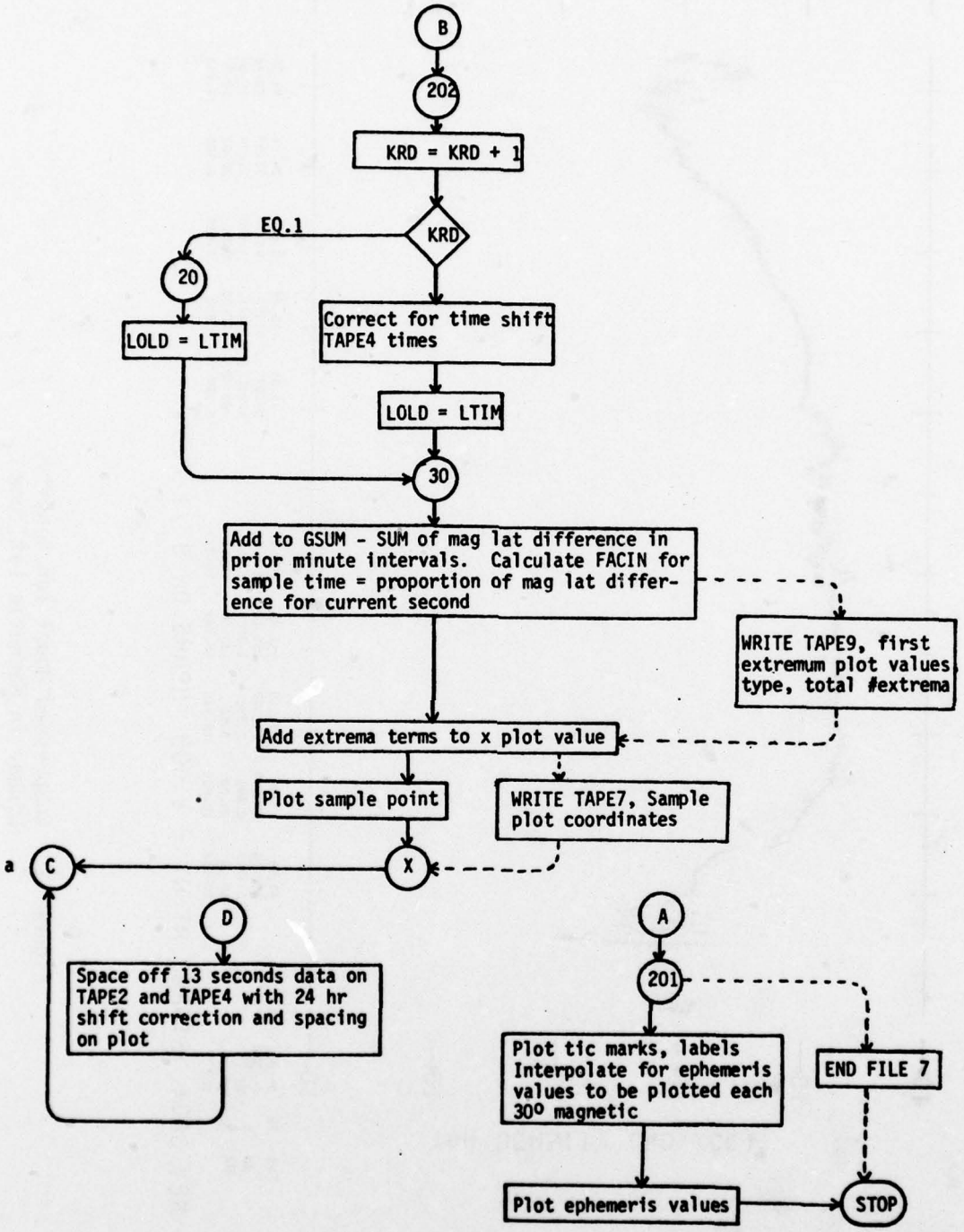

Figure 10b. Program TXCGM Flow Chart

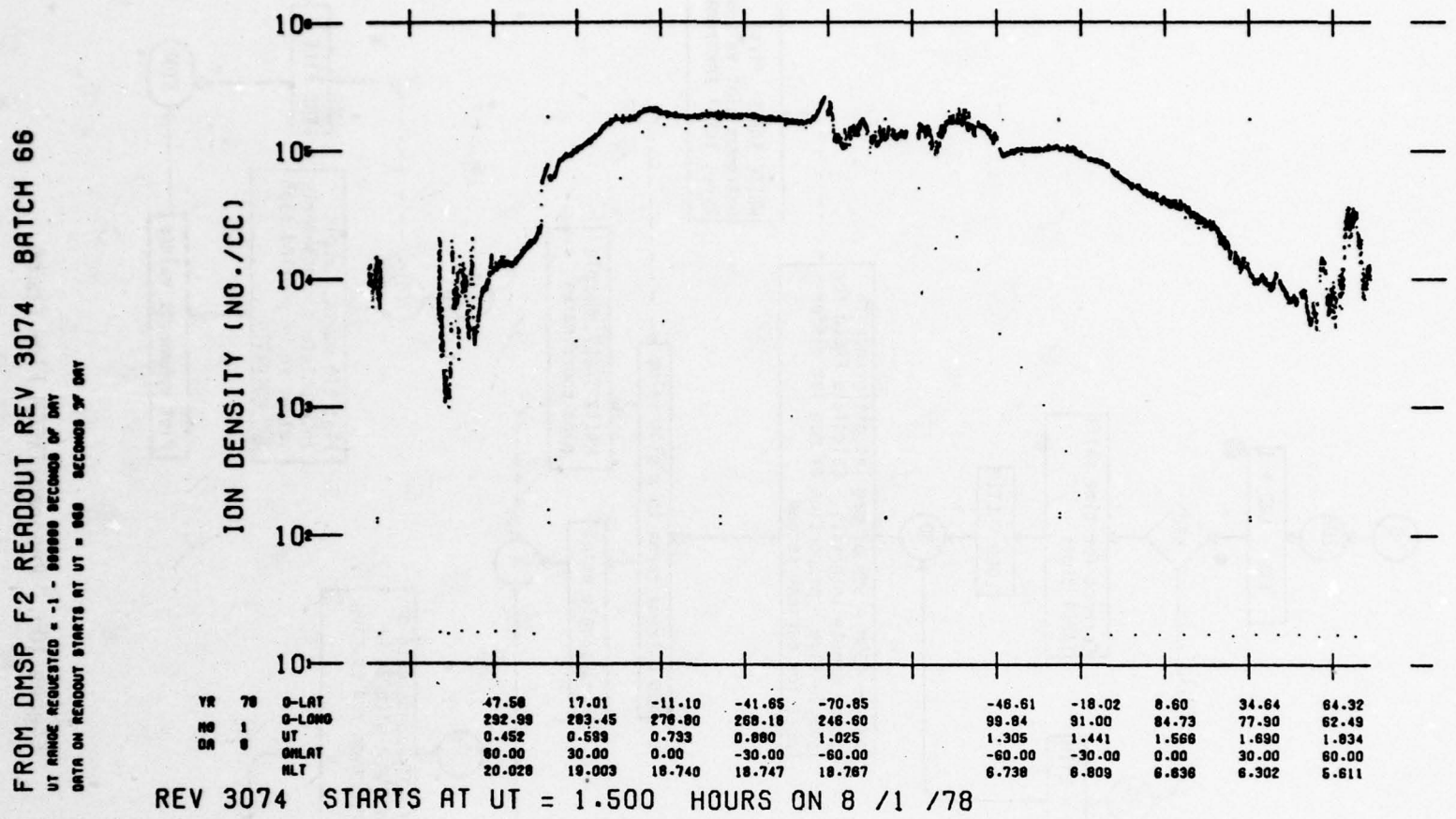

Figure 11. Compressed Model Ion Density.
Linear in Magnetic Latitude

magnetic latitude (either from -90° to 90° or from 90° to -90°) in a three dimensional presentation. The objective is to display qualitative changes in the density "surface" from orbit to orbit, over the course of about a day. Hidden points are not eliminated, but a viewing perspective is chosen so that few hidden points will occur. To this end, a fixed perspective has been chosen; but this can be altered by changing data statements in the program. The assumptions about the three dimensional coordinate system are:

a) The first semi-orbit is in the y=0 plane with magnetic latitude along the x axis and densities along the z axis. Successive semi-orbits are at y=1/2", 1", 1-1/2", etc. planes. The expected density values are scaled between z=0, z=3. The semi-orbit magnetic latitude is scaled between x=0, x=6.

b) The coordinates of the eye are (-10.",-10.",10."). The line-of-sight is from the eye to the point (3",3",2"). The eye vertical is the z axis.

c) The projection plane is perpendicular to the line-of-sight and is 5" from (3,3,2) along the line-of-sight toward the eye.

d) The coordinate system in the projection plane is oriented so that its y axis is parallel to the line from Z to F in the 3D system. The intersection point has the coordinates (B,C) in the plane coordinate system, where Z is (3,3,0) and F is (3,3,2).

Mathematics of Transformation

The 3D coordinates of the eye are in array E. Those of the sighted point are in array F, both arrays dimensioned 3. The distance from E to F is

$$DE = \sum_{i=1}^{3} (E(i) - F(i)^2)^{1/2}$$

The unit vector along the line-of-sight from F to E is

$$\frac{E(i) - F(i)}{DE} \qquad i = 1,\ldots,3$$

So the point along the line 5" from F is

$$P(i) = F(i) + 5[(E(i) - F(i))/DE] \qquad i = 1,\ldots,3$$

The equation for the plane through P is

$$(x-P(1))\ (E(1)-F(1)) + (y-P(2))\ (E(2)-F(2)) + (z-P(3))\ (E(3)-F(3)) = 0$$

For an arbitrary point A(1), A(2), A(3), the equation for the line to E is given by

$$x = (E(1) - A(1)) * T$$
$$y = (E(2) - A(2)) * T$$
$$z = (E(3) - A(3)) * T$$

Substituting

$$\sum_{i=1}^{3} [((E(i) - A(i))T - P(i))\ (E(i) - F(i))] = 0$$

Solving for T

$$T = \frac{\sum_{i=1}^{3} [P(i)\ (E(i) - F(i))]}{\sum_{i=1}^{3} [(E(i) - F(i))\ (E(i) - A(i))]}$$

Then the coordinates for the intersection point are

$$X(i) = (E(i) - A(i)) * T \qquad i = 1,\ldots,3$$

Now, to select the unit vectors in the plane (in 3D coordinates), we solve for the intersection point of the line through (3,3,0) and (3,3,2) and the projection plane. The equation for the line is

$$x = 3,\ y = 3,\ z$$

Solving for z coordinate

$$S(3) = \frac{(P(1) - 3)\ (E(1) - 3) + (P(2) - 3)\ (E(2) - 3)}{(E(3) - 2)} + P(3)$$

with $S(1) = 3,\ S(2) = 3$

The unit vector in the y direction in the plane U is

$$U(i) = (P(i) - S(i))/DU \qquad i = 1,\ldots,3$$

where

$$DU = \left(\sum_{i=1}^{3} (P(i) - S(i))^2\right)^{1/2}$$

The vector $P \rightarrow (3,3,2)$ is along the line-of-sight, so $\overline{G}$ is a unit vector perpendicular to $\overline{U}$ where

$$G(1) = \frac{3 - P(1)}{DG}, \quad G(2) = \frac{3 - P(2)}{DG}, \quad G(3) = \frac{2 - P(3)}{DG}$$

with

$$DG = \left[(3 - P(1))^2 + (3 - P(2))^2 + (2 - P(3))^2 \right]^{1/2}$$

So the x unit vector in the plane, $\overline{V}$, is given by

$$\overline{G} \times \overline{U}$$

where

$$V(1) = G(2) * U(3) - U(2) * G(3)$$
$$V(2) = G(3) * U(1) - G(1) * U(3)$$
$$V(3) = G(1) * U(2) - U(1) * G(2)$$

The origin in the plane system is

$$\phi(i) = P(i) - B * V(i) - C * U(i) \qquad i = 1,\ldots,3$$

where $B = -1$, $C = 0$. So the x coordinate of X is $(\overline{X - \phi}) * \overline{V}$, or

$$W(1) = \sum_{i=1}^{3} [(X(i) - \phi(i)) * V(i)]$$

and the y coordinate is

$$W(2) = \sum_{i=1}^{3} [(X(i) - \phi(i)) * U(i)]$$

where W(1), W(2) are the coordinates of X in the projection plane coordinate system.

In the main program PERP, E, F, Z are defined in data statements; B and C are entered as defined variables; P, S, U, V and G are calculated; and A is redefined as necessary to call subroutine PLAN. PLAN calculates T, X and W.

Input File Preparation

Program TXCGM is modified slightly to write files called TAPE7 and TAPE9. TAPE7 contains all the plot coordinates for the ion plot versus geomagnetic latitude of one readout. TAPE9 contains for the readout the x coordinate of the first pole (XFIR), the indicator (MXMN) of whether the pole is the north (1) or south (-1) pole, and the total number (KEX) of poles in the readout. TXCGM so modified is run successively through the readouts which are to be included in the three dimensional plot. After each run of TXCGM, an end of file is inserted on TAPE7, but none on TAPE9.

Program RECAT then uses TAPE7 and TAPE9 as input, and produces TAPE1, which has plot information starting at the first pole, and the indicator MXMN as the first record. RECAT is flow charted in Figure 12.

Finally program INPRP (Fig. 13) selects the semi-orbits desired (card data, 1 = first set, -1 = set shifted by 90°), and writes TAPE6, which contains the semi-orbits to be plotted.

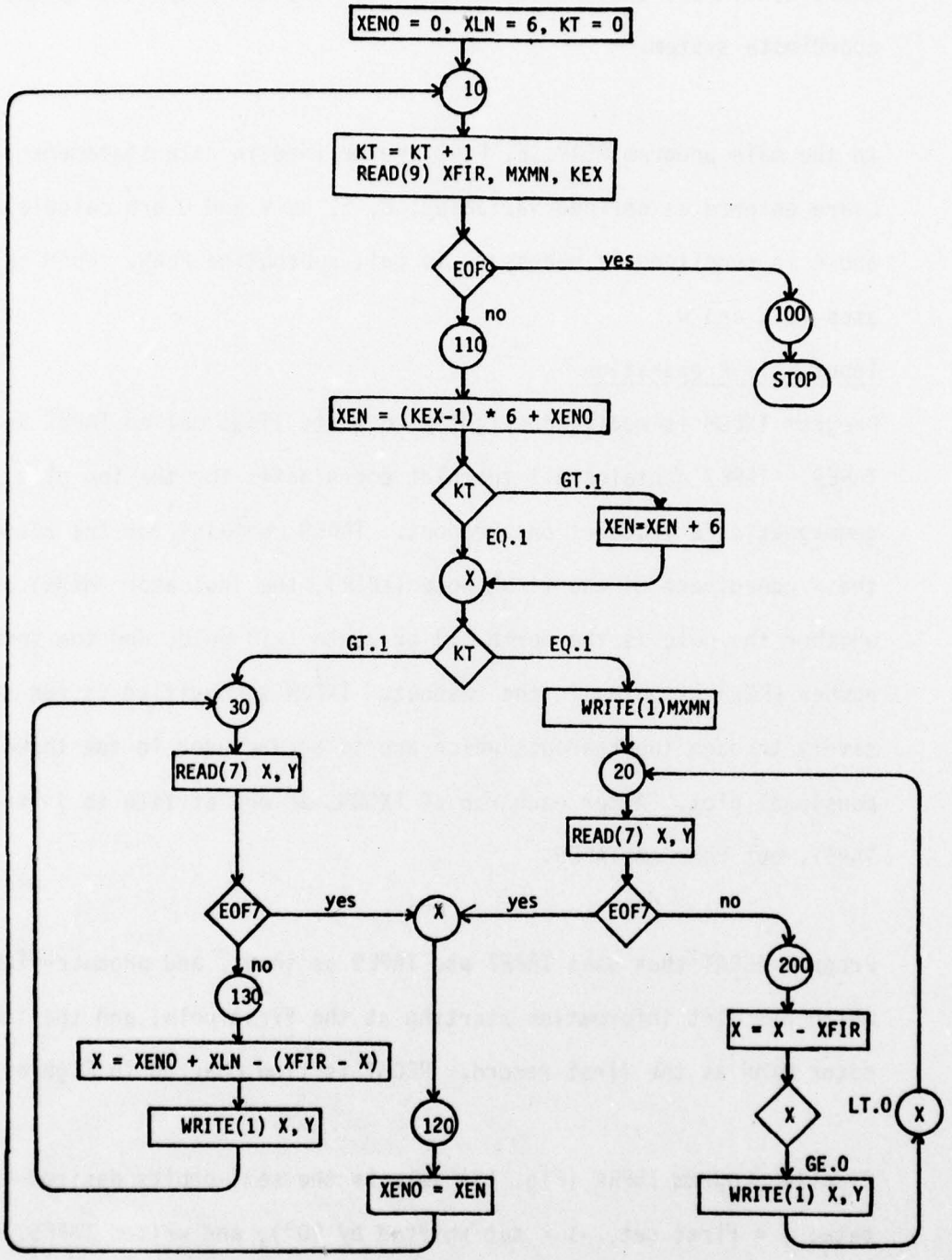

Figure 12. Program RECAT Flow Chart

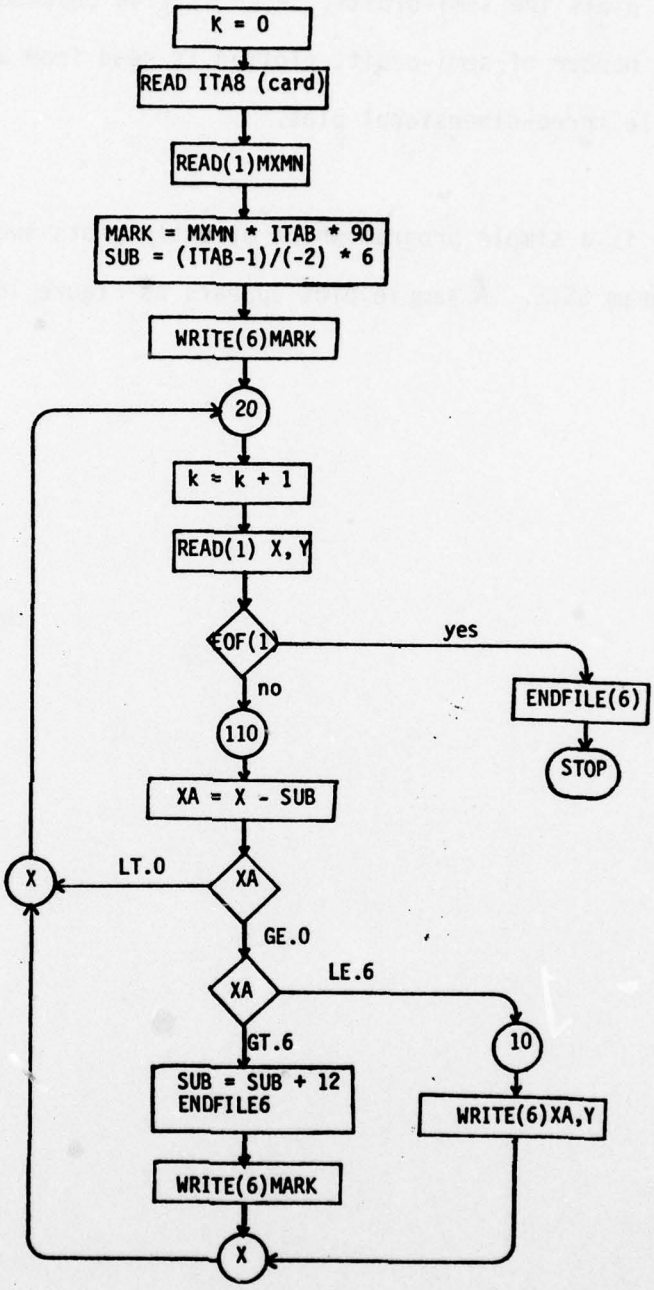

Figure 13. Program INPRP Flow Chart

PERP then plots the semi-orbits. PERP is flow charted in Figure 14. The total number of semi-orbits plotted is read from a card. Figure 15 is a sample three-dimensional plot.

5. PLORB is a simple program which directly plots sweep data as output from program SSIE. A sample plot appears as Figure 16.

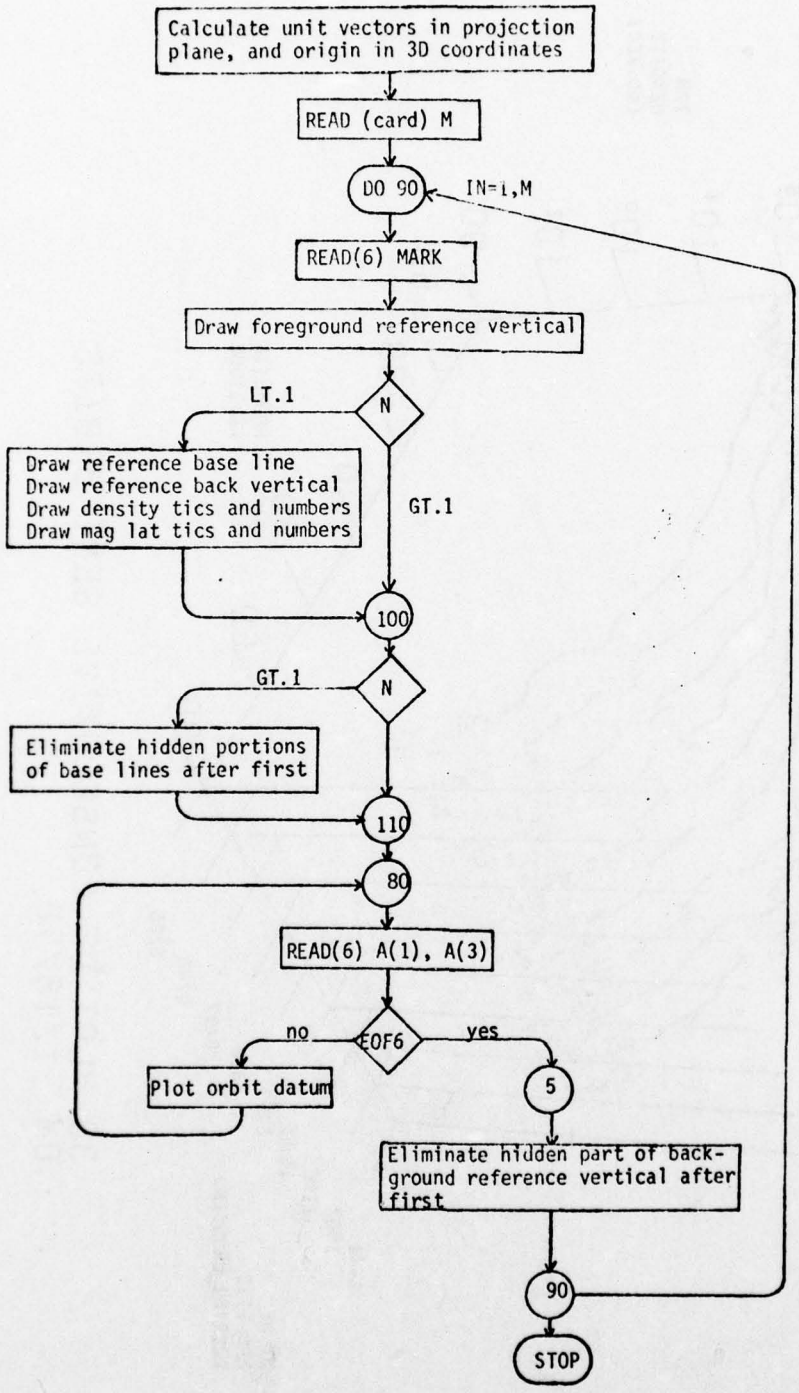

Figure 14. Program PERP Flow Chart

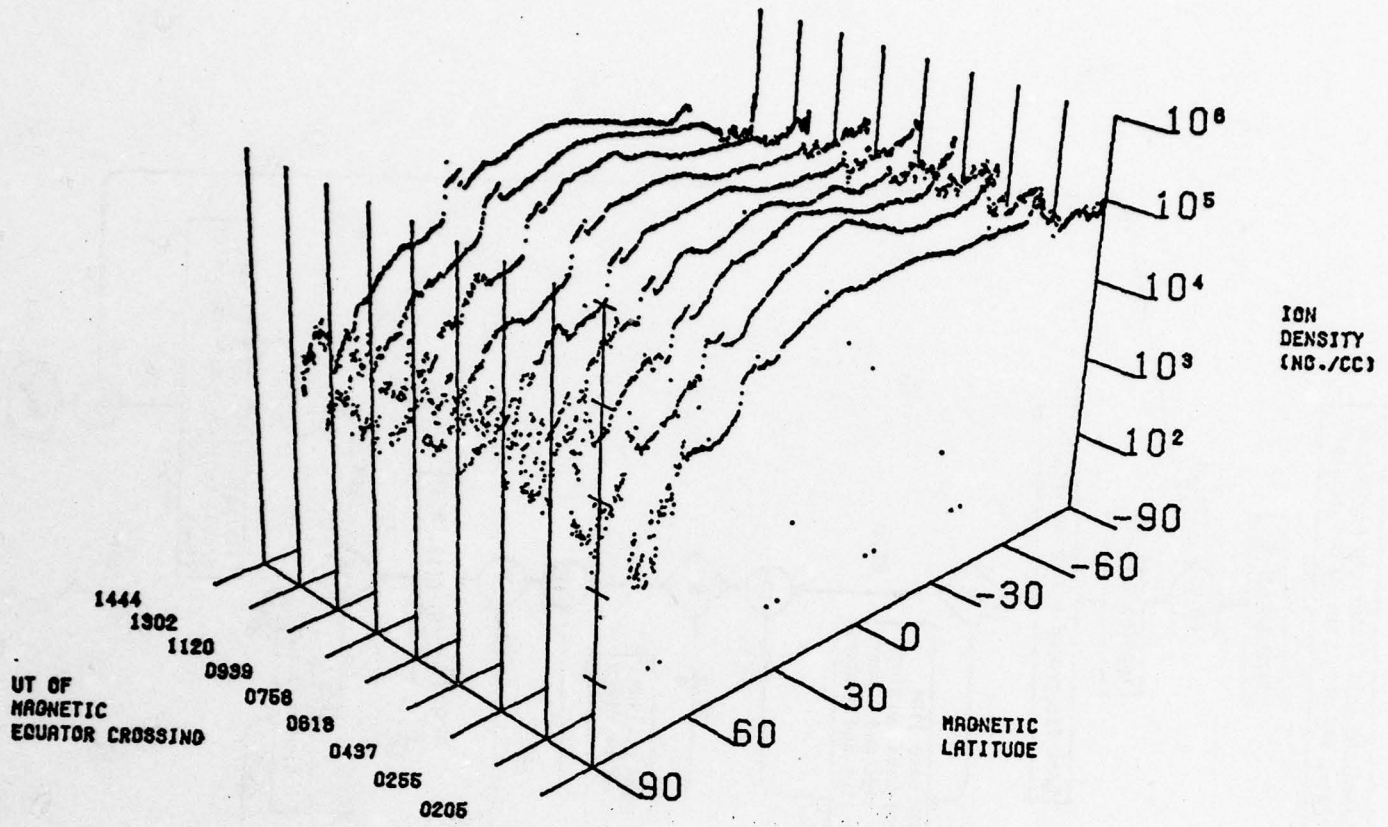

Figure 15. 3D Mode 1 Successive Semi-Orbits
Ion Density vs. Magnetic Latitude

Figure 16. Mode 2 Sweep Plots Sample

4.3 SSIE Output File Changes

The organization of the SSIE output file was described in Reference 2. Since that report, there have been several changes in the structure, and the following will supersede the output file description in Reference 2.

The processed file (output) from the SSIE analysis program fits the description of the DMSP Special Sensor Data Preprocessed Circular File Subsystem Specification of AFGWC, revised 3 July 1976, with the following exceptions.

1. The processed file is 22016 sectors long, addressable 0-22015. Each data set is one minute of data, but is 420 words, or 15 sectors, long. The one additional sector is included in the ephemeris group (header) making that group 60 words in length, rather than 32 as in the preprocessed file.

2. As in the preprocessed file, one second of data is contained in six 36 bit words, the first being a time-synch word, and the remaining five containing 20 nine bit words of data. In the processed file, the seconds themselves are in time order, but one second of data is repeated as it appears in the input file* (Ref. 2, pp. 73-74).

* The program has the option to include ion density approximation in the ion data words.

3. The 60 word data set header (ephemeris group) for the output file is as follows:

First Sector of Minute

Word	Contents	
1	Latitude, radians, 0-PI/2, fp.	First data/time in minute
2	Longitude, radians, 0-PI/2, fp.	
3	Altitude, NM, fp.	
4	Julian Date, 1-366, integer	
5	Seconds from 0000Z on JD, 0-86399, int.	
6		Last data/time in minute
7		
8	As in words 1-5	
9		
10		
	Earth center coordinates, time of word 5	
11	X fp	
12	Y fp	
13	Z fp	
	Earth center coordinates, time of word 10	
14	X fp	
15	Y fp	
16	Z fp	
17	Orbit anomaly angle, rad, fp. Time of word 5	
18	Orbit anomaly angle, rad, fp. Time of word 10	
19	JD of latest sweep pair start time, integer, 1-366	
20	Seconds from 0000Z, integer 0-86399.	

t_0 designates time at midpoint of the electron sweep. If the start of an electron sweep occurs within a minute, the time in words 19-20 will be between the time in 4-5 and 9-10.

21 Electron density at t_0 for latest sweep not starting in current minute, CM^{-3}, fp.

22 Electron density at t_0 for sweep starting in current minute if there is one - otherwise, same value as wd 21. CM^{-3}, fp.

23 Ratio of electron density at t_0, to measured current at sensor potential equal to resting bias voltage for the same sweep as in word 21.

24 As in word 23 for same sweep as in word 22.

25 Electron temperature at t_0 for latest sweep - current minute sweep if one starts in it, deg K, fp.

26 Vehicle potential with respect to plasma at t_0, same sweep as in 25, volts, fp.

The numbers contained in the following five words take their values at t_0 + 17, midway into the ion sweep following the latest electron sweep.

27 N(1) H^+ density

28 N(2) O^+ density

Second Sector of Minute

1	TEMP	Average ion temperature
2	AMU	Average ion mass
3	PHISIX	Vehicle pot wrt plasma

The following, Scale Height, is computed at t_0 + 8.5, midway between the two sweeps.

4	HP	Scale Height

The following 4 words contain coefficients for transforming raw voltage to applied voltages after a linear fit of raw voltages and times.

For electron sweep:

APEVL(mv) = XTIME(mv) * AVEB + AVEA

For ion sweep:

APIVL(mv) = XTIME(mv) * AVIB + AVIA

Raw voltages are obtained from monitor data words. At present nominal voltages are being used, since monitor words are noisy. The logic is included for future use.

5	AVEA
6	AVEB
7	AVIA
8	AVIB

The following four words contain coefficients for transforming raw voltages to logs of amps. They are recalculated every 1024 seconds.

For electron sweeps:

AMPEL(NEL) = AINE + BSLE * IEL * .01

For ion sweeps:

AMPIO(NIO) = AINI + BSLI * ION * .01

9 AINE

10 BSLE

11 AINI

12 BSLI

References

1. "Analysis and Programming for Research in Physics of the Upper Atmosphere", Logicon Inc. Final Report, AFGL-TR-76-0231, September 1976.

2. "Analysis and Research for Integrated Systems in Physics of the Atmosphere", Logicon, Inc. Final Report, AFGL-TR-77-0265, November 1977.

3. Fletcher, R., and Powell, M. J. D., "Rapidly Convergent Descent Method for Minimization", The Computer J., Vol. 6, p. 163, (1963).

5. Plasma Bulk Motion

5. Plasma Bulk Motion

Initiator: P. Wildman

Project No: 2311 Problem No: 4701

5.1 Introduction

Disturbances and irregularities in the ionosphere and magnetosphere, particularly in the polar and auroral regions, affect electromagnetic wave communications, detection, tracking, guidance, and early warning defense systems. Ambient plasma bulk motion is an important factor in forecasting ionospheric and and magnetospheric plasma meteorology and in understanding the processes leading to polar region irregularities (Fig. 1). Such irregularities are already known to cause the scintillations in satellite signals received at ground stations (Ref. 1) and in radar signals over the horizon (Ref. 2). This work supports research projects at AFGL involving in situ sensing by satellites of plasma bulk motion as well as plasma densities and temperatures. The satellites concerned are S3-2 and S3-3 flown at ionospheric and magnetospheric altitudes, respectively. The on board sensors are divided into three groups: the planar ion sensor array, the non-planar ion sensor array, and the spherical Langmuir-type electron sensor.

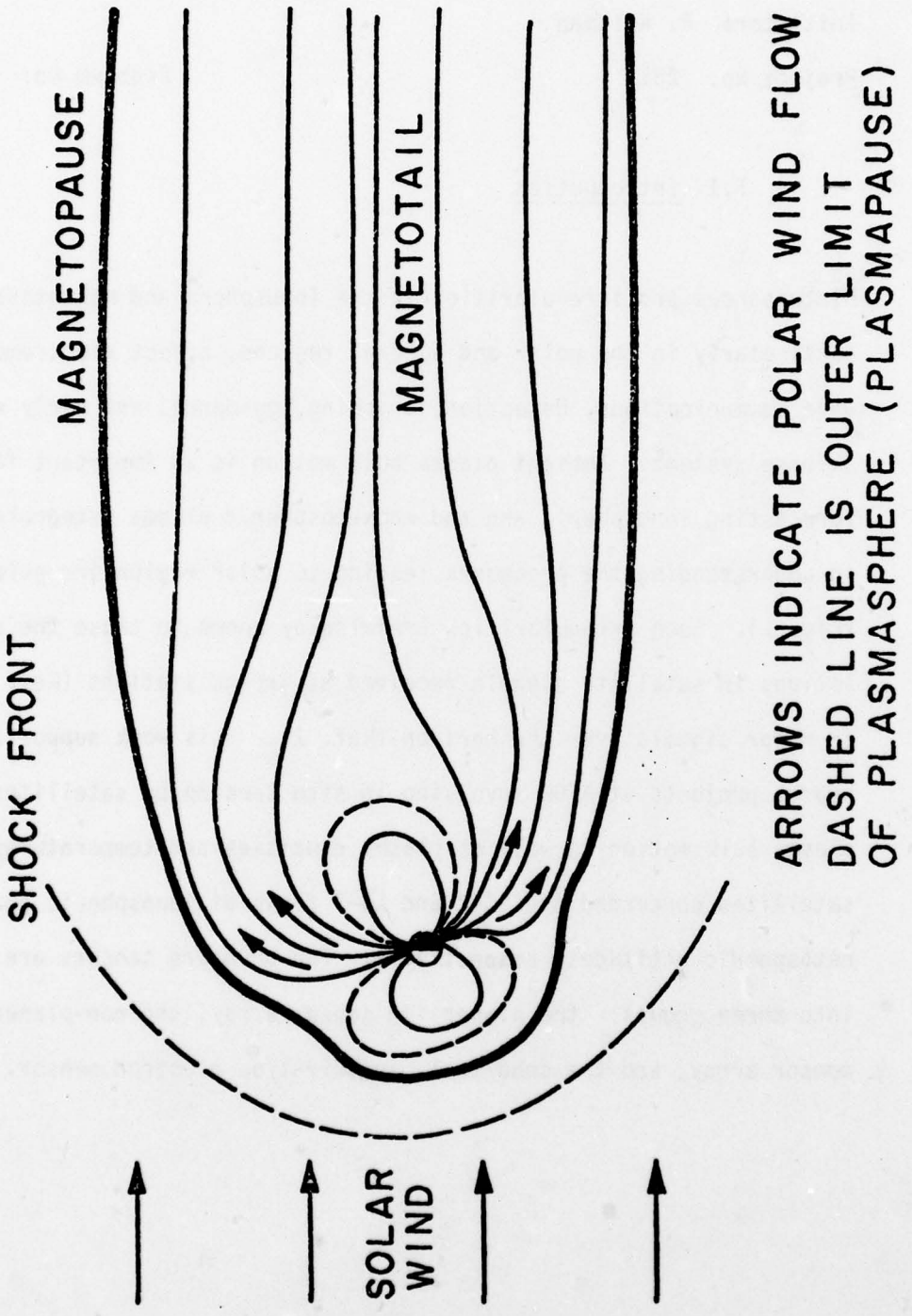

Figure 1. Plasma Flows in the Earth's Environment

5.2 Data Processing

For data processing, three types of data tapes are required, viz., the plasma data tape, the satellite attitude (OM) data tape, and the satellite ephemeris (ORMAG) data tape. The structures of these data are documented in References 3 and 4.

The satellite signals consist of several patterns which have to be recognized. They are the telemetry (TM) applied voltage sweeps, electron sensor real sweeps, electron calibrates, ion calibrates, and range switchings. The flow chart of Figure 2 outlines the data processing and computational schemes. Figure 3 displays some typical raw data of electron and ion currents measured on satellite S3-3.

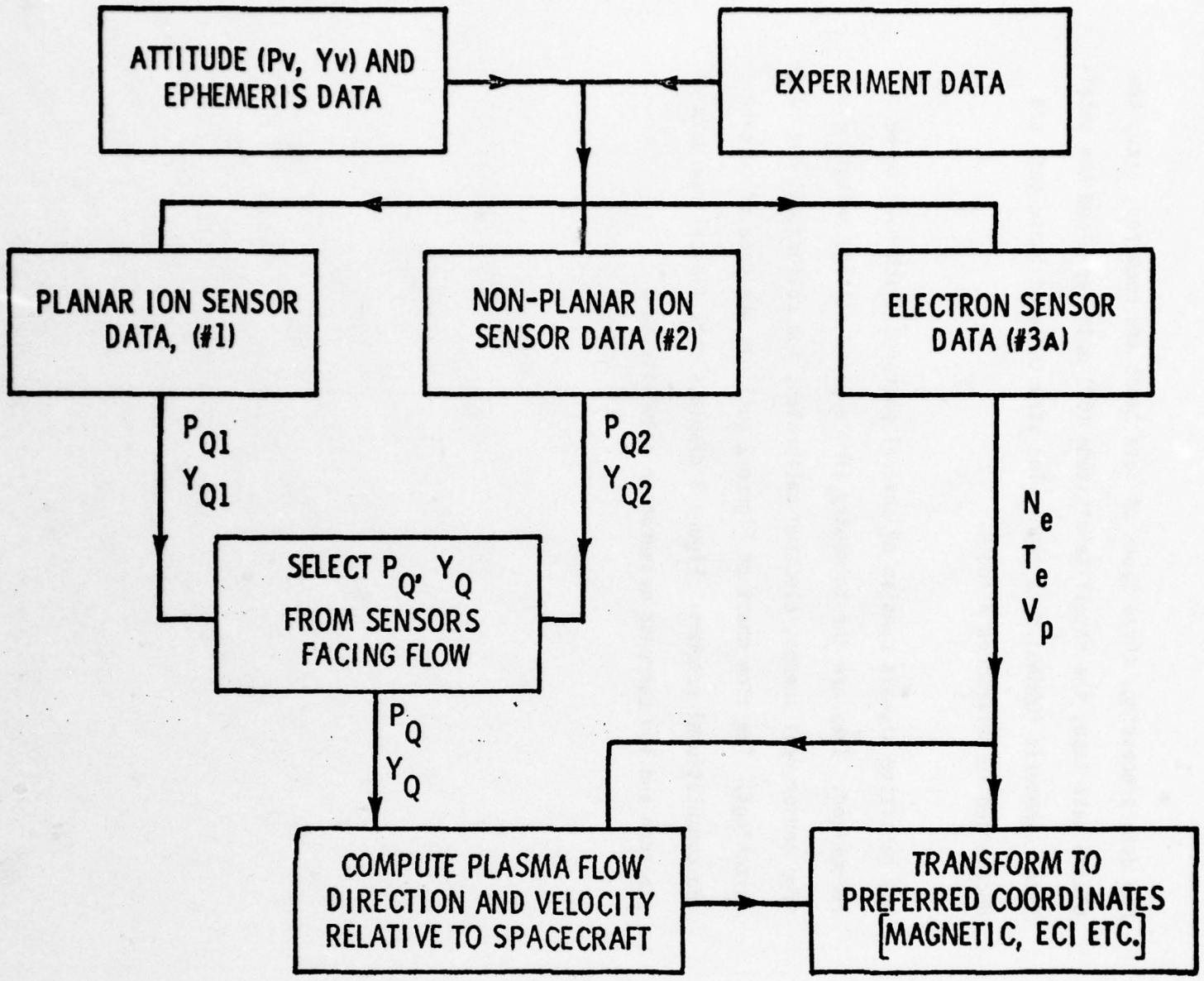

Figure 2. Plasma Flow (Polar Wind) Data Flow

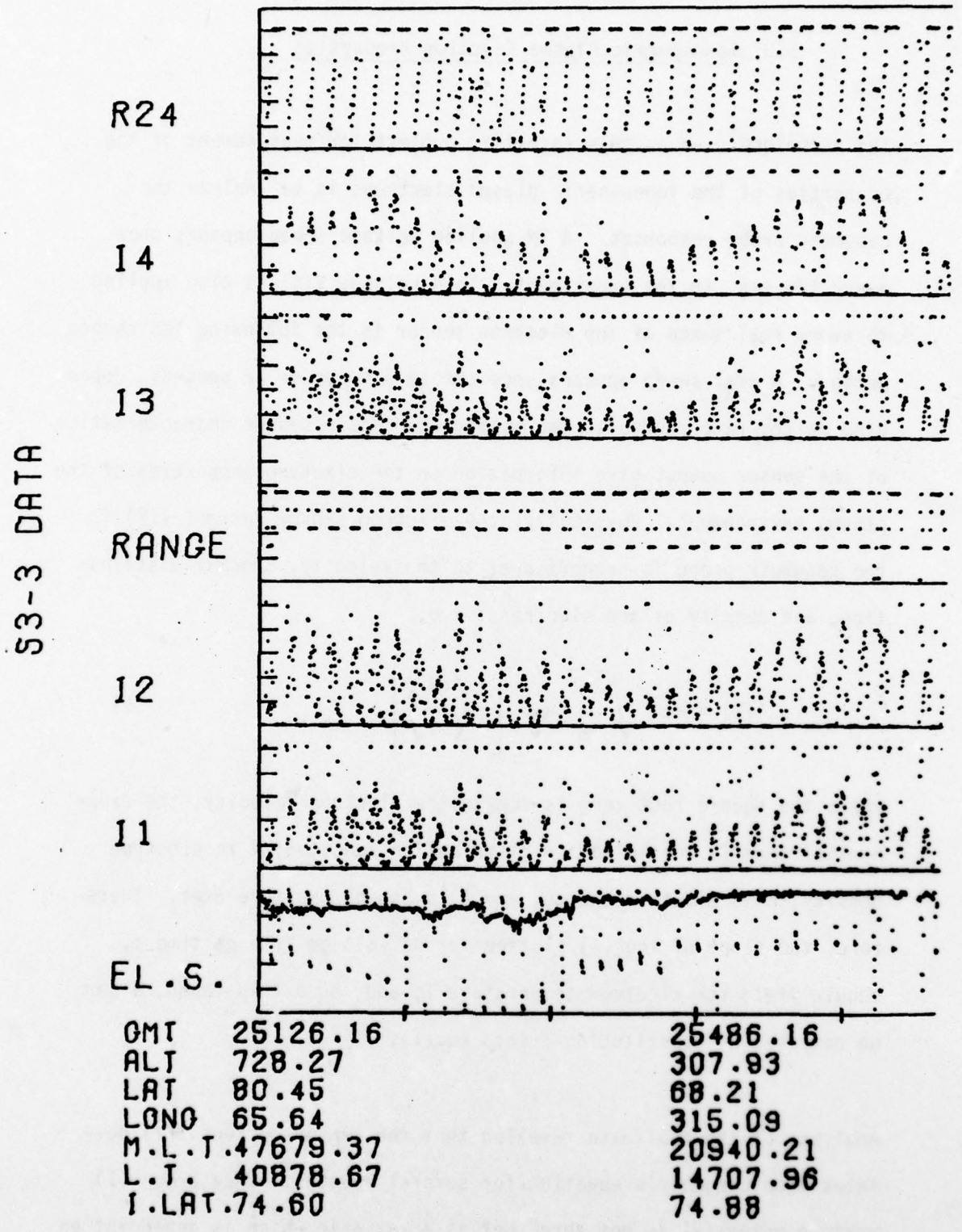

Figure 3. Electron and Ion Currents - Raw Data

5.3 Ionospheric Plasma Electron Properties

The technique used on this satellite project for measurement of the properties of the ionospheric plasma electrons is to analyze the Langmuir probe responses. A TM applied voltage sweep appears once every 128 sec. in the experiment. This voltage V(t) is also applied to every real sweep of the electron sensor in the following 128 second period. A real sweep appears once per 16 seconds or 32 seconds, depending on the rate control. The voltage-current response characteristics of the sensor output give information on the electron properties of the plasma environment. Physically, the electron sensor current I(V) in the Langmuir probe is proportional to the velocity, thermal distribution, and density of the electrons; i.e,

$$I(V) \propto NeA \sqrt{\frac{2kT}{m}} \exp\left[-\left(\frac{eV}{kT}\right)\right] \qquad (1)$$

where the square root term is due to the electron velocity, the exponential term is the Boltzmann distribution function, N is electron density, e is electron charge, and A is sensor aperture area. Therefore, the slope of $\log_e(I)$ plotted versus voltage V(t) at time t, should yield the electron temperature T; and, once T is found, N can be computed by substituting T into eq.(1).

Analysis of the real data revealed that the sensor-current I(V) deviates from Langmuir's equation for several reasons. They are: (1) vehicle potential is not zero, but is a variable which is dependent on

environment; (2) the effective aperture area is affected by the plasma sheath surrounding the sensor and the vehicle; (3) there often exists at the same region more than one species of electrons, characterized by different densities and temperatures; (4) geometry of grids in the sensor; (5) secondary electron emissions and also photo electron emissions from the sensor. Figure 4 shows a typical current-voltage pattern during a real sweep of the electron sensor.

The vehicle potential variations in the ionosphere are related to the phenomenon of spacecraft charging (Ref. 5). It has been determined that whenever the relative vehicle potential is greater than about 6V, the sweep lies outside the region of validity of the presently known theory, and the data has to be rejected. The plasma sheath is a result of the well known Debye shielding property of plasmas (Ref. 6). The presence of multi-electron species characterized by their individual temperatures and densities is due to electron flows in the ionosphere, especially in events such as energetic electron precipitations in auroral and red arc regions and in polar plasma flow regions. Photoemissions and secondary emissions are electrons knocked off the sensor's outer surface by solar photons and energetic electrons respectively.

In order to provide an analytically tractable model, it is assumed that only two species of electrons are present; i.e., the amount of a third species is negligible. Mathematically, the sensor current becomes expressed as the sum of contributions of I_1 and I_2 from the two species and I_3 from the secondary and photoemissions.

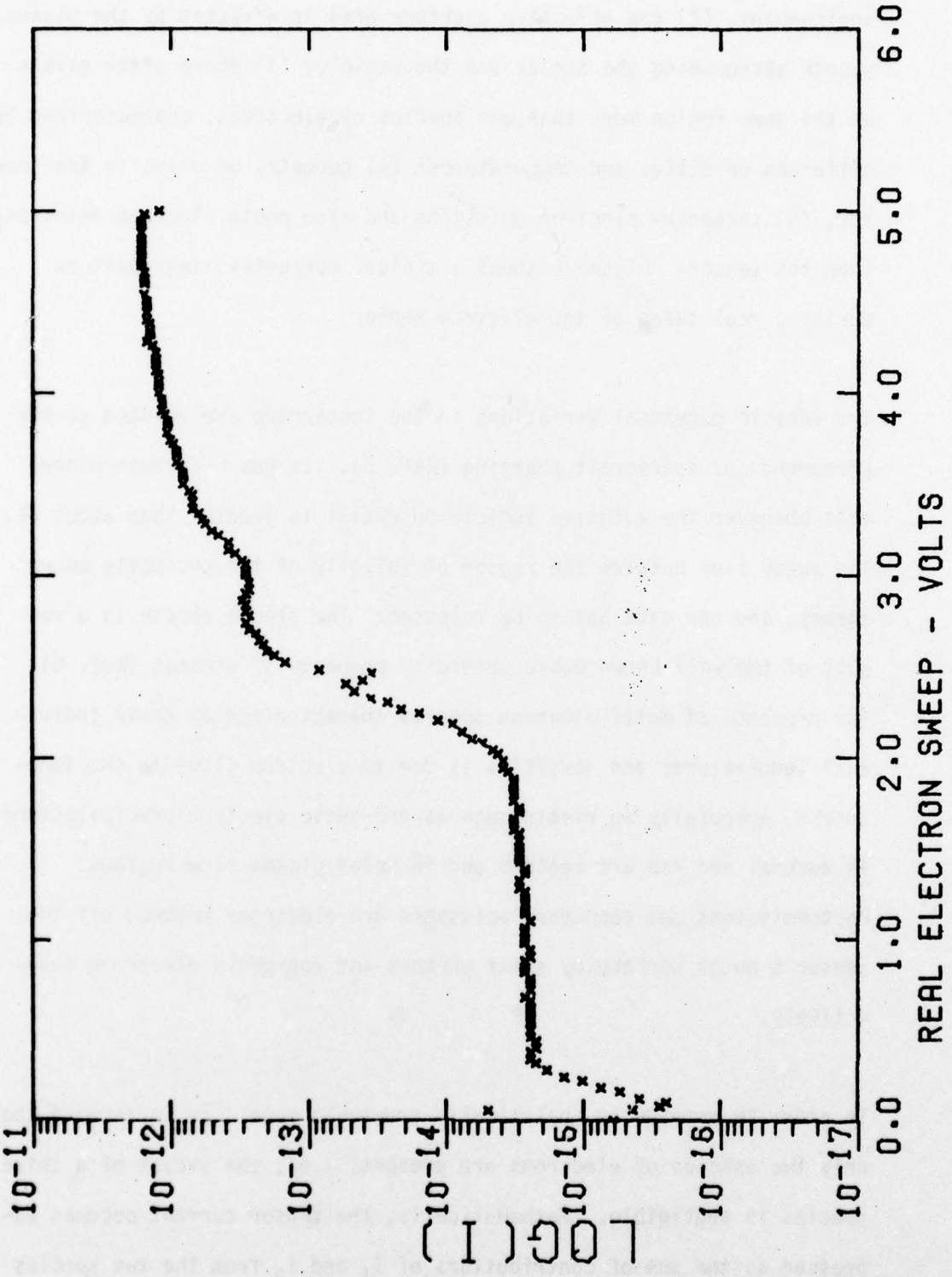

Figure 4. Typical Current-Voltage Pattern During Real Sweep of Electron Sensors

$$I(V) = I_1(N_1,T_1,V) + I_2(N_2,T_2,V) + I_3(V)$$

$$I(V) = \sum_{i=1}^{2} 4\, r^2\, \xi N_i e \sqrt{\frac{kT_i}{2\pi m}} \left[1 - \frac{r^2 - R^2}{r^2} \exp \left(- \frac{R^2}{r^2 - R^2} \frac{eV}{kT_i} \right) \right]$$

$$+ \exp (a + bV) \qquad (2)$$

where $V = V_s + \Phi$, where Φ is the vehicle potential, and V_s is the applied voltage on the sensor, r is sheath radius, R grid radius, ξ transmission factor, k Boltzmann constant, e electron charge, N electron density, T electron temperature, and i labels the species. Each sweep pattern is the superposition of the sweep patterns corresponding to two single species. The expression I(V) is invariant under permutation of the indices i (=1,2), and the lower temperature species has a density much higher than that of the other species. To determine the parameters that characterize the physical contents of the sweeps, the method of steepest descent of Fletcher and Powell (Ref. 7,8) is used for fitting the sweep patterns. The parameters to be determined are N_i, T_i, Φ, r, a and b. Occasionally, the results of a sweep have to be rejected because of over saturation of data, broken sweep due to existence of a time gap in which no signal was received on the ground, too much noise in data, excessive vehicle potential due to spacecraft charging, excessive photoemission overshadowing the true signals, or simply overshooting in the rapid descent technique. Rejection codes are listed in Table 1. Usually, the sweep results are very useful. The scheme of electron density correction computation at the end of

every real sweep is shown in Figure 5. Figure 6 displays the profile of electron temperature determined by means of S3-3 data. The measurement of such a profile above 1,000 km has not previously been mapped thoroughly because of the limit imposed by the apogee of satellites.

Table 1. Rejection Code used in the computer data processing of Real Sweeps.

Data Rejection Code	Reason
1	Wild data, lying outside three standard deviations.
2	Temperature density data mismatched.
3	Temperature below 600°K.
4	Magnitude of vehicle potential greater than 6 volts.
5	Steepest descent method does not work.

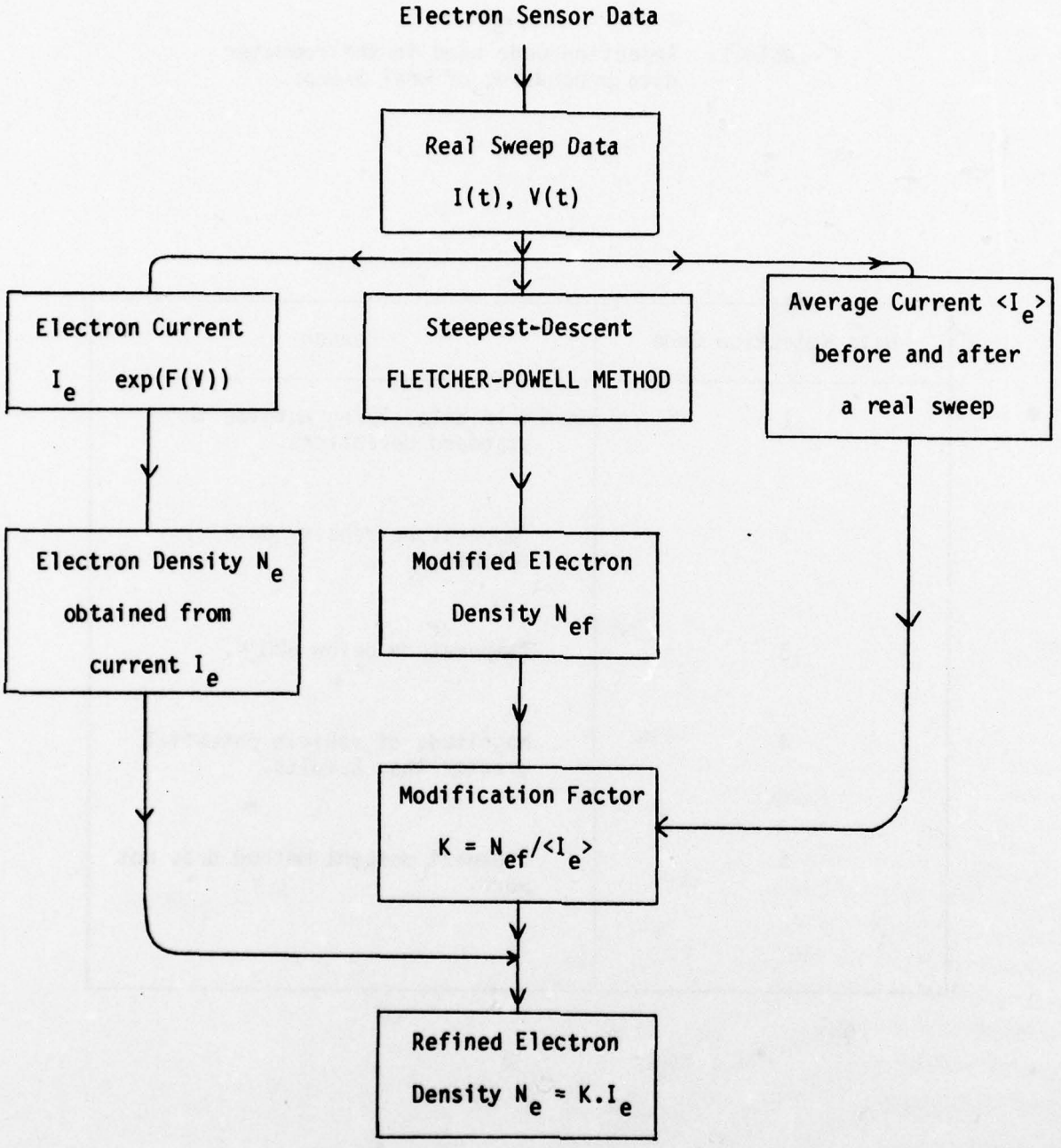

Figure 5. Scheme of Real Sweep Electron Density Computation.

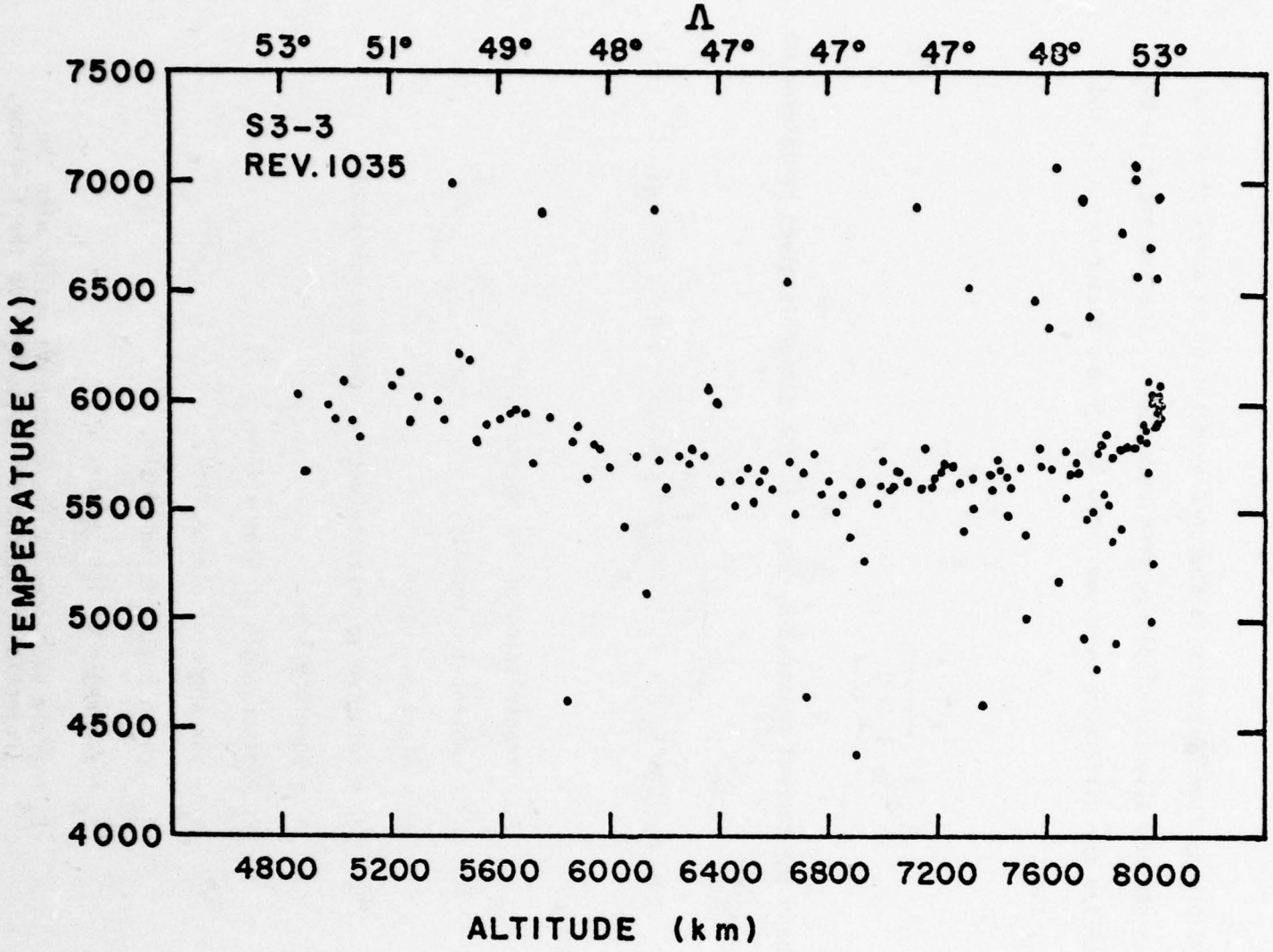

Figure 6. Profile of Electron Temperature Mapped by Satellite S3-3 at Magnetospheric Altitudes

5.4 Determination of the Plasma Flow Direction

The plasma flow direction is measured by means of an array of plasma ion sensors slightly displaced from each other. The technique is to utilize the difference over sum ratio R_{ij} of two measurements I_i and I_j; i.e.,

$$R_{ij} = \frac{I_i - I_j}{I_i + I_j} \tag{3}$$

where the current measured by the i-th ion sensor is given by References 9 and 10.

$$I = \xi Ne\, Aq\, [\text{Cos } Y_Q \text{ Cos } Y_S \text{ Cos}(P_Q - P_S + E_t) + \text{Sin } Y_Q \text{ Sin } Y_S] \tag{4}$$

where:

ξ = transmission of the aperture,

N = ambient ion density,

e = electron charge,

q = relative velocity between plasma and spacecraft,

A = aperture area,

P_Q = pitch angle of plasma flow,

Y_Q = yaw angle of plasma flow,

P_S = pitch angle of ion sensor,

Y_S = yaw angle of ion sensor,

E_t = angle subtended by the spacecraft x-axis with the projection of spacecraft velocity V on the XZ-plane, with the satellite spinning about the y-axis.

The ion sensors are not symmetrically mounted about the array centroid. As a result, the use of only two sensors, i and j, is not sufficient for the determination of flow direction. An algorithm has been worked out by Lai et al (Ref. 11) utilizing the x ratio, defined by

$$x = \frac{R_{13} + \tan(2\alpha)\tan\varepsilon}{R_{13} - \tan(2\alpha)\cot\varepsilon}$$

where 2α is the angle between the normals of any two adjacent sensors, γ and ε, are the skew angles about the y-axis and z-axis deviating from the array center line, (see Table 2). The plasma flow pitch and yaw angles are given by solving the following equations (Ref. 12)

$$R_{24}\ \frac{1 - x}{1 + x\,R_{24}} = \tan\alpha\,\tan(-P_Q + \gamma - E_t) \qquad (5)$$

$$\tan(P_Q + E_t - \gamma) = \frac{-R_{24}\left[1 - x\right]}{\tan\alpha\left[1 + xR_{24}\right]} \qquad (6)$$

Since x is a function of R_{13}, all four ion sensor measurements are needed simultaneously for the determination of plasma flow direction. Once the flow direction is determined, the magnitude of flow velocity can be derived from the relative flow magnitude measured by the sensors, and the vehicle velocity.

Table 2. Skew Sensor Pitch and Yaw Angles

Sensor No.	1	2	3	4
P_S	$-(\alpha-\gamma)$	$-(\alpha-\gamma)$	$-(\alpha-\gamma)$	$(\alpha+\gamma)$
Y_S	$-(2\alpha+\varepsilon)$	$-\varepsilon$	$-(2\alpha-\varepsilon)$	$-\varepsilon$

5.5 Blockage of Ion Flows and Non-linear Function Fitting

After careful analysis of a considerable number of orbits of real satellite data, it became clear that for cases where the Mach number of the satellite's motion relative to the ambient plasma is large ($M >> 1$), the current measured by a sensor is severely limited when the plasma flow vector intercepts a portion of the spacecraft surface reaching the surface aperture. When the flow vector does not intercept the satellite surface, the current does behave similarly to that detected by an "unobstructed" sensor, as formulated by Lai et al (Refs. 11,12).

For the case when the Mach number of the satellite motion relative to the ambient plasma is near or greater than 1 ($M \gtrsim 1$), the current measured by a sensor is less than that which would be measured by an "unobstructed" sensor for all directions of the flow vector.

To model exactly the shapes of the obstructions of flow to the sensor would require an algorithm that would not be efficient for the analysis of a large volume of data. Instead, the obstructions are approximated by a series of wedges with wedge angles ϕ_1 and ϕ_2 and centered on the sensor's apertures (Ref. 13). As a result, the analytical expression of the current measured by a sensor looking out of the satellite spin plane becomes (Ref. 13):

$$I_{out} = 1/2\ NeA(a/\pi)^{1/2} \int_0^\infty v_z \left\{ \text{erf}\left[\sqrt{a}(v_z \cot \phi_1 + q \cos \eta)\right] \right. \qquad (7)$$

$$\left. + \text{erf}\left[\sqrt{a}(v_z \cot \phi_2 - q \cos \xi)\right] \right\} \exp\left[-a(v_z - q \cos \theta)^2\right] dv_z \ .$$

where υ, the velocity of plasma particles, is just an integration variable here; q is the measured velocity of plasma flow; and θ is defined later.

Similarly, the analytical expression for the in-plane sensor current becomes

$$I_{in} = 1/2\ NeA(a/\pi)^{1/2} \int_0^{\infty} \upsilon_z \left\{ \text{erf}\left[\sqrt{a}(\upsilon_z \cot \phi_1 + q \cos \eta)\right] + \text{erf}\left[\sqrt{a}(\upsilon_z \cot \phi_2 - q \cos \xi)\right] \right\} \exp\left[-a(\upsilon_z - q \cos \theta)^2\right] d\upsilon_z \quad (8)$$

where

$$q \cos \theta = (\underline{v} + \underline{w}) \cdot \underline{L},$$

$$q \cos \eta = (\underline{v} + \underline{w}) \cdot \underline{M},$$

$$q \cos \xi = \sqrt{q^2 - (q \cos \eta)^2 - (q \cos \theta)^2},$$

$$[\underline{v}] = |v| \begin{bmatrix} \cos Y_q \cos P_q \\ \sin Y_q \\ \cos Y_q \sin P_q \end{bmatrix},$$

$$[\underline{w}] = \begin{bmatrix} -D_x \cos Y_q \cos P_q + D_y \sin Y_q \cos P_q + D_z \sin P_q \\ -D_x \sin Y_q - D_y \cos Y_q \\ -D_x \cos Y_q \sin P_q + D_y \sin Y_q \sin P_q - D_z \cos P_q \end{bmatrix}$$

$$[\underline{L}] = \begin{bmatrix} \cos P_s \cos Y_s \\ \sin Y_s \\ \cos Y_s \sin P_s \end{bmatrix}$$

$$[\underline{M}] = \begin{bmatrix} x & \\ -(\cos Y_s \sin Y_s \cos P_s)/x & \\ -[(\cos Y_s)^2 \cos P_s \sin P_s]/x & \end{bmatrix}$$

$$x = (\cos^2 Y_s \sin^2 P_s + \sin^2 Y_s)^{1/2}$$

and $$\text{erf}(x) = \frac{2}{\sqrt{\pi}} \int_0^x \exp(-t^2)\, dt$$

These integrals can be calculated with good accuracy with Gaussian quadrature. To determine the plasma flow parameters use is made of methods for fitting non-linear functions to data. Numerical values of parameters are found by a search in parameter space for the "solution" that yields a minimum in the difference between the expected and real values of the function. The search algorithm is based on the method of parameter optimization developed by Fletcher and Powell (Refs. 7,8). Using the methods described in this section, we have computed the plasma flow data for many orbits (Figs. 7,8). In particular, a very high (9.8 km/s) flow velocity of plasma was discovered to be associated with a large poleward electric field structure (see Section 6) at the plasmapause during the May 1976 magnetic storm (Ref. 14).

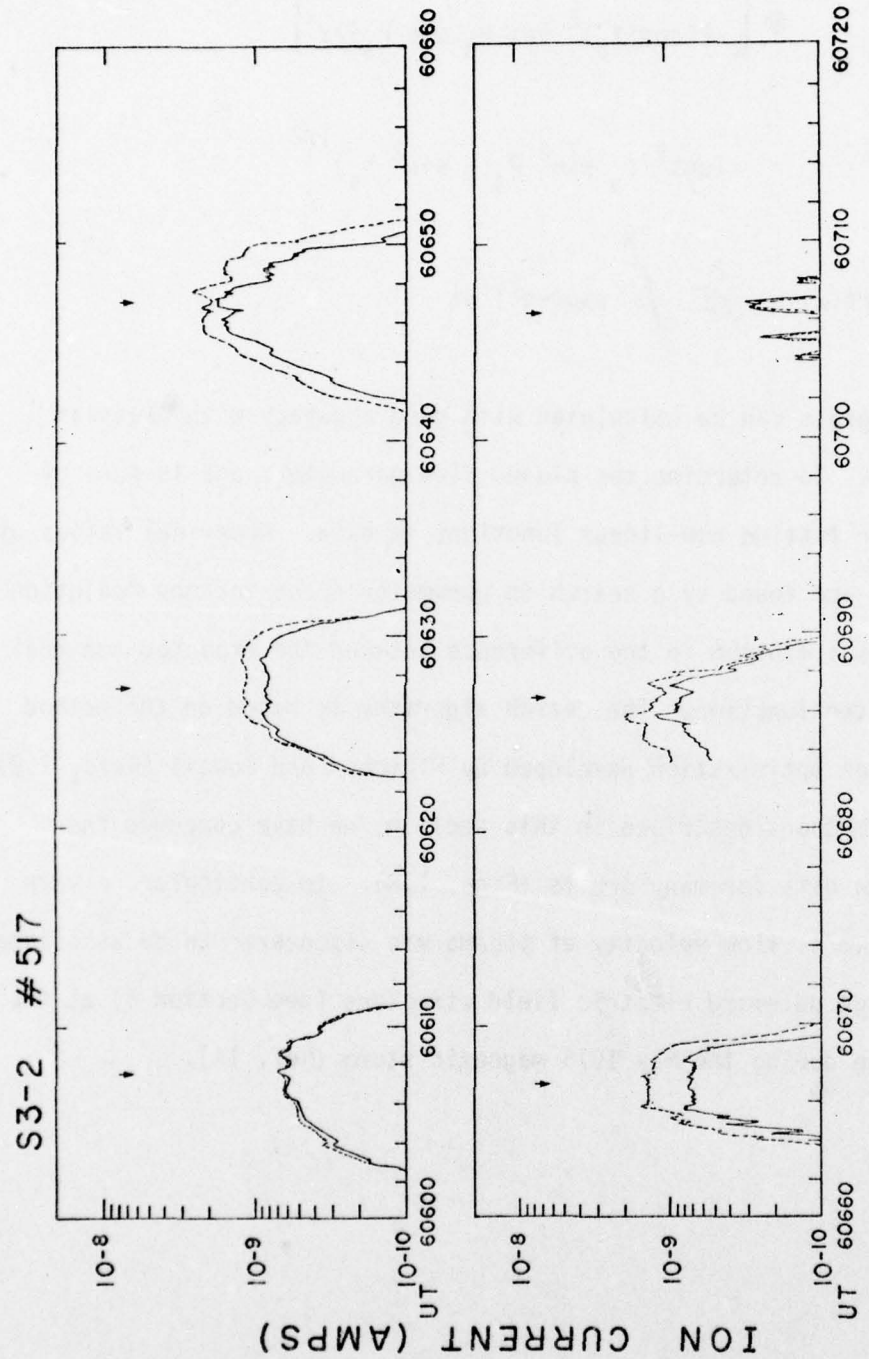

Figure 7. Typical Ion Currents Measured by a Four Sensor Array

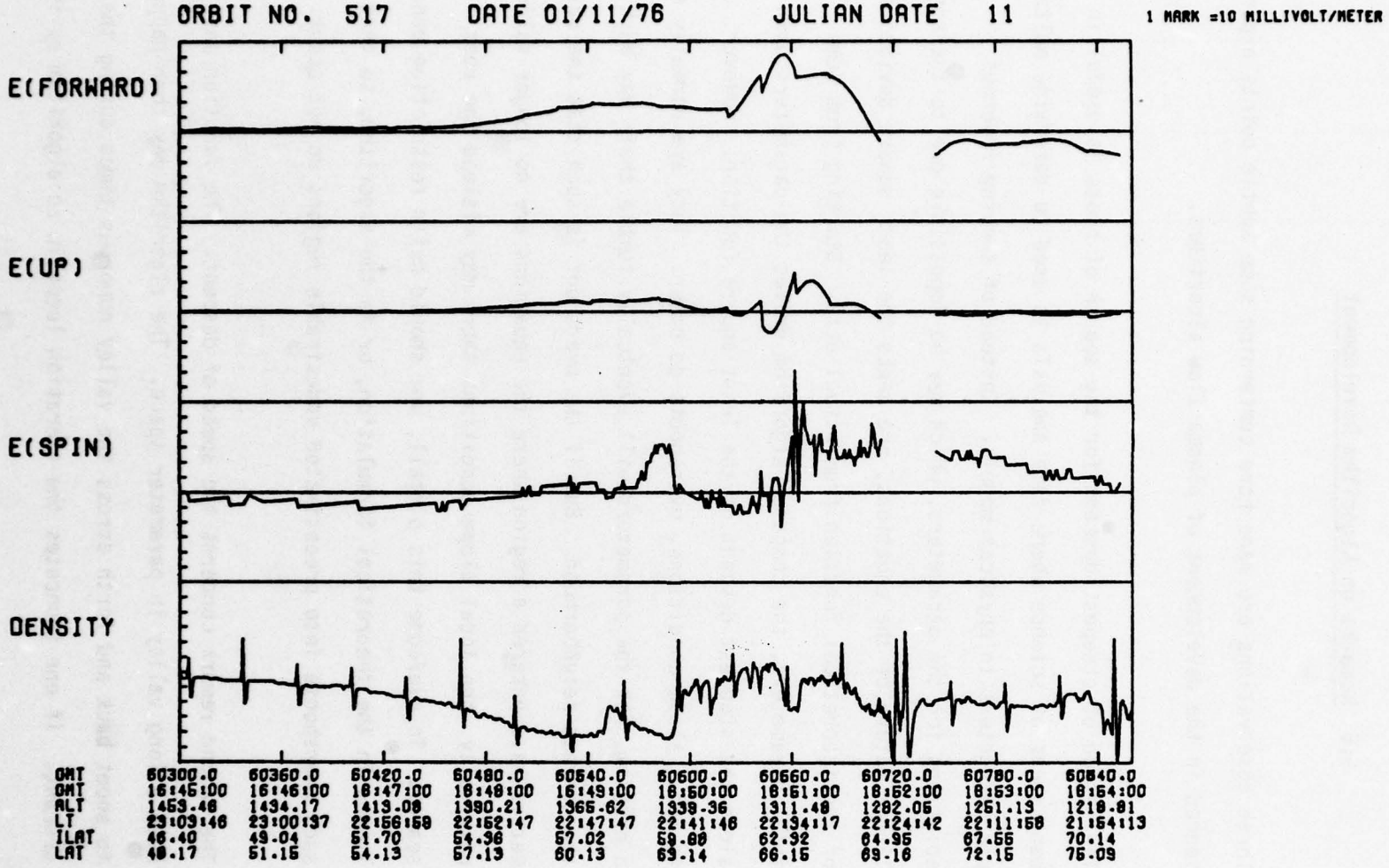

Figure 8. Strip Plots for the Correlated Study of Ionospheric Electric Field Components and Plasma Electron Properties

5.6 Remarks on Algorithm Development

Three observations are made here concerning some subtle points experienced in the development of plasma flow algorithms.

The method of steepest descent for the search of roots is useful in many areas of science where data analysis is used to determine multiple parameters in physical models. Instead of seeking rigorous solutions for the parameters, which may be impossible due to the nonlinear nature of the equations, one seeks the least square deviation of the theoretical function from actual data. Starting from some trial parameters, the computer algorithm drives the parameters down along the steepest descent of the least square function. However, due to local slope conditions, overshoots do occur. They are normally not a problem, for the parameters will eventually fumble their way back to the correct neighborhood. But if the overshoot is such that the parameters have entered a region where the equations are no longer valid physically, the local slope conditions there may mislead the root search. To overcome this pitfall, one should build restriction conditions in the theoretical formulation, or in the algorithm, so that such overshoots into preestimated undesirable regions do not occur.

The second remark concerns the speed of descent. The function may have a long valley in parameter space. The algorithm may then happen to shoot back and forth across the valley numerous times during the descent. If one truncates the iteration loops in an algorithm by im-

posing a certain number for maximum search trials, one might end up at a set of parameters nowhere near the true solutions. To avoid this pitfall, one should scale the parameters so that the long valley deforms into a conical depression. This would greatly enhance accuracy of solutions and minimize computer time. This is a potentially important consideration.

The third remark concerns the mathematical function erf(x) as computed by the CDC-6600. When the argument is negative, no diagnostic indication is given by the computer. It simply gives a zero value, so that any computation involving erf(negative) would give a meaningless result; and the programmer-analyst would not know why. The remedy is simply to use erf(-x) = -erf(x) in the algorithms. CDC should rectify this situation in the future, or at least warn users.

References

1. Sagalyn, R. C., Smiddy, M., and Ahmed, M., "High Latitude Irregularities in the Top Side Ionosphere based on ISIS-1 Thermal Ion Probe Data", J. Geophys. Res. 79, p. 425, (1974).

2. Headrick, J. M., and Skolnick, M. I., "Over-the-Horizon Radar in the HF Band", Proc IEEE, Vol. 62, No. 6, pp. 664-673, June 1974.

3. The Boeing Co., Document No. D233-10002-1.

4. McInerney,R. E., and Abelowitz, A., "Magnetic Field Package", AFCRL-TR-73-0356, (1973).

5. Sagalyn, R. C., and Burke, W. J., "Injun V Observations of Vehicle Potential Fluctuations at 2500 km" in Proc. Spacecraft Charging Technology Conference, AFGL-TR-77-0051, (1977).

6. Walker, E. H., "Plasma Sheath and Screening Around a Stationary Charged Sphere and Rapidly Moving Charged Body", in "Interactions of Space Vehicles with an Ionized Atmosphere" (ed. S. Singer), Pergamon Press, (1965).

7. Fletcher, R., and Powell, M. J. D., "Rapidly Convergent Descent Method for Minimization", The Computer J., Vol. 6, p. 163, (1963).

8. Powell, M. J. D., "A Method for Minimizing a Sum of Squares of Non-Linear Functions without Calculating Derivatives", The Computer J., Jan. (1965).

9. Sagalyn, R. C., and Smiddy. M., "Positive Ion Measurements of Spacecraft Attitude: Gemini X and XII", J. Spacecraft and Rockets, Vol. 6, No. 9, (1969).

10. Smiddy, M., Stuart R. D., "An Analysis of the Behaviour of a Multi-Grid Spherical Sensor in a Drifting Maxwellian Plasma", AFCRL-69-0013, (1969).

11. Lai, S. T., Smiddy, M., and Wildman, P., "Satellite Sensing of Low Energy Plasma Bulk Motion", *Bull. Amer. Meteor. Soc.*, Vol. 57, No. 8, p. 108, (1976).

12. Lai, S. T., Smiddy, M., and Wildman, P., "Satellite Sensing of Low Energy Plasma Bulk Motion", Proceedings of the Seventh Conference of Aerospace and Aeronautical Meteorology and Symposium on Remote Sensing from Satellites, Amer. Meteor. Soc. & AIAA, p. 302-306, (1976). Also, AFGL-TR-76-0281, (1976).

13. Rich, F. J., and Wildman, P., "A Model for the Electrical Current Collected by a Planar Aperture Ion Collector With a Partially Blocked Field of View", AFGL-TR-77-0096, (1976).

14. Smiddy, M., Kelley, M., Burke, W., Rich, F., Sagalyn, R., Shuman, B., Hayes, R., and Lai, S., "Intense Poleward-Directed Electric Fields Near the Ionospheric Projection of the Plasmapause", Geophys. Res. Lett., Vol. 4, No. 11, pp. 543-546, November 1977.

6. Ionospheric Electric Fields

6. Ionospheric Electric Fields

Initiator: M. Smiddy

Project No: 2311 Problem No: 4702

6.1 Introduction

Electric fields are an important aspect of the ionospheric-magnetospheric region of space. The plasma in this region, and the associated electromagnetic fields, form the environment of the Air Force's satellite systems, with which they experience important interactions. The reconnection of the magnetic field lines frozen in the solar wind induces electric fields which are subsequently mapped down into the polar magnetosphere and ionosphere. Electric fields perturb the ambient plasma flow, affecting electromagnetic wave communications, especially in the polar region. In order to map the global distribution of these electric fields and their associated currents, the Air Force scientific satellite S3-2 was launched into a nearly polar orbit.

6.2 Rotating Satellite Boom Sensor System

The S3-2 satellite featured three pairs of deployable, mutually orthogonal booms. It had an initial apogee, perigee, inclination, and spin period of 1556 km, 240 km, 96.3°, and 20 seconds respectively (Ref. 1). The electric field sensors were carbon coated spheres of 3.81 cm radius, four of which were mounted on the ends of 13.72m long triaxial cable wire booms deployed in the radial force field of the spinning satellite. Two other sensors were mounted on the ends of two rigid booms deployed parallel to the spin axis with a tip-to-tip 11.18m electrode separation. Data were obtained from only one of the wire boom pairs in the satellite spin plane and from the axial pair of sensors. Experimental techniques for making double probe electric field measurements have been described elsewhere (Refs. 2,3).

The frequency components of the data from the sensors were predominantly at spin frequency and orbit frequency. However, other frequencies corresponding to various oscillation modes may be present during periods of perturbation to the satellites' motion. These effects are especially pronounced during the transient response periods following boom deployment, spin orientation maneuver, etc. A comprehensive study of the mode dynamics of the rotating satellite has been fully documented in the References 4, 5, and 6, and will not be discussed further here.

The booms in the spin plane detected predominantly sinusoidal electric fields due to the rotational behavior of the satellite. The predominant

electric field measured is the induced field ($\underline{v} \times \underline{B}$), where $\underline{v}$ is the velocity of the satellite and $\underline{B}$ is the magnetic field. This induced field is a relativity effect (Ref. 7). Furthermore, the rotating frame of the earth introduces a Coriolis effect (Ref. 8) ($\underline{\omega} \times \underline{r}$) which also has to be subtracted in order to separate the genuine electric field, $\underline{E}_{true}$, from the measured field $\underline{E}_{meas}$. Thus,

$$\underline{E}_{meas} = \underline{E}_{true} + (\underline{v} - \underline{\omega}_e \times \underline{r}) \times \underline{B} \qquad (1)$$

where $\underline{\omega}_e$ is the earth's rotational angular velocity, and $\underline{r}$ is the position vector of the spacecraft measured from the center of the Earth.

6.3 Data Structure and Processing Techniques

For data reduction and computation, three types of input data are required. They are: (1) electric field experiment data, (2) satellite sensor attitude (OM) data, and (3) ephemeris and magnetic field (ORMAG) data. The structures of these data are tabulated in the References 9, 10, and 11. The electric field experiment data are in the fifth file of every tape of the satellites's raw data. The experimental data contain six channels of sensor signals with various high and low gains. These signals are given in telemetry counts, which can be converted to voltages by a simple conversion factor.

A central idea for the determination of the various geophysical parameters from experimental data is the fitting of curves using theoretical formulations based on physical considerations. The main program system for this project employs curve fitting techniques using satellite orbital frequency ω_o and spin frequency ω_s. Transformations of spacecraft and geophysical coordinates are also crucial in the computation algorithms. Some of the transformation matrices are documented in Reference 12.

6.4 The DC-Offset

Due to the relatively superior sensitivity of the instruments on this satellite, a new feature has been detected in the nature of the electric field data. It is the DC-offset, V(t), which is a very slowly varying function with some orbital periodicity. Correlation analysis using eq. (1), has been carried out in order to determine whether the DC-offset of the radial boom system would mirror that of the axial and thus allow for rigorous correction. I.e.,

$$V_{\text{Booms 5-6}}(t) = a + b * V_{\text{Booms 1-2}}(t) \qquad (2)$$

This would be the case, for example, if the effect were due to a monolayer of O^+ ions on the spheres. However, the data does not support this relationship. The axial voltage level tracks the plasma density even in a pure H^+ plasma. This occurs even equatorward of the light ion trough. One view (Ref. 13) is that the offset V(t) is not a real electric field variation but some complicated function of plasma density and electric field. Thus, the offset V(t) is an instrumental and environmental effect and must be subtracted off if true electric field in the ionosphere is to be determined.

$$\underline{E}_{\text{true}} = \underline{E}_{\text{meas}} - (\underline{v} - \omega_e \times \underline{r}) \times \underline{B} - V(t) \qquad (3)$$

The method of DC-offset subtraction is as follows. For lower latitudes

(<60°), where the earth's magnetic field lines are closed, the ambient electric field is vanishingly small because of the lack of solar wind induced effects mapping down along open magnetic field lines. Therefore, any voltage that remains after subtraction of the induced field ($\underline{v} \times \underline{B}$) can be attributed to the sphere's DC-offset. By deleting regions above 60°, and by fitting a slowly varying function (eq. 4) with orbital periodicity ω_o^{-1} to this voltage, one can determine, approximately, the contact potential for an entire orbit.

$$V(t) = \sum_{i=1}^{n} A_i \sin i\omega_o t + \sum_{i=1}^{n} B_i \cos i\omega_o t + C \qquad (4)$$

In addition, there is another instrumental/environmental effect. The instruments operate with a calibration sequence every 512 seconds. But during and immediately after a calibration sequence, the satellite data show an exponentially recovering pattern for about 40 to 60 seconds. These post-calibration data must be deleted before the treatment using eq.(4) can be used.

6.5 Program System and Description

The main analysis is presently executed by means of a highly integrated system of programs as depicted in the flow chart of Figure 1. Figure 2 represents a more detailed flow chart of some of the initial operations shown in Figure 1: calibration, v x B subtraction, and Fourier or polynomial offset fit. Similarly, Figure 3 illustrates, in greater detail, some of the final processing steps: main processing, geophysical transformations, and special techniques for fitting DC offsets.

Initial processing unpacks the raw data file, recognizes data words, converts data to raw voltages by the appropriate amplifier gain, removes amplifier bias, subtracts the induction field, and eliminates calibration sequences. Interactive processing displays the intermediate data on a CRT graphics console, permits editing, and performs various functional fits to the edited data while allowing the user to vary pertinent parameters. Plots of the final fit and a deck of coefficient cards are output on option. The program also has a Butterworth filtering routine and an optional correlation analysis routine. A non-interactive version can also be used optionally, and is presently the adopted version in the consolidated automated program system. Since one set of sensors in the spin plane is inoperative, an instantaneous determination of $\underline{E}(t)$ is not possible. However, if $\underline{E}(t)$ varies at a rate slower than the spin frequency of the satellite, then the field can be resolved. More specifically, if the frequency

spectrum of E(t), defined by

$$\underline{\Sigma}(\omega) = \int \underline{E}(t) e^{i\omega t} dt \qquad (5)$$

is bounded so that $|\underline{\Sigma}(\omega)| = 0$ for $\omega > \omega_s$, then one can determine $\underline{E}$ unambiguously. For most orbits studied, this seems to be the case. The Main Program System then determines $\underline{E}$ by fitting a function of the form

$$V(t) = A(t) \sin(\omega_s t) + B(t) \cos(\omega_s t) + C(t) \qquad (6)$$

to the spinning boom voltage. A(t) and B(t) are expressed in terms of a predetermined number of Chebyshev polynomials, such that their frequency content does not exceed ω_s. Since the voltage measured is given by

$$V(t) = \underline{E}(t) \cdot \underline{R}(t),$$

where $$\underline{R}(t) = R_o (\sin(\omega_s t)\, x + \cos(\omega_s t)\, y), \qquad (7)$$

one sees that A(t) and B(t) are the x and y components of $\underline{E}$, expressed in a coordinate system defined at t=0. The offset is adequately given by C(t) in (6), provided that it does not vary rapidly compared to spin frequency. The third component of the electric field is measured directly by the axial boom, with offset subtracted, as described in section 6.4.

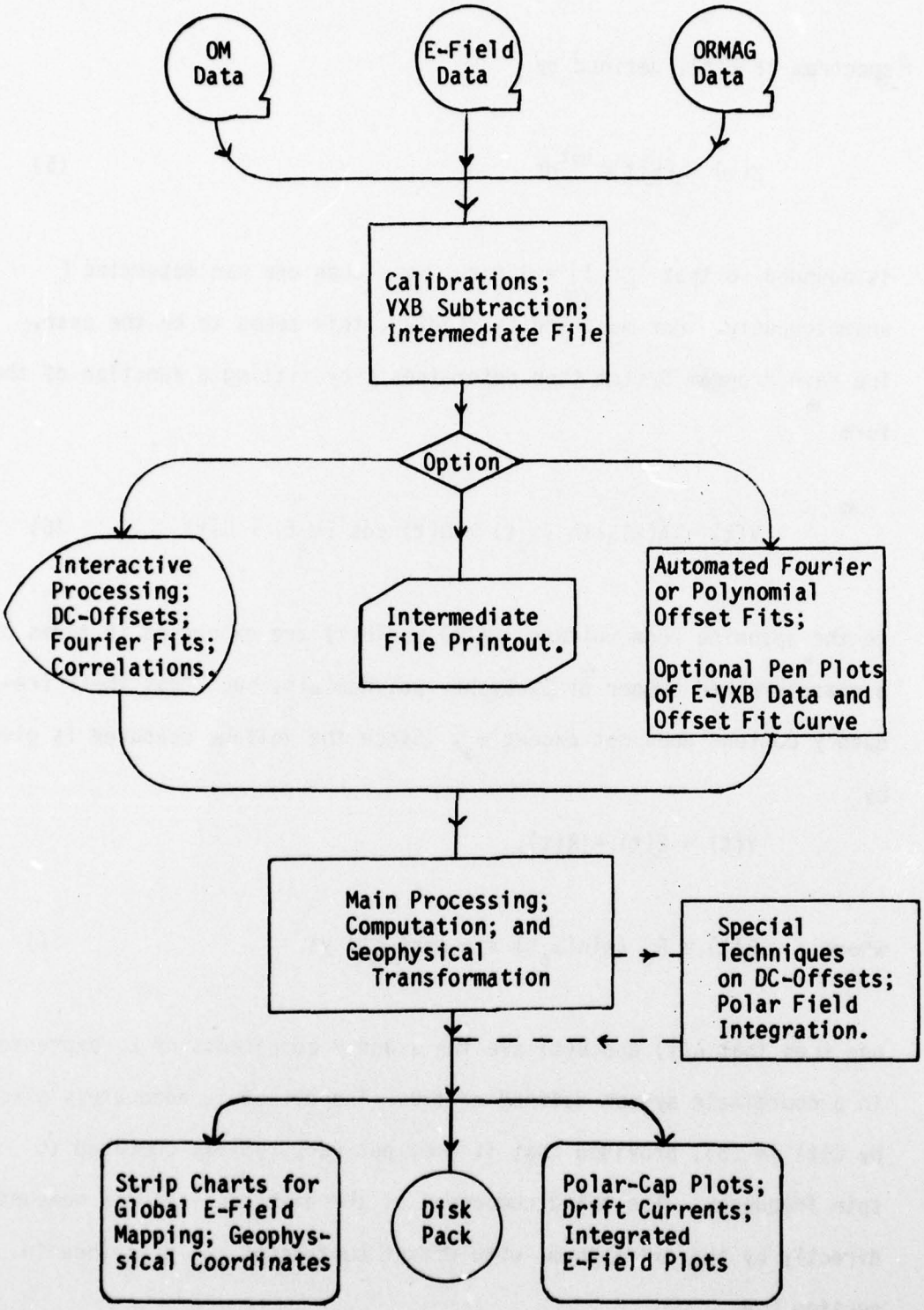

Figure 1. Flow Chart of Consolidated Program System for Electric Field Analysis

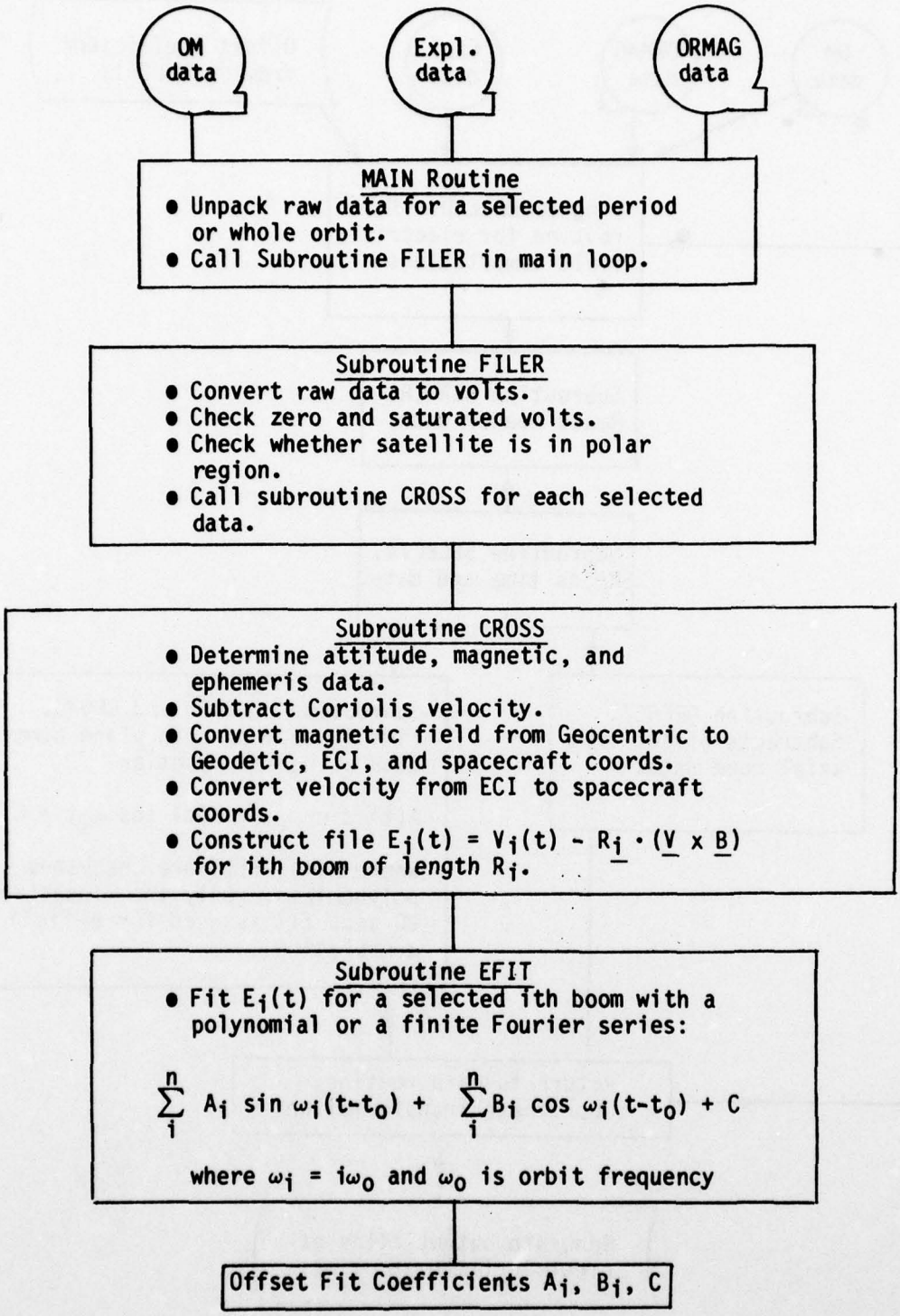

Figure 2. Flow Chart for the Functional Description of Program OBTFILEFIT.

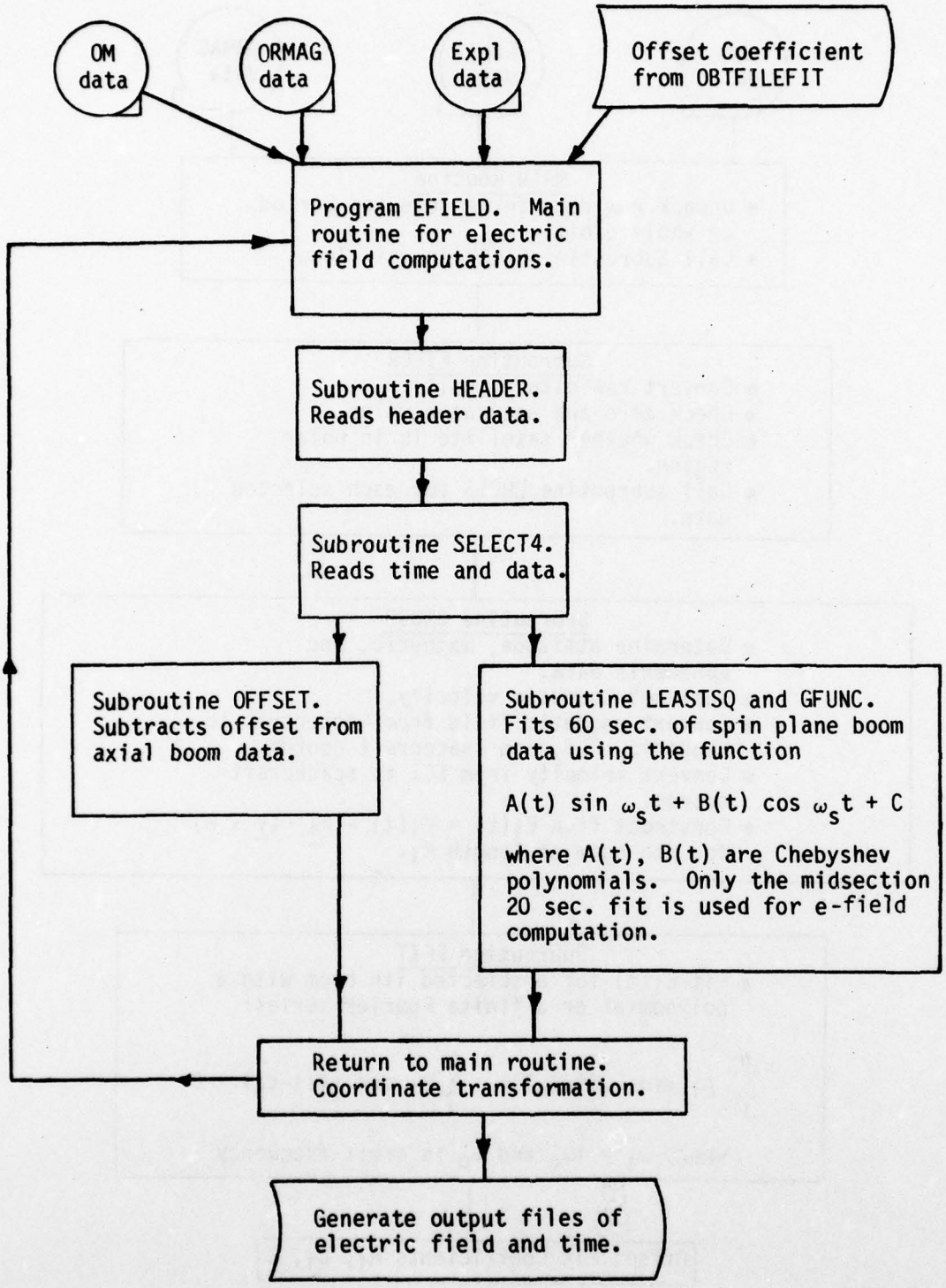

Figure 3 . Flow Chart for the Functional Description of Program EFIELD.

6.6 Presentation of Results

The electric field results obtained from the EFIELD program are transformed to various geophysical coordinate systems, written on a disc pack file, and plotted a strip charts and polar plots. In the strip charts, the ionospheric electric field magnitude and components are plotted for a whole orbit in earth centered inertial, geomagnetic, satellite local vertical, or optionally solar magnetic coordinates. A typical strip chart is shown in Figures 4 and 5. In the polar plots, the geomagnetic components of electric fields measured by the satellite on polar passes are presented (Fig. 6). A line is drawn from each satellite position in the direction of the electric field, with its length proportional to the field strength. The circles show constant invariant latitudes. The satellite track is not a straight line because the magnetic pole is displaced from the geographic pole. Magnetic local time advances counterclockwise from midday, at the top. The drift current map (Fig. 7) is generated from the electric field polar plot, by computing the convective drift velocity from the electric field and a knowledge of the earth's magnetic field. Using the techniques outlined in these sections, hundreds of orbits of satellite data have been processed and the electric fields mapped. In particular, the largest electric field structure ever detected at low altitudes in the ionosphere has been discovered (Ref. 1). The event took place during a magnetic storm and the field structure was in the evening sector near the ionospheric projection of the plasmapause. The main pulse directed magnetically northward. No significant elec-

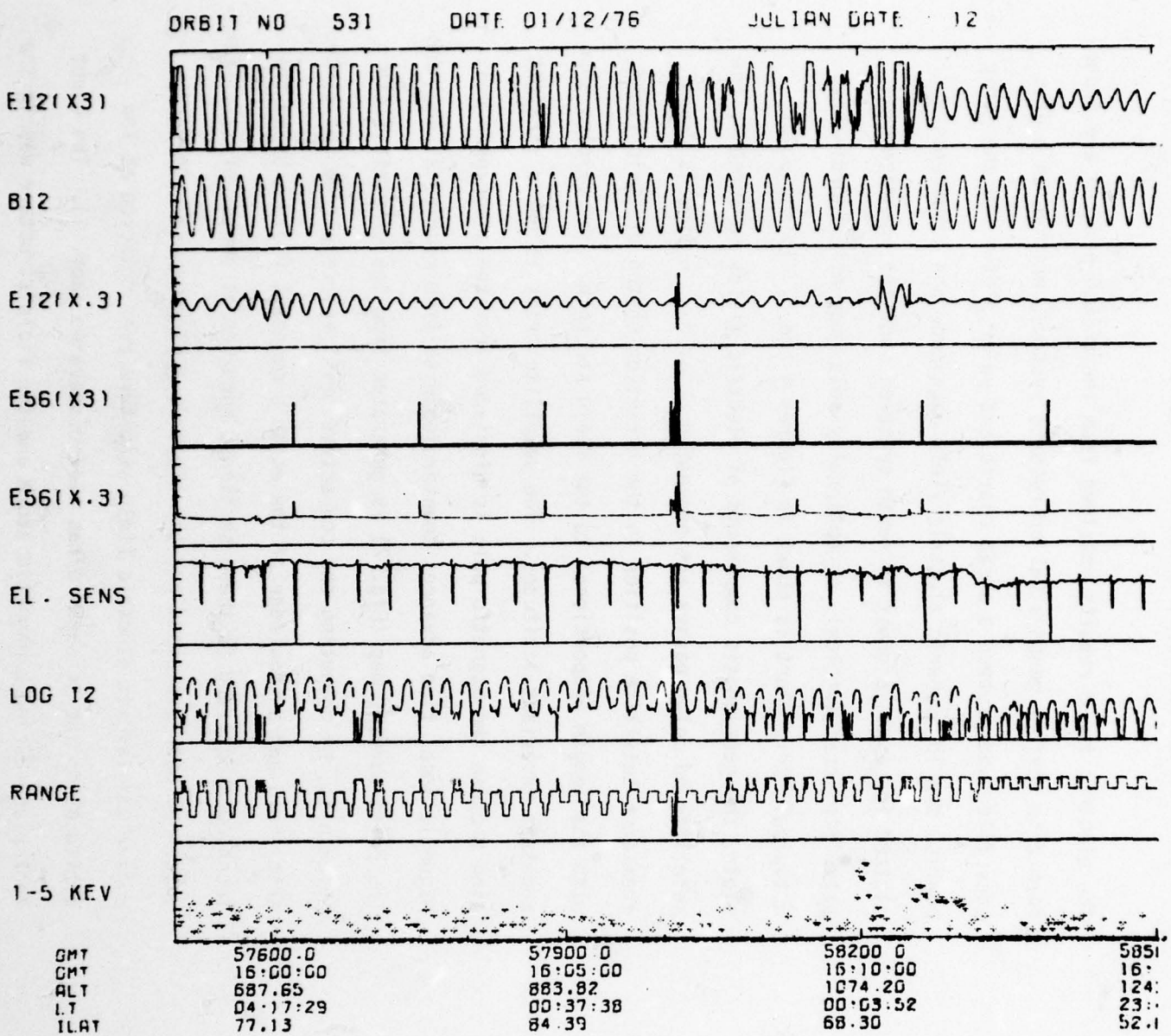

Figure 4. Strip Chart Plot of Measurements from the E-Field, Plasma Motion, and High-Energy Particle Flux Experiments

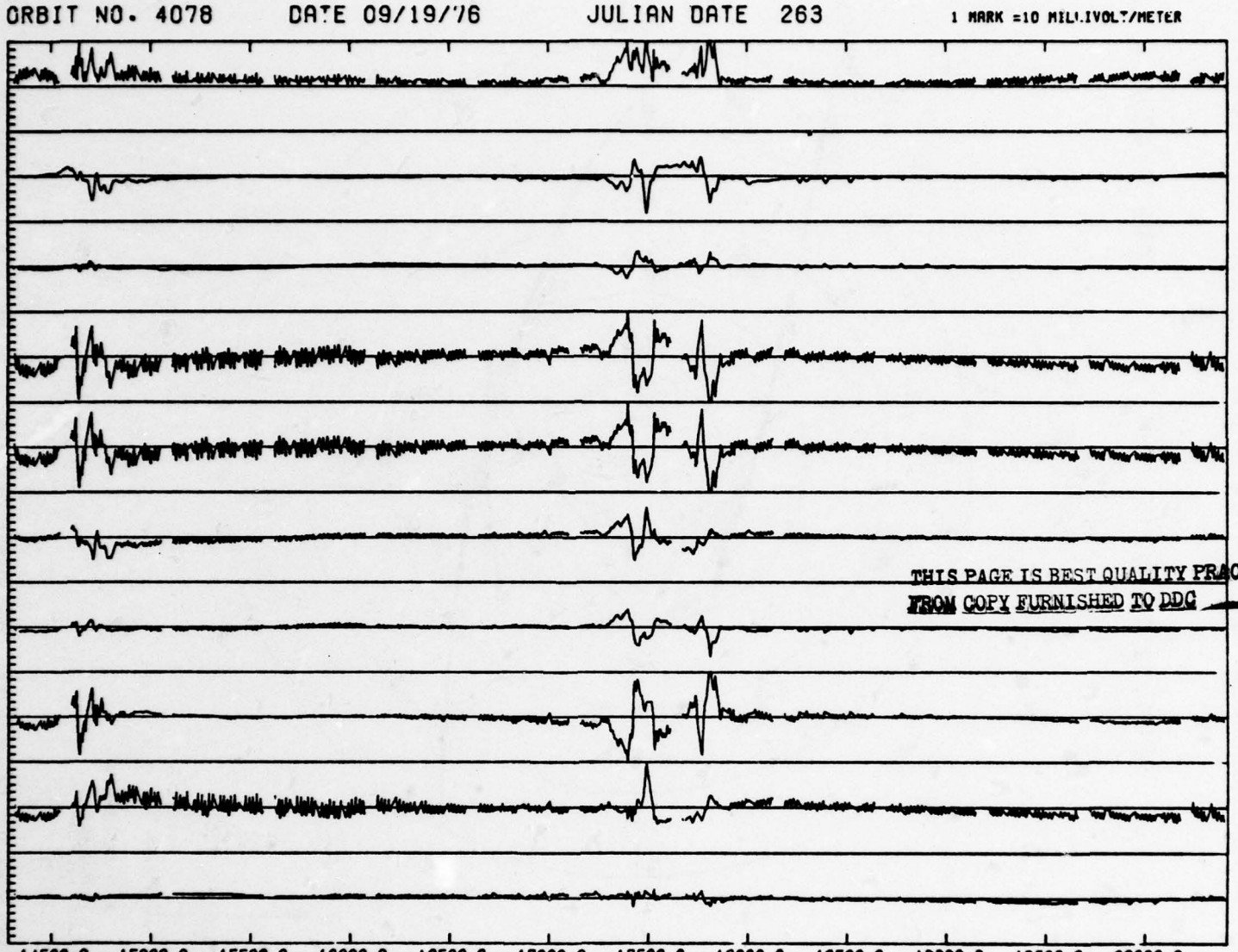

Figure 5. In top-to-bottom sequence: Electric Field Magnitude and Components Computed in Local Vertical, Earth Centered Inertial, and Geomagnetic Coordinate Systems. Ephemeris data are listed below the abscissa.

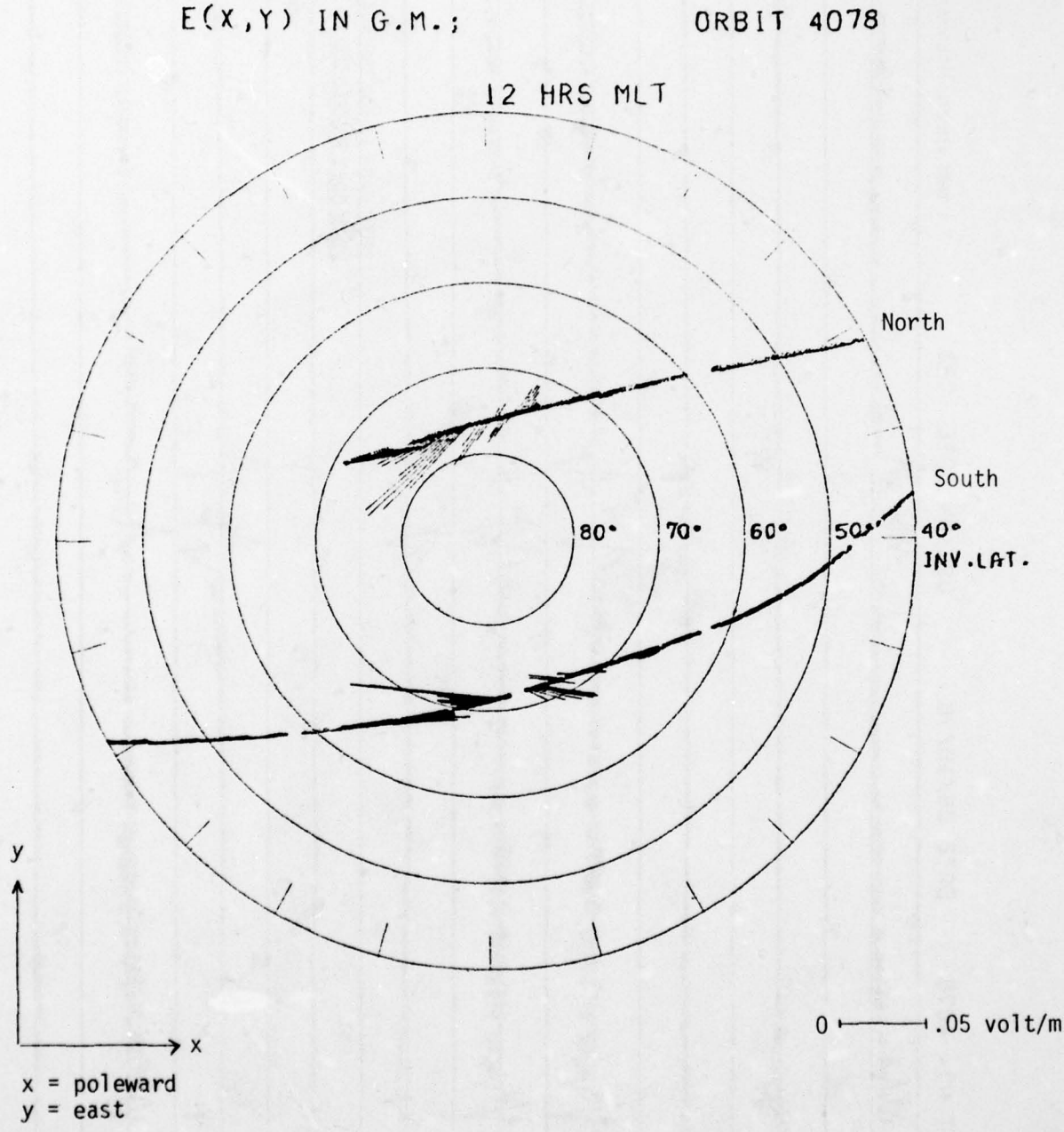

Figure 6. Geomagnetic Components of Polar Electric Field Mapped on a Background of Invariant Latitude and Magnetic Local Time

AD-A062 488 LOGICON INC LEXINGTON MA F/G 4/1
RESEARCH, ANALYSIS, DEVELOPMENT, AND APPLICATION OF HIGHLY INTE--ETC(U)
OCT 78 J N BASS, K H BHAVNANI, S T LAI F19628-78-C-0049
UNCLASSIFIED AFGL-TR-78-0204 NL

3 OF 3
AD A062488

END
DATE FILMED
3-79
DDC

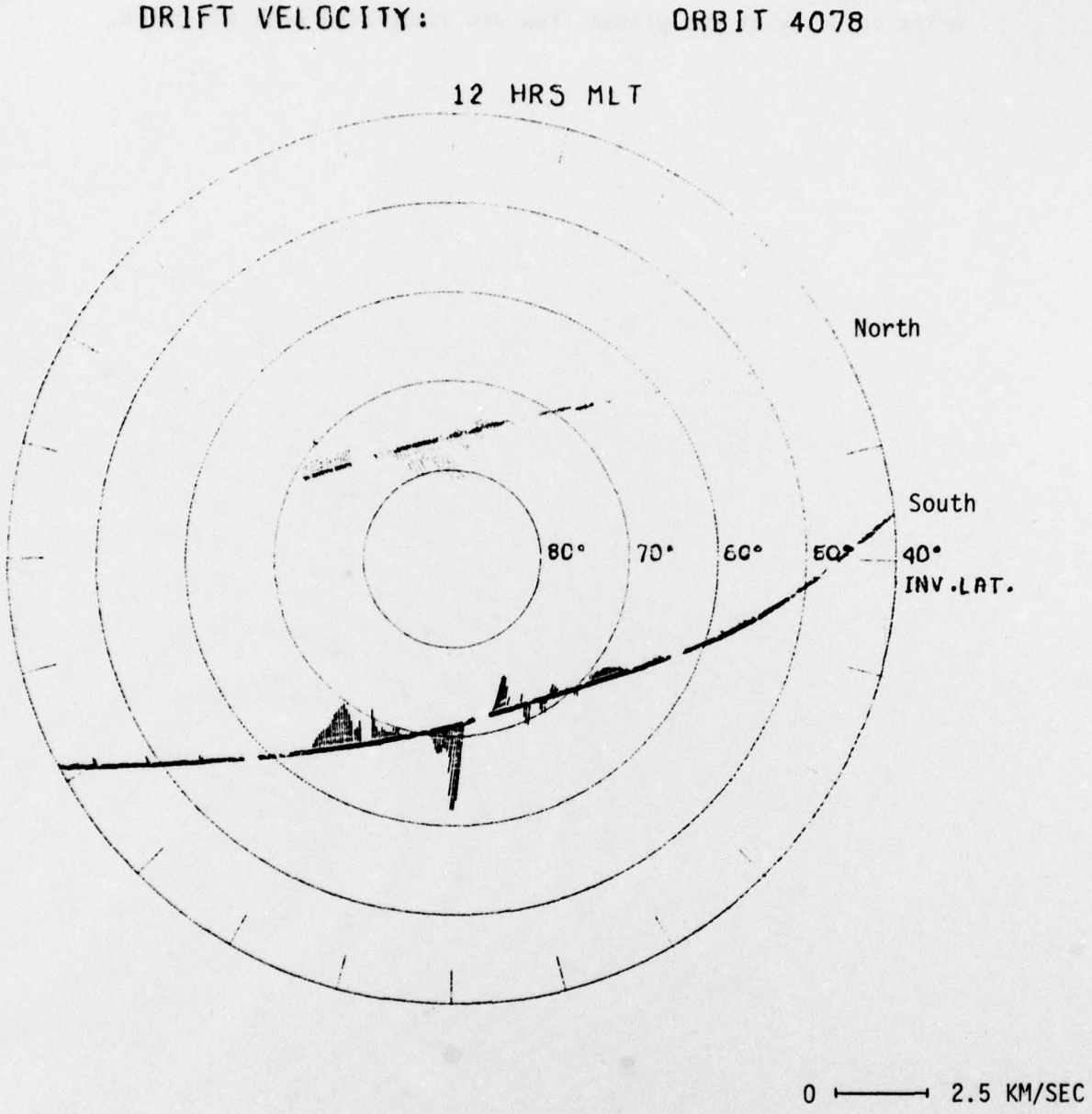

Figure 7. Drift Current Map Generated from the Polar Electric Field Map by Computing the Convective Drift Velocity from the Electric Field and a Knowledge of the Earth's Magnetic Field

tric field aligned with the magnetic field showed up. A very high drift velocity of the plasma flow was associated with the pulse.

6.7 Cross Polar Cap Potential

For dawn-dusk orbits where the electric field is predominantly in the forward direction of the satellite, the drift current must be perpendicular to the trajectory. For cross polar potential calculations, the integral $\Phi = \int \underline{E} \cdot d\underline{s}$ is digitally approximated by $\Phi = \sum_i \Delta\Phi_i$. More specifically, let E_r be the component of electric field measured by the radial detectors (dipole booms 1-2) and $\Delta\underline{s}$ be the distance which the vehicle which has moved perpendicular to $\underline{B}$ in time Δt

$$\Delta\underline{s} = \frac{\underline{B} \times (\underline{v} \times \underline{B})}{B^2} \Delta t$$

where the velocity $\underline{v}$ must be defined in the same reference frame as $\underline{E}$ (i.e., rotating or not). Thus, for each half spin period τ, the potential change $\Delta\Phi_i$ is calculated by using (Ref. 14)

$$\Delta\Phi_i = -\underline{E}_{r,i} \frac{\underline{B} \times (\underline{v} \times \underline{B})}{B^2} \tau$$

The total $\Phi_n = \sum_i^n \Delta\Phi_i$ is then plotted at each incremental time Δt. Calculated cross polar cap potential drops range between 20 and about 80 kilovolts. The implications of these observations for our understanding of high latitude convective patterns and their relation to the orientation of the interplanetary magnetic field have been presented (Ref. 15). A typical Φ polar plot is shown in Figure 8.

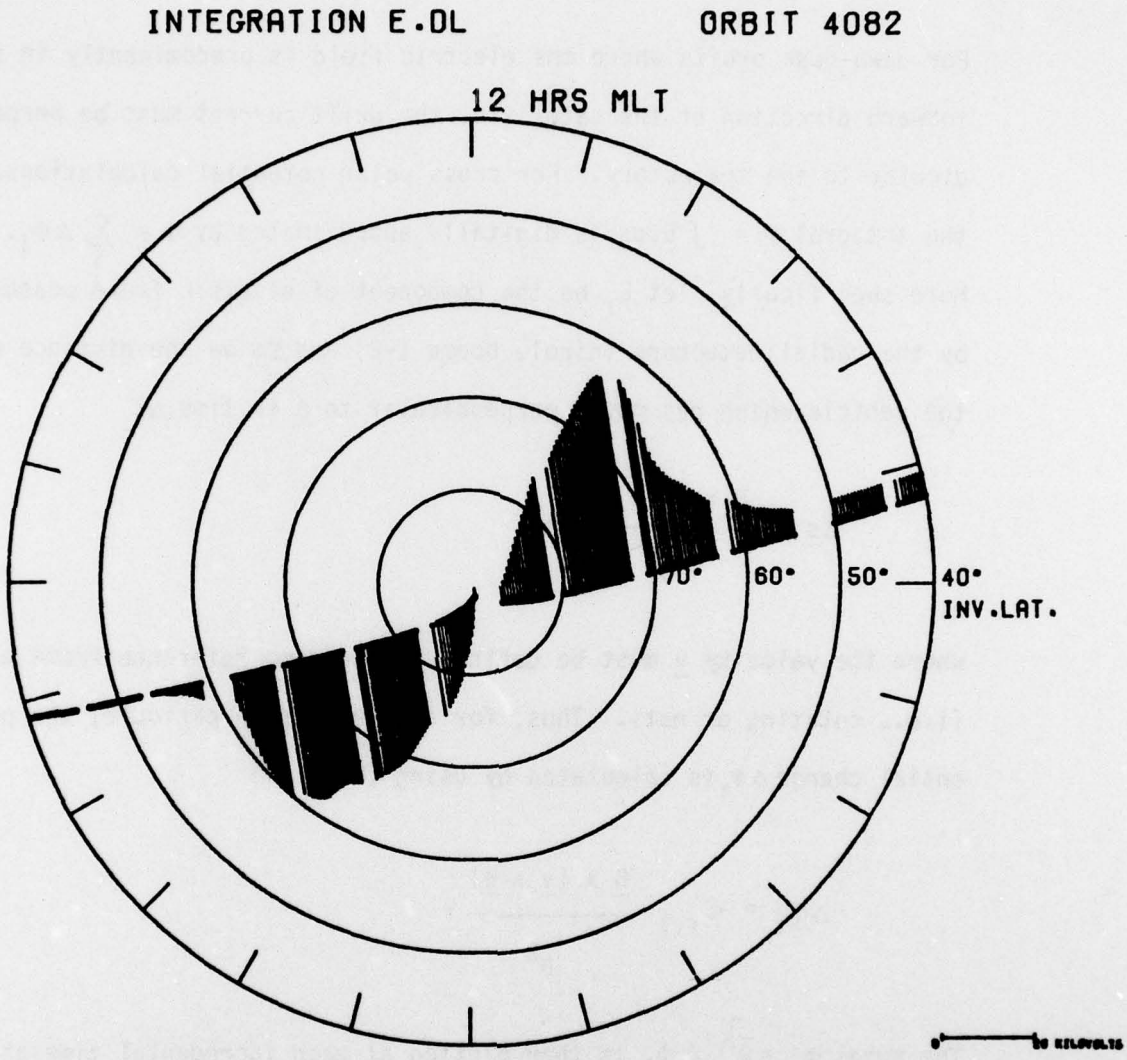

Figure 8. Cross Polar Cap Electric Field Integration

6.8 Polar Electric Fields and Plasma Convective Flows In High Latitudes

The phenomenon of electric field reversals in the high latitude regions near the dawn-dusk meridian has been known for several years (Refs. 16, 17). The field reversals are consistent with convective patterns of plasma flow in these regions. The patterns of electric fields and plasma flows are highly dependent on solar winds and therefore on interplanetary magnetic fields (IMF). Using satellite S3-2 results, morphological classification of these patterns has been achieved (Refs. 18,19), and compared with earlier works (Ref. 20).

For data analysis, orbits were chosen from those of the last four months of 1976 when S3-2 was near the dawn-dusk meridian. They were selected if: (1) the satellite passed to invariant latitudes > 80°, and (2) hourly averaged values of the interplanetary magnetic field (IMF) were available. A total of 43 northern and 48 southern polar cap passes satisfied these criteria.

For the benefit of those not experienced in this field, a digest is given as follows.

In Figure 9, morphological patterns of polar plasma convection are displayed.

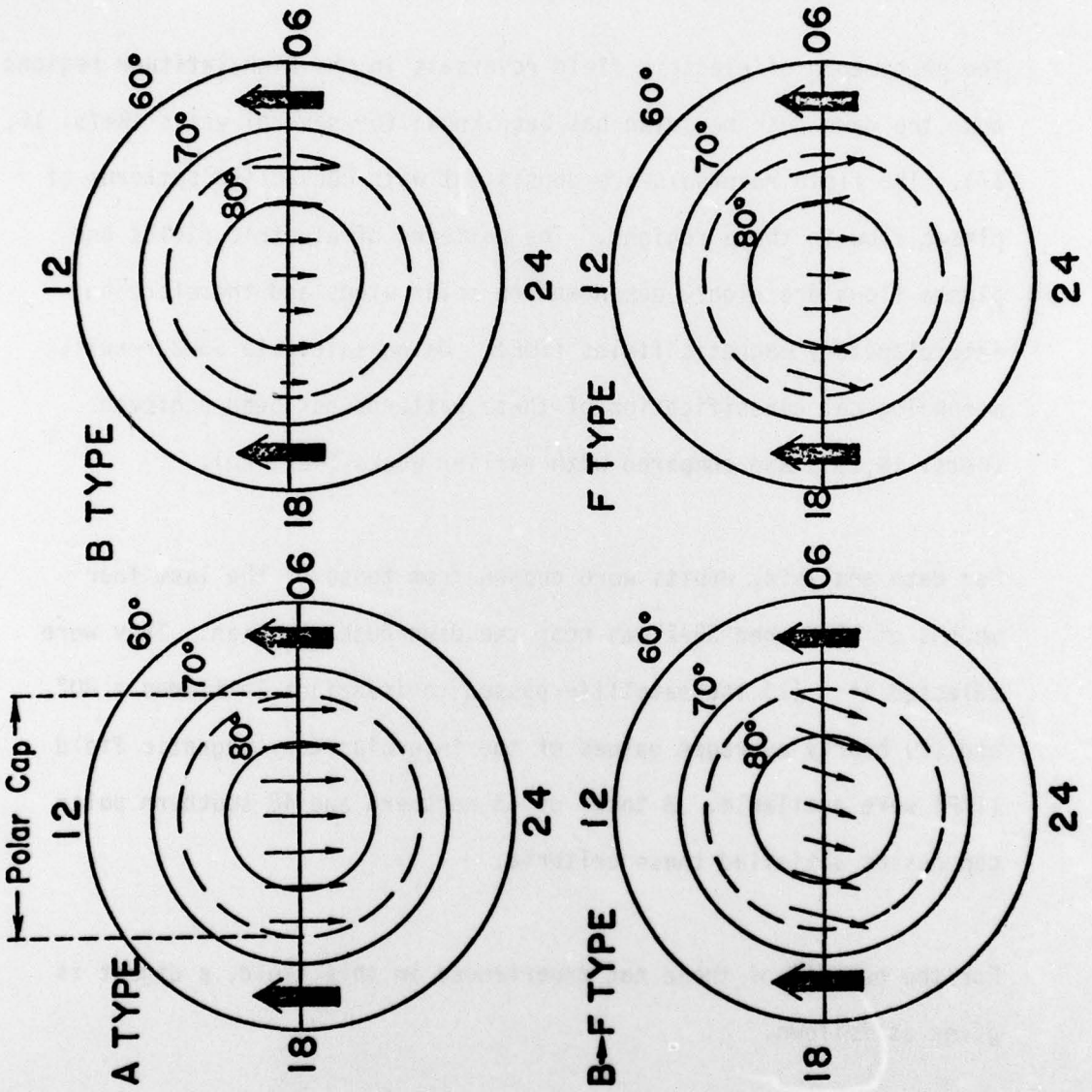

Figure 9. Morphological Patterns of Convection Currents in the Polar Region

The flow in the mid portion of the pattern is anti-sunward and that in the outer portion of the pattern sunward, completing the convection. The magnetic field $\underline{B}$ in the polar region is practically downward so that the flow ($\underline{E} \times \underline{B}$) is due to an electric field in the dawn-dusk direction, with reversals occurring twice in the poleward auroral zones, as shown in Figure 10.

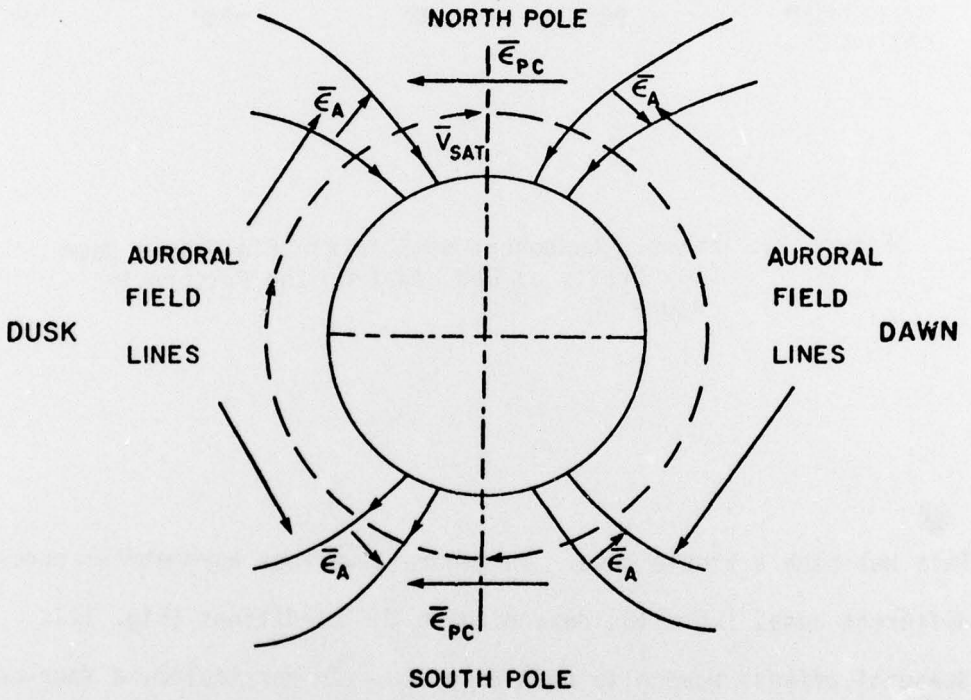

Figure 10. Electric Field Reversals in Auroral Regions in a Dawn-Dusk Cross Section

Thus, a satellite would measure on its dawn-dusk trajectory a forward component of the electric field as portrayed in Figure 11.

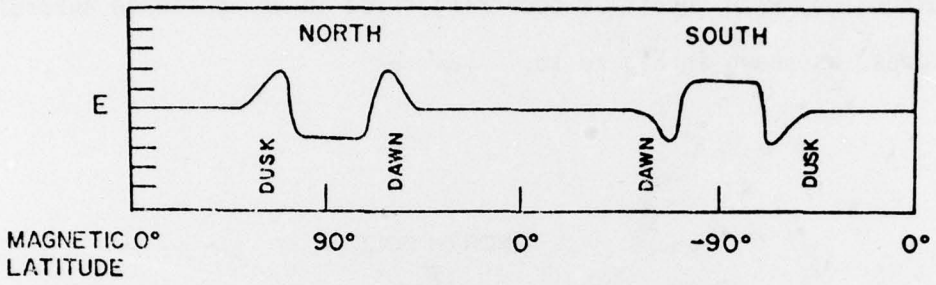

Figure 11. Forward Component of Electric Field in a Dawn Dusk Orbit, as Deduced from the Pattern in Figure 10

This has been a simple case. In general, various asymmetries occur in different cases (Ref. 18) depending on IMF conditions (Fig. 12). Seasonal effects have also been observed. In particular, a four-cell convection pattern (Fig. 12) with sunward flow in the middle has also been discovered, (Ref. 19), agreeing with the theoretical conjecture of Maezawa, (Ref. 21).

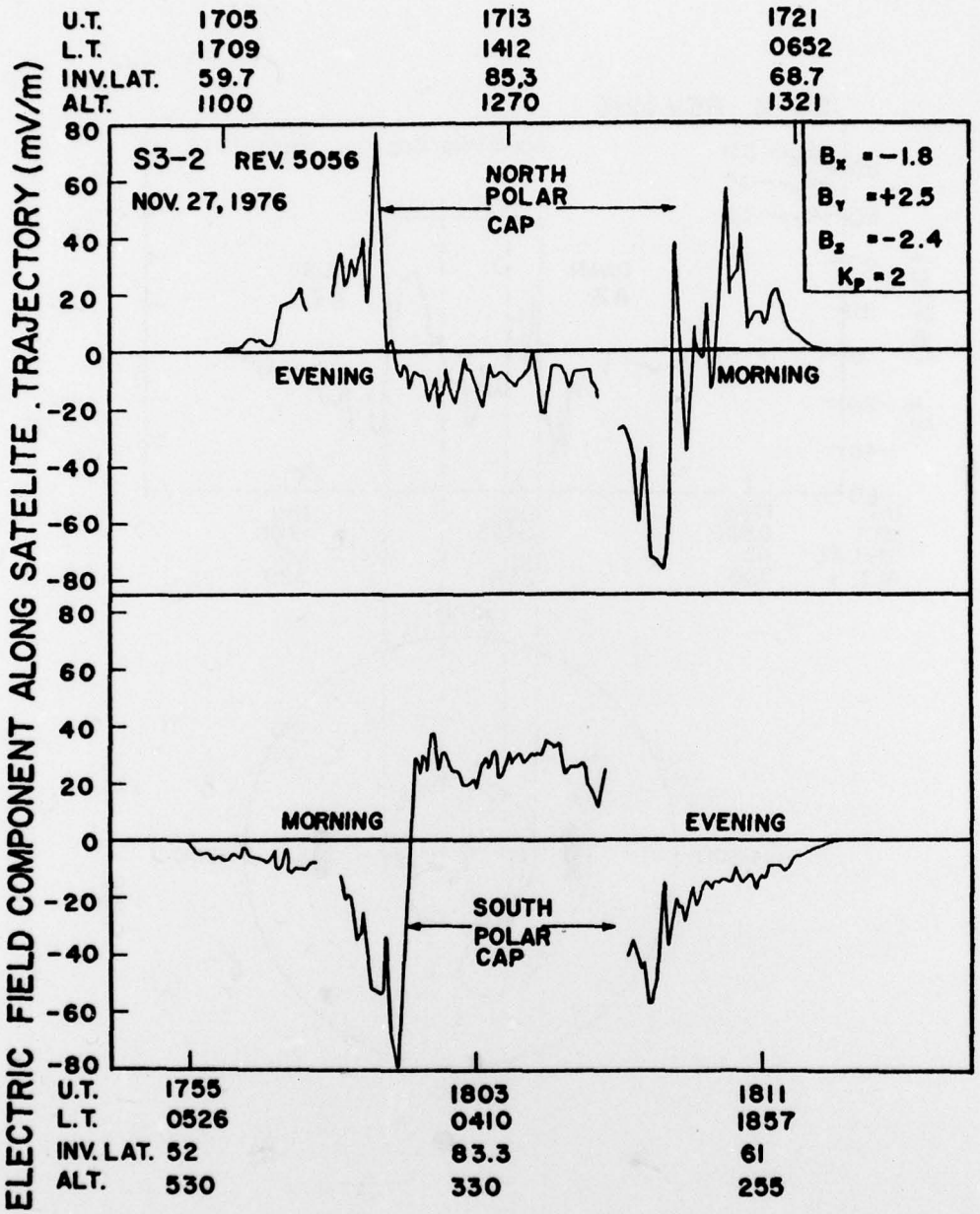

Figure 12. Forward Component of Electric Field Measured by Satellite S3-2 in a Dawn Dusk Orbit

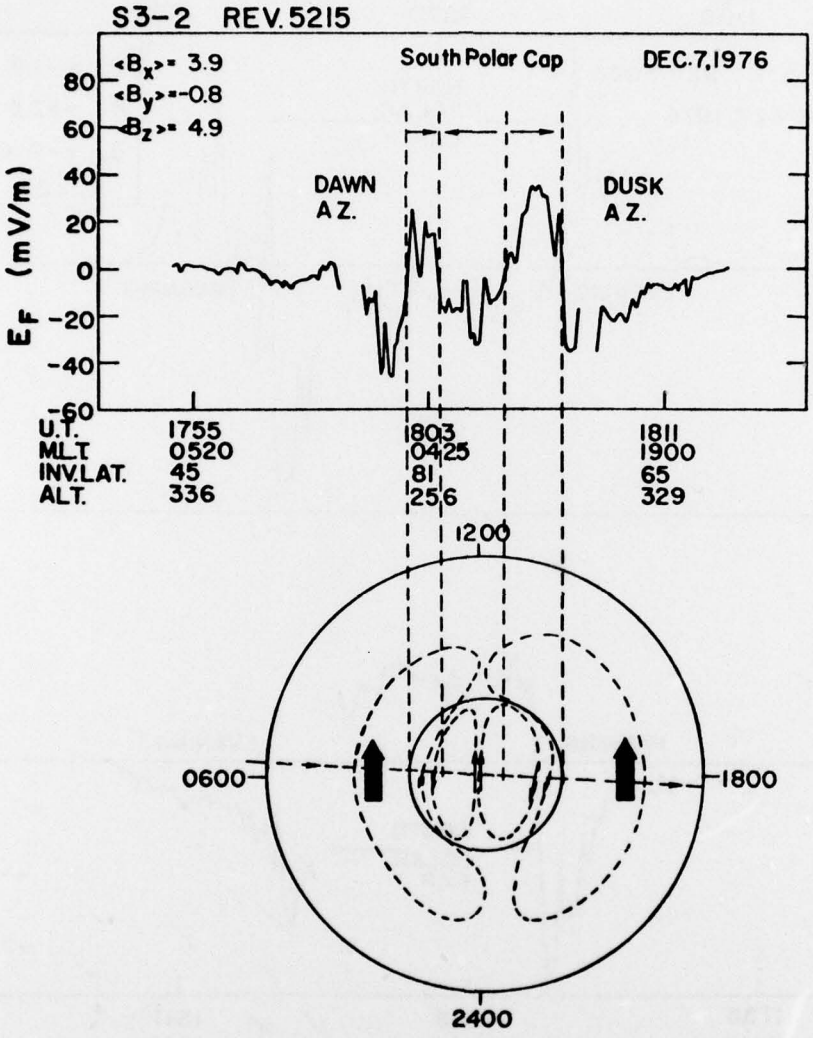

Figure 13. Forward Component of Electric Fields Measured by Satellite S3-2 Traversing a Four Cell Drift Flow Pattern in the Polar Region

6.9 Anomalous Resistivity along Magnetic Field Lines

Due to the helical motion of charged particles along magnetic field lines $\underline{B}$, the probability of particle collision is mainly in the directions transverse to $\underline{B}$. The particles move practically as free particles along $\underline{B}$ and provide negligible resistivity. This the reason why electrical resistivity is substantial only in directions transverse to $\underline{B}$; and electrical fields parallel to $\underline{B}$ are practically zero. However, interesting plasma interaction events occur in the ionosphere and magnetosphere. On rare occasions, anomalous resistivity along $\underline{B}$ appears.

Electric fields parallel to $\underline{B}$ have been clearly found in one of the S3-2 orbits: orbit 517B has been studied in very careful detail. Large local fluctuation of magnetic field appeared, due to the presence of strong current j_z (i.e., $\partial By/\partial x = j_z$) in the local vertical system (Fig. 14). Strong electric fields, including substantial components along B, were found. The event occurred after the satellite entered the O^+ region, where the energetic electrons excited the O^+ to cause visible arcing (Fig. 15). The gyrofrequency of oxygen ion has been identified in the FFT power spectrum of electric field data. The plasma ion current (Fig. 16) showed significant change in amplitude when entering the O^+ region, because the heavy O^+ ion mass (compared to the H^+ mass) renders a great difference between forward sensor ion current and backward sensor ion current. The particle energy counter clearly indicated an inverted V event during this period. The forward

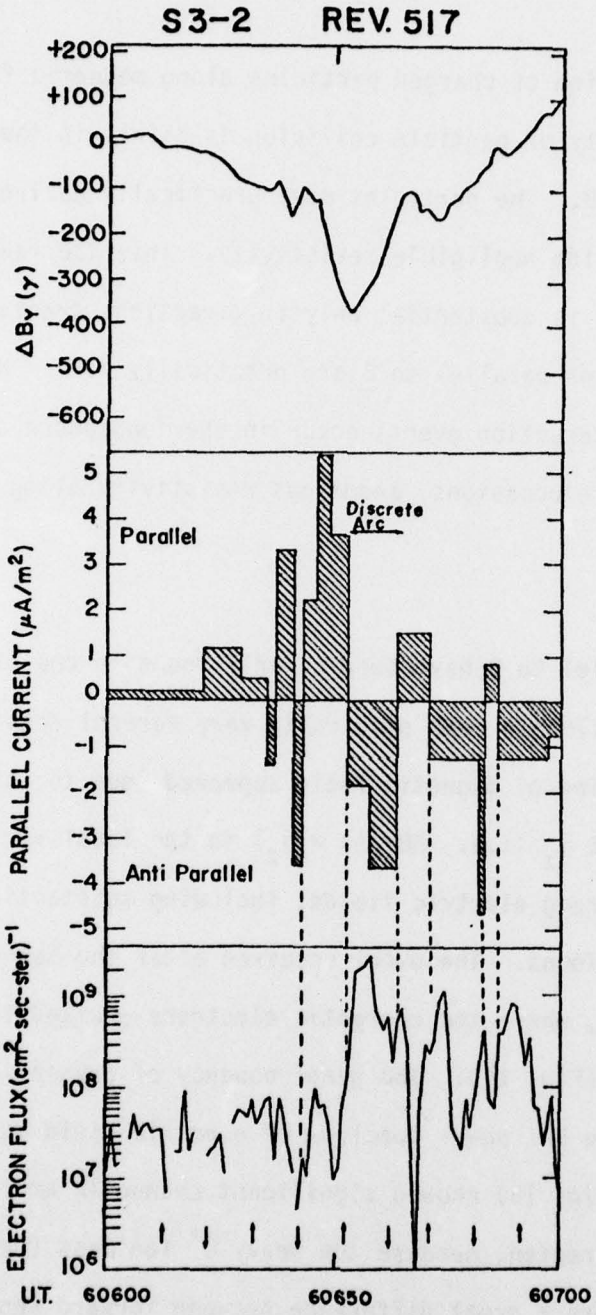

Figure 14. Disturbance in Magnetic Field Associated with Parallel Currents During the Satellite S3-2 Traverse of an Inverted "V" Event

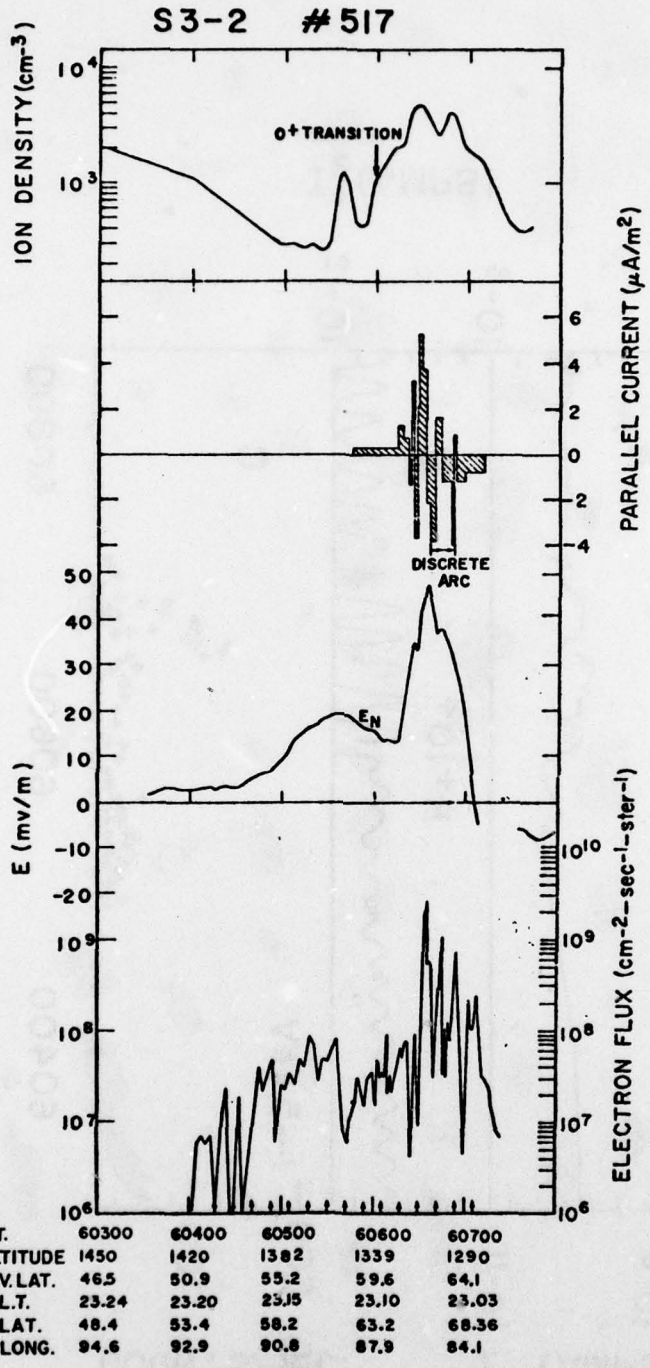

Figure 15. The arcing phenomenon occurs in 0^+ region. The forward component of electric field shows a sudden rise and then abrupt fall into negative values.

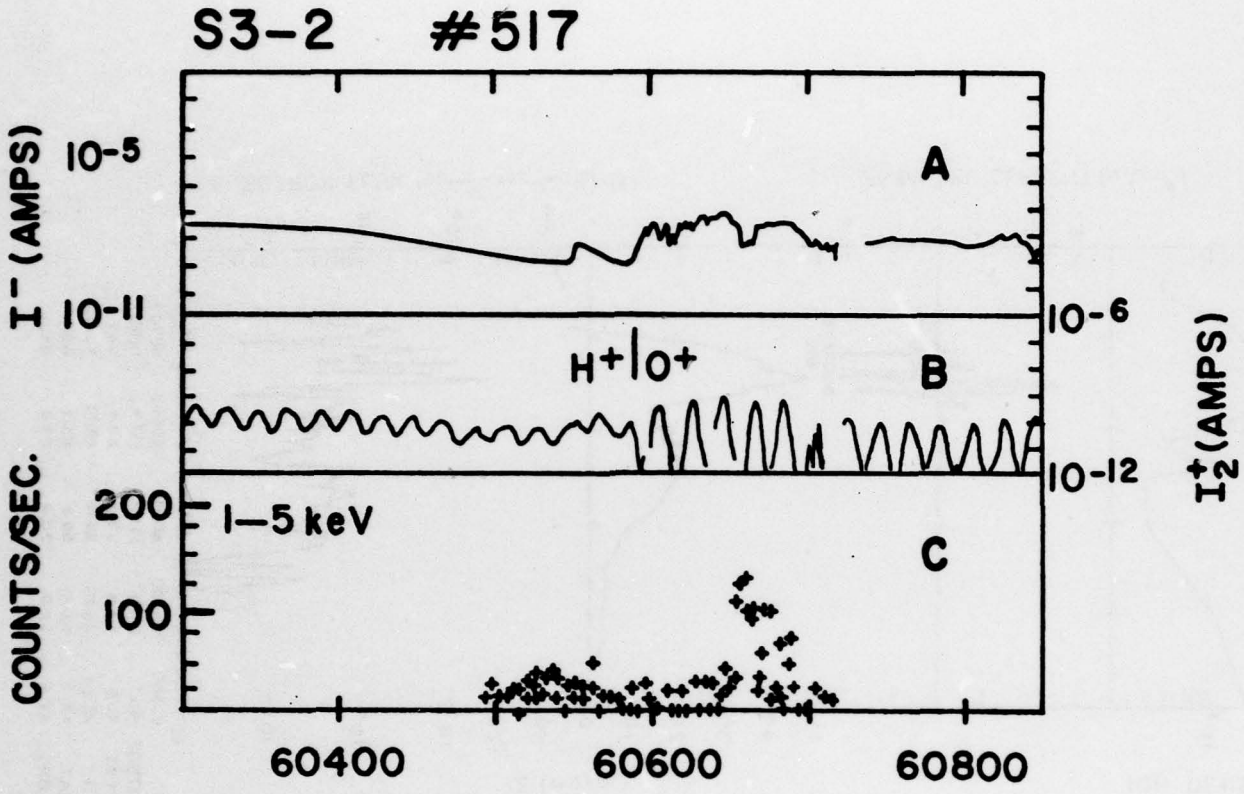

Figure 16. Electron density (A), ion sensor current (B), and Particle Energy counter (C) measurements, showing an inverted "V" event occurring shortly after the satellite enters O^+ region.

component of $\underline{E}$ shows a sharp rise as the satellite enters the inverted V region and drops rapidly into negative values as the satellite leaves. These exciting results will be written up as a paper intended for publication (Ref. 22).

References

1. Smiddy, M., Kelley, M., Burke, W., Rich, F., Sagalyn, R., Shuman, B., Hayes, R., and Lai, S., "Intense Poleward-Directed Electric Fields Near the Ionospheric Projection of the Plasmapause", Geophys. Res. Lett. 4, No. 11, pp. 543-546 (1977).

2. Mozer, F. S., "Analyses of Techniques for Measuring DC and AC Electric Fields in the Magnetosphere", pp. 273-312.

3. Fahleson, U., "Theory of Electric Field Measurements Conducted in the Magnetosphere with Electric Probes", Space Sci. Rev., 7 pp. 238-262 (1967).

4. Lai, S. T., Mahon, H., and Smiddy, M., "Dynamics of Wire Boom Oscillations on a Spinning Satellite, Part I: Lagrangian Equations of Motion and Transient Response", (accepted for publication, J. Appl. Math & Phys.)

5. Lai, S. T., Mahon, H., and Smiddy, M., "Dynamics of Wire Boom Oscillations on a Spinning Satellite, Part II: Normal Modes in Spin Plane", (accepted for publication, J. Appl. Math. & Phys.)

6. Lai, S. T., Mahon, H., and Smiddy, M., "Dynamics of Wire Boom Oscillations on a Spinning Satellite, Part III: Normal Modes out of Spin Plane", (to be submitted to J. Appl. Math, & Phys.)

7. Landau, L. D., and Lifshitz, I., Classical Theory of Fields, 3rd Edition, Addison-Wesley, (1973).

8. Goldstein, H., Classical Mechanics, Addison-Wesley, Reading Mass., (1950).

9. The Boeing Co., Document No. D233-10002-1.

10. The Boeing Co., Document No. D233-10036-2.

11. McInerney, R. E., and Abelowitz, A., "Magnetic Field Package", Air Force Report No. AFCRL-TR-73-0356, (1973).

12. Lai, S. T., Smiddy, M., and Wildman, P., "Satellite Sensing of Low Energy Plasma Bulk Motion", Proceedings of the Seventh Conference of Aerospace and Aeronautical Meteorology and Symposium on Remote Sensing from Satellites, Amer. Meteor. Soc. & AIAA, pp. 302-306, (1976). Also, AFGL-TR-76-0281, (1976).

13. Kelley, M. C., Private Communication.

14. Kelley, M. C., Private Communication.

15. Smiddy, M., Burke, W., Kelley, M., and Lai, S., "Electric Fields at High Latitudes near the Dawn-Dusk Meridian", Trans. Am. Geophys. U., Vol. 59, No. 4, p. 360,(1978).

16. Cauffman, D. P., "Electric Field Reversals in the Magnetosphere", Ph.D. Thesis, University of Iowa, (1970).

17. Cauffman, D. P., and Gurnett, D. A., "Satellite Measurements of High Latitude Convection E-Fields", Space Sci. Rev. 13, p. 369, (1972).

18. Burke, W. J., Sagalyn, R. C., Smiddy, M., Kelley, M. C., and Lai, S. T., "Electric Fields at High Latitudes in the Topside Ionosphere near the Dawn-Dusk Meridian", presented at COSPAR, (1978); accepted for publication, Space Research, (1978).

19. Burke, W. J., Kelley M. C., Sagalyn, R. C., Smiddy, M., and Lai, S. T., "Polar Cap Electric Field Structure with Northward Interplanetary Magnetic Field", submitted to J. Geophys. Res., (1978).

20. Heppner, J. P., "Polar-Cap Electric Field Distribution Related to the Interplanetary Magnetic Field Direction", J. Geophys. Res., 77, p. 4877, (1972).

21. Maezawa, K., "Magnetospheric Convection Induced by the Positive and Negative Z Components of the Interplanetary Magnetic Field: Quantitative Analysis Using Polar Cap Magnetic Records", J. Geophys. Res. 81, p. 2289, (1976).

22. Burke, W. J., Kelley, M. C., Sagalyn, R. C., Smiddy M., Hardy, D. A., and Lai, S. T., (to be published).